Tracing the Evolution of the Earth System through an Isotopic Record of Proterozoic Sulfate

Peter W. Crockford

Department of Earth and Planetary Sciences

McGill University
Montreal, Quebec
August, 2017

A thesis submitted to McGill University in partial fulfillment of the requirements of the degree of Doctor of Philosophy

For my family, friends and mentors,

thanks for getting me this far

Acknowledgements

My work at McGill began with a project idea proposed to me by Dr. Boswell Wing exploring Neoproterozoic Snowball Earth glaciations. This project kicked off an exploration into Earth history utilizing isotopic tools that ultimately became what is now this thesis. The reality of this endeavor is that it is the product of a large team of people who came together to support me through providing samples, ideas, laboratories, friendship and mentorship, and if I attempted to fully do justice to the gratitude deserved to everyone involved it would likely dwarf some of the chapters in this thesis. First and foremost I owe a huge debt of gratitude to Dr. Boswell Wing (Boz) and Galen Halverson who ultimately gave me a shot to restart my academic pursuits. Without them taking a chance on me I am certain I would be in some miserable job in the middle of nowhere. Boz has been an amazing mentor and friend over the past four years, always supportive of the many intellectual detours I took during my time at McGill. Galen facilitated some of my best memories over my PhD with adventures on Baffin Island, Yukon, Australia and Spain and has been an unshakeable rock through my whole time at McGill always ensuring that my chief concern is producing quality science, and to never worry about funding even as complications arose in my last year. Both Boz and Galen have set a very high bar in supervising students, doing scientific research as well as how to teach, and I hope one day I can live up to their examples.

Special thanks needs to go out to my fellow PROPS members who welcomed me into the group from my first days at McGill. I would like to single out Marcus Kunzmann, Grant Cox, Andre Pellerin and Thi Hao Bui who showed me the ropes in the lab, and field, as well as help me navigate how to be successful in graduate school. I would also like to give a special shout out to Sarah Worndle who was my partner-in-crime through many of my adventures to the North and South and has been a great friend through my time at McGill. And thanks to Tim Gibson, Malcolm Hodgskiss, Jesse Collangelo-Lillis and all PROPS members for creating a great workspace to share ideas and do my work.

Thanks to Dr. Huiming Bao for welcoming me into the OASIC group at LSU where I thoroughly enjoyed all of my visits and am so greatful for all of the mentorship Dr. Bao has provided over my PhD. The success of all my trips to LSU was in a large part due to the help of Justin Hayles, who aided in analysis and more importantly great discussions over beer after work at the Chimes. Although many of my side-projects have not made it into this thesis, I would like to thank Dr. Andre Poirier, for all of his help with my work at GEOTOP, Dr. John Higgins at Princeton, Dr. Yuichiro Ueno at Tokyo Tech, Dr. Noah Planavsky at Yale, Dr. Joel Savarino at IGGE and Dr. Tristan Horner at WHOI who welcomed me into their labs and broadened my interests and expertise that have played a large role in shaping work I plan to do into the future.

It goes without saying, thank you to my family and friends who supported me through my PhD. First my parents Devi and Dennis for always providing love and support over the past 32 years. Thanks to my friends Devin Stark and Evan Riddel for always making time to talk. And special thanks to Ichiko Sugiyama who has been so supportive over the past few years often making sure I don't work myself to death as well as coming to the lab with me late nights and weekends, and being so patient as I scrambled to stay on top of manuscripts, presentations and proposals. Thanks to the EPS department, that provided an amazing home and for all the hard work of the faculty and staff (Angela, Anne, and Kristy) for creating such a supportive environment. I'd like to give special thanks to Anita Mountjoy whose countless dinners have often been the cure for homesickness, and to Dr. Bjorn Sundby who has been so much help with both academic and life advice. And thanks to all of my EPS friends especially Nils Backeberg, Lucas Kavenaugh and Kalina Malowany who have been such a pleasure to make so many great memories with during my time in Montreal. And finally I would like to thank Paul Hoffman, who in 2011 gave me the opportunity to work with him in Namibia. This experience rejuvenated my excitement in science and ultimately gave me the confidence to pursue a PhD. Paul's friendship and support has been invaluable over the past years, and I look forward to future lively discussions and debates.

Funding over my time at McGill has been provided through an NSERC CREATE, CATP program as well as an NSERC PGS-D fellowship as well as NSERC and FQNRT funding through Dr. Boswell Wing and Dr. Galen Halverson. I would like to thank the Mineralogical Association of Canada for both a travel grant and scholarship, the Geological Society of America for a student research grant, McGill University GREAT and Mobility programs, McGill EPS for a McGregor Scholarship, and NSTP/PCSP for funding work on Baffin Island. I would like to thank MITACS, the Japanese Society for the Promotion of Science and Campus France for funding my summer research in Japan in 2016 and France in 2017. And thank you to the Agouron Institute Geobiology Fellowship Program, Dr. Itay Halevy and Dr John Higgins for providing me with the piece of mind that I have a future in academia beyond McGill.

Abstract

Beginning with the oxygenation of the surface environment and concluding with Snowball Earth glaciations and diversification of animals, the Proterozoic Earth witnessed some of the most dramatic shifts to the Earth System. These transitions are burdened with many unanswered questions largely surrounding the composition of the atmosphere and nature of the biosphere. Sulfate has the ability to document many of these changes in the sedimentary record through its isotopes. Specifically, recent analytical advances over the past few decades have opened new abilities to constrain atmospheric chemistry, identify specific microbial metabolisms and gauge the size of the biosphere. In this thesis an isotopic record of Proterozoic sulfate is presented where over 400 samples from 35 different formation spanning Earth's earliest evaporites at 2.35 Ga to Ediacaran aged deposits were measured for both major ($\delta^{18}O$, $\delta^{34}S$) and minor ($\Delta^{17}O$, $\Delta^{33}S$) isotopes.

Neoproterozoic samples deposited in the immediate aftermath of the Marinoan Snowball Earth reveal a dynamic sulfur cycle through $\Delta^{17}O$, $\delta^{34}S$ and $\Delta^{33}S$ results. I expand the current footprint of the $\Delta^{17}O$ anomaly, which has been one of the major pillars in support of the Snowball Earth Hypothesis. Through expanding to three new paleo-continents in North America, Brazil and Norway I provide further evidence that deglaciation from the Marinoan was rapid and synchronous. Further, these results lay a foundation to interrogate the post-Marinoan sedimentary record for local, global or globally local perturbations to the Earth System.

Contrasting highly dynamic Cryogenian records, I explore the mid-Proterozoic through sulfates from the 1.4 Ga Sibley Group. Here similar large $\Delta^{17}O$ anomalies similar

to the Cryogenian are observed, However, in the absence of any evidence of glaciation, these results imply a significantly smaller biosphere generating oxygen at this time, and likely over much of the mid-Proterozoic. To obtain a more synoptic view of the Proterozoic I complement Cryogenian and Sibley data sets with 32 other formations spanning the Proterozoic. This comprehensive record depicts dramatic changes to the Earth system through five unique Proterozoic stages. What stands out is that underlying many of these changes may be dramatic shifts in the size of the biosphere and marine sulfate reservoir.

Résumé

De l'oxygénation de l'atmosphère terrestre à une probable glaciation totale de la surface de la Terre et à la diversification animale, le Protérozoïque est marqué par plusieurs évènements qui constituent des changements majeurs pour le système Terre. Cependant, de nombreuses questions concernant ces grandes transitions, notamment sur la composition de l'atmosphère et la constitution de la biosphère lors de ces évènements, demeurent toujours sans réponse. Le sulfate possède la caractéristique de pouvoir documenter ces changements à travers l'étude de sa composition isotopique. Par ailleurs, au cours des dernières décennies, le développement de nouvelles techniques d'analyses ont permis une meilleure compréhension de la chimie atmosphérique, des métabolismes microbiens et une meilleure estimation de la taille de la biosphère dans le passé. Dans ce travail de thèse, un enregistrement isotopique du sulfate ($\delta^{18}O$, $\delta^{34}S$, $\Delta^{17}O$ et $\Delta^{33}S$) datant du Protérozoïque est présenté. 400 échantillons prélevés sur 35 évaporites reparties sur la Terre et datés entre 2,35 Ga et la période de l'Ediacaran ont été analysés.

Les analyses isotopiques en $\Delta^{17}O$, $\delta^{34}S$ et $\Delta^{33}S$ réalisées sur des échantillons du néo-Protérozoïque déposés immédiatement après la période du Marinoan (vers 635 Ma soit la fin du Cryogenian qui se caractérise par période de glaciation totale de la Terre) révèlent un cycle de soufre avec une dynamique spécifique. Les résultats obtenus dans cette étude complètent les enregistrements déjà disponibles de l'anomalie $\Delta^{17}O$ du sulfate datant du Marinoan et grâce auxquels l'hypothèse d'une Terre complètement englacée a pu être confortée. Ces nouveaux résultats, et la répartition géographique des échantillons avec lesquels ils ont été obtenus, révèlent que la déglaciation du Marinoan a été rapide et particulièrement synchrone. En outre, ces résultats constituent une base utile à une

meilleur compréhension des enregistrements de perturbations locales à globales issus des dépôts sédimentaires post-Marinoan.

Dans un deuxième temps j'ai travaillé sur des échantillons du mid-Protérozoïque datant de 1,4 Ga (séquence du Sibley group), soit une période dynamiquement différente du Cryogenian. Les anomalies en $\Delta^{17}O$ alors mesurées montrent des valeurs assez comparables à celles observées lors du Cryogenian. Ces résultats impliquent, en tenant compte des preuves suggérant une probable absence de glaciation à cette période, la présence d'une biosphère génératrice d'oxygène de taille significativement plus petite à ce moment-là et probablement sur une large partie du mid-Protérozoïque.

Afin de couvrir plus largement cette étude sur la période étudiée, le jeu de données obtenues pour le Cryogenian et le Sibley a été complété par l'analyse de 32 autres échantillons couvrant le Protérozoïque. Cet enregistrement complet révèle des changements majeurs dans le système Terre au long des cinq périodes spécifiques du Protérozoïque. Avec pour la plupart de ces changements des larges modifications de la taille de la biosphère et du réservoir de sulfate d'origine océanique.

Preface and Author Contributions

This thesis contains an introduction followed by four chapters of original research. Each chapter contains an individual preface highlighting the importance of the respective work and contributions of all participants of this work. The work within this thesis was conducted between September 2013 and August 2017. Below I summarize author contributions for chapters within this thesis as well as other works that were conducted during my time at McGill.

Chapters contained within this thesis have been previously published or are currently in review. This work was not possible without the combined efforts of multiple co-authors summarized by chapter below:

Chapter 2: Peter W. Crockford, Benjamin R. Cowie, Boswell A. Wing and David T. Johnston conceived the project. Field-work and sample collection was performed by Galen P. Halverson, Paul F. Hoffman and Francis A. Macdonald. Sulfur isotope analysis was performed by Ichiko Sugiyama, Thi Hao Bui and Andre Pellerin. Oxygen isotope analysis was performed by Peter W. Crockford, and Justin A. Hayles. The manuscript was written by Peter W. Crockford and Benjamin R. Cowie with input from all co-authors most notably Boswell A. Wing and David T. Johnston.

Chapter 3: Peter W. Crockford conceived the project. Samples were collected by Malcolm S.W. Hodgskiss, Gabriel Uhlein and Fabricio Caxito. Oxygen isotope analysis were performed by Peter W. Crockford, and Justin Hayles. Peter W. Crockford interpreted the data and wrote the manuscript with input from all co-authors most notably

Galen P. Halverson.

Chapter 4: Peter W. Crockford, Noah J. Planavsky and Boswell A. Wing conceived the project. Noah J. Planavsky, Andrey Bekker, and Philip Fralick collected samples. Peter W. Crockford and Justin A. Hayles performed oxygen isotope analyses. Peter W. Crockford and Thi H. Bui performed sulfur isotope analyses. Peter W. Crockford wrote the manuscript with input from all co-authors listed above as well as Dr. Huiming Bao.

Chapter 5: Peter W. Crockford and Boswell A. Wing conceived the project. Peter W. Crockford, Marcus Kunzmann, Galen P. Halverson, Boswell A. Wing, Andrey Bekker, Robert Rainbird, Grant Cox, Sarah Worndle, Timothy Gibson, Aivo Lepland, Nicholas Swanson-Hysell, Sharad Master, Bulusu Sreenivas, Anton Kuznetsov, and Valery Krupenik collected samples. Peter W. Crockford, Justin A. Hayles and Yongbo Peng performed oxygen isotope analyses. Peter W. Crockford and Thi Hao Bui performed sulfur isotope analyses. Peter W. Crockford interpreted the data, and wrote the manuscript with input from Marcus Kunzmann, Andrey Bekker, Grant Cox, Timothy Gibson, Justin Hayles, Yongbo Peng, Huiming Bao, Sarah Worndle, Aivo Lepland Galen Halverson, Sarah Worndle, and Boswell A. Wing.

Before arriving at McGill I produced other works that were published during my time here:

1. **Crockford, P.W.,** Telmer, K., and Best, M. (2014). Dissolution kinetics of Devonian carbonates at circum-neutral pH, 50bar pCO**2**, 105 C, and 0.4 M: The importance of complex brine chemistry on reaction rates. Applied Geochemistry, 41, 128-134.

2. Canil, D., **Crockford, P.W.,** Telmer, K., and Rossin, R. (2015) Mercury abundances in the crust and mantle and relevance to the moderately volatile element budget of the Earth. Chemical Geology, 396, 134-142

3. Hoffman, P.F., Bellfroid, E.J., **Crockford, P.W.,** De Moor, A., Halverson, G.P., Hodgin, B., Hodgskiss, M.S.W., Holtzman, B.K., Jasechko, G.R., Johnston, B.W., and Lamothe, K.G. (2016) A misfit Cryogenian diamictite in the Vrede domes, Northern Damara Zone, Namibia: Chuos (Sturtian) or Ghaub (Marinoan) Formation? Moraine or Palaeovalley?. Communications of the Geological Survey of Namibia, 17, 1-16

During my time at McGill I also co-authored other publications that did not make it into this thesis. Contributions to these works included sample collection, data generation and analysis as well as manuscript preparation. These works include:

1. Cox, G.M., Jarrett, A., Edwards, D., **Crockford, P.W.,** Halverson, G. P., Li, ZX, Collins, A. S. (2016) The Mesoproterozoic Roper Seaway. Chemical Geology 440, 101-114

2. Kunzmann, M., Bui, T.H., **Crockford, P.W.,** Halverson, G. P., Scott, C., Lyons, T.W., Wing, B.A., (2017) Bacterial sulfur disproportionation constrains timing of Neoproterozoic oxygenation. Geology. 45, 207-210

3. Macdonald, F.A., Karabinos, P.M., Crowley, J.L., Hodgin, E.B., **Crockford, P.W.,** Delano, J., Bridging the gap between the foreland and hinterland II: geochronology and tectonic setting of Ordovician magmatism and basin formation on the Laurentian margin of New England and Newfoundland. American Journal of Science, 317, 555-596

4. Horner, T.J., Pryer, H.V., Nielsen, S.G., **Crockford, P.W.,** Gauglitz, J.M., Wing, B.A., and Rickets, R.D. Pelagic Barite Precipitation at micromolar ambient sulphate. Nature Communications *accepted*

5. Nelson, L., Strauss, J.V., **Crockford, P.W.,** Cox, G.M., Macdonald, F.A., Johnson, B.G.,Ward, W., Colpron, M., and McClelland, W.C., Geochemical constraints on the evolution of the pre-Mississippian sedimentary rocks in the North Slope of Yukon and Alaska. GSA Special Papers in review

6. Gibson, T.M., Shih, P.M., Fischer, W.W., Cumming, V.M., Creaser, R.A., **Crockford, P.W.,** Hodgskiss, M.S.W., Worndle-Quoex, S., Rainbird, R.H., Skulski, T.M., Halverson, G.P. Precise age of Bangiomorpha Pubescencs dates the emergence of eukaryotic photosynthesis. *Geology* submitted

Contents

List of Tables

List of Figures

1. Introduction

The Proterozoic Eon represents Earth's middle age and spans nearly half of all its history (2.5-0.542 Ga). Sedimentary units deposited over this interval record enormous changes to both the biosphere and the biogeochemical cycles that support it (Lyons et al., 2014; Reinhard et al., 2016; Stuecken et al., 2016; Koehler et al., 2017; Fig. 1.1). Many of these changes are likely a consequence of the emergence of oxygenic photosynthesizers excreting free oxygen to the surface environment and eventually dominating global primary production (Sessions et al., 2009). This new flux of free oxygen to the surface environment and likely growth of the biosphere would have ushered in a dramatic shift in the redox state of Earth's surface environment that may have allowed for more metabolically active forms of life to emerge as well as an expansion of the environments they inhabited (Knoll and Bauld, 1989; Des Marais, 2001; Catling et al., 2005; Scott et al., 2008; Kharecha et al., 2005; Holland, 2006; Mills et al., 2014; Judson et al., 2016; Fig. 1.1). While much evidence is derived from various redox proxies and biogeochemical models, this broad progression in oxygenation of the surface environment between the Archean and Phanerozoic (Fig 1.1; Cloud, 1972; Garrels and Perry, 1973; Lyons et al., 2014) is borne out in macro-scale features such as the disappearance of banded Iron formations (Isley and Abbott, 1999), the disappearance of rounded pyrite and uraninite grains deposited in fluvial settings (Roscoe, 1973; Rasmussen et al., 1999), and the appearance of fossilized animals in sedimentary units (Fig. 1.1; Knoll, 1992; Erwin et al., 2011). This inferred rise of atmospheric oxygen from these macro-scale features is reflected in ancient marine geochemical records with evidence of persistent subsurface anoxia with varying degrees of ferruginous and euxinic conditions as well as different degrees of surface water oxygenation (Canfield, 1998; Arnold et al., 2004; Poulton et al., 2010; Planavsky et al., 2011; Kunzmann et al., 2015; Hardisty et al., 2017; Fig. 1.1). Changes in the surface environment over the Proterozoic however, were not limited to a rise in the oxidative capacity of the atmosphere and marine environment. For example the early Proterozoic sun was almost 20% less luminous than present day, however there is only evidence for glacially derived sediments at the beginning and end of this Eon suggesting an important role for increased atmospheric greenhouse gas inventories to compensate for this reduced solar output (Fig. 1.1; Gough, 1981). Continental arrangements appear to have been very diverse from supercontinents to spread out micro-continents (Li et al., 2013) which would both change the albedo of the Earth but also the nature of margins (Bradley, 2011) where much of the complex interplay between the biosphere, atmosphere, hydrosphere and geosphere takes place (Campbell and Allen, 2008). All of these features provide a fascinating series of events to be reconstructed and an exciting opportunity to study the Earth under a far different geochemical regime than the modern.

While great strides have been made in refining models of atmospheric chemistry (Goldblatt et al., 2006; Laakso and Schrag, 2013; Daines et al., 2016; Wolf and Toon, 2014), and timing the emergence of different branches in the tree of life (Hug et al., 2015), the Proterozoic remains riddled with uncertainty. For example atmospheric oxygen levels over the mid-Proterozoic span orders of magnitude from less than 0.1% PAL (Present Atmospheric Level) to 10% PAL (O_2 1 PAL ≈ 209,500 ppm; Planavsky et al., 2014; Canfield et al., 2005; Fig. 1.1) and recent estimates potentially place Neoproterozoic levels as high as 50% PAL (Blamey et al., 2017). What mixture of greenhouse gases that compensated for a faint young sun over this interval is also debated with atmospheric CO_2 (pCO_2) estimates spanning from modern levels to over 200 PAL (CO_2 PAL = 280 ppm; Sheldon et al, 2013; von Paris et al., 2008; Fig. 1.1) and the role of methane continually debated (Pavlov et al., 2003; Olson et al., 2016; Fiorella and Sheldon, 2017). As important as atmospheric chemistry and the temperature of the Earth surface environment is the productivity of the biosphere, however estimates on how this has varied through Earth history remain sparse and without geochemical proxies in the sedimentary record.

Matters become increasingly complicated over both Paleoproterozoic and Neoproterozoic glaciations where their initiations and terminations remain enigmatic (Hoffman et al., 1998; Kopp et al., 2005) and the composition of the atmosphere and survival of the biosphere over these intervals hotly debated (Hoffman, 2016). Importantly the pace at which the Earth entered these events and recovered remains elusive as radiometric dating techniques lack the resolution to provide such clarity. What is clear, is that the combination of factors that ultimately drove changes and maintained stability of the Earth System over the Proterozoic requires further investigation.

Advances in analytical capabilities over the past decades and the development of geochemical proxies that can provide globally integrated signatures are providing an ability to test outstanding questions over the Proterozoic as well as provide new insights. In many cases however, data is incredibly sparse over this interval of Earth history. This is particularly notable for triple oxygen ($\Delta^{17}O$) isotopes that have a proven ability to provide information on the ancient atmosphere and biosphere where the current record only extends slightly beyond the Cryogenian (Bao et al., 2008; Wing, 2013; Fig. 2.1).

This thesis explores the Proterozoic environment through new oxygen and sulfur isotopic measurements within sedimentary sulfate minerals. Specifically this thesis addresses:

1. What was the pace of recovery from the Marinoan Snowball Earth glaciation? (Chapters 2 and 3)
2. Can local from global geochemical signals in the recovery from the Marinoan Snowball Earth be distinguished? (Chapter 3)
3. Has global primary production varied throughout Earth history? (Chapters 4 and 5)
4. How rapid was oxygenation across the *GOE*? (Chapter 5)
5. How has the size of the global marine sulfate reservoir responded to changes in the surface environment? (Chapters 2 and 5)

In Chapters 2 and 3 $\Delta^{17}O$ anomalies associated with the Marinoan Snowball Earth glaciation are extended to three new paleocontinents (modern day Canada, Brazil, and Norway). In Chapter 2 $\Delta^{17}O$ data is combined with sulfur isotopes and timing estimates are calculated for the time required to impart and remove anomalous $\Delta^{17}O$ values from the global marine sulfate reservoir. As tying geographically disparate strata together in time has been a challenge for post-Marinoan strata, in Chapter 3 it is argued that $\Delta^{17}O$ anomalies provide such a time horizon, and thus locations that posses it are the best candidates to evaluate global from local geochemical signals. In Chapters 4 and 5 isotopic records of sulfate are extended to the first evaporites in the sedimentary record deposited at 2.35 Ga. Chapter 4 focuses on the 1.4 Ga Sibley Group where it is argued that large $\Delta^{17}O$ anomalies reflect reduced global primary production from modern levels across the mid-Proterozoic. In Chapter 5 a compilation of new oxygen and sulfur isotope data spanning the entire Proterozoic is presented and broad trends are discussed in the context of the evolving Earth surface environment.

Figures

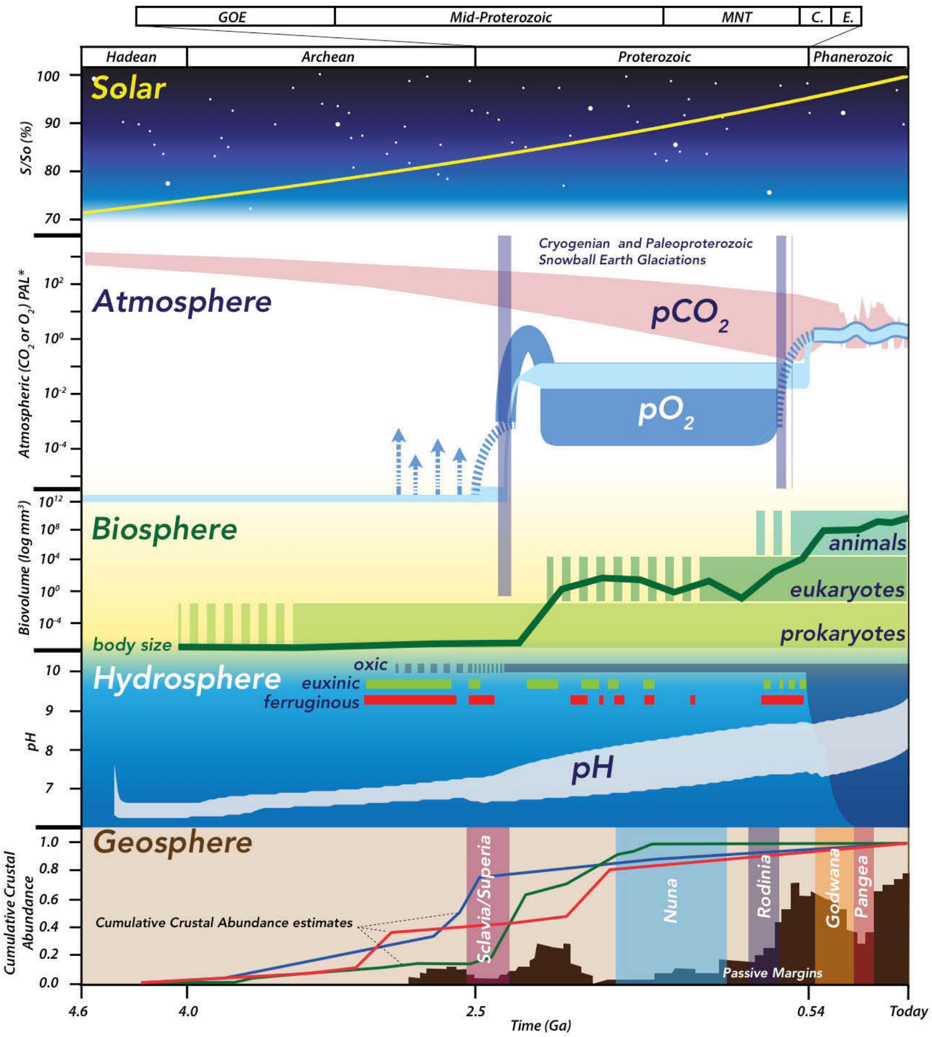

Figure. 1.1: Schematic of changes to the Earth System over geologic time. Estimates for major changes to the Earth System are outlined for Solar, Atmosphere, Biosphere, Hydrosphere and Geosphere presented from top to bottom, respectively. At the top we track changes in solar output relative to present levels calculated from Gough et al., 1981. Below we track proposed trajectories of atmospheric CO_2 and O_2 levels presented relative to Present Atmospheric Levels (PAL; 280 ppm CO_2; 209,500 ppm O_2). The CO_2 field is taken from the 1D model of von Paris et al., 2008 from 4.6-0.6 Ga, and using estimates from Franks et al., 2014 and Berner, 2006. The O_2 field is based on combined proxy data compiled by Lyons et al., 2014 with average estimates in light blue, and a broader range presented in purple/dark blue?. Overlaying atmospheric estimates are panglacial intervals so called Snowball Earth events in blue lines (Hoffman et al., 1998; Kirschvink et al., 2000). Below the biosphere panel depicts changes in maximum body sizes of organisms over Earth history, as summarized by Payne et al., 2011, and overlain with the diversity of the biosphere separated into prokaryote, eukaryote and animals with dashed bars representing uncertainty in origin. Below in the hydrosphere panel we plot marine redox conditions (Hardisty et al., 2017; Anbar et al., 2007; Planavsky et al., 2011) together with a predicted evolution of seawater pH values (Halevy and Bachan, 2017). Finally at the base of the figure in the geosphere panel we plot the distribution of passive margins through time (dark brown; Bradley, 2011), supercontinents (and cratonic amalgamations e.g. Sclavia/Superia) through Earth history, and crustal growth curves from Jacobsen, 1988 (red), Ying, 2011 (green) and Taylor and Mclennan, 1985 (blue).

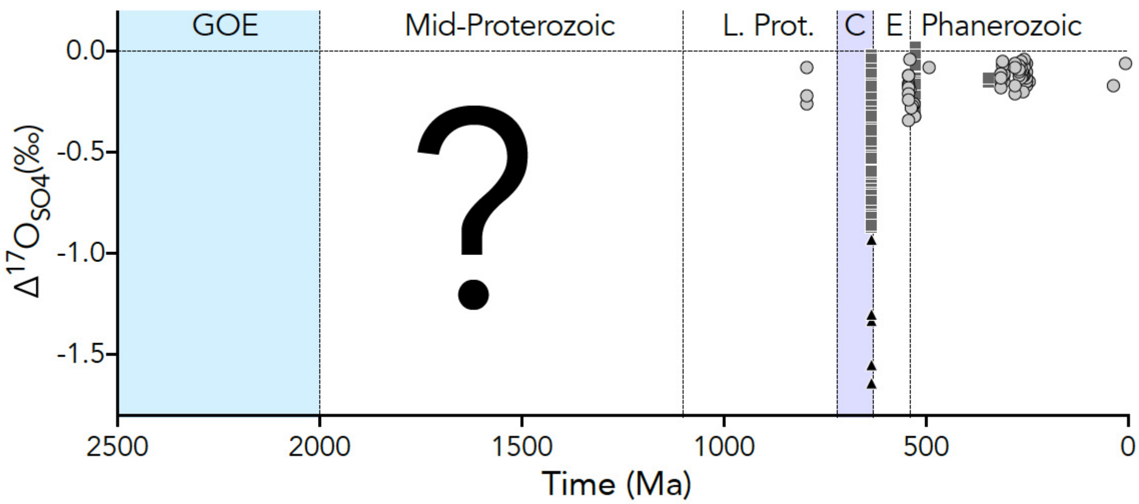

Figure. 1.2: Existing triple oxygen ($\Delta^{17}O$) data within sulfates from Bao et al., 2008; 2009; 2012 and Crockford et al., 2016, extending back to 750 Ma.

Bibliography

Arnold, G.L., Anbar, A.D., Barling, J. and Lyons, T.W., 2004. Molybdenum isotope evidence for widespread anoxia in mid-Proterozoic oceans. *Science*, *304*(5667), pp.87-90.

Bao, H., Lyons, J.R. and Zhou, C., 2008. Triple oxygen isotope evidence for elevated CO2 levels after a Neoproterozoic glaciation. *Nature*, *453*(7194), pp.504-506.

Bao, H., Fairchild, I.J., Wynn, P.M. and Spötl, C., 2009. Stretching the envelope of past surface environments: Neoproterozoic glacial lakes from Svalbard. *Science*, *323*(5910), pp.119-122.

Bao, H., Chen, Z.Q. and Zhou, C., 2012. An 17 O record of late Neoproterozoic glaciation in the Kimberley region, Western Australia. *Precambrian Research*, *216*, pp.152-161.

Berner, R.A., 2006. GEOCARBSULF: a combined model for Phanerozoic atmospheric O_2 and CO 2. *Geochimica et Cosmochimica Acta*, *70*(23), pp.5653-5664.

Blamey, N.J., Brand, U., Parnell, J., Spear, N., Lécuyer, C., Benison, K., Meng, F. and Ni, P., 2016. Paradigm shift in determining Neoproterozoic atmospheric oxygen. *Geology*, *44*(8), pp.651-654.

Bradley, D.C., 2011. Secular trends in the geologic record and the supercontinent cycle. *Earth-Science Reviews*, *108*(1), pp.16-33.

Campbell, I.H. and Allen, C.M., 2008. Formation of supercontinents linked to increases in atmospheric oxygen. *Nature Geoscience*, *1*(8), p.554.

Canfield, D.E., 1998. A new model for Proterozoic ocean chemistry. *Nature*, *396*(6710), pp.450-453.

Canfield, D.E., 2005. The early history of atmospheric oxygen: homage to Robert M. Garrels *Annu. Rev. Earth Planet. Sci.*, *33*, pp.1-36.

Catling, D.C., Glein, C.R., Zahnle, K.J. and McKay, C.P., 2005. Why O_2 Is Required by Complex Life on Habitable Planets and the Concept of Planetary" Oxygenation Time". *Astrobiology*, *5*(3), pp.415-438.

Cloud, P., 1972. A working model of the primitive Earth. *American Journal of Science*, *272*(6), pp.537-548.

Crockford, P.W., Cowie, B.R., Johnston, D.T., Hoffman, P.F., Sugiyama, I., Pellerin, A., Bui, T.H., Hayles, J., Halverson, G.P., Macdonald, F.A. and Wing, B.A., 2016.

Triple oxygen and multiple sulfur isotope constraints on the evolution of the post-Marinoan sulfur cycle. *Earth and Planetary Science Letters*, *435*, pp.74-83.

Daines, S.J., Mills, B.J. and Lenton, T.M., 2017. Atmospheric oxygen regulation at low Proterozoic levels by incomplete oxidative weathering of sedimentary organic carbon. *Nature Communications*, *8*

Des Marais, D.J., 2001. Isotopic evolution of the biogeochemical carbon cycle during the Precambrian. *Reviews in Mineralogy and Geochemistry*, *43*(1), pp.555-578.

Erwin, D.H., Laflamme, M., Tweedt, S.M., Sperling, E.A., Pisani, D. and Peterson, K.J., 2011. The Cambrian conundrum: early divergence and later ecological success in the early history of animals. *science*, *334*(6059), pp.1091-1097.

Fiorella, R.P. and Sheldon, N.D., 2017. Equable end Mesoproterozoic climate in the absence of high CO2. *Geology*, *45*(3), pp.231-234.

Franks, P.J., Royer, D.L., Beerling, D.J., Van de Water, P.K., Cantrill, D.J., Barbour, M.M. and Berry, J.A., 2014. New constraints on atmospheric CO2 concentration for the Phanerozoic. *Geophysical Research Letters*, *41*(13), pp.4685-4694.

Goldblatt, C., Lenton, T.M. and Watson, A.J., 2006. Bistability of atmospheric oxygen and the Great Oxidation. *Nature*, *443*(7112), pp.683-686.

Garrels, R.M. and Perry, E.A., 1974. Cycling of carbon, sulfur, and oxygen through geologic time. *The sea*, *5*, pp.303-336.

Gough, D.O., 1981. Solar interior structure and luminosity variations. *Solar Physics*, *74*(1), pp.21-34.

Halevy, I. and Bachan, A., 2017. The geologic history of seawater pH. *Science*, *355*(6329), pp.1069-1071.

Hardisty, D.S., Lu, Z., Bekker, A., Diamond, C.W., Gill, B.C., Jiang, G., Kah, L.C., Knoll, A.H., Loyd, S.J., Osburn, M.R. and Planavsky, N.J., 2017. Perspectives on Proterozoic surface ocean redox from iodine contents in ancient and recent carbonate. *Earth and Planetary Science Letters*, *463*, pp.159-170.

Hoffman, P.F., Kaufman, A.J., Halverson, G.P. and Schrag, D.P., 1998. A Neoproterozoic snowball earth. *Science*, *281*(5381), pp.1342-1346.

Hoffman, P.F., 2016. Cryoconite pans on Snowball Earth: supraglacial oases for Cryogenian eukaryotes?. *Geobiology*, *14*(6), pp.531-542.

Holland, H.D., 2006. The oxygenation of the atmosphere and oceans. *Philosophical Transactions of the Royal Society of London B: Biological Sciences*, *361*(1470), pp.903-915.

Hug, L.A., Baker, B.J., Anantharaman, K., Brown, C.T., Probst, A.J., Castelle, C.J., Butterfield, C.N., Hernsdorf, A.W., Amano, Y., Ise, K. and Suzuki, Y., 2016. A new view of the tree of life. *Nature Microbiology*, *1*, p.16048.

Isley, A.E. and Abbott, D.H., 1999. Plume-related mafic volcanism and the deposition of banded iron formation. *Journal of Geophysical Research: Solid Earth*, *104*(B7), pp.15461-15477.

Jacobsen, S.B., 1988. Isotopic constraints on crustal growth and recycling. *Earth and Planetary Science Letters*, *90*(3), pp.315-329.

Judson, O.P., 2017. The energy expansions of evolution. *Nature Ecology & Evolution*, *1*, p.0138.

Kharecha, P., Kasting, J. and Siefert, J., 2005. A coupled atmosphere–ecosystem model of the early Archean Earth. *Geobiology*, *3*(2), pp.53-76.

Kirschvink, J.L., Gaidos, E.J., Bertani, L.E., Beukes, N.J., Gutzmer, J., Maepa, L.N. and Steinberger, R.E., 2000. Paleoproterozoic snowball Earth: Extreme climatic and geochemical global change and its biological consequences. *Proceedings of the National Academy of Sciences*, *97*(4), pp.1400-1405.

Knoll, A.H., 1992. Vendian microfossils in metasedimentary cherts of the Scotia group, Prins Karls Forland, Svalbard. *Palaeontology*, *35*(4), pp.751-774.

Koehler, M.C., Stüeken, E.E., Kipp, M.A., Buick, R. and Knoll, A.H., 2017. Spatial and temporal trends in Precambrian nitrogen cycling: a Mesoproterozoic offshore nitrate minimum. *Geochimica et Cosmochimica Acta*, *198*, pp.315-337.

Kopp, R.E., Kirschvink, J.L., Hilburn, I.A. and Nash, C.Z., 2005. The Paleoproterozoic snowball Earth: a climate disaster triggered by the evolution of oxygenic photosynthesis. *Proceedings of the National Academy of Sciences of the United States of America*, *102*(32), pp.11131-11136.

Knoll, A.H. and Bauld, J., 1989. The evolution of ecological tolerance in prokaryotes. *Earth and Environmental Science Transactions of The Royal Society of Edinburgh*, *80*(3-4), pp.209-223.

Kunzmann, M., Halverson, G.P., Scott, C., Minarik, W.G., Wing, B.A., 2015. Geochemistry of Neoproterozoic black shales from Svalbard: implications for oceanic redox conditions spanning Cryogenian glaciations. *Chemical Geology, 417*, 383-393.

Laakso, T.A. and Schrag, D.P., 2014. Regulation of atmospheric oxygen during the Proterozoic. *Earth and Planetary Science Letters*, *388*, pp.81-91.

Li, Z.X., Evans, D.A. and Halverson, G.P., 2013. Neoproterozoic glaciations in a revised global palaeogeography from the breakup of Rodinia to the assembly of Gondwanaland. *Sedimentary Geology*, *294*, pp.219-232.

Lyons, T.W., Reinhard, C.T. and Planavsky, N.J., 2014. The rise of oxygen in Earth/'s early ocean and atmosphere. *Nature*, *506*(7488), pp.307-315.

Mills, D.B., Ward, L.M., Jones, C., Sweeten, B., Forth, M., Treusch, A.H. and Canfield, D.E., 2014. Oxygen requirements of the earliest animals. *Proceedings of the National Academy of Sciences*, *111*(11), pp.4168-4172.

Olson, S.L., Reinhard, C.T. and Lyons, T.W., 2016. Limited role for methane in the mid-Proterozoic greenhouse. *Proceedings of the National Academy of Sciences*, *113*(41), pp.11447-11452.

Pavlov, A.A., Hurtgen, M.T., Kasting, J.F. and Arthur, M.A., 2003. Methane-rich Proterozoic atmosphere?. *Geology*, *31*(1), pp.87-90.

Payne, J.L., McClain, C.R., Boyer, A.G., Brown, J.H., Finnegan, S., Kowalewski, M., Krause, R.A., Lyons, S.K., McShea, D.W., Novack-Gottshall, P.M. and Smith, F.A., 2011. The evolutionary consequences of oxygenic photosynthesis: a body size perspective. *Photosynthesis Research*, *107*(1), pp.37-57.

Planavsky, N.J., McGoldrick, P., Scott, C.T., Li, C., Reinhard, C.T., Kelly, A.E., Chu, X., Bekker, A., Love, G.D. and Lyons, T.W., 2011. Widespread iron-rich conditions in the mid-Proterozoic ocean. *Nature*, *477*(7365), pp.448-451.

Planavsky, N.J., Reinhard, C.T., Wang, X., Thomson, D., McGoldrick, P., Rainbird, R.H., Johnson, T., Fischer, W.W. and Lyons, T.W., 2014. Low Mid-Proterozoic atmospheric oxygen levels and the delayed rise of animals. *Science*, *346*(6209), pp.635-638.

Poulton, S.W., Fralick, P.W. and Canfield, D.E., 2010. Spatial variability in oceanic redox structure 1.8 billion years ago. *Nature Geoscience*, *3*(7), p.486.

Rasmussen, B. and Buick, R., 1999. Redox state of the Archean atmosphere: evidence from detrital heavy minerals in ca. 3250–2750 Ma sandstones from the Pilbara Craton, Australia. *Geology*, *27*(2), pp.115-118.

Reinhard, C.T., Planavsky, N.J., Gill, B.C., Ozaki, K., Robbins, L.J., Lyons, T.W., Fischer, W.W., Wang, C., Cole, D.B. and Konhauser, K.O., 2016. Evolution of the global phosphorus cycle. *Nature*. 541 (7637), pp. 386-389.

Roscoe, S.M., 1973. The Huronian Supergroup, a Paleoaphebian succession showing evidence of atmospheric evolution. *Geological Association of Canada, Special Paper*, *12*, pp.31-47.

Scott, C., Lyons, T.W., Bekker, A., Shen, Y.A., Poulton, S.W., Chu, X.L. and Anbar, A.D., 2008. Tracing the stepwise oxygenation of the Proterozoic ocean. *Nature*, *452*(7186), p.456.

Sessions, A.L., Doughty, D.M., Welander, P.V., Summons, R.E. and Newman, D.K., 2009. The continuing puzzle of the great oxidation event. *Current Biology*, *19*(14), pp.R567-R574.

Sheldon, N.D., 2013. Causes and consequences of low atmospheric pCO_2 in the Late Mesoproterozoic. *Chemical Geology*, *362*, pp.224-231

Stüeken, E.E., Kipp, M.A., Koehler, M.C. and Buick, R., 2016. The evolution of Earth's biogeochemical nitrogen cycle. *Earth-Science Reviews*, *160*, pp.220-239.

Taylor, S.R. and McLennan, S.M., 1985. The continental crust: its composition and evolution.

von Paris, P., Rauer, H., Grenfell, J.L., Patzer, B., Hedelt, P., Stracke, B., Trautmann, T. and Schreier, F., 2008. Warming the early Earth—CO_2 reconsidered. *Planetary and Space Science*, *56*(9), pp.1244-1259.

Wing, B.A., 2013. A cold, hard look at ancient oxygen. *Proceedings of the National Academy of Sciences*, *110*(36), pp.14514-14515.

Wolf, E.T. and Toon, O.B., 2014. Controls on the Archean climate system investigated with a global climate model. *Astrobiology*, *14*(3), pp.241-253.

Ying, J.F., Zhou, X.H., Su, B.X. and Tang, Y.J., 2011. Continental growth and secular evolution: Constraints from U-Pb ages and Hf isotope of detrital zircons in Proterozoic Jixian sedimentary section (1.8–0.8 Ga), North China Craton. *Precambrian Research*, *189*(3), pp.229-238.

Preface to Chapter 2

Between 717 and 635 million years ago, the Earth was engulfed from poles to equator in ice-sheets in two long lasting glaciations named the Sturtian and Marinoan. These so called Snowball Earth glaciations are a recent addition to the known history of the Earth and have become the forefront of excitement in Precambrian Geology. One of the major lines of evidence that laid to rest much of the debate surrounding these highly controversial events, was the discovery of large mass-independent triple oxygen isotope anomalies discovered within sulfate minerals in post-Marinoan sequences. These large oxygen isotope anomalies are only possible under two scenarios: an extremely reduced capacity of the biosphere to produce oxygen, or extremely high levels of atmospheric CO_2. Subsequent work ruled out the former interpretation making these isotopic anomalies a key piece of evidence for the existence of the second snowball Earth glaciation, the reason being that extremely high CO_2 levels would be required to end the Snowball Earth climate, and that such high CO_2 levels are only achievable when the Earth surface and atmosphere are segregated by icesheets.

In this Chapter we extended the oxygen isotope anomaly to a new location (northwest Canada; paleo-Laurentia) and present these results alongside multiple sulfur isotope data. This combined isotopic data set is then compared to existing data from south China. Trends in oxygen and sulfur isotopes appear to follow a consistent stratigraphic trajectory toward sulfate with a progressively heavier isotopic composition. Such a pattern appearing on two geographically disparate continents is likely only possible under two scenarios: either global drivers are producing similar local isotopic signatures, or these two locations are monitoring the evolution of the global marine sulfate reservoir. We calculate scenarios that could impart and subsequently eliminate such signatures from the global marine sulfate reservoir in order to provide upper estimates of the timing of deposition of these deposits and underlying cap carbonate units at a finer resolution than is possible through existing radiometric means. This exercise reveals two important insights into the post-Marinoan Earth: first the sulfur cycle at this time was no different to the modern with respect to process but was far different with respect to the magnitude of fluxes and size of reservoirs, and second the post-Marinoan sulfate reservoir was at its smallest size compared to the following 635 million years, and possibly since the Archean.

2. Triple oxygen and multiple sulfur isotope constraints on the evolution of the post-Marinoan sulfur cycle

Abstract

Triple oxygen isotopes within post-Marinoan barites have played an integral role in our understanding of Cryogenian glaciations. Reports of anomalous $\Delta^{17}O$ values within cap carbonate hosted barites however have remained restricted to South China and Mauritania. Here we extend the $\Delta^{17}O$ anomaly to northwest Canada with our new measurements of barites from the Ravensthroat cap dolostone with a minimum $\Delta^{17}O$ value of -0.75‰. For the first time we pair triple oxygen with multiple sulfur isotopic data as a tool to identify the key processes that controlled the post-Marinoan sulfur cycle. We argue using a dynamic 1-box model that the observed isotopic trends both in northwest Canada and South China can be explained through the interplay between sulfide weathering, microbial sulfur cycling and pyrite burial. An important outcome of this study is a new constraint placed on the size of the post-Marinoan sulfate reservoir (≈0.1% modern), with a maximum concentration of less than 10% modern. Through conservative estimates of sulfate fluxes from sulfide weathering and under a small initial sulfate reservoir, we suggest that observed isotopic trends are the product of a dynamic sulfur cycle that saw both the addition and removal of the $\Delta^{17}O$ anomaly over four to five turnovers of the post-Marinoan marine sulfate reservoir.

2.1 Introduction

The dramatic climate transition observed at the boundary between the Cryogenian and Ediacaran periods (635 Ma) is well documented but poorly understood. The Snowball Earth Hypothesis postulates that during this transition, Earth's oceans were frozen in a runaway ice-albedo feedback that was finally disrupted by the gradual, syn-glacial build-up of volcanogenic greenhouse gases (primarily CO_2) in Earth's atmosphere (Hoffman et al., 1998). The Snowball Earth event at the end of the Cryogenian period (the 635 Ma Marinoan glaciation) is marked by "cap carbonate" deposits and, in several regions of the world, thin intervals of barite ($BaSO_4$) (Hoffman et al., 2011; Macdonald et al., 2013). The recent discovery of large deficits in ^{17}O – ^{16}O ratios, relative to those expected from the ^{18}O – ^{16}O ratios in Snowball-associated barites, has drawn new attention to these deposits (Bao et al., 2008; Peng et al., 2011).

Stratospheric production of ozone preferentially concentrates the heavy oxygen isotopes (^{17}O and ^{18}O) in equal proportions relative to their lighter counterpart (^{16}O) (Thiemens and Heidenreich, 1983), and isotopic exchange results in the enrichment of stratospheric gases, principally CO_2, in the two heavy isotopes of oxygen (Yung et al., 1991; Yung et al., 1997). Conversely, stratospheric O_2 bears the isotopically lighter fraction, and is anomalously enriched in ^{16}O, and depleted in ^{17}O (Luz et al., 1999). This stratospheric isotopic anomaly is mixed into the tropospheric O_2 reservoir, where it can lead to ^{17}O depletions in tropospheric O_2. These ^{17}O depletions are tempered in the troposphere by O_2 generated through oxygenic photosynthesis (Luz et al., 1999), which is sourced ultimately from the hydrosphere and carries no mass- independent ^{17}O anomaly. Mass exchange between the stratosphere-troposphere seems to be relatively insensitive to changing atmospheric compositions (Butchart et al., 2006), therefore, the unique oxygen isotope signatures in post-Marinoan barites likely reflect perturbations to either biospheric productivity (Sansjofre et al., 2011), atmospheric CO_2 levels (Bao et al., 2008), or possibly both (Cao and Bao, 2013; Wing, 2013).

Transfer of the atmospheric isotope signal to marine sulfate starts with oxidative weathering of sulfide minerals, producing aqueous sulfate with up to 25% of its oxygen from tropospheric O_2 (Balci et al., 2007; Bao et al., 2008; Kohl & Bao, 2011). Rivers transport this sulfate to the oceans where it, and the isotopic anomaly it carries, is diluted into the standing stock of marine sulfate. Sulfate also fuels microbial sulfur cycling (MSC) in marine environments. The sulfide produced along the reductive branch of MSC can be re-oxidized to sulfate (Jorgensen, 1990), leading to a flux of isotopically normal ($\Delta^{17}O = 0$) sulfate back into the marine pool (Peng et al., 2011). This same set of processes (sulfide weathering and MSC) carry sulfur isotope consequences for the marine sulfate reservoir, mediated by the fraction of sulfur that leaves the marine environment through pyrite burial. The sulfide produced from sulfate reduction will be enriched in ^{32}S, leaving a sulfate counterpart that is enriched in ^{34}S. As preserved in the sedimentary record, sulfur isotopic differences between sulfates and sulfides are related to both oceanic sulfate concentrations (Gomes and Hurtgen, 2015, Bradley et al., 2015) and organic carbon availability, as manifest through sulfate reduction rates in marine sediments (Leavitt et al., 2013). Re-oxidative sulfur cycling can amplify this isotopic difference between reduced and oxidized forms of sulfur (Canfield and Thamdrup, 1994) but it also produces characteristic ^{33}S – ^{32}S fractionations that enable it to be distinguished from MSC's reductive branch (Johnston et al., 2005; Pellerin et al., 2015a, Wu et al., 2010). Coupled oxygen and sulfur isotope measurements from post-Marinoan barite, therefore, are a potentially powerful tool to resolve not only atmospheric compositions, but also the dominant metabolic contributions and critical fluxes into and out of the marine reservoir during this unique time in Earth history.

Although considerable attention has been given to the dynamics of the sulfur cycle across the Cryogenian-Ediacaran transition, many outstanding questions remain. For example, the initial size of the marine sulfate reservoir at the end of the Marinoan glacial episode, and the rapidity of its growth to typical Phanerozoic levels is still unknown. Sulfur isotope fractionations between sulfate and sulfide in different post-Marinoan sedimentary packages have been used to argue for an initial sulfate reservoir of late Archean proportions that grew to Phanerozoic levels over ≈30 million years (Halverson & Hurtgen, 2007). Alternatively, large depletions in ^{34}S in sulfides from black shales have been interpreted to reflect a more immediate oxidative response, with the growth of a sizable sulfate reservoir occurring at a rate that was more than an order of magnitude more rapid (Sahoo et al., 2012). The microbial dynamics of the sulfur cycle over this interval are also uncertain, with the suggestion of a broad interval of enhanced re-oxidative sulfur cycling preceding the Marinoan glacial interval, (Canfield and Teske, 1996) as well as a vigorous oxidative component of MSC drawing down marine sulfate levels in the earliest Ediacaran (Peng et al., 2011). Given the complicated relationship between atmospheric oxygen, marine sulfate levels, and the intensity of microbial sulfur re-oxidation, these conflicting results make it difficult to reconstruct the nature of the ocean – atmosphere system in the aftermath of the Marinoan glaciation.

In this study we provide new data and interpretation of the post-Marinoan sulfur cycle through the isotopic record within barite fans from the Mackenzie Mountains in northwest Canada (Fig. 2.1). This dataset includes the first paired triple oxygen and multiple sulfur isotope measurements from a Marinoan-aged barite. These data are interpreted within a time-dependent model of post-glacial sulfate cycling to explain observed isotopic trends and the environmental conditions accompanying barite deposition. By extending the record of the ^{17}O anomaly in barite to another paleo-continent, we link these isotopic shifts to the global operation of the post-Marinoan sulfur cycle. Through this approach we make new estimates for the size of the post-Marinoan sulfate reservoir and the impact of re-oxidative sulfur cycling. These results provide model-dependent estimates for the time interval captured by both barite units and underlying cap carbonates.

2.2 Materials and Methods:

Sample Description

Two predominant morphologies of macroscopic barite occur in Marinoan cap dolostones worldwide. The first type is diagenetic, forming void filling crustose cements (Shields et al., 2007) and tepee-like breccias interpreted as subaqueous (Jiang et al., 2006) or vadose (Zhou et al., 2010) in origin. The second type – seafloor barite fans – are primary and abiogenic. These barite fans grew directly into the water column, and they are preserved within an iron and manganese-rich dolomicrite matrix. Seafloor barite structures are found above or within cap dolostone units commonly below buildups of aragonite fans (Hoffman et al., 2011).

Seafloor barite is the primary barite morphology observed in the Ravensthroat Formation cap dolostone in the southern and central portions of the Mackenzie Mountains in the northern Canadian Cordillera (Hoffman et al., 2011; Macdonald et al., 2013) (Fig. 2.1). The geological and chemostratigraphic succession in the Mackenzie Mountains is similar to other cap carbonate successions elsewhere, representing a transgressive sequence with large negative shifts in carbon isotope ratios occurring at the top of the cap dolostone unit (Hoffman & Halverson, 2011).

Barite layers in the Ravensthroat Formation immediately overlying the cap dolostone, are typically 4–10 cm thick, and consist of bladed crystals and upward-fanning rosettes (Fig. 2.1c). The upward-oriented growth habit, sediment drape that thins over crystal terminations, and presence of crystal fragments as detrital material within the sediment matrix indicate the barite was deposited at the sediment-water interface. Importantly, there are three distinct generations of barite that were sequentially deposited at the top of the Ravensthroat Formation (Fig. 2.1). The first generation structures (Type B1) are 1–2 cm in height and consist of fine fans of barite blades originating from common nucleation centers and draped with laminated peloidal Fe-rich dolomite sediment (Arnaud et al., 2011) (Fig. 2.1c). The B1 structures are covered by larger (2–3 cm) internally laminated fans and rosettes (Type B2) interspersed within the dolomite matrix. The uppermost barite structures (Type B3) are even larger (3–4 cm) and consist of fans that have coalesced into digitate groups with more widely spaced internal laminations. These latest formed barites are inclusion rich, and have thin rinds of inclusion-free barite separated by Fe-rich sediment infill (Fig. 2.1c). The preservation of these delicate textures, together with systematic isotopic trends identified here, suggest that barites from northwest Canada have not been affected by any post-depositional geochemical modification. The occurrence of equivalent units on four other paleo-continents (Kennedy, 1996; Bao et al., 2008; Hoffman et al., 2011) suggests global similarity of depositional processes and timing among the Marinoan seafloor barite units.

Oxygen Isotope Measurements

Triple oxygen isotope measurements followed the methods detailed by Bao et al. (2008). Barite powders were dissolved and re-precipitated as pure barite via a modified DTPA (diethylenetriaminepentaacetic acid) procedure to remove any potential contamination from non-sulfate bearing minerals (Bao, 2006). This involved first dissolving the samples in a 0.05 M DTPA, 0.1 M NaOH solution over 12 hours in a sample shaker. Samples were subsequently acidified with 6 M HCl in a water bath at 80 ˚C to drive off any CO_2, thereby preventing the formation of witherite during the reprecipitation of barite (Bao & Thiemens, 2000). Pyrite oxidation was not a large concern in contamination of samples since pyrite abundance was determined through high-resolution micrographs, and determined to be a maximum concentration of 0.5% within the micrite phase. Samples were then loaded onto a stainless steel stage and placed under a BrF_5 atmosphere for 12 hours to react with any trace water in the samples. Oxygen gas was generated with a CO_2 -laser fluorination system on approximately 10 mg of sample powder. Typical yields of $O_{2(g)}$ were between 25–35% on the barite sample powder, resulting in approximately 25 μmol of $O_{2(g)}$ for analysis. Triple oxygen isotope compositions of O_2 derived from barite were measured on a Thermo MAT 253 in dual-inlet mode in the OASIC laboratory at Louisiana State University, and are expressed as:

$$\Delta^{17}O = \delta'^{17}O - (0.52 \times \delta'^{18}O) \quad (1)$$

where, $\delta'^{i}O = \ln({}^{i}R_{sample}/{}^{i}R_{SMOW}) \times 1000$, ${}^{i}R = {}^{i}O/{}^{16}O$ and i is 17 and 18.

Results are presented on the SMOW scale (cf. Bao et al., 2008). Repeat measurements on pure $BaSO_4$ laboratory standards yielded a 1σ analytical uncertainty for $\Delta^{17}O$ measurements of less than 0.05‰.

Microdrilled barite powders were also analyzed for their $\delta^{18}O$ values via a TC/EA coupled to a Thermo Delta V configured in continuous flow mode at Harvard University. Each sample was run in duplicate, with an established standard deviation of 0.3‰ (1σ) for replicate analyses of in-house standards. The composition of unknowns was calibrated against international standards (IAEA SO5, IAEA SO6, and NBS-127) that were interspersed through each run (See Johnston et al., 2014 for additional detail). Values are expressed as:

$$\delta^{18}O = ({}^{18}R_{sample} - {}^{18}R_{standard})/{}^{18}R_{standard} \times 1000 \quad (2)$$

where ${}^{18}R = {}^{18}O/{}^{16}O$.

Sulfur Isotope Measurements

Multiple sulfur isotope measurements ($\delta^{34}S$, $\Delta^{33}S$, $\Delta^{36}S$ values) were performed by reacting powdered barite samples first in a boiling Cr-reducing solution (Canfield et al., 1986), which liberated minor H_2S from trace sulfides in the barite. Modal analysis showed that these sulfides always formed less than 0.3 mole % of the sulfur in a given sample. The resulting powders were then rinsed repeatedly with Milli-Q H_2O and dried over night. To measure the isotopic composition of the sulfates approximately 10 mg of the dried powder was then reacted with 15 mL of Thode reduction solution at 100 ˚C (Thode et al., 1961), which converts sulfate to H_2S. Hydrogen sulfide gas was carried through a N_2 gas stream and was bubbled through a Zn acetate solution where it was converted to ZnS. Samples were then precipitated as Ag_2S after reaction with 0.2 M $AgNO_3$. Dried Ag_2S samples were reacted with $F_{2(g)}$ in nickel bombs at 250 °C, to generate pure $SF_{6(g)}$. The isotopic composition of $SF_{6(g)}$ was first purified via gas chromatography and analyzed on a Thermo MAT-253 in dual inlet mode in the Stable Isotope Laboratory at McGill University. Results were normalized to repeated measurements of international reference material IAEA-S-1, with a defined $d^{34}S$ value of -0.3‰ on the Vienna Canyon Diablo Troilite (V-CDT) scale. We took the $\delta^{33}S$ value of IAEA-S-1 to be -0.061‰ V-CDT. Sulfur isotope compositions are expressed as:

$$\delta^{i}S = ([{}^{i}R_{sample}/{}^{i}R_{V\text{-}CDT}]-1) \times 1000 \qquad (3)$$

where ${}^{i}R = {}^{i}S/{}^{32}S$ and i is 33, 34, or 36, and

$$\Delta^{i}S = \delta^{i}S - 1000\times([1+(\delta^{34}S/1000)]^{i\lambda} - 1) \qquad (4)$$

where i is 33 or 36. We calculated $\Delta^{33}S$ and $\Delta^{36}S$ values through reference mass dependent exponents, of ${}^{33}\lambda = 0.515$, and ${}^{36}\lambda = 1.9$, representative of equilibrium sulfur isotope exchange at high temperatures. Uncertainty (1σ) on the entire analytical procedure is estimated to be better than 0.1‰ for $\delta^{34}S$, 0.01‰ for $\Delta^{33}S$ and 0.2‰ for $\Delta^{36}S$.

2.3 Results

The sequential nature of three barite textures allows geochemical signatures to be placed in relative chronological order. Values of $\Delta^{17}O$, $\delta^{18}O$, $\delta^{34}S$, and $\Delta^{33}S$ all show clear trends with the progression from the earliest formed barite (B1) to the latest (B3) (Fig. 2.2). Type B1 captures the largest negative $\Delta^{17}O$ values and lightest $\delta^{18}O$ values with a mean value of -0.66‰ and 17.95‰ respectively. In the later formed type B3 barite, the $\Delta^{17}O$ signal is diminished and $\delta^{18}O$ values progressively heavier, reaching -0.12‰ and 19.51‰ respectively (Fig. 2.2a; Table 2.1). Similar isotopic trends were observed in sulfur data that showed a mean $\delta^{34}S$ value of 29.5‰, and a $\Delta^{33}S$ value of ≈ -0.04‰. The $\delta^{34}S$ and $\Delta^{33}S$ values increase reaching averages of 45‰ and 0.08‰ respectively for type B3 (Fig. 2.2b; Table 2.1). These observations suggest that the seafloor barite horizon was sourced from a sulfate pool with an evolving isotopic composition. In the analysis that follows, we take the near linear positive covariation of $\Delta^{17}O$ and $\delta^{34}S$ as the primary geochemical signal to be modeled, and reserve the positive covariation of $\Delta^{33}S$ with $\delta^{34}S$ as an independent test of the model predictions.

2.4 Discussion

Existing Interpretations of the Isotopic Evolution of post-Marinoan Seafloor Barite

There are three published models for the sulfur and/or oxygen isotope evolution of post-Marinoan barites. One conceptual model for barite deposition called on the upwelling of anoxic barium- and sulfide-rich but sulfate-poor deep waters into an oxygenated surface ocean (Hurtgen et al., 2006). Upon mixing of these two water masses, aqueous sulfide would have been oxidized, providing a ^{34}S-depleted source of sulfate and driving barite supersaturation (Hurtgen et al., 2006). This type of sulfide oxidation would deposit sulfate with the Δ^{17}O of ocean water (Δ^{17}O ≈ 0‰ VSMOW), leading either to negative covariation between δ^{34}S and Δ^{17}O or a wide range of δ^{34}S at a Δ^{17}O ≈ 0‰ (cf. carbonate-associated sulfate from W2 dolomites of Bao et al., 2009). However, we observe a positive correlation between δ^{34}S and Δ^{17}O and significantly non-zero Δ^{17}O, suggesting that an alternative process is required for the barites reported here (Table 2.1) and elsewhere (Bao et al., 2008; Peng et al., 2011).

A second conceptual model associates the formation of Marinoan-age void-filling barite cements and crusts with the deposition of barite in methane-rich cold seeps on the modern day seafloor (Shields et al. 2007). Modern cold-seep barite is spatially localized with a wide range of δ^{34}S values that do not follow a coherent stratigraphic order (Torres et al., 2003). In contrast, the Ravensthroat barite layer has a broad spatial distribution, and exhibits a monotonic stratigraphic variation of δ^{34}S values (Table 2.1; Fig. 2.2). Although modern cold seeps appear to encompass a similar range in δ^{34}S values, δ^{18}O values from the Ravensthroat barite plot in a much more limited range (Table 2.1). Therefore this places the Ravensthroat barites on a very different δ^{18}O – δ^{34}S trend than these previously suggested modern analogues (Shields et al., 2007; Antler et al., 2015).

These observations suggest that an actualistic interpretation based on modern cold seep barites is not appropriate for the barites studied here.

Finally, a third coupled $\Delta^{17}O$ and $\delta^{34}S$ record in Marinoan barite from South China has been quantitatively reproduced in a model of the sulfur cycle after a Snowball Earth (Peng et al., 2011). This model starts with a standing pool of isotopically anomalous sulfate in the post-glacial ocean. It requires intense microbial sulfate reduction (MSR) to drive sulfate $\delta^{34}S$ to more positive values, and nearly equally intense re-oxidation of the sulfide to reset sulfate $\Delta^{17}O$ toward a value of 0‰ (Peng et al., 2011). Importantly the model can only generate a positive covariation between $\delta^{34}S$ and $\Delta^{17}O$ if no sulfate is supplied to the ocean through oxidative weathering of continental rocks or sediments. Consumption of a "closed" sulfate reservoir by net sulfate reduction leads to continually increasing $\delta^{34}S$ values through a continual decline of the total amount of sulfate in the post-Marinoan ocean in this model (Peng et al., 2011). This characteristic contrasts with evidence for growth of the marine sulfate reservoir during the Ediacaran period (Halverson & Hurtgen, 2007; Sahoo et al., 2012). In addition, the model's suggestion of an apparent oxidative inversion, where modern levels of sulfide re-oxidation in the ocean are sustained in the face of limited oxidative weathering of continental sulfide minerals, runs counter to evidence for the immediate resumption of oxygenic primary productivity in the post-glacial photic zone (Kunzmann et al., 2013) in a post-Marinoan ocean that was anoxic overall (Johnston et al., 2013). It is further difficult to envision how the oxidizing capacity in the ocean is kept separate from the troposphere. These challenges led us to develop a new quantitative interpretation of the unique isotopic trends preserved in post-Marinoan seafloor barites.

Isotopic Evolution of the post-Marinoan Sulfur Cycle

The variability in $\delta^{34}S$ observed within global cap carbonate sequences requires either a diminished global sulfate reservoir, or local processes that act simultaneously on nearly every paleo-continent producing isotopic trends of the same magnitude and direction (Hurtgen et al., 2006). The oxygen and sulfur isotopic signatures preserved within the Ravensthroat barite are similar to those in post-Marinoan barite preserved on other paleo-continents as well as isotopic signatures preserved within cap carbonates in Australia (Shields et al., 2007; Bao et al., 2008; Peng et al., 2011; Bao et al., 2012). As a result, this consistency points toward a common solution, and one that operates on a global-scale.

We assert that the basic processes of the marine sulfur cycle (MSR, pyrite burial, and sulfate input from continental weathering) are able to reproduce the collective isotopic observations when operating under realistic conditions for the post-Marinoan oceans. First, the anomalous oxygen isotope composition in the barites resulted from the specific atmospheric and biospheric state that evolved during the Marinoan glaciation (Bao et al., 2008), and was carried to the ocean via the oxidative weathering of continental sulfides (Bao et al., 2009). Enhanced oxidative weathering was likely behind the inferred increase in the size of the marine sulfate reservoir as the Ediacaran period progressed, requiring the flux of sulfate from the continents outpace sulfate removal through pyrite burial (Halverson and Hurtgen, 2007; Sahoo et al., 2012). In order to test this scenario, we constructed a dynamic 1-box model of the marine sulfur cycle (cf. Halverson and Hurtgen, 2007). The model is described in Equations 5−7, where all calculations were performed using delta notation, and key model inputs and outputs are conceptually summarized in figure 2.3 and detailed in table 2.2.

$$dM_S / dt = F_W - F_W \times f_{py} \quad (5)$$

$$d(Ms \times \delta^{34}S_S)/dt = F_w \times \delta^{34}S_W - f_{py} \times F_W \times (\delta^{34}S_S + {}^{34}\varepsilon) \quad (6)$$

$$d(Ms \times \Delta^{17}O_S)/dt = F_w \times \Delta^{17}O_W - f_{py} \times F_W \times (\Delta^{17}O_S) \quad (7)$$

The initial isotopic composition of the marine sulfate reservoir is set at $\Delta^{17}O_{S0}$ = -0.1‰ (Bao et al., 2012) and $\delta^{34}S_{S0}$ = +15‰ (Halverson and Hurtgen, 2007). The model has two free parameters: (1) the fraction (f_{py}) of the flux of sulfate coming into the system by weathering (F_w) that leaves the system via pyrite burial ($F_{pyrite\ burial}$) where $f_{py} = F_{pyrite\ burial}/F_w$; and (2) the fractionation associated with MSR that is imparted to the pyrite leaving the system [$^{34}\varepsilon = (^{34}\alpha - 1) \times 1000 \approx \delta^{34}S_{py} - \delta^{34}S_s$, where $^{34}\alpha = ([^{34}S/^{32}S]_{py}/[^{34}S/^{32}S]_S)$]. Re-oxidation of sulfide to sulfate is not considered directly in this model (Figs. 2.3a and 2.3b), although the potential sulfur isotope consequences of re-oxidation are explored later.

We forced the model with an initial pulse of ^{17}O-depleted sulfate with $\Delta^{17}O_W$ = -4.2‰, and $\delta^{34}S_W$ = +5‰, which represents one plausible observationally constrained estimate of the isotopic composition of weathering-derived sulfate following the Marinoan glaciation (Bao et al., 2009; Halverson and Hurtgen, 2007; Figs. 2.3c and 2.3d). The assumption of a constant isotopic composition for weathering-derived sulfate is a simplification, and the isotopic composition of atmospheric O_2 is likely to be globally homogeneous at the timescales considered here. However strict transfer of this isotopic homogeneity to sulfate derived from oxidation of terrestrial sulfides is unlikely. The minimum $\Delta^{17}O$ value observed in the barite dataset ($\Delta^{17}O_{min}$ = -1.0‰) is interpreted to reflect the minimum $\Delta^{17}O$ value reached by the marine sulfate reservoir, and constrains the duration of the initial pulse of ^{17}O-depleted sulfate carried by continental run-off as a result (Fig. 2.3c). This timing also constrains the period over which the specific pO_2 and pCO_2 necessary to generate the prescribed $\Delta^{17}O$ were present. We assume that the $\Delta^{17}O$ values carried by F_w decreased the $\Delta^{17}O$ of marine sulfate from -0.1‰ to a minimum value of -1‰, and upon reaching this value barite deposition initiated. This assumption enables a timing estimate of the duration of the initial ^{17}O depleted pulse from continental run-off, and also provides a maximum duration for the deposition of the underlying cap dolostone. The shift from isotopically anomalous riverine $\Delta^{17}O$ values to isotopically normal values characterized by $\Delta^{17}O_W$ = -0.1‰ is taken as a step function in the model (Fig. 2.3c). Although the transition from a high pCO_2 syn-glacial atmosphere with limited primary production to a more characteristic Ediacaran environment with lower pCO_2 values and renewed primary production is unlikely to be instantaneous, it appears to be rapid (Sansjofre et al., 2011; Bao et al., 2012; Killingsworth et al., 2013; Kunzmann et al., 2013).

The forcing used here captures the first-order isotopic consequences of this transition without adding unconstrained temporal complexity. The progression of marine sulfate isotope compositions toward steady-state values of $\Delta^{17}O_S$ = -0.1‰ tracks dilution with isotopically normal riverine sulfate (Fig. 2.3c), while the $\delta^{34}S$ value approaching 45‰ reflects fractionation associated with sulfate removal through MSR, modified by the relative fraction of pyrite burial compared to weathering (Fig. 2.3d). These isotopic endpoints are fixed by our measurements from northwest Canada (Table 2.1), which are corroborated by previous studies in South China and Mauritania (Bao et al., 2008; Peng et al., 2011; Killingsworth et al., 2013). The evolution of the model is set by the passage of sulfate turnover times (t = M_{S0}/F_W; the ratio of the initial mass of marine sulfate to the influx of sulfate from continental weathering).

In figure 2.4 we present a sensitivity analysis of the model to changing parameters ($^{34}\varepsilon$, f_{py}). The reference model used $^{34}\varepsilon$ = -42‰ and f_{py} = 0.95 to reproduce the $\Delta^{17}O$ and $\delta^{34}S$ evolution of the B1–B3 barite layers (Fig. 2.4). Although the reference $^{34}\varepsilon$ value is near the upper limit of measured $\delta^{34}S$ differences between pyrite and carbonate associated sulfate in Marinoan cap dolostones (Hurtgen et al., 2005, 2006), it is within the range of theoretical predictions (Wing and Halevy, 2014) and experimental determinations (Sim et al., 2011, Leavitt et al 2013, Bradley et al., 2015) of MSC at low sulfate concentrations. The reference model generated a close isotopic match in model time for each of the barite horizons, thus we consider it a plausible set of conditions to explain coherent stratigraphic variations observed here. We tested each model run for fidelity with the rock record by verifying that the model output $\Delta^{17}O$ values corresponding with measured B1 (-0.66), B2 (-0.39), and B3 (-0.12) were produced within the same model time period as the equivalent measured $\delta^{34}S$ values for B1 (29.1 ± 4.3), B2 (39.5 ± 4.4) and B3 (44.4 ± 2.5). Dotted circles in figure 2.4 indicate compatibility among model and data. Three model cases (Figs. 2.4a, 2.4e, and 2.4i) were found to be compatible with all measured data requiring a value for f_{py} near 1, and a value for $^{34}\varepsilon$ near -40‰. Independently increasing the reference model $^{34}\varepsilon$ to -37‰ or lowering $^{34}\varepsilon$ to -47‰ without changing f_{py} resulted in a poor model fit (Figs. 2.4d and 2.4f). A decreasing sulfate reservoir size with time was investigated by increasing f_{py} to 1.05, thereby requiring consumption of the standing pool of sulfate. Increasing f_{py} above 1 did not result in compatible solutions with $^{34}\varepsilon$ set at -42‰ or -47‰ (Figs. 2.4b and 2.4c), but was compatible with $^{34}\varepsilon$ = -37‰. Decreasing f_{py} to 0.85 resulted in a model fit with less compatibility as $^{34}\varepsilon$ values increased (Figs. 2.4g and 2.4h). Thus, there is a narrow range of parameters that can be used in this model to reproduce the isotopic measurements in the Ravensthroat formation, resulting in a narrow set of non-unique solutions that are consistent with current understanding of MSC. Our model suggests that f_{py} needs to be close to, but not greater than one and $^{34}\varepsilon$ values are approximately -40‰, which is typical for $^{34}\varepsilon$ values in marine sediments (Leavitt et al., 2013).

These results highlight three important features of the post-Marinoan marine sulfur cycle. First, the marine sulfate reservoir was predisposed to isotopic modification in the immediate aftermath of the Marinoan glaciation. Second, these isotopic changes occurred over approximately four to five turnover times for sulfate (τ = 4-5). Third, since the deposition of the cap dolostones occurred prior to the barite layers, the duration of the initial ^{17}O depleted weathering pulse suggests that the cap dolostones were deposited in less than one turnover time of the marine sulfate reservoir (τ = 0.3).

$\Delta^{33}S$ – $\delta^{34}S$ patterns in Post-Marinoan Seafloor Barite

In contrast to previous models of the post-Marinoan sulfur cycle (Peng et al., 2011), the reference presented here explains the data set without contributions from sulfide re-oxidation. Measured multiple sulfur isotope values provide an independent test of this prediction (Fig. 2.2b). Sulfur-based microbial metabolisms can lead to small $\delta^{33}S$ – $\delta^{34}S$

deviations from the reference mass law defined by $^{33}\lambda = 0.515$ through their impact on sulfur isotope fractionation factors. The exponential relationship between fractionation factors of different isotope pairs is typically expressed through λ values, where, for example, $^{33}\alpha = {^{34}\alpha}^{33\lambda}$. Through an equation like (7) for $\delta^{33}S$, we incorporated fractionation of ^{33}S-^{32}S associated with MSC and pyrite burial in the reference model ($^{34}\varepsilon = -42‰$; $f_{py} = 0.95$), and predicted the $\Delta^{33}S - \delta^{34}S$ patterns that result from different values of $^{33}\lambda$. Starting from an initial of $\delta^{34}S_{S0} = +15‰$ and $\Delta^{33}S_{S0} = -0.05$ (Scott et al., 2014), the $\Delta^{33}S - \delta^{34}S$ trajectory from the Ravensthroat barite is inconsistent with $^{33}\lambda$ values associated with re-oxidative sulfur cycling via microbial disproportionation of elemental sulfur or sulfite (Fig. 2.2b; $^{33}\lambda = 0.515 - 0.520$; Johnston et al., 2005; Pellerin et al., 2015a), but falls along the lower limit of predictions based on laboratory and theoretical studies of $^{33}\lambda$ values generated by MSR only (Fig. 2.2b; $^{33}\lambda = 0.505 - 0.515$) (Farquhar et al., 2003; Johnston et al., 2005; Wu et al., 2010; Leavitt et al., 2013; Wing and Halevy, 2014; Pellerin et al., 2015b).

Our inference that the $\Delta^{33}S - \delta^{34}S$ patterns reflect primarily MSR is reinforced by the $\delta^{18}O$ values of the Ravensthroat barite. Although they were not modeled due to a lack of constraints on the $\delta^{18}O$ of the post-glacial hydrosphere, similar $\delta^{18}O$ values, along with elevated $\delta^{34}S$ values, are characteristic of sulfate undergoing active MSR in modern environments (Antler et al. 2013; 2015). In general, the additional isotopic evidence presented here is further support for a post-Marinoan global marine sulfate reservoir that is driven by post-glacial resumption of continental weathering, MSR, and pyrite burial.

Sulfate Source to Post-Marinoan Seafloor Barite

In figure 2.5, we plot the results of the reference model of marine sulfate evolution in $\delta^{34}S$ and $\Delta^{17}O$ space, overlain by the Ravensthroat barite data. The ability of the model to reproduce the measured patterns implies that the sulfate source to the seafloor barite in northwest Canada could be a global seawater reservoir. As a consequence, the modeled seawater sulfate values could plausibly be compositional end-members during barite deposition on other paleo-continents.

Previously published $\delta^{34}S$ and $\Delta^{17}O$ values from well preserved barites with little to no diagenetic overprinting from South China (Fig. 2.5; Peng et al., 2011) scatter away from modeled oceanic values and toward higher $\Delta^{17}O$ and lower $\delta^{34}S$, thus requiring a second source of sulfate. One possible explanation is that the South China succession may represent a system with a stronger riverine influence than that of northwest Canada. This is evidenced through barite deposition occurring over a larger stratigraphic interval in South China in shallower carbonate facies that would plausibly have faster accumulation rates than the northwest Canada samples (Peng et al., 2011). We suggest that isotopically normal riverine sulfate (with a $\Delta^{17}O$ value of −0.1‰ after the initial pulse of ^{17}O depleted sulfate) is mixed with an open ocean sulfate pool (with an evolving $\Delta^{17}O$) during the time of barite deposition in South China, creating a spectrum of compositions between these end-members (Fig. 2.5). This mixing relationship suggests that the South China barite layers record up to 50% dilution of marine sulfate via sulfate supplied by rivers. Together with our model solution, this interpretation of the South China dataset provides a globally consistent framework for the isotopic evolution of these and other post-Marinoan barite deposits.

Calibrating the size of the post-Marinoan sulfate reservoir

The reference model constrains the residence time of marine sulfate during the immediate aftermath of the Marinoan glaciation, if the timeframes of cap dolostone and barite accumulation can be estimated. There is only a single estimate of the time interval represented by post-Marinoan seafloor barite horizons: $2.1 \pm 7.8 \times 10^5$ yrs estimated by correlating $\delta^{13}C$ patterns from the Marinoan sections in South China (Killingsworth et al., 2013). In contrast, there is a wide range of estimates for the time interval represented by the cap dolostones, from $\approx 10^3$ yrs (oceanographic models; Hyde et al., 2000), $\approx 10^4$ yrs (modeling of sea level changes; Creveling and Mitrovica, 2014), $\approx 10^5$ yrs (paleomagnetic reversal frequencies; Trindade et al., 2003), to $\approx 10^6$ yrs (Ca and Mg isotope modeling; Kasemann et al., 2014). If the duration of barite accumulation was 2×10^5 yrs (Killingsworth et al., 2013), then the modeling presented here suggests that $\Delta^{17}O$ ingrowth into the marine sulfate reservoir and, by inference, the deposition of the cap dolostone occurred on the order of $\approx 10^4$ years. This timescale is consistent with a recent estimate of the lifetime of a post-glacial meltwater plume in the post-Marinoan ocean (Liu et al., 2014). Under this timescale, the reference model suggests that the residence time of sulfate in the post-Marinoan ocean was $\approx 4–5 \times 10^4$ yrs (Fig. 2.4).

We suggest a modern weathering flux is a plausible estimate of post-glacial sulfate supply to the marine reservoir. Given the absence of mass-independent sulfur isotope fractionation in the barites, it is unlikely pO_2 levels dropped to sufficiently low values during the glaciation to hinder pyrite oxidation (Reinhard et al., 2013), while a vigorous post-glacial hydrologic cycle (Kasemann et al., 2014) would likely outpace modern riverine input. With a modern flux of sulfate from continental weathering, a residence time of ≈ 10^4 yrs implies a small marine sulfate reservoir at the end of the Marinoan glacial interval (Fig. 2.6; ≈ 0.1% of modern marine sulfate). For a barite accumulation interval of 10^6 yrs (the maximum allowed by chronologic uncertainties; Killingsworth et al., 2013) and a larger sulfate supply from enhanced post-Marinoan continental weathering (10 × modern; Kasemann et al., 2014), an upper limit to the post-Marinoan sulfate pool approaching 10% modern is implied (Fig. 2.6). These values bracket published estimates of marine sulfate concentrations at the start of the Ediacaran period (1% of modern; Halverson and Hurtgen, 2007). Low but increasing sulfate concentrations appear to have been maintained throughout the deposition of the seafloor barite, as the coupled oxygen and sulfur isotope variations require that much, but not all, of the sulfate coming into the post-Marinoan ocean was reduced to sulfide and sequestered as pyrite.

2.5 Conclusions

In this study we have extended the previously reported $\Delta^{17}O$ anomalies in post-Marinoan marine barite precipitates to a new paleo-continent, highlighting the global nature of this geochemical horizon. By pairing these results with coeval multiple sulfur isotope analyses we provide new insights into the post-Marinoan sulfur cycle and climate. First we demonstrate the dynamic nature of the sulfur cycle, where the $\Delta^{17}O$ anomaly can be imparted and subsequently eliminated in four to five turnovers of the marine sulfate reservoir. Second, our results suggest that this can be achieved through oxidative weathering coupled to microbial sulfate reduction and pyrite burial, without much contribution from re-oxidative fluxes. Further, and a target for subsequent work, is the implication that the post-Marinoan atmosphere (here involving CO_2, O_2 and gross primary production) was evolving in a fashion whereby the magnitude of the tropospheric $\Delta^{17}O$ anomaly in O_2 crashed as the ocean-atmosphere recovered following the glaciation. Third, we show that the initial post-Marinoan sulfate reservoir was smaller than at other times in the Ediacaran, possibly 0.1% of the modern with and upper limit of 10% modern. Finally our results appear to be most consistent with recent timing estimates of cap carbonate deposition on the order of ~10^4 yrs, reminiscent of timescales that have come to characterize typical glacial-interglacial cycles. Together these findings highlight that the post-Marinoan sulfur cycle was not different from the modern with respect to important processes, however, it was likely unfamiliar with respect to magnitudes of sources and sinks.

Acknowledgements

We give special thanks to Dr. Huiming Bao for enlightening discussions about triple oxygen isotopes and for access to the OASIC laboratory at Louisiana State University. We would also like to thank two anonymous reviewers and Pierre Cartigny for constructive reviews and AE Gideon Henderson for editorial guidance that greatly improved this manuscript. The National Science and Engineering Research Council of Canada supported this work through a Canadian Astrobiology Training Program PhD Fellowship to PWC and NSERC CREATE and Discovery Grants RGPIN-2014-06626 to BAW. Fieldwork was supported by NSF grant EAR-0417422 (PFH). The Stable Isotope Laboratory at McGill is supported by the FQRNT through the GEOTOP research center. Cowie and Johnston were funded through the MIT-Harvard node of the NASA NAI as well as a NSF CAREER award to DTJ.

Tables

Table 2.1: $\Delta^{17}O$ (1σ analytical uncertainty = 0.05‰), $\delta^{34}S$ (1σ analytical uncertainty < 0.1‰), $\Delta^{33}S$ (1σ analytical uncertainty < 0.01‰), and $\Delta^{36}S$ (1σ analytical uncertainty < 0.2‰) stable isotope ratios for Type B1, B2 and B3 barite textures from NW Canada. Analyses of barites for $\delta^{18}O$ represent micro-drilled sub samples of individual barite layers (NM = not measured).

Sample	$\Delta^{17}O$	$\delta^{18}O$	$\delta^{34}S$	$\Delta^{33}S$	$\Delta^{36}S$	Texture
2-1	-0.75	18.77	26.66	-0.023	-0.62	B1
2-2	-0.66	17.12	29.89	-0.036	-0.67	B1
2-4	-0.56	NM	30.82	-0.037	-0.75	B1
4-1	-0.36	18.33	40.70	0.009	-0.51	B2
4-2	-0.36	18.98	41.98	0.026	-0.64	B2
4-3	-0.37	NM	37.99	0.002	-0.99	B2
4-4	-0.47	NM	37.45	-0.019	-0.09	B2
3-1	-0.20	19.51	45.53	0.073	-0.16	B3
3-2	-0.08	19.78	43.04	0.086	-0.29	B3
3-3	-0.08	19.25	44.54	0.083	0.32	B3

Table 2.2: Summary of reference model input parameters with end-member possibilities considered in model sensitivity tests.

Parameter	Description	Reference Model Value	Sensitivity Tests
M_{So}	Initial marine sulfate concentration	$3 \cdot 10^{16}$ mol	-
F_W	Weathering flux of sulfate	$3 \cdot 10^{12}$ mol·yr^{-1}	≈$3 \cdot 10^{11}$ – $3 \cdot 10^{13}$ mol·yr^{-1}
$\Delta^{17}O_{W0}$	$\Delta^{17}O$ value of initial sulfate weathering flux	-4.2‰	-
$\Delta^{17}O_{S0}$	$\Delta^{17}O$ value of initial marine sulfate reservoir	-0.1‰	-
$\Delta^{17}O_{min}$	Minimum $\Delta^{17}O$ value reached by marine sulfate	-1.0‰	-
$\Delta^{17}O_{WS}$	$\Delta^{17}O$ value of sulfate of sulfate weathering flux once $\Delta^{17}O_{min}$ (-1.0‰) is achieved	-0.1‰	-
$\Delta^{17}O_S$	Calculated $\Delta^{17}O$ of marine sulfate	-	-
$\delta^{34}S_W$	$\delta^{34}S$ value of sulfate weathering flux	+5.0‰	-
$\delta^{34}S_{S0}$	$\delta^{34}S$ value of initial sulfate reservoir	+15.0‰	-
$\delta^{34}S_{py}$	$\delta^{34}S$ of pyrite produced from MSC	-	-
$\delta^{34}S_S$	Calculated $\delta^{34}S$ of marine sulfate	-	-
$^{34}\varepsilon$	≈ the difference in $\delta^{34}S$ values of sulfate and sulfide	-42‰	-37‰ – -47‰
f_{py}	Fraction of sulfate leaving the system via pyrite burial	0.95	0.85 – 1.05
τ	Marine sulfate residence time	10^4 yrs	>10^3, <10^6 yrs

Figures

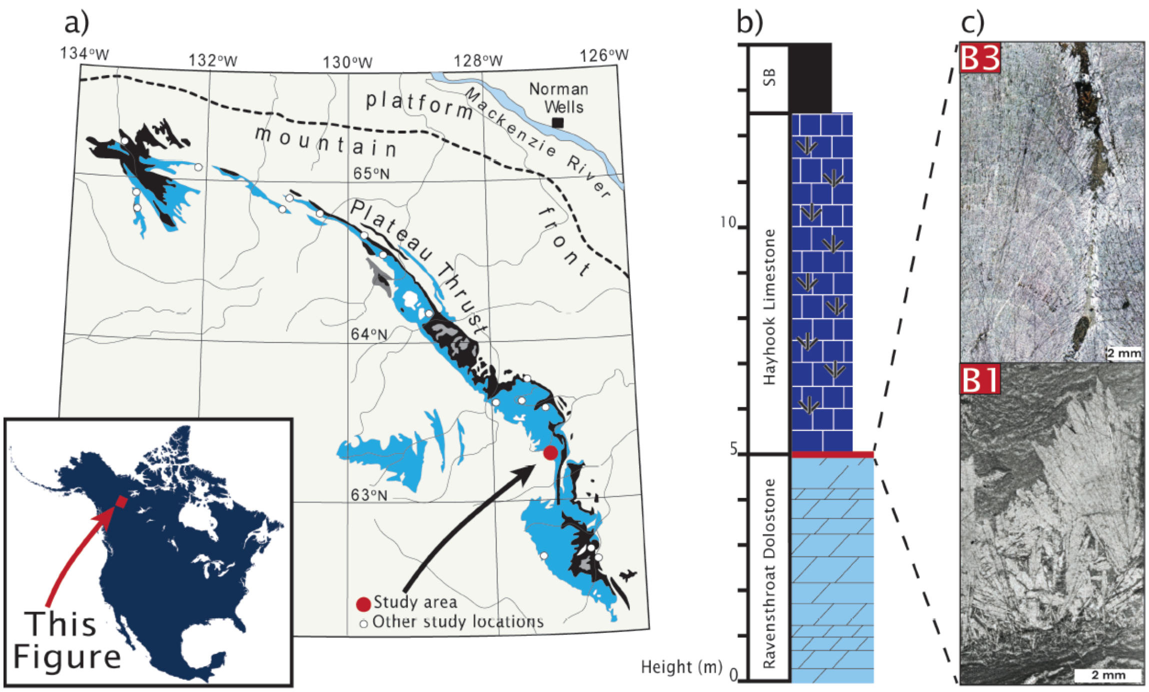

Figure 2.1: (A) Exposed Neoproterozoic stratigraphy in the Mackenzie Mountains in northwest Canada where barites from this study were sampled. (B) Stratigraphic log outlining barite occurrence at the top of the Ravensthroat cap dolostone, underlying the Hayhook Limestone (C) Digital photomicrographs of barite fans taken in unpolarized light in ~3mm-thick polished thin sections, where examples of the change in textures observed in the barite unit are observed with basal bladed crystal fans in the B1 horizon and digitate groups with widely spaced laminations in the B3 horizon.

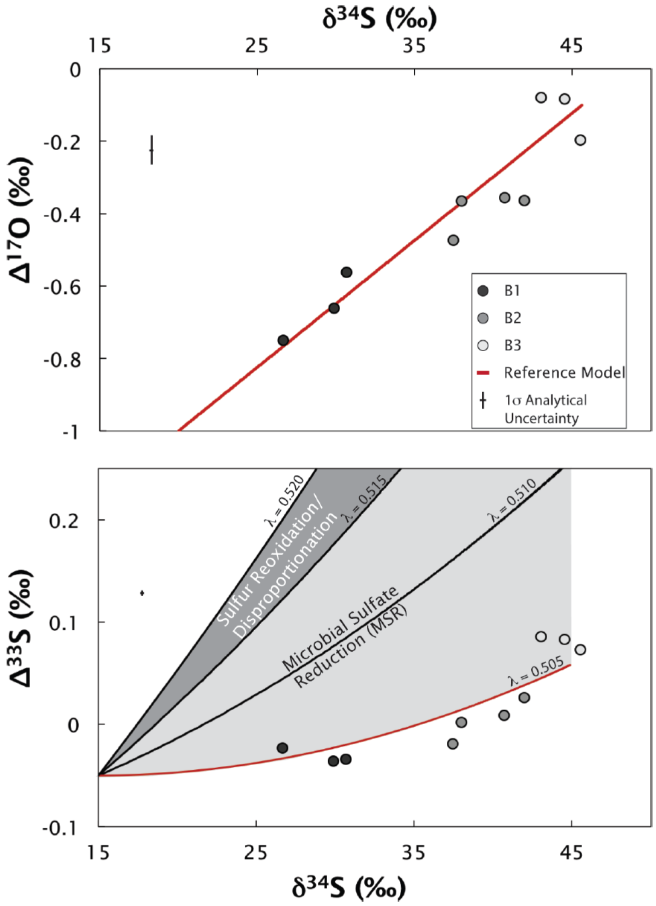

Figure 2.2: (A) Ravensthroat Formation barite $\Delta^{17}O$ and $\delta^{34}S$ data plotted on the reference model solution ($^{34}\varepsilon$ = -42 and f_{Py} = 0.95) for sulfate isotope values. (B) Ravensthroat Formation barite $\Delta^{33}S$ and $\delta^{34}S$ data plotted on reference model solution for sulfate isotope values calculated for varying values of $^{33}\lambda$. Analytical uncertainty is represented by the black cross beneath figure legends.

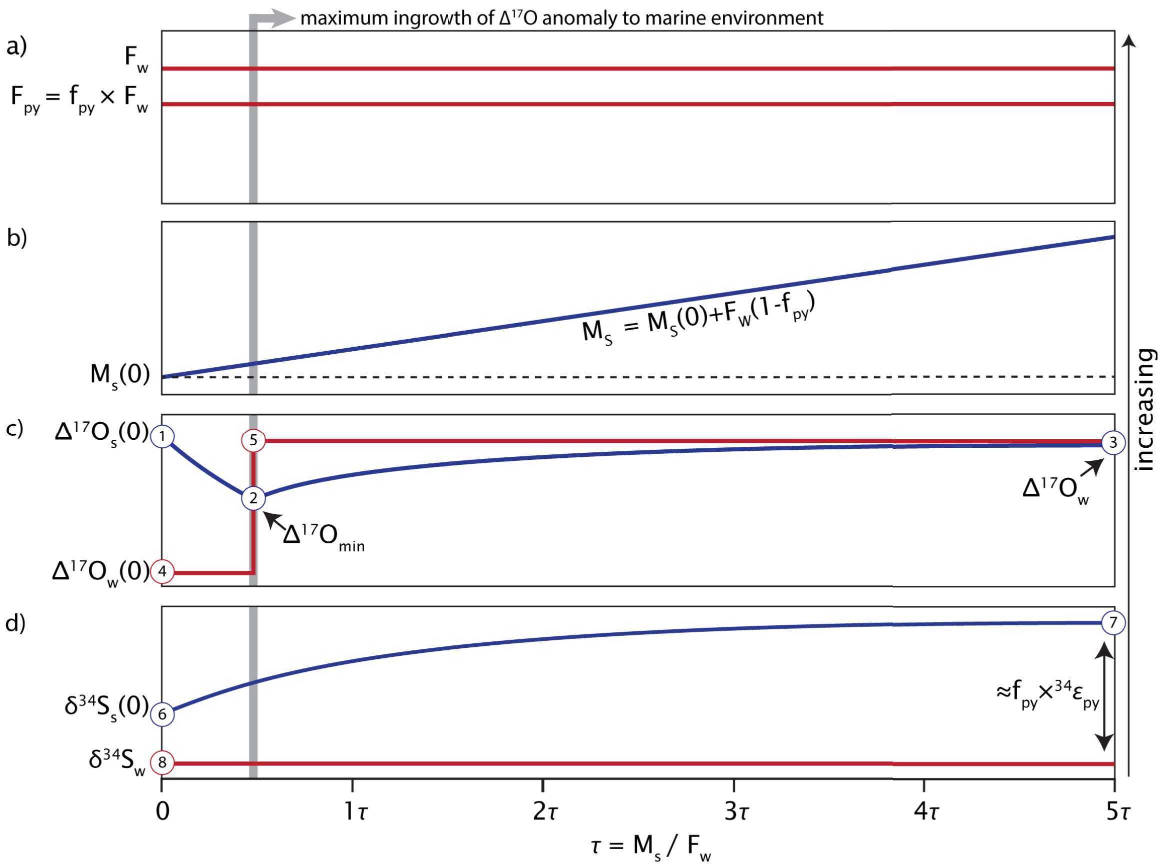

Figure 2.3: Qualitative description of reference model forcing and responses: f_{py}, F_W, $\Delta^{17}O_W$, $\delta^{34}S_W$ and M_s, $\Delta^{17}O_s$, $\delta^{34}S_s$ over five turnover periods (t) of the marine sulfate reservoir. Model forcing is shown in red, while responses are shown in blue and the critical transition in F_W when the maximum $\Delta^{17}O$ anomaly is imparted to the marine environment is marked with the grey line. Numerical values are not assigned along y-axes, however increases in vertical height correspond to increasing values. Circles filled with numbers 1-8 correspond to reference model values, as set by observations (1: initial marine $\Delta^{17}O$ value = -0.1‰, 2: minimum marine $\Delta^{17}O$ value = -1‰, 3: $\Delta^{17}O$ marine at isotopic steady-state = -0.1‰, 4: initial $\Delta^{17}O$ value of weathering flux= -4.2‰, 5: $\Delta^{17}O$ value of weathering flux after maximum marine anomaly is reached = -0.1‰, 6: initial marine $\delta^{34}S$ value = +15‰, 7: $\delta^{34}S$ marine at isotopic steady-state = +45‰, 8: riverine $\delta^{34}S$ value = +5‰). (a) Sulfate input is slightly greater than sulfate output, and both are unchanged for the duration of the model. (b) The mass of the sulfate reservoir increases linearly with model time. (c) $\Delta^{17}O_s$ responds to a step function change in $\Delta^{17}O_W$, reaching a steady state value equal to $\Delta^{17}O_W$. (d) $\delta^{34}S_s$ responds to the fractionation associated with microbial sulfur cycling (^{34}e), reaching a steady state value modulated by the magnitude of f_{py}.

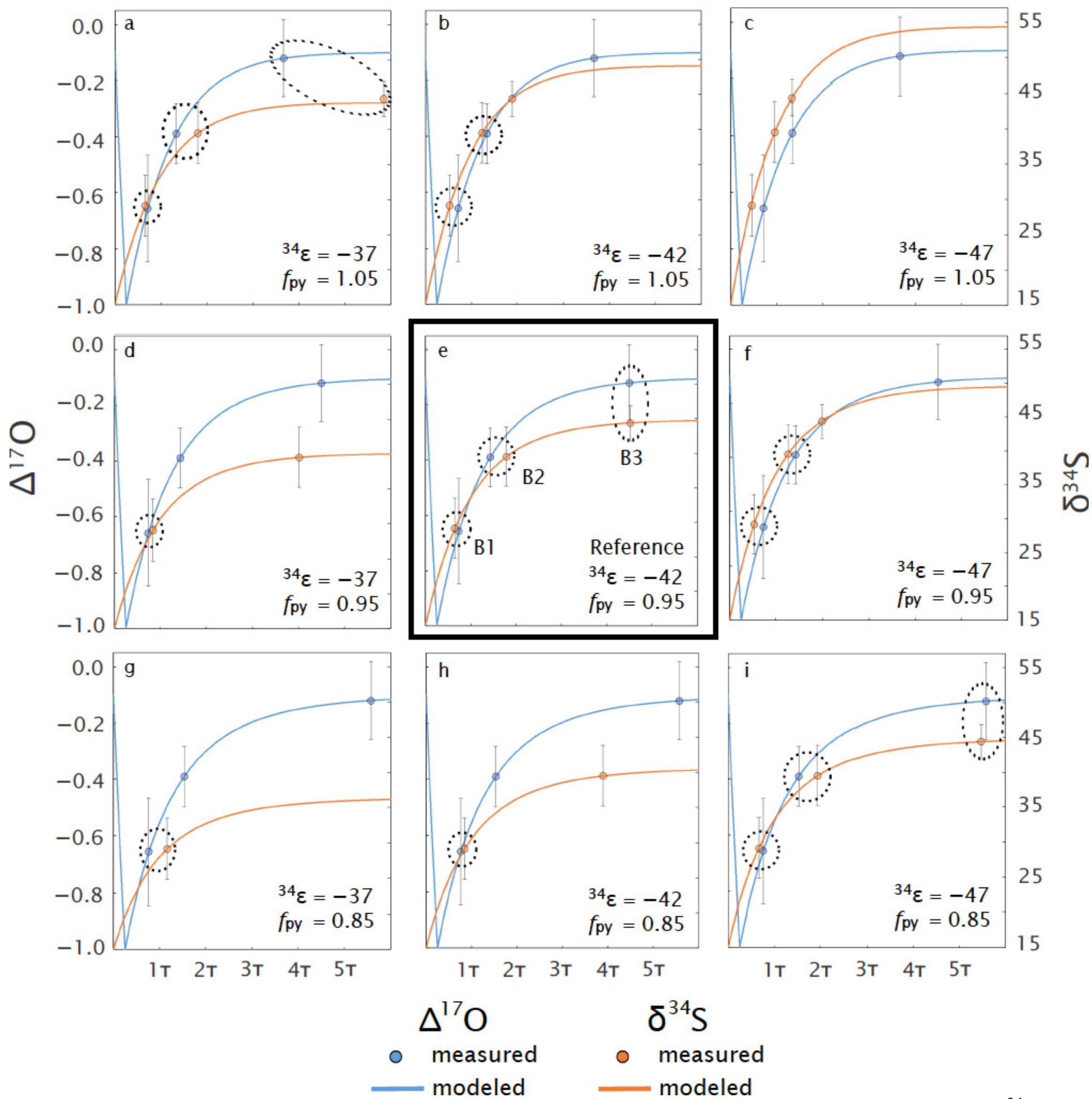

Figure 2.4: Model sensitivity to changes in isotope fractionation between sulfate and sulfide ($^{34}\varepsilon$) and pyrite burial flux (f_{py}) relative to weathering flux (F_W). Data points represent the mean isotopic compositions of barite layers B1−B3. Error bars represent 2σ on the mean of the measurements from each respective layer. Dotted circles indicate agreement in model time between the mean values ±2σ for $\Delta^{17}O$ and $\delta^{34}S$.

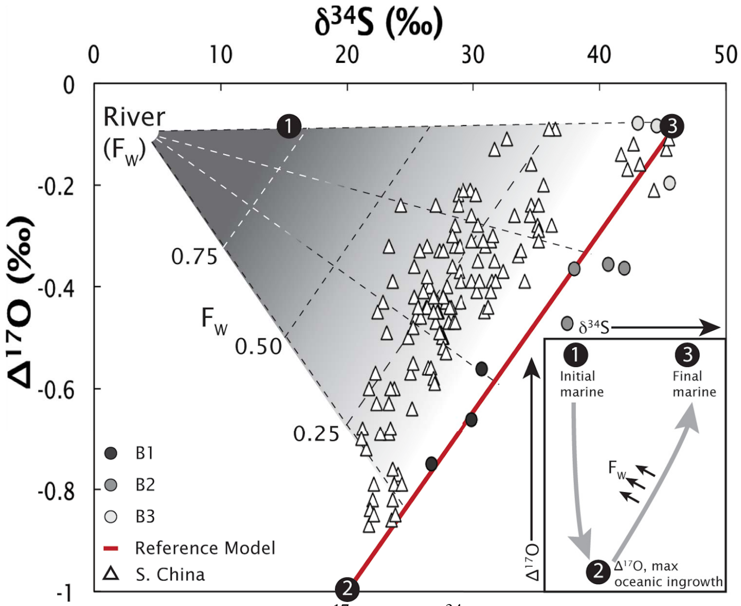

Figure 2.5: Cross-plot of Δ^{17}O and δ^{34}S values from the reference model ($^{34}\varepsilon = -42‰, f_{Py} = 0.95$) from the Ravensthroat Formation barites from northwest Canada (B1, B2 and B3), and from the Doushantou Formation barites from South China (Peng et al., 2011). Mixing between the evolving marine sulfate reservoir (model) and postglacial riverine sulfate creates a mixing surface by which contributions from each end-member can be determined for the South China data set. Marine sulfate isotopic composition evolves from an initial composition (1) to the most extreme ^{17}O values where F_W steps from Δ^{17}O = -4.2‰ to Δ^{17}O = -0.1‰ (2), and finally marine isotopic values captured in barites evolve along the red line to a final isotopic composition (3). Please refer to Fig 2.2. for analytical uncertainty.

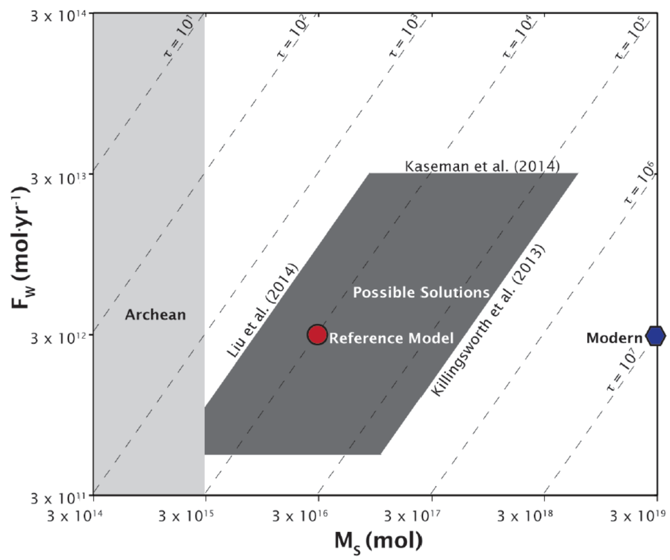

Figure 2.6: Summary of estimated upper and lower potential limits on turnover times of the marine sulfate reservoir (M_S/F_W) and F_W (see Jamieson et al., 2013; Killingsworth et al., 2013; Kasemann et al., 2014; Liu et al., 2014). Gridlines represent varying residence time values (t) in years. Model solutions compatible with the Ravensthroat $\Delta^{17}O$ and $\delta^{34}S$ data are represented in the dark grey box, which deviates from the t isolines in the lower left to disregard solutions that have a M_S below estimated Archean sulfate concentrations (shown as a light grey box). The reference model solution is represented by the red circle where $M_S/F_W = 10^4$ years. The modern sulfur cycle is represented as a blue hexagon, and plots well outside of the possible post-Marinoan solutions.

Bibliography

Antler, G., Turchyn, A. V., Rennie, V., Herut, B., & Sivan, O. (2013). Coupled sulfur and oxygen isotope insight into bacterial sulfate reduction in the natural environment. *Geochimica et Cosmochimica Acta*, *118*, 98-117.

Antler, G., Turchyn, A. V., Herut, B., & Sivan, O. (2015). A unique isotopic fingerprint of sulfate-driven anaerobic oxidation of methane. *Geology*, G36688-1.

Arnaud, E., Halverson, G. P., & Shields-Zhou, G. (Eds.). (2011). The geological record of neoproterozoic glaciations. Geological Society of London.

Balci, N., Shanks III, W. C., Mayer, B., & Mandernack, K. W. (2007). Oxygen and sulfur isotope systematics of sulfate produced by bacterial and abiotic oxidation of pyrite. *Geochimica et Cosmochimica Acta*, *71*(15), 3796-3811.

Bao, H. (2006). Purifying barite for oxygen isotope measurement by dissolution and reprecipitation in a chelating solution. *Analytical chemistry*, *78*(1), 304-309.

Bao, H., Lyons, J. R., & Zhou, C. (2008). Triple oxygen isotope evidence for elevated CO_2 levels after a Neoproterozoic glaciation. *Nature*, *453*(7194), 504-506.

Bao, H., Fairchild, I. J., Wynn, P. M., & Spötl, C. (2009). Stretching the envelope of past surface environments: Neoproterozoic glacial lakes from Svalbard. *Science*, *323*(5910), 119-122.

Bao, H., Chen, Z. Q., & Zhou, C. (2012). An $\Delta^{17}O$ record of late Neoproterozoic glaciation in the Kimberley region, Western Australia. *Precambrian Research*, *216*, 152-161.

Bradley, A. S., Leavitt, W. D., Schmidt, M., Knoll, A. H., Girguis, P. R., & Johnston, D. T. (2015). Patterns of sulfur isotope fractionation during Microbial Sulfate Reduction. *Geobiology*.

Butchart, N., Scaife, A. A., Bourqui, M., De Grandpré, J., Hare, S. H. E., Kettleborough, J., Langematz U., Manzini, E., Sassi, F., Shibata, K., Shindell, D., Sigmond, M. (2006). Simulations of anthropogenic change in the strength of the Brewer–Dobson circulation. *Climate Dynamics*, *27*(7-8), 727-741.

Canfield, D. E., & Thamdrup, B. (1994). The production of 34S-depleted sulfide during bacterial disproportionation of elemental sulfur. *Science*, *266*(5193), 1973-1975.

Canfield, D. E., & Teske, A. (1996). Late Proterozoic rise in atmospheric oxygen concentration inferred from phylogenetic and sulphur-isotope studies. *Nature*, *382*(6587), 127-132.

Canfield, D. E., Raiswell, R., Westrich, J. T., Reaves, C. M., & Berner, R. A. (1986). The use of chromium reduction in the analysis of reduced inorganic sulfur in sediments and shales. *Chemical Geology*, *54*(1), 149-155.

Cao, X., & Bao, H. (2013). Dynamic model constraints on oxygen-17 depletion in atmospheric O2 after a snowball Earth. *Proceedings of the National Academy of Sciences*, *110*(36), 14546-14550.

Creveling, J. R., & Mitrovica, J. X. (2014). The sea-level fingerprint of a Snowball Earth deglaciation. *Earth and Planetary Science Letters*, *399*, 74-85.

Farquhar, J., Johnston, D. T., Wing, B. A., Habicht, K. S., Canfield, D. E., Airieau, S., & Thiemens, M. H. (2003). Multiple sulphur isotopic interpretations of biosynthetic pathways: implications for biological signatures in the sulphur isotope record. *Geobiology*, *1*(1), 27-36.

Gomes, M. L., & Hurtgen, M. T. (2015). Sulfur isotope fractionation in modern euxinic systems: Implications for paleoenvironmental reconstructions of paired sulfate–sulfide isotope records. *Geochimica et Cosmochimica Acta*, *157*, 39-55.

Halverson, G. P., & Hurtgen, M. T. (2007). Ediacaran growth of the marine sulfate reservoir. *Earth and Planetary Science Letters*, *263*(1), 32-44.

Hoffman, P. F., Kaufman, A. J., Halverson, G. P., & Schrag, D. P. (1998). A Neoproterozoic snowball earth. *Science*, *281*(5381), 1342-1346.

Hoffman, P. F., & Halverson, G. P. (2011). Neoproterozoic glacial record in the Mackenzie Mountains, northern Canadian Cordillera. *Geological Society, London, Memoirs*, *36*(1), 397-412.

Hoffman, P. F., Macdonald, F. A., & Halverson, G. P. (2011). Chemical sediments associated with Neoproterozoic glaciation: iron formation, cap carbonate, barite and phosphorite. *Geological Society, London, Memoirs*, *36*(1), 67-80.

Hurtgen, M. T., Arthur, M. A., & Halverson, G. P. (2005). Neoproterozoic sulfur isotopes, the evolution of microbial sulfur species, and the burial efficiency of sulfide as sedimentary pyrite. *Geology*, *33*(1), 41-44.

Hurtgen, M. T., Halverson, G. P., Arthur, M. A., & Hoffman, P. F. (2006). Sulfur cycling in the aftermath of a 635-Ma snowball glaciation: Evidence for a syn-glacial sulfidic deep ocean. *Earth and Planetary Science Letters*, *245*(3), 551-570.

Hyde, W. T., Crowley, T. J., Baum, S. K., & Peltier, W. R. (2000). Neoproterozoic 'snowball Earth'simulations with a coupled climate/ice-sheet model. *Nature*, *405*(6785), 425-429.

Jamieson, J. W., Wing, B. A., Farquhar, J., & Hannington, M. D. (2013). Neoarchaean seawater sulphate concentrations from sulphur isotopes in massive sulphide ore. *Nature Geoscience*, *6*(1), 61-64.

Jiang, G., Kennedy, M. J., Christie-Blick, N., Wu, H., & Zhang, S. (2006). Stratigraphy, sedimentary structures, and textures of the late Neoproterozoic Doushantuo cap carbonate in South China. *Journal of Sedimentary Research*, *76*(7), 978-995.

Jørgensen, B. B. (1990). A thiosulfate shunt in the sulfur cycle of marine sediments. *Science*, *249*(4965), 152-154.

Johnston, D. T., Wing, B. A., Farquhar, J., Kaufman, A. J., Strauss, H., Lyons, T. W., Kah, L., & Canfield, D. E. (2005). Active microbial sulfur disproportionation in the Mesoproterozoic. *Science*, *310*(5753), 1477-1479.

Johnston, D. T., Poulton, S. W., Tosca, N. J., O'Brien, T., Halverson, G. P., Schrag, D. P., & Macdonald, F. A. (2013). Searching for an oxygenation event in the fossiliferous Ediacaran of northwestern Canada. *Chemical Geology*, *362*, 273-286.

Kasemann, S. A., Pogge von Strandmann, P. A., Prave, A. R., Fallick, A. E., Elliott, T., & Hoffmann, K. H. (2014). Continental weathering following a Cryogenian glaciation: Evidence from calcium and magnesium isotopes. *Earth and Planetary Science Letters*, *396*, 66-77.

Kennedy, M. J. (1996). Stratigraphy, sedimentology, and isotopic geochemistry of Australian Neoproterozoic postglacial cap dolostones: deglaciation, $d^{13}C$ excursions, and carbonate precipitation. *Journal of Sedimentary Research*, *66*(6).

Killingsworth, B. A., Hayles, J. A., Zhou, C., & Bao, H. (2013). Sedimentary constraints on the duration of the Marinoan Oxygen-17 Depletion (MOSD) event. *Proceedings of the National Academy of Sciences*, *110*(44), 17686-17690.

Kohl, I., & Bao, H. (2011). Triple-oxygen-isotope determination of molecular oxygen incorporation in sulfate produced during abiotic pyrite oxidation (pH= 2–11). *Geochimica et Cosmochimica Acta*, *75*(7), 1785-1798.

Kunzmann, M., Halverson, G. P., Sossi, P. A., Raub, T. D., Payne, J. L., & Kirby, J. (2013). Zn isotope evidence for immediate resumption of primary productivity after snowball Earth. *Geology*, *41*(1), 27-30.

Leavitt, W. D., Halevy, I., Bradley, A. S., & Johnston, D. T. (2013). Influence of sulfate reduction rates on the Phanerozoic sulfur isotope record. *Proceedings of the National Academy of Sciences*, *110*(28), 11244-11249.

Liu, C., Wang, Z., Raub, T. D., Macdonald, F. A., & Evans, D. A. (2014). Neoproterozoic cap-dolostone deposition in stratified glacial meltwater plume. *Earth and Planetary Science Letters*, *404*, 22-32.

Luz, B., Barkan, E., Bender, M. L., Thiemens, M. H., & Boering, K. A. (1999). Triple-isotope composition of atmospheric oxygen as a tracer of biosphere productivity. *Nature*, *400*(6744), 547-550.

Macdonald, F. A., Strauss, J. V., Sperling, E. A., Halverson, G. P., Narbonne, G. M., Johnston, D. T., Kunzmann, M., Schrag, D. P., Higgins, J. A. (2013). The stratigraphic relationship between the Shuram carbon isotope excursion, the oxygenation of Neoproterozoic oceans, and the first appearance of the Ediacara biota and bilaterian trace fossils in northwestern Canada. *Chemical Geology*, *362*, 250-272.

Pellerin, A., Bui, T. H., Rough, M., Mucci, A., Canfield, D. E., & Wing, B. A. (2015). Mass-dependent sulfur isotope fractionation during reoxidative sulfur cycling: A case study from Mangrove Lake, Bermuda. *Geochimica et Cosmochimica Acta*, *149*, 152-164.

Pellerin, A., Anderson-Trocmé, L., Whyte, L. G., Zane, G. M., Wall, J. D., & Wing, B. A. (2015). Sulfur Isotope Fractionation during the Evolutionary Adaptation of a Sulfate-Reducing Bacterium. *Applied and Environmental Microbiology*, *81*(8), 2676-2689.

Peng, Y., Bao, H., Zhou, C., & Yuan, X. (2011). $\Delta^{17}O$-depleted barite from two Marinoan cap dolostone sections, South China. *Earth and Planetary Science Letters*, *305*(1), 21-31.

Reinhard, C. T., Lalonde, S. V., & Lyons, T. W. (2013). Oxidative sulfide dissolution on the early Earth. *Chemical Geology*, *362*, 44-55.

Sahoo, S. K., Planavsky, N. J., Kendall, B., Wang, X., Shi, X., Scott, C., Anbar, a., Lyons, T.W., Jiang, G. (2012). Ocean oxygenation in the wake of the Marinoan glaciation. *Nature*, *489*(7417), 546-549.

Sansjofre, P., Ader, M., Trindade, R. I. F., Elie, M., Lyons, J., Cartigny, P., & Nogueira, A. C. R. (2011). A carbon isotope challenge to the snowball Earth. *Nature*, *478*(7367), 93-96.

Scott, C., Wing, B. A., Bekker, A., Planavsky, N. J., Medvedev, P., Bates, S. M., Yun, M. & Lyons, T. W. (2014). Pyrite multiple-sulfur isotope evidence for rapid expansion and contraction of the early Paleoproterozoic seawater sulfate reservoir. *Earth and Planetary Science Letters*, *389*, 95-104.

Shields, G. A., Deynoux, M., Strauss, H., Paquet, H., & Nahon, D. (2007). Barite-bearing cap dolostones of the Taoudéni Basin, northwest Africa: sedimentary and isotopic evidence for methane seepage after a Neoproterozoic glaciation. *Precambrian Research*, *153*(3), 209-235.

Thiemens, M. H., & Heidenreich, J. E. (1983). The mass-independent fractionation of oxygen: A novel isotope effect and its possible cosmochemical implications. *Science*, *219*(4588), 1073-1075.

Thode, H. G., Jan Monster, and H. B. Dunford (1961). "Sulphur isotope geochemistry." *Geochimica et Cosmochimica Acta. 25*(3), 159-174.

Torres, M. E., Bohrmann, G., Dubé, T. E., & Poole, F. G. (2003). Formation of modern and Paleozoic stratiform barite at cold methane seeps on continental margins. *Geology*, *31*(10), 897-900.

Trindade, R. I. F., Font, E., D'Agrella-Filho, M. S., Nogueira, A. C. R., & Riccomini, C. (2003). Low-latitude and multiple geomagnetic reversals in the Neoproterozoic Puga cap carbonate, Amazon craton. *Terra Nova*, *15*(6), 441-446.

Wing, B. A. (2013). A cold, hard look at ancient oxygen. *Proceedings of the National Academy of Sciences*, *110*(36), 14514-14515.

Wing, B. A., & Halevy, I. (2014). Intracellular metabolite levels shape sulfur isotope fractionation during microbial sulfate respiration. *Proceedings of the National Academy of Sciences*, *111*(51), 18116-18125.

Wu, N., Farquhar, J., Strauss, H., Kim, S. T., & Canfield, D. E. (2010). Evaluating the S-isotope fractionation associated with Phanerozoic pyrite burial. *Geochimica et Cosmochimica Acta*, *74*(7), 2053-2071.

Yung, Y. L., DeMore, W. B., & Pinto, J. P. (1991). Isotopic exchange between carbon dioxide and ozone via O (1D) in the stratosphere. *Geophysical Research Letters*, *18*(1), 13-16.

Yung, Y. L., Lee, A. Y., Irion, F. W., DeMore, W. B., & Wen, J. (1997). Carbon dioxide in the atmosphere: Isotopic exchange with ozone and its use as a tracer in the middle atmosphere. *Journal of Geophysical Research: Atmospheres (1984–2012)*, *102*(D9), 10857-10866.

Zhou, C., Bao, H., Peng, Y., & Yuan, X. (2010). Timing the deposition of ^{17}O-depleted barite at the aftermath of Nantuo glacial meltdown in South China. *Geology*, *38*(10), 903-906.

Preface to Chapter 3

A proliferation of radiometric dating applied to Neoproterozoic strata has resolved many debates surrounding the chronology of the Sturtian and Marinoan glaciations. These advances have brought to light two long lasting glaciations of 59 (Sturtian) and 4 Myr (Marinoan) duration allowing for new explorations contrasting these enigmatic events. Along with new radiometric ages has come a number of geochemical studies exploring post-glacial and interglacial sequences attempting to constrain weathering rates, primary production and marine redox conditions across these intervals of Earth history. Unfortunately the errors associated with current radiometric dates are at best an order of magnitude too large to explore the pace of geochemical evolution predicted from numerous geochemical and modeling studies. This shortcoming prevents correlation of geographically disparate strata that is required in order to elucidate the global, local or globally local nature of revealed geochemical trends.

In this chapter we further extend the $\Delta^{17}O$ anomaly to two new paleo-continents with samples from the Nyborg formation of northern Norway, and the Bambui group of Brazil. These new results together with anomalies revealed at five other locations provide a large global footprint of this signal. Importantly, as the appearance and disappearance of $\Delta^{17}O$ anomalies are either tied to the evolution of the atmosphere or marine sulfate reservoir, their existence is by nature transient. In Chapter 2 we calculated the end-member scenario of imparting and removing $\Delta^{17}O$ anomalies from the marine sulfate reservoir suggesting a likely timescale on the order of 10^4 years. Therefore in this Chapter we put forward that $\Delta^{17}O$ anomalies can be utilized as an important geochemical datum that offers the ability to tie geochemical trends together in time. We further argue that the distribution and location of $\Delta^{17}O$ anomalies both geographically and stratigraphically provides further evidence for rapid deglaciation from the Marinoan as well as further evidence that deglaciation was indeed synchronous.

3. Linking paleocontinents through triple oxygen isotope anomalies

Abstract

A central tenet of the Neoproterozoic Snowball Earth hypothesis is that glaciations ended synchronously. This condition is borne out by recent U-Pb and Re-Os geochronology, which establishes that the end of the Sturtian and Marinoan (i.e. Cryogenian) glaciations occurred globally at ca. 659 and 635 Ma, respectively. However, the timescale of deglaciation is much less than the intrinsic error of even the highest-resolution dating techniques, and by consequence calibrating the pace and synchronicity of biogeochemical recovery from Cryogenian glaciations remains a challenge. Given the importance of obtaining a globally synoptic view of paleoenvironmental conditions and biological evolution during these extraordinary transitions, robust correlations and chronologies are imperative. Here we suggest that triple oxygen isotope ($\Delta^{17}O$) anomalies recorded globally in Marinoan post-glacial cap carbonate sequences provide a unique time datum that can be used to cross-correlate these strata and track the geochemical evolution of the oceans during deglaciation. We extend the footprint of the $\Delta^{17}O$ anomaly to two new paleocontinents with results from Brazil and northern Norway that display anomalous $\Delta^{17}O$ values of -1.05 and -1.02‰, respectively. Seven paleocontinents are now known to preserve this unique geochemical signature, and the prediction is that it should be found on others, where it will serve as a precise time marker during the recovery from the Marinoan Snowball Earth.

3.1 Introduction

Neoproterozoic glacial deposits are widespread with sedimentological and paleomagnetic data indicating that ice-sheets existed at low latitudes and altitudes (Hoffman et al., 1998; Hoffman and Li, 2009). Large carbon isotope anomalies preceding two Cryogenian (ca. 720–635 Ma) glaciations (Prave et al., 2009; Halverson et al., 2010) and the global occurrence of sedimentologically and geochemically unique cap carbonate sequences above glacial diamictites and associated strata, favor the Snowball Earth hypothesis over competing explanations for low-latitude glaciation in the Neoproterozoic. This hypothesis asserts that Earth effectively froze over completely, plunging it into a highly stable climatic state dominated by the high albedo of ice. This ice albedo effect could only be overcome through the accumulation of extraordinary amounts of CO_2 in the atmosphere (Hoffman et al., 1998; Bao et al., 2008), perhaps accompanied by decreased albedo as continental ice sheets gradually retreated (Benn et al., 2015) or accumulation of dust in the low-latitudes (Abbot and Pierrehumbert, 2010). Whereas the Snowball Earth hypothesis was unsurprisingly controversial, it made the key predictions that the glaciations should have been global in extent and long-lived, terminating synchronously.

The global extent of the Cryogenian glaciations is borne out by a combination of paleomagnetic data and paleogeographic reconstructions (Hoffman and Li, 2009). Early compilations of radiometric age constraints on Neoproterozoic glaciations led some authors to conclude that they were diachronous, and hence inconsistent with snowball glaciation (e.g., Allen and Etienne, 2005). However, a surge in new radiometric ages has firmly established that the two Cryogenian glaciations were long-lived and ended synchronously. Results from high-precision U-Pb zircon dating and Re-Os dating of organic-rich sediments converge to indicate that the older Cryogenian (i.e., Sturtian) glaciation initiated between 717.5-716.3 Ma

(Macdonald et al. 2010) and terminated between 659.3-658.5 Ma (Rooney et al., 2014; 2015) and that the younger Cryogenian (i.e., Marinoan) glaciation initiated between 649.9-639 Ma (Kendall et al., 2006; Prave et al., 2016) and terminated between 636 – 634.7 Ma (Zhang et al., 2005; Condon et al., 2005; Calver et al., 2013; Rooney et al., 2015; Prave et al., 2016).

Despite new radiometric ages, most Cryogenian glacial successions remain poorly dated. Fortunately, the geological records of the Sturtian and Marinoan glaciations and the *cap carbonate sequences* that were deposited after these glaciations can be distinguished via a combination of sedimentological observations, stratigraphic context, and geochemical data (Kennedy et al., 1998; Hoffman and Schrag, 2002; Halverson et al., 2005). In fact, the cap carbonate sequence post-dating the Marinoan snowball glaciation is so widespread and idiosyncratic that it serves as the basis for the definition of the start of the Ediacaran Period (Knoll et al., 2006). This cap carbonate sequence begins with a transgressive systems tract (TST) that encompasses a basal cap dolostone and ends with a maximum flooding surface that commonly lies within organic-rich shales. The thick, overlying high-stand systems tract (HST) fills the substantial accommodation space that was generated during the long-lived glaciation (Hoffman et al., 1998), but left underfilled by the unusually low sediment accumulation rates characteristic of snowball glaciations (Partin and Saddler, 2016). In contrast, the Sturtian cap carbonate sequence typically lacks a TST, beginning instead at the maximum flooding surface (Halverson et al., 2005).

If the correlation and ages of the Cryogenian glaciations and their respective cap carbonates are well established, the chronology of recovery from snowball glaciations remains fuzzy. Geochemical and oceanographic modelling (Crockford et al., 2016; Yang et al., 2017) imply that the post-Marinoan rise in sea level should have persisted between 10^4 – 10^5 years, which is less than the current precision of radiometric dating techniques. Given that deposition of cap dolostones is diachronous (Hoffman et al., 2007) and that the relative timing is spatially heterogeneous due to competing factors of glacial eustasy, thermal expansion, self-gravitation, and isostatic rebound (Creveling and Mitrovica, 2014), it is difficult to generate a globally synoptic snapshot of the global ocean during glacial meltback and subsequent warming. However, extremely negative $\Delta^{17}O$ anomalies documented in sulfate-bearing minerals in multiple post-Marinoan cap dolostones (Bao et al., 2008; Bao et al., 2012; Crockford et al., 2016) present a unique opportunity to identify a globally isochronous datum within the cap carbonate sequences that fortuitously also closely approximates the Cryogenian-Ediacaran boundary.

3.2 Triple oxygen ($\Delta^{17}O$) isotopes

$\Delta^{17}O$ anomalies are generated through the destruction and reforming of ozone (O_3) in the stratosphere that imparts a mass-independent enrichment of ^{17}O into O_3 and CO_2 and a corresponding depletion of ^{17}O in residual O_2 (Wen and Thiemens, 1993). The magnitude of ^{17}O depletion, denoted as a negative $\Delta^{17}O$ value [$\Delta^{17}O = ln(\delta^{17}O+1) - 0.5305 \times ln(\delta^{18}O+1)$; see supplemental], is proportional to both pCO_2 levels and the rate of dilution by the gross O_2 export of the biosphere to the troposphere, which is proportional to gross primary production (*GPP)* (Yung et al., 1997; Luz et al., 1999). One pathway that translates atmospheric $\Delta^{17}O$ signatures to the Earth surface environment is through sulfide oxidation, where a portion of the anomaly (≈8-30%) is incorporated and robustly retained into product sulfate (Kohl and Bao, 2012; Balci et al., 2007). This sulfate can then be preserved in the geological record (e.g. barite, gypsum, carbonate associate sulfate—CAS) provided deposition occurs before isotopic signatures are reset in response to significant microbial cycling and/or dilution by a large standing sulfate reservoir.

3.3 Extending the $\Delta^{17}O$ horizon

Neoproterozoic glacial and periglacial sequences have been reported in 48 locations for the Marinoan; five of these sequences bear anomalous $\Delta^{17}O$ signatures. These anomalies occur in syn-Marinoan CAS extracted from lacustrine carbonates in the Wilsonbreen Formation in Svalbard (Bao et al., 2009), post-Marinoan CAS in the Moonlight Valley cap dolostone of northern Australia (Bao et al, 2012), and most commonly, enigmatic barite horizons deposited at or near the top of cap dolostones within the post-glacial TST (Bao et al., 2008; Hoffman et al., 2011; Crockford et al., 2016). Barite-bearing horizons typically occur discontinuously on paleotopographic highs at the transition from cap dolostones to deeper water carbonate or shale facies, range from a few millimeters to centimeters in thickness (rarely they are over a meter in thickness; Killingsworth et al., 2013), and occur as either seafloor cements or diagenetic crusts (Hoffman et al. 2011). These barite-hosted $\Delta^{17}O$ anomalies have been identified in the Jbeliat Group of Mauritania, the Doushantuo Formation of South China, and the Ravensthroat Formation of northwestern Canada (Bao et al., 2008; Crockford et al., 2016). The limited stratigraphic interval within which these anomalies occur, particularly as seen in northwest Canada, further highlights the transiency of these events and their utility as chronostratigraphic markers (Crockford et al., 2016; Fig. 3.1).

To expand the geographic footprint of existing reports of anomalous $\Delta^{17}O$ bearing sulfate, we measured $\Delta^{17}O$ values from post-Marinoan seafloor barites in two new localities: the Sete Lagoas Formation (lower Bambuí Group) of east-central Brazil (cf. Caxito et al., 2012), and the Nyborg Formation (Vestertana Group) of northern Norway (Rice et al., 2011). Samples from Brazil typically display a bladed crystal habit and occur along paleo-highs on granitic basement between 1 and 8 cm thick. Similar to Brazilian samples, the Norwegian barites outcrop along basement highs and are typically bladed crystals and rosettes, with barite beds 1–30 cm thick. Although the age of units in both locations has previously been controversial, most recent studies suggest both are Marinoan in age based on a combination of sequence stratigraphic, sedimentological, and isotopic characteristics (Caxito et al., 2012; Halverson et al., 2005). Here we report $\Delta^{17}O$ values as negative as -1.05‰ and -1.02‰ from Brazil and Norway, respectively (Fig. 3.1). These $\Delta^{17}O$ values are of similar magnitude to minimum values observed in South China (-0.87‰; Peng et al., 2011) and northwestern Canada (-0.84‰; Crockford et al., 2016) (Fig. 3.1). They also provide additional support for a Marinoan age for these two units, making them temporally equivalent to dated units in South China and northwestern Canada, and expand the occurrence of Marinoan $\Delta^{17}O$ anomalies to seven paleo-continents (Fig. 3.1).

3.4 Neoproterozoic $\Delta^{17}O$ anomalies are unique to the Marinoan glaciation

At present, $\Delta^{17}O$ anomalies below < -0.4‰ are known only from Marinoan-aged glacial deposits or the TSTs at the base of the associated cap carbonate sequences. The interpretation of this geochemical signal has been controversial because varying *GPP* or $p\text{CO}_2$ levels can lead to the generation of anomalous $\Delta^{17}O$ values under very different atmospheric conditions. Evidence of relatively high levels of primary production in the aftermath of the Marinoan (Kunzmann et al., 2013) coupled to more in-depth modeling of the generation of $\Delta^{17}O$ anomalies over Cryogenian glaciations (Cao and Bao, 2013), strongly support initial interpretations of extremely elevated $p\text{CO}_2$ levels (Hoffman et al., 1998; Bao et al., 2008). Explaining the restriction of extreme $\Delta^{17}O$

anomalies to only the Marinoan glaciation, however, remains a challenge. To date, no anomalous $\Delta^{17}O$ signals have been documented in association with the end of the Sturtian glaciation, despite the fact that high pCO_2 levels are predicted due its longevity (ca. 58 Myrs; Macdonald et al., 2010; Rooney et al., 2014; 2015). However, this missing signal is most likely accounted for by the absence of appropriate strata to capture the $\Delta^{17}O$ anomalies. The post-Sturtian cap carbonate sequence lacks a TST, and hence it does not record the early recovery from snowball glaciation. By comparison with the Marinoan cap carbonate sequence, in which the $\Delta^{17}O$ anomaly is preserved within the TST, it follows that by the time the post-Sturtian cap carbonate began to be deposited, any $\Delta^{17}O$ anomaly had already disappeared due to mixing with the global ocean and post-glacial sulfur cycling. Hence, the prediction is that unless syn-Sturtian terrestrial sulfates (or sulfate-rich carbonates) or a rare post-Sturtian TST is discovered, no post-Sturtian $\Delta^{17}O$ anomaly should be preserved.

3.5 Marinoan $\Delta^{17}O$ anomalies are short-lived

The extraordinary atmospheric pCO_2 levels required to escape a Snowball climate state (>0.01 – 0.3 bar; Caldeira and Kasting, 1992; Bao et al., 2009), combined with the positive ice-albedo feedback, would drive very rapid melting and prevent a protracted history of ice advance and retreat during deglaciation. Therefore the $\Delta^{17}O$ anomaly event represents an extreme atmospheric state that is intrinsically short-lived and corroborates stratigraphic and geochronological data that indicate that the Marinoan cap carbonate successions were deposited synchronously (Hoffman et al., 1998). That is, regardless of their translation into the geologic record, anomalous $\Delta^{17}O$-bearing horizons represent a finite window of opportunity when atmospheric O_2 possessed significantly anomalous $\Delta^{17}O$ values and surface ocean conditions were appropriate for capturing it. This finite window is expressed in the sedimentary record with similar magnitudes of post-glacial anomalies over multiple paleo-continents. Importantly, this expression appears insensitive to paleolatitude (Fig. 3.1).

Existing estimates for the time scale of Marinoan deglaciation indicate that it is rapid and synchronous, occurring over an interval ($<10^5$ years) that is unresolvable using current radiometric techniques. Although the origins of the most common $\Delta^{17}O$-bearing units (barites) remains debated, hypotheses for the origins of sulfate captured within it require either continental margins strongly influenced by continental weathering, which allows them to capture the isotopic signal of evolving atmospheric conditions, or changing isotopic composition of the global marine sulfate reservoir. Importantly both hypotheses allow timing estimates to be made on the occurrence and disappearance of sulfate with anomalous $\Delta^{17}O$ signatures. Crockford et al., (2016) calculated that even in the case where $\Delta^{17}O$ anomalies are imparted and subsequently removed from the global marine sulfate reservoir with a wide range of plausible sulfate input and output fluxes, the time scale must have been between 10^3-10^6 years. This broad estimate is consistent with recent modeling of the time scale for mixing of the stratified, post-Marinoan ocean ($\approx 5 \times 10^4$ yrs; Yang et al., 2017).

Calculations have also been made to apply timing estimates to scenarios where barite records track local conditions along multiple margins, where isotopic signals should be more tightly coupled to the atmosphere than in the open ocean. In such scenarios, rapidly evolving atmospheric chemistry away from a composition that permits the inception of large stratospheric anomalies occurs on timescales less than 10^5- 10^6 years (Cao and Bao, 2013). Therefore, the stratigraphic context of the anomaly in the different sections, combined with simple modeling considerations of how they developed, imply that $\Delta^{17}O$ anomalies must have been short-lived relative to the post-glacial transgression and should occur globally. Therefore, we argue that $\Delta^{17}O$ anomalies are the best existing geochemical datum to cross-correlate basal Ediacaran strata and further integrate global geochemical signals. In this regard, they are analogous to the Ir anomaly marking the Cretaceous-Paleogene boundary and similarly implicate an extreme event in Earth's history.

3.6 Conclusions

Correlatable datums across widespread geographic locations are paramount in reconstructing accurate temporal geochemical records to track the evolution of Earth's surface environment after Snowball Earth glaciations. We present new triple oxygen isotope data from the Nyborg Formation of Norway and the Bambuí Group of Brazil, extending the record of Marinoan $\Delta^{17}O$ anomalies to seven paleo-continents. These new localities create a wide geographic footprint of $\Delta^{17}O$ signals that are correlatable to radiometrically dated units. $\Delta^{17}O$ anomalies are likely unique to Marinoan aged strata and of shorter duration than uncertainty on existing radiometric techniques. These factors make $\Delta^{17}O$ anomalies a valuable tie point for cross-correlating cap carbonate sequences from different paleo-continents and comparing other geochemical signals within them that track the rapid evolution of the Earth surface environment spanning the Cryogenian-Ediacaran boundary.

Acknowledgements

The Authors wish to thank Dr. Huiming Bao for providing laboratory facilities for analysis and lively discussion. PWC acknowledges funding from an NSERC PGS-D grant and funding under Boswell A. Wing from the Natural Sciences and Engineering Research Council of Canada and the Fonds de Recherche du Québec–Nature et Technologies (FRQNT). FC acknowledges funding from FAPEMIG (Brazil) through grants APQ-00914-14 and PPM-00539-15.

Figures

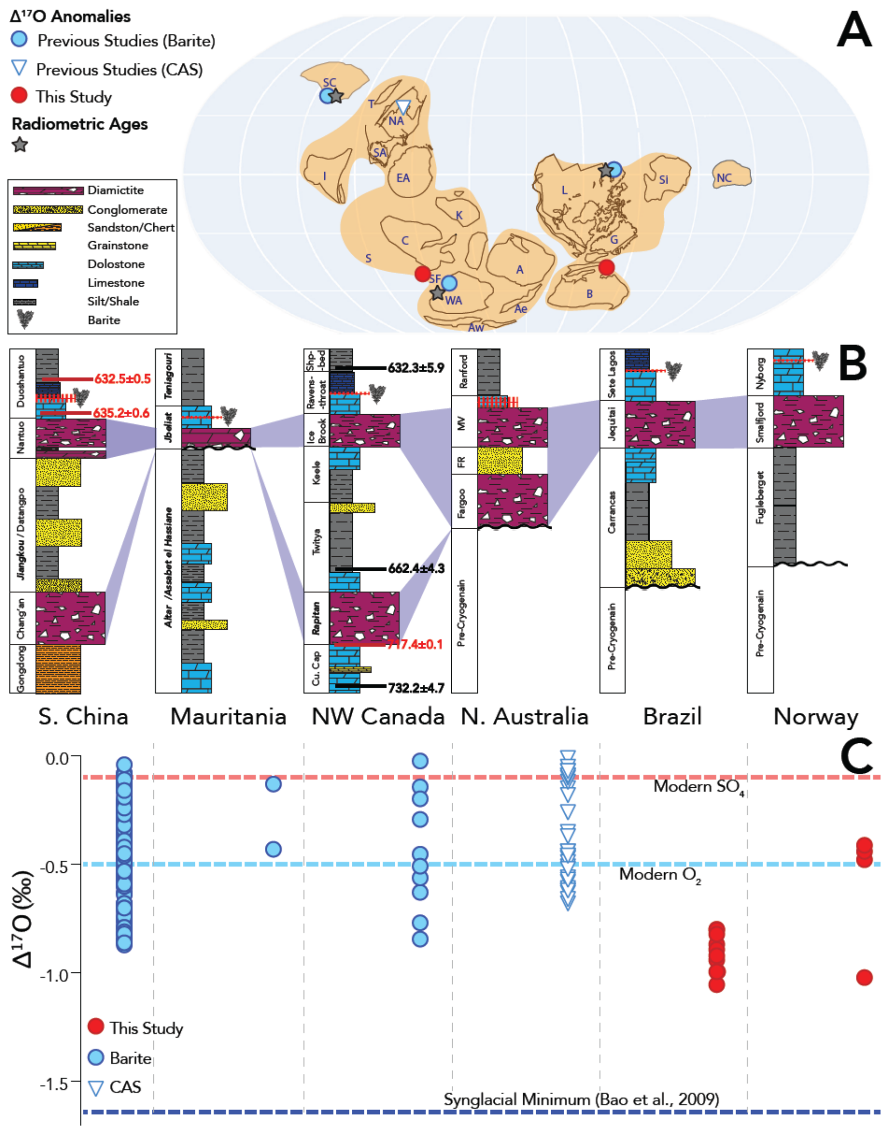

Figure 3.1. Geochronological data, stratigraphy, paleogeography, and $\Delta^{17}O$ data: A) a paleo-reconstruction map at 635 Ma from Li et al. (2013) with sample locations from this (red circles) and previous studies (blue circles, white triangle) reporting $\Delta^{17}O$ data. Locations of current radiometric ages are plotted as grey stars. B) Simplified Cryogenian stratigraphic columns from (left to right) south China, Mauritania, northwest Canada, northern Australia, Brazil and northern Norway including existing geochronological data (U-Pb red; Condon et al., 2005; Zhang et al., 2005; Macdonald et al., 2010; Re-Os black; Rooney et al., 2015; Rooney et al., 2014). Bolded italicized names on stratigraphic columns represent groups and other labels represent formations. Red dashed lines indicate anomalous $\Delta^{17}O$ values, and locations with barite occurrences include symbols. C) All measured $\Delta^{17}O$ data from this study and from previous works (Bao et al., 2008; Peng et al., 2011; Bao et al., 2012; Killingsworth et al., 2013; Crockford et al., 2016) with barite data from previous studies plotted as blue circles, from this study in red circles and CAS data as blue and white triangles. Modern seawater $\Delta^{17}O_{SO4}$ is plotted as a red dashed line, modern $\Delta^{17}O_{O2}$ as a blue dashed line, and syn-glacial minimum $\Delta^{17}O$ values in dark blue (Bao et al., 2009). Uncertainty on all $\Delta^{17}O$ data for the total analytical procedures summarized in SI is +/- 0.05‰.

Bibliography

Abbot, D.S. and Pierrehumbert, R.T. (2010). Mudball: surface dust and Snowball Earth deglaciation. *Journal of Geophysical Research: Atmospheres*, 115(D3).

Allen, P.A. and Etienne, J.L. (2008). Sedimentary challenge to snowball Earth. *Nature Geoscience, 1*(12), 817-825.

Balci, N., Shanks, W.C., Mayer, B. and Mandernack, K.W. (2007). Oxygen and sulfur isotope systematics of sulfate produced by bacterial and abiotic oxidation of pyrite. *Geochimica et Cosmochimica Acta*, *71*(15), 3796-3811.

Bao, H., Fairchild, I.J., Wynn, P.M. and Spötl, C. (2009). Stretching the envelope of past surface environments: Neoproterozoic glacial lakes from Svalbard. *Science*, *323*(5910), 119-122.

Bao, H., Lyons, J.R. and Zhou, C. (2008). Triple oxygen isotope evidence for elevated CO_2 levels after a Neoproterozoic glaciation. *Nature*, *453*(7194), 504-506.

Bao, H., Chen, Z.Q. and Zhou, C. (2012). An ^{17}O record of late Neoproterozoic glaciation in the Kimberley region, Western Australia. *Precambrian Research*, *216*, 152-161.

Benn, D.I., Le Hir, G., Bao, H., Donnadieu, Y., Dumas, C., Fleming, E.J., Hambrey, M.J., McMillan, E.A., Petronis, M.S., Ramstein, G. and Stevenson, C.T. (2015). Orbitally forced ice sheet fluctuations during the Marinoan Snowball Earth glaciation. *Nature Geoscience*, *8*(9), 704-707.

Caldeira, K. and Kasting, J.F. (1992). Susceptibility of the early Earth to irreversible glaciation caused by carbon dioxide clouds. *Nature, 359*(6392), 226-229.

Calver, C.R., Crowley, J.L., Wingate, M.T.D., Evans, D.A.D., Raub, T.D. and Schmitz, M.D. (2013). Globally synchronous Marinoan deglaciation indicated by U-Pb geochronology of the Cottons Breccia, Tasmania, Australia. *Geology*, *41*(10), 1127-1130.

Cao, X. and Bao, H., 2013. Dynamic model constraints on oxygen-17 depletion in atmospheric O2 after a snowball Earth. *Proceedings of the National Academy of Sciences*, *110*(36), 14546-14550.

Caxito, F.A., Halverson, G.P., Uhlein, A., Stevenson, R., Dias, T.G., Uhlein, G.J. (2012). Marinoan glaciation in east central Brazil. *Precambrian Research*, *200*, 38-58.

Condon, D., Zhu, M., Bowring, S., Wang W., Yang, A., Jin, Y. (2005). U-Pb dates from the Neoproterozoic Duoshantuo formation, China. *Science, 308*(5718), 95-98.

Creveling, J.R. and Mitrovica, J.X. (2014). The sea-level fingerprint of a Snowball Earth deglaciation. *Earth and Planetary Science Letters*, *399*, 74-85.

Crockford, P.W., Cowie, B.R., Johnston, D.T., Hoffman, P.F., Sugiyama, I., Pellerin, A., Bui, T.H., Hayles, J., Halverson, G.P., Macdonald, F.A. and Wing, B.A. (2016). Triple oxygen and multiple sulfur isotope constraints on the evolution of the post-Marinoan sulfur cycle. *Earth and Planetary Science Letters*, *435*, 74-83.

Halverson, G.P., Wade, B.P., Hurtgen, M.T. and Barovich, K.M. (2010). Neoproterozoic chemostratigraphy. *Precambrian Research*, *182*(4), 337-350.

Halverson, G.P., Hoffman, P.F., Schrag, D.P., Maloof, A.C. and Rice, A.H.N. (2005). Toward a Neoproterozoic composite carbon-isotope record. *Geological Society of America Bulletin*, *117*(9-10), 1181-1207.

Hoffman, P.F., Kaufman, A.J., Halverson, G.P. and Schrag, D.P. (1998). A Neoproterozoic snowball earth. *Science*, *281*(5381), 1342-1346.

Hoffman, P.F. and Li, Z.X. (2009). A palaeogeographic context for Neoproterozoic glaciation. *Palaeogeography, Palaeoclimatology, Palaeoecology, 277*(3), 158-172.

Hoffman, P.F. and Schrag, D.P. 2002. The snowball Earth hypothesis: testing the limits of global change. *Terra nova*, *14*(3), 129-155.

Hoffman, P.F., Halverson, G.P., Domack, E.W., Husson, J.M., Higgins, J.A. and Schrag, D.P. (2007). Are basal Ediacaran (635 Ma) post-glacial "cap dolostones" diachronous? *Earth and Planetary Science Letters*, *258*(1), 114-131.

Hoffman, P.F., Macdonald, F.A. and Halverson, G.P. (2011). Chemical sediments associated with Neoproterozoic glaciation: iron formation, cap carbonate, barite and phosphorite. *Geological Society, London, Memoirs*, *36*(1), 67-80.

Kendall, B., Creaser, R.A. and Selby, D. (2006). Re-Os geochronology of postglacial black shales in Australia: Constraints on the timing of "Sturtian" glaciation. *Geology*, *34*(9), 729-732.

Kennedy, M.J., Runnegar, B., Prave, A.R., Hoffmann, K.H. and Arthur, M.A. (1998). Two or four Neoproterozoic glaciations? *Geology*, *26*(12), 1059-1063.

Killingsworth, B.A., Hayles, J.A., Zhou, C. and Bao, H. (2013). Sedimentary constraints on the duration of the Marinoan Oxygen-17 Depletion (MOSD) event. *Proceedings of the National Academy of Sciences*, *110*(44), 17686-17690.

Knoll, A., Walter, M., Narbonne, G., Christie-Blick, N. (2006). The Ediacaran Period: a new addition to the geologic time scale. *Lethaia*, *39*(1), 13-30.

Kohl, I. and Bao, H. (2011). Triple-oxygen-isotope determination of molecular oxygen incorporation in sulfate produced during abiotic pyrite oxidation (pH= 2–11). *Geochimica et Cosmochimica Acta*, *75*(7), 1785-1798.

Kunzmann, M., Halverson, G.P., Sossi, P.A., Raub, T.D., Payne, J.L. and Kirby, J. (2013). Zn isotope evidence for immediate resumption of primary productivity after snowball Earth. *Geology*, *41*(1), 27-30.

Li, Z.X., Evans, D.A. and Halverson, G.P. (2013). Neoproterozoic glaciations in a revised global palaeogeography from the breakup of Rodinia to the assembly of Gondwanaland. *Sedimentary Geology, 294,* 219-232.

Luz, B., Barkan, E., Bender, M.L., Thiemens, M.H. and Boering, K.A. (1999). Triple-isotope composition of atmospheric oxygen as a tracer of biosphere productivity. *Nature*, *400*(6744), 547-550.

Macdonald, F.A., Schmitz, M.D., Crowley, J.L., Roots, C.F., Jones, D.S., Maloof, A.C., Strauss, J.V., Cohen, P.A., Johnston, D.T. and Schrag, D.P. (2010). Calibrating the cryogenian. *Science*, *327*(5970), 1241-1243.

Partin, C.A. and Sadler, P.M. (2016). Slow net sediment accumulation sets snowball Earth apart from all younger glacial episodes. *Geology*, *44*(12), 1019-1022.

Peng, Y., Bao, H., Zhou, C. and Yuan, X. (2011). ^{17}O-depleted barite from two Marinoan cap dolostone sections, south China. *Earth and Planetary Science Letters*, *305*(1), 21-31.

Prave, A.R., Condon, D.J., Hoffmann, K.H., Tapster, S. and Fallick, A.E. (2016). Duration and nature of the end-Cryogenian (Marinoan) glaciation. *Geology*, *44*(8), 631-634.

Prave, A.R., Fallick, A.E., Thomas, C.W. and Graham, C.M. (2009). A composite C-isotope profile for the Neoproterozoic Dalradian Supergroup of Scotland and Ireland. *Journal of the Geological Society*, *166*(5), 845-857.

Rice, A.H.N., Edwards, M.B., Hansen, T.A., Arnaud, E. and Halverson, G.P. (2011). Glaciogenic rocks of the Neoproterozoic Smalfjord and Mortensnes formations, Vestertana Group, E. Finnmark, Norway. *Geological Society, London, Memoirs*, *36*(1), 593-602.

Rooney, A.D., Macdonald, F.A., Strauss, J.V., Dudás, F.Ö., Hallmann, C. and Selby, D. (2014). Re-Os geochronology and coupled Os-Sr isotope constraints on the Sturtian snowball Earth. *Proceedings of the National Academy of Sciences*, *111*(1), 51-56.

Rooney, A.D., Strauss, J.V., Brandon, A.D. and Macdonald, F.A. (2015). A Cryogenian chronology: Two long-lasting synchronous Neoproterozoic glaciations. *Geology*, *43*(5), 459-462.

Shields, G.A., Deynoux, M., Strauss, H., Paquet, H. and Nahon, D. (2007). Barite-bearing cap dolostones of the Taoudéni Basin, northwest Africa: sedimentary and isotopic evidence for methane seepage after a Neoproterozoic glaciation. *Precambrian Research*, *153*(3), 209-235.

Wen, J. and Thiemens, M.H., (1993). Multi-isotope study of the O (1D)+ CO_2 exchange and stratospheric consequences. *Journal of Geophysical Research: Atmospheres*, *98*(D7), 12801-12808.

Yang, J., Jansen, M.F., Macdonald, F.A. and Abbot, D.S. (2017). Persistence of a freshwater surface ocean after a snowball Earth. *Geology*, 45(7) 615-618.

Yung, Y.L., DeMore, W.B. and Pinto, J.P. (1991). Isotopic exchange between carbon dioxide and ozone via O (1D) in the stratosphere. *Geophysical Research Letters*, *18*(1), 13-16.

Zhang, S., Jiang, G., Zhang, J., Song, B., Kennedy, M.J. and Christie-Blick, N. (2005). U-Pb sensitive high-resolution ion microprobe ages from the Doushantuo Formation in south China: Constraints on late Neoproterozoic glaciations. *Geology*, *33*(6), 473-476.

3.7 Supplementary Information

Methods

All samples were cut to remove weathered edges, and then crushed by hand in a cleaned agate mortar and pestle. Samples (≈20 mg) were then dissolved into a 1 M sodium hydroxide (NaOH) – 0.05 M diethylenetriaminepentaacetic acid (DTPA) solution and shaken for 12 hours. Samples were then filtered and acidified with double distilled 6 N HCl, followed by the addition of drops of concentrated $BaCl_2$ solution allowing samples to reprecipitate. Samples were allowed to sit for 12 hours followed by centrifuging and washing with deionized water three times. Samples were then dried for 24 hours. This total procedure was then repeated once more before analysis (Bao et al., 2006).

For analysis samples (≈10 mg) were loaded onto a stainless steel plate and loaded into a chamber and flooded with $BrF_{5(g)}$. Samples were then heated with a CO_2 laser releasing $O_{2(g)}$ from $SO_{4(s)}$ with ≈30-40% yields. Samples were then run through a series of cryo-focusing steps to remove impurities and collected onto mol-seive. Samples of pure $O_{2(g)}$ were then analyzed on a Thermo MAT-253 on dual inlet mode. Repeated measurements of inter-laboratory standards yielded a maximum uncertainty (1σ) on the entire analytical procedure to be < 0.5‰.

In the wet chemistry steps pyrite oxidation within $BaSO_4$ was not calculated to be a significant contaminant to justify removal through a chromium reduction solution as abundances of pyrite within samples was determined by microscopy (Crockford et al., 2016) to be a maximum of 0.5% in micritic phases and far less within $BaSO_4$. Although sample yields from lazing are not 100% repeated tests by Bao et al., (2008) determined no significant fractionations during this process, therefore we argue measured $\Delta^{17}O$ results are reflective of original SO_4 values.

Geological Settings

The Sete Lagoas Cap Carbonate

The post-Marinoan cap carbonate in east central Brazil is represented by the first ~35 m of the Sete Lagoas Formation, Bambuí Group, which sharply overlies Neoproterozoic glaciogenic rocks of the Jequitaí Formation (with no evidence of reworking or hiatus), Mesoproterozoic sedimentary basins, or crystalline basement rocks of the São Francisco craton (Vieira et al., 2007; Caxito et al., 2012; Alvarenga et al., 2014). The Sete Lagoas cap dolomite forms the base of a cap carbonate interval and displays unusual sedimentary features, that resemble many other post-Marinoan cap carbonate units worldwide, such as the distinguishable pale yellow to pink color of laminated and peloidal dolostones, its variable, although small average thickness (2 to 5 m), the presence of giant wave ripples, barite beds and finally the distinct negative carbon isotopic excursion with $\delta^{13}C$ values decreasing upward (-2 to -6.5‰) (Caxito et al., 2012; Alvarenga et al., 2014). These dolomites are overlain by a thicker (10 to 50 m) interval of laminated limestones containing seafloor cements (aragonite pseudomorphs and locally barites), negative $\delta^{13}C$ values and $^{87}Sr/^{86}Sr$ data constantly around 0.7074-0.7077. The Sete Lagoas cap carbonate occurs basin wide, despite the pink dolomite interval being locally absent in some cases, preserving only the 10s of meters of limestones with recurrent seafloor cements. The recently discovered late Ediacaran *Cloudina* index fossil in the middle Sete Lagoas Formation (Warren et al., 2014) suggests an unconformity separating the lower post-Marinoan cap carbonate interval from the remaining late Ediacaran Bambuí basin (Uhlein et al., 2016).

In the central part of the basin (northern Minas Gerais), the Sete Lagoas Formation outcrops above gneissic rocks of a former basement paleo-high. Its first 10 m represents the cap carbonate interval, with a 1 m-thick pale pink dolomite overlain by laminated limestones. The sampled barite levels are the first documented occurring in the Bambuí Group and are located in the last centimeters of cap dolomite. It comprises mainly thin (1 to 8 cm) and stratiform levels of white to light blue barite minerals with a pearly lustre, bladed crystal habit and high specific gravity (~4.5 g/cm^3) (Fig. S3.1). Laterally, the barite levels occur as veins and as major void-filling cement in tepee structures.

The Nyborg Cap Carbonate

The Marinoan glaciation in northern Norway is recorded in the Gaissa Basin in the Tanafjord-Varangerfjord region. This succession preserves a portion of the interglacial period (Grasdal Formation), which is separated from the overlying Marinoan diamictite (Smalfjord Formation) and Marinoan cap carbonate (Nyborg Formation) by a subglacial erosion surface (Rice et al., 2012). Owing to a lack of radiometric ages in the Gaissa Basin, this package of sedimentary rocks is interpreted to correspond the Marinoan glaciation through use of carbon isotope chemostratigraphy, and stratigraphic and sedimentological correlation (Halverson et al., 2005; Rice et al., 2012). The Nyborg Formation may be deposited either on top of the Smalfjord Formation or crystalline rocks of the Fennoscandian Shield. Barite samples collected from the Nyborg Formation were found conformably overlying the crystalline basement in lenses and horizons ranging in thickness between 1 and 30 cm. Morphology of barite units range from massive to bedded, with some outcrops exhibiting rosettes and bladed morphology.

Supplementary Tables

Table S3.1: Triple oxygen ($\Delta^{17}O_{SO4}$) data from Brazil and Finnmark (northern Norway) samples. Total analytical error on individual analyses is less than 0.05‰.

Sample Name	*Description*	$\Delta^{17}O$(‰)
PCSL-1	Sete Lagoas Fm. Brazil	-0.87
PCSL-2	Sete Lagoas Fm. Brazil	-0.80
PCSL-3	Sete Lagoas Fm. Brazil	-0.90
PCSL-4	Sete Lagoas Fm. Brazil	-0.80
PCSL-5	Sete Lagoas Fm. Brazil	-0.82
PCSL-6	Sete Lagoas Fm. Brazil	-1.05
PCSL-7	Sete Lagoas Fm. Brazil	-0.99
PCSL-8	Sete Lagoas Fm. Brazil	-0.89
PCSL-9	Sete Lagoas Fm. Brazil	-0.92
MF1505-0.5	Nyborg Fm. northern Norway	-0.41
MF1504-0.28	Nyborg Fm. northern Norway	-1.02
MF1505-0.65	Nyborg Fm. northern Norway	-0.48
MF1501-0.15	Nyborg Fm. northern Norway	-0.44

Supplementary Figures

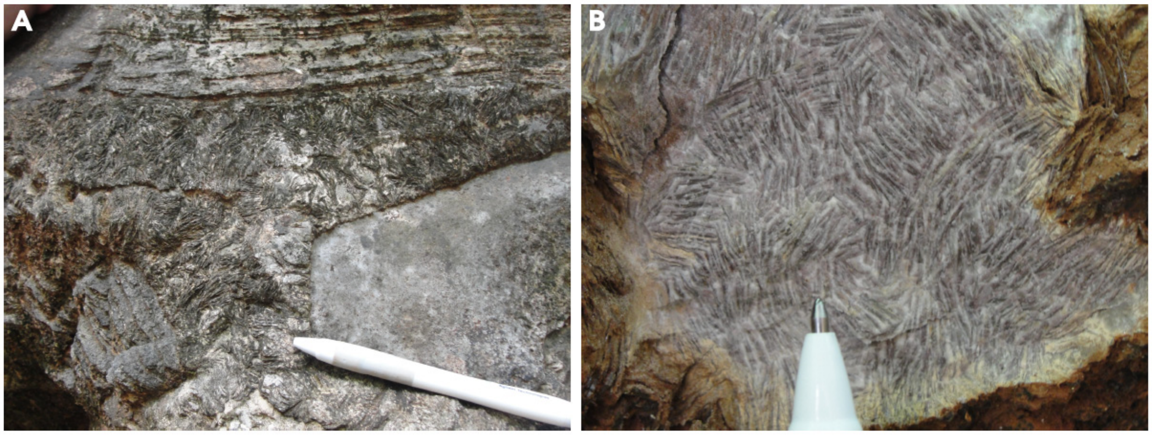

Figure S3.1: Images of barite occurrences from the Sete Lagoas Formation, Brazil.

The Nyborg Cap Carbonate

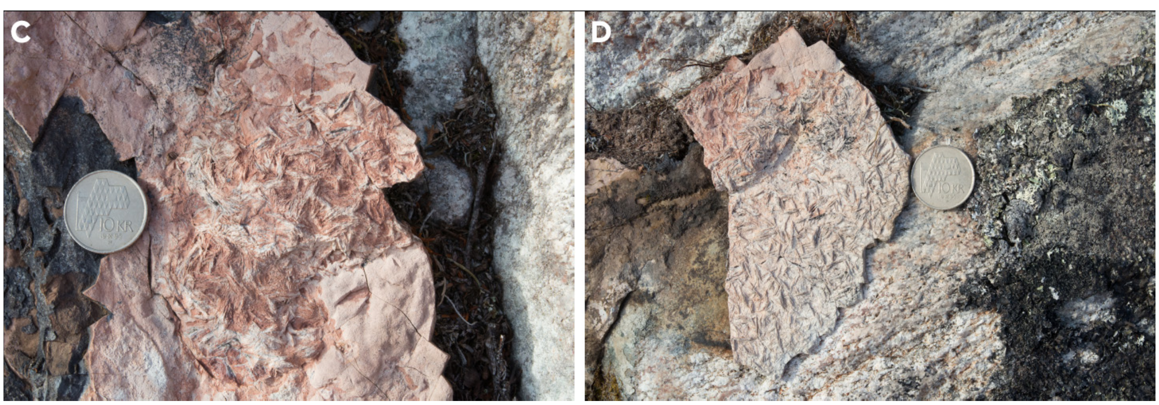

Figure S3.2: Images of barite occurrences from the Nyborg Formation, Norway.

Bibliography

Alvarenga, C.J., Santos, R.V., Vieira, L.C., Lima, B.A. and Mancini, L.H. (2014). Meso-Neoproterozoic isotope stratigraphy on carbonates platforms in the Brasilia Belt of Brazil. *Precambrian Research*, *251*, 164-180.

Bao, H. (2006). Purifying barite for oxygen isotope measurement by dissolution and reprecipitation in a chelating solution. *Analytical chemistry*, *78*(1), 304-309.

Bao, H., Lyons, J.R. and Zhou, C. (2008). Triple oxygen isotope evidence for elevated CO_2 levels after a Neoproterozoic glaciation. *Nature*, *453*(7194), 504-506.

Crockford, P.W., Cowie, B.R., Johnston, D.T., Hoffman, P.F., Sugiyama, I., Pellerin, A., Bui, T.H., Hayles, J., Halverson, G.P., Macdonald, F.A. and Wing, B.A. (2016). Triple oxygen and multiple sulfur isotope constraints on the evolution of the post-Marinoan sulfur cycle. *Earth and Planetary Science Letters*, *435*, 74-83.

de Andrade Caxito, F., Halverson, G.P., Uhlein, A., Stevenson, R., Dias, T.G. and Uhlein, G.J. (2012). Marinoan glaciation in east central Brazil. *Precambrian Research*, *200*, 38-58.

Halverson, G. P., Hoffman, P. F., Schrag, D. P., Maloof, A. C., & Rice, A. H. N. (2005). Toward a Neoproterozoic composite carbon-isotope record. *Geological Society of America Bulletin*, *117*(9-10), 1181-1207.

Rice, A. H. N., Edwards, M. B., & Hansen, T. A. (2012). Neoproterozoic glacial and associated facies in the Tanafjord-Varangerfjord area, Finnmark, North Norway. *Field Guides*, *26*, 1-83.

Uhlein, G.J., Uhlein, A., Halverson, G.P., Stevenson, R., Caxito, F.A., Cox, G.M. and Carvalho, J.F. (2016). The Carrancas Formation, Bambuí Group: A record of pre-Marinoan sedimentation on the southern São Francisco craton, Brazil. *Journal of South American Earth Sciences*, *71*, 1-16.

Vieira, L.C., Trindade, R.I., Nogueira, A.C. and Ader, M. (2007). Identification of a Sturtian cap carbonate in the Neoproterozoic Sete Lagoas carbonate platform, Bambuí Group, Brazil. *Comptes Rendus Geoscience*, *339*(3), 240-258.

Warren, L.V., Quaglio, F., Riccomini, C., Simões, M.G., Poiré, D.G., Strikis, N.M., Anelli, L.E. and Strikis, P.C. (2014). The puzzle assembled: Ediacaran guide fossil Cloudina reveals an old proto-Gondwana seaway. *Geology*, *42*(5), 391-394.

Preface to Chapter 4

Tracking the extent of life on our planet through time is essential for a basic understanding of the broad co-evolution of ecology and the oxygen and carbon cycles. But, until now, there were essentially no empirical constraints on the size of the biosphere for most of Earth's history. In this chapter we present the first empirical evidence for limited primary productivity in Earth's middle age. Although we build from observations in one time interval, our work suggests a limited amount of photosynthetic productivity through most of Earth's history, in contrast to the traditional view of relatively constant productivity though time. Specifically, we present new triple oxygen isotope ($\Delta^{17}O$) data preserved within 1.4 Ga sulfate from the Sibley Group of Ontario Canada. We report the largest $\Delta^{17}O$ depletions observed outside of the Cryogenian period. As first reported by Bao et al., (2008), these signatures have previously only been found in sulfate minerals associated with Neoproterozoic 'snowball Earth' events. In those environments, anomalous $\Delta^{17}O$ values are interpreted to reflect the high CO_2 concentrations that were required from deglaciation. However, there are no glacial deposits found within about 700 million years on either side of the samples we studied.

Building on the interpretations in the discovery paper of anomalous $\Delta^{17}O$ values in modern O_2 (first reported by Luz et al., 1999), we use the range of published estimates for CO_2 in the Mesoproterozoic to constrain gross primary production (GPP) at that time to about 2-20% of modern *GPP*. This provides a straightforward mechanism for maintaining the low O_2 levels that seem to characterize the Proterozoic. This chapter addresses a long-standing and fundamental question about the history of life on our planet. Our findings provide a critical -previously missing- piece of information about

Earth's middle ages. We demonstrate that limited primary production would be a central driver in maintaining low atmospheric O_2 levels over the Proterozoic Eon and cement the idea that the Proterozoic oxygen, carbon and nutrient cycles where fundamentally different than in the Phanerozoic or Archean.

4. Limited primary production sustained low mid-Proterozoic oxygen levels

Abstract

A protracted increase in gross primary production (*GPP*) through Earth's history has commonly been evoked. However there is no direct evidence that the global biosphere was less productive before the rise of complex eukaryotic ecosystems. Here we present a suite of triple oxygen isotope ratios ($\Delta^{17}O$) from ca. 1.4 Ga sedimentary sulfates from Ontario Canada in order to evaluate this assumption. We report the most negative $\Delta^{17}O$ values ($\Delta^{17}O$ = -1.03‰) in sulfates observed outside of the terminal Cryogenian period. We interpret this observation as a direct reflection of the balance between ancient pCO_2 and *GPP* levels imparted to 1.4 Ga tropospheric O_2. Considering current Proterozoic atmospheric pCO_2 and pO_2 estimates, the results imply that mid-Proterozoic *GPP* was likely between 2-20% of the modern biosphere and that 1.4 Ga pO_2 levels were greater than 0.4% modern. When compared to estimates of Phanerozoic *GPP* and models for Archean primary production, our results suggest that an increasingly more productive biosphere accompanied the broad secular pattern of increasing atmospheric O_2 over geologic time.

4.1 Main Text

Modern primary producers perform oxygenic photosynthesis, providing O_2 to the atmosphere and fixing carbon to fuel initial heterotrophic consumption in the global biosphere. Although Proterozoic O_2 levels are vigorously debated, multiple lines of evidence point to a low-oxygen surface environment compared to the modern (Lyons et al., 2014). In this low-oxygen world oxygenic gross primary production (*GPP*) over the mid-Proterozoic has been widely assumed to be less than *GPP* in more recent Earth history (Anbar and Knoll, 2002). This assumption is so deeply entrenched that mechanistic explanations for low-oxygen surface environments largely focus on how to limit the productivity of the mid-Proterozoic biosphere (Johnston et al., 2009; Laakso and Schrag, 2014; Sánchez-Baracaldo et al., 2014; Derry, 2015) despite the lack of direct empirical evidence for lower productivity at this time. The mid-Proterozoic biosphere may indeed have been significantly nutrient limited when compared to the modern biosphere (Reinhard et al., 2017), however proposals for sustaining the apparent environmental stasis that characterized this interval of Earth history (Brasier and Lindsay, 1998; Payne et al., 2011) would be strengthened if their key components could be validated from the geologic record. Here we examine the assumption that the mid-Proterozoic biosphere was less productive than more recent biospheres through application of the triple oxygen isotope proxy.

A record of the productivity of the biosphere is embedded within the isotopic composition of tropospheric O_2. Stratospheric photochemical reactions preferentially concentrate heavy oxygen isotopes (^{17}O, ^{18}O) in O_3, leaving residual O_2 anomalously enriched in ^{16}O and characterized by a negative $\Delta^{17}O$ value [$\Delta^{17}O$ = $ln(\delta^{17}O+1)$ –

$0.5305 \times ln(\delta^{18}O+1)$; see Supplementary Information] (Miller, 2002; Angert et al., 2003). Photochemical and modeling experiments indicate that isotopic exchange between stratospheric CO_2 and this heavy oxygen from O_3 photolysis imparts a positive $\Delta^{17}O$ value in CO_2 (Wen and Thiemens, 1993; Yung et al., 1991; Young et al., 2014). It follows from mass balance that O_2 exiting the stratosphere carries a negative $\Delta^{17}O$ value with the magnitude of this anomaly proportional to CO_2 levels (pCO_2; Luz et al., 1999; Blunier et al., 2002). This stratospheric O_2 mixes with tropospheric O_2 produced through photosynthesis that carries ^{16}O, ^{17}O, and ^{18}O in isotopically normal proportions, with a near-zero $\Delta^{17}O$ value that principally reflects the isotopic composition of source water (Luz et al., 1999; Luz and Barkan, 2010). Therefore, the $\Delta^{17}O$ value of tropospheric O_2 reflects a balance between the proportion of O_2 supplied from the stratosphere versus that derived from photosynthesis (Luz et al., 1999; Bender et al., 1994) as well as the size of the O_2 reservoir where these fluxes compete. Because photosynthetic carbon fixation is in approximate stoichiometric proportion to O_2 production, the $\Delta^{17}O$ anomaly in modern tropospheric O_2 is a direct measure of *GPP* (Luz et al., 1999). Accordingly, given independent estimates of contemporaneous CO_2 levels, ancient atmospheric $\Delta^{17}O$ signatures can provide constraints on ancient *GPP* and pO_2 levels.

Sedimentary sulfate minerals have the unique potential to preserve atmospheric oxygen in the geologic record. This is a consequence of the abiotic or biologically mediated oxidative weathering of sulfide leading to a sizeable amount (21-34 mole % abiotic (Kohl and Bao, 2012); 8-15 mole % biologically mediated (Balci et al., 2007)) of oxygen from tropospheric O_2 being incorporated into product sulfate. In addition to the proportion of sulfide oxidized by O_2 relative to other oxidants, the $\Delta^{17}O$ value of aqueous sulfate is affected by the ratio of sulfide to sulfate minerals in the source rocks undergoing oxidative weathering as well as the intensity and style of microbial sulfur cycling in the aqueous environment (Antler et al., 2013; Pellerin et al., 2015). Despite the fact that microbial sulfur cycling may completely erase the tropospheric O_2 isotopic signature in aqueous sulfate, modern marine sulfate carries a muted but resolvable negative average $\Delta^{17}O$ value (Bao et al., 2008; Cowie and Johnston, 2016; $\Delta^{17}O$ > -0.08‰) that is, in part, an expression of the $\Delta^{17}O$ value in modern tropospheric O_2[14,25] (Young et al., 2014; Barkan and Luz, 2005;≈ -0.5‰). Terrestrial sulfate-rich evaporative settings have the highest potential to sample newly formed sulfate from oxidative weathering, and therefore are likely to capture more pristine atmospheric isotope signatures than marine settings. Such environments are conducive to rapid precipitation of gypsum, anhydrite, or other sulfate salts (Hardie, 1968), and minimize the isotopic consequences of repeated cycles of microbial sulfate reduction and re-oxidation (Ryu et al., 2006). In sum, both marine and non-marine sulfate minerals can capture negative atmospheric $\Delta^{17}O$ signatures, but there is likely to be a shift to less pronounced negative values in marine settings due to more pronounced isotopic exchange with water during microbial sulfur cycling.

To search for an undiluted $\Delta^{17}O$ signature of mid-Proterozoic tropospheric O_2 we sampled drill core from the Rossport Formation of the Sibley Group in Ontario, Canada, which is comprised of lacustrine and sabkha sediments with abundant gypsum veins, and nodules and has an estimated depositional age of ca. 1.4 Ga with 1.1 Ga dykes that cross cut the sedimentary package providing an absolute minimum age (Rogala et al., 2007; see Supplementary Information). We measured the oxygen ($\Delta^{17}O$, $\delta^{18}O$) and sulfur ($\delta^{34}S$,

$\Delta^{33}S$) isotope compositions of evaporitic sulfate chemically extracted from 68 samples, and found $\Delta^{17}O$ values as negative as -1.03‰, far below the $\Delta^{17}O$ value of modern tropospheric O_2, and Phanerozoic marine sulfates (Fig. 4.1). Importantly these results by nature indicate the first near-direct sampling of mid-Proterozoic atmospheric O_2 and the minimum $\Delta^{17}O$ value provides a constraint on the size of this reservoir. The only geological examples with comparable $\Delta^{17}O$ values are those from marine barites and carbonate associated sulfate (CAS) deposited in the aftermath of the Marinoan glaciation (Bao et al., 2008; Bao et al., 2012; Crockford et al., 2016) and slightly older CAS in carbonates deposited in syn-deglacial lakes (Bao et al., 2009). The $\Delta^{17}O$ data from syn-Marinoan glacial lake carbonate-associated sulfates have a long tailed distribution that is drawn out toward the most negative $\Delta^{17}O$ values (down to ≈ -1.64‰), and correlate closely with co-measured $\delta^{34}S$ values (Fig. 4.2; see Supplementary Information; Bao et al., 2009). These characteristics reflect mixing of sulfate derived from sulfide oxidation with other sulfate sources, likely catalyzed through intense microbial sulfur cycling (Bao et al., 2009). These features are not observed in the $\Delta^{17}O$ dataset from the Sibley Group, which display a normal distribution (Fig. 4.1) with a mean of -0.68‰ and a standard deviation of 0.13‰, and only weakly correlate with co-measured $\delta^{34}S$ values (Fig. 4.2; see Supplementary Information). Further, the isotopically light $\delta^{34}S$ and negative $\Delta^{33}S$ values suggest weak microbial sulfur cycling with very limited sulfide reoxidation at the time the Sibley sulfates were deposited (Fig. 4.2). Like the post-Marinoan barites ($\Delta^{17}O_{min}$ = -0.86‰ and $\Delta^{17}O_{mean}$ = -0.41‰), the Sibley Group sulfates appear to carry a clear isotopic signal of atmospheric O_2 that is primarily modulated by the amount of O_2 incorporated into sulfate during sulfide oxidation rather than weathering and redeposition of pre-existing sulfate minerals or intense re-oxidative microbial sulfur cycling (Fig. 4.2).

Sulfate minerals with $\Delta^{17}O$ values that are far more negative than modern tropospheric O_2 must have been deposited under an atmosphere that bore little resemblance to the modern with respect to its chemistry and magnitude of fluxes into and out of the O_2 reservoir. As a result the relationship between $\Delta^{17}O$ and *GPP* cannot be calibrated using modern values (Luz et al., 1999; Blunier et al., 2002; Bao et al., 2008). In this light, isotopic mass balance calculations designed to simulate atmospheric conditions capable of generating large $\Delta^{17}O$ anomalies demonstrate that the $\Delta^{17}O$ value of tropospheric O_2 reflects three key variables: pCO_2, pO_2, and *GPP* with other control parameters (eg. troposphere-stratosphere exchange) exerting considerably less influence (Cao and Bao, 2013). Under a high *GPP* scenario, as may be the case for the immediate aftermath of the Marinoan glaciation (Kunzmann et al., 2013), ultra-high atmospheric pCO_2 (>350 Present Atmospheric Levels (PAL); 1 PAL = 280 ppm CO_2) is the only viable way to impart a significantly negative $\Delta^{17}O$ value to tropospheric O_2 (Cao and Bao, 2013; ≈ -30‰ or lower), thus confirming a key prediction of the snowball Earth theory (Kirschvink, 2002). Alternatively, similarly negative $\Delta^{17}O$ values can be generated in low pO_2 conditions where *GPP* is greatly diminished, effectively lengthening the residence time of O_2 in the atmosphere. Here we use an isotopic mass balance approach (Cao and Bao, 2013) with independent estimates for mid-Proterozoic pCO_2 and pO_2 levels in an effort to provide new constraints on the composition of the mid-Proterozoic atmosphere and productivity of the biosphere (*GPP*; see Supplementary Information).

We derive a $\Delta^{17}O$ value of 1.4 Ga tropospheric O_2 by correcting the most negative $\Delta^{17}O$ value from Sibley sulfate (-1.03‰) for the partial incorporation of atmospheric O_2 during biologically mediated sulfide oxidation (Balci et al., 2007; ≈ 8-15 mole%) that dominates natural environments in the modern (Percak-Dennett et al., 2017) and likely did so throughout the mid-Proterozoic. Again, this approach is conservative, as post-weathering processes can only remove anomalous $\Delta^{17}O$ values and cannot impart them, leading to estimates for *GPP* that are strict maximums both in modern and ancient environments. With these considerations, 1.4 Ga tropospheric O_2 had a $\Delta^{17}O$ value that was between -6.8 and -12.9‰ (cf. modern tropospheric O_2 ≈ -0.5‰; Young et al., 2014; Barkan and Luz, 2005). The CO_2 content of the atmosphere at this time was likely higher than today, given a lack of evidence for glaciation under a less luminous sun and mounting evidence that CO_2 was the predominant greenhouse gas driving mid-Proterozoic warming (Olson et al., 2016). This is consistent with estimates of mid-Proterozoic pCO_2 from geochemical proxies and climate models that when compiled together suggest pCO_2 levels between 2-30 PAL at 1.4 Ga (Mills et al., 2014; Wolf and Toon, 2014; Sheldon, 2013; see Supplementary Information). Estimates for mid-Proterozoic O_2 levels span a wider range (Planavsky et al., 2014; Cole et al., 2016; Zhang et al., 2016; Holland et al., 1989; Liu et al., 2015; Daines et al., 2017; Canfield et al., 2005; Sperling et al., 2013; Runnegar, 1991) from less than 0.001 to 0.01 PAL for inhibited Fe-Mn-Cr oxidation in terrestrial settings implied by paleosol studies and calibrations of the Cr isotope proxy (Planavsky et al., 2014; Cole et al., 2016) to less than 0.1 PAL for box models calculating the O_2 levels required to remove persistent oceanic anoxia (Canfield, 2005) that is a near-ubiquitous feature of the mid-Proterozoic marine redox record (Reinhard et al., 2013; Cox et al., 2016).

Even within this wide range of pO_2 (0.001-0.1 PAL) and pCO_2 estimates (2-30 PAL) the $\Delta^{17}O$ results reported here provide the first evidence that limited mid-Proterozoic primary production was indeed a biogeochemical reality. For example, if pO_2 was in the middle of the range of most estimates (0.01-0.04 PAL; Fig. 4.3) model solutions for $\Delta^{17}O$ values between -6.8 and -12.9‰ for tropospheric O_2 imply that mid-Proterozoic *GPP* operated between 2 and 20% of modern values (Fig. 4.3). Outside of these conditions, trade-offs take place, requiring O_2 and CO_2 inventories at the extremes of currently estimated ranges. Under a low O_2 atmosphere, (pO_2 = 0.001 PAL; Fig. 4.3) our results place mid-Proterozoic *GPP* at <<10% of the modern value. However such conditions are only achievable if CO_2 levels were extremely low (pCO_2 < 1 PAL; Fig. 4.3), providing evidence against such low pO_2 estimates. Within suggested 1.4 Ga pCO_2 estimates (2-30 PAL) the lowest pO_2 level achievable is 0.004 PAL. At the other end of the O_2 spectrum (pO_2 = 0.1 PAL), however, *GPP* values still do not reach modern values (50% modern) at 30 PAL pCO_2 (Fig. 4.3). Further the maximum pCO_2 level capable of providing values within a pO_2 range of 0.001-0.1 PAL is 53 PAL. In sum, under a broad range of independent estimates for mid-Proterozoic pCO_2 and pO_2, the negative $\Delta^{17}O$ values that may have typified mid-Proterozoic O_2 require that the 1.4 Ga biosphere was less productive than both its modern and Phanerozoic counterparts.

Our oxygen isotope measurements represent the first empirical constraint on the relative carbon fixation capacity of the mid-Proterozoic biosphere suggesting at 1.4 Ga it operated at 2-20% of modern levels. This finding represents a critical calibration point for biogeochemical hypotheses that have had to assume *GPP* levels of the mid-Proterozoic biosphere (e.g. $<10\%$ modern, Derry, 2015; $\approx 0.3\%$ modern, Laakso and Schrag, 2014), and reveal a far different oxygen cycle in operation during the mid-Proterozoic when compared to earlier and later times. Such an oxygen cycle may be reflected in the uniformly low $\delta^{13}C$ values that characterize carbonate rocks through much of the Proterozoic, potentially suggesting a weaker and static carbon cycle (Buick et al., 1995). As Archean (Kharecha et al., 2005; Canfield et al., 2006; Ward et al., 2016) and Phanerozoic (Wing et al., 2013) *GPP* estimates bookend the lower and upper limits of the range inferred here, this suggests that primary production may have progressively increased throughout Earth's history in concert with the broad two-step history of O_2 in Earth's atmosphere.

Acknowledgements

PWC acknowledges funding from an NSERC PGS-D grant and funding under Boswell A. Wing from the Natural Sciences and Engineering Research Council of Canada and the Fonds de Recherche du Québec–Nature et Technologies (FRQNT).

Figures

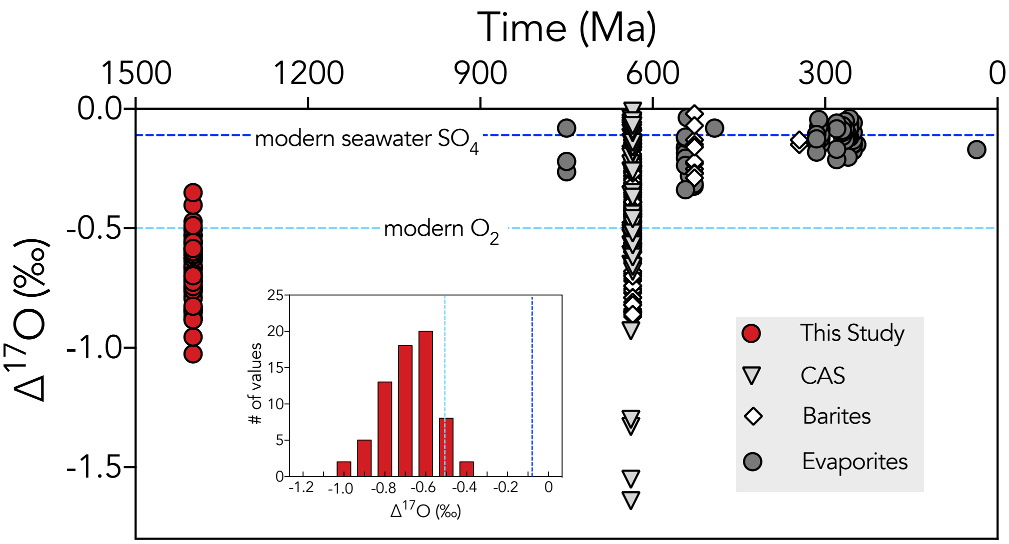

Figure 4.1. Compiled $\Delta^{17}O$ data in barites (white diamonds), carbonate-associated sulfate (CAS; grey triangles), and evaporites (grey or red circles) and new data from this study (Bao et al., 2008; Bao et al., 2012; Crockford et al., 2016; Bao et al., 2009). Analytical uncertainty on $\Delta^{17}O$ measurements (1σ) is less than 0.05‰. Results are compared to average values of modern marine sulfate (dark blue dashed line; Bao et al., 2008) and modern tropospheric O_2 $\Delta^{17}O$ values (light blue dashed line; Luz et al., 1999; Luz and Barkan, 2011). Next to new data is a histogram of values displaying the distribution of values.

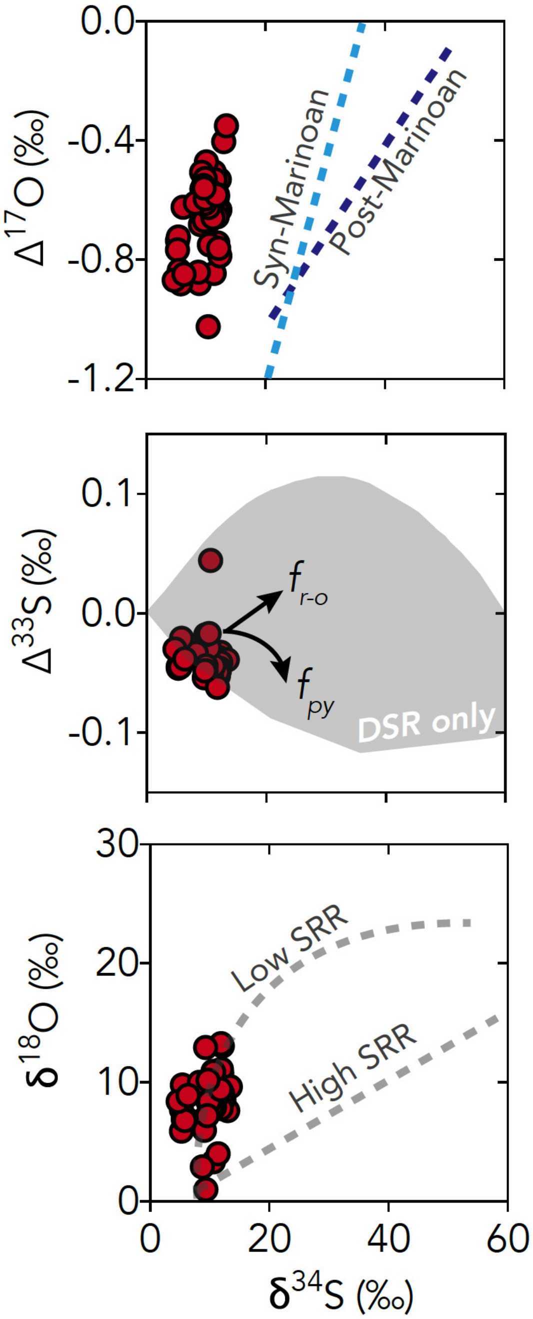

Figure 4.2. In the top panel we present $\delta^{34}S$ and $\delta^{18}O$ data against sulfate reduction rate (SRR) curves from Ref. 21 and data from this study falls along the low SRR path (Antler et al., 2013). The bottom panel presents $\delta^{34}S$ and $\Delta^{17}O$ data where only a weak correlation is observed (R^2 95% confidence = 0.084) compared to Marinoan barite (dark blue dashed line) and Marinoan CAS (light blue dashed light) cf. supplementary information. Total analytical uncertainty on $\delta^{34}S$ and $\delta^{18}O$ measurements is estimated at 0.1 and 0.5‰ respectively.

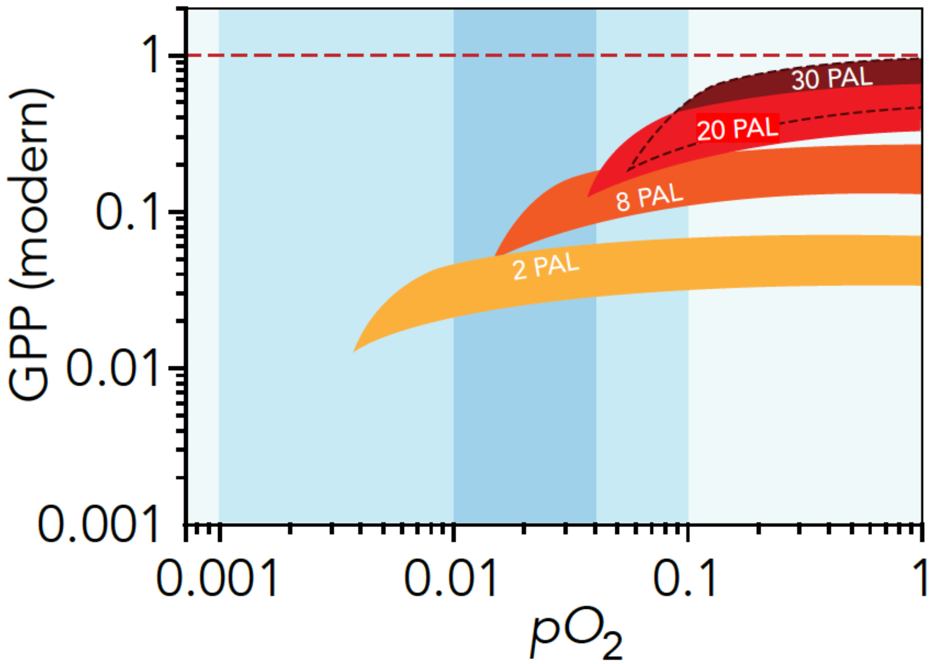

Figure 4.3. Modeling results based on $\Delta^{17}O$ values of tropospheric O_2 between -6.8 and -12.9‰. *GPP*-pO_2 solution fields are presented at different pCO_2 values relative to preindustrial levels (PAL): 30 PAL (dark red), 20 PAL (red), 8 PAL (orange) and 2 PAL (yellow). Upper bounds of solution fields represent $\Delta^{17}O$ = -6.8‰ (15% O_2 incorporation) and lower bounds represent $\Delta^{17}O$ = -12.9‰ (8% O_2 incorporation). Blue fields represent O_2 estimates with light blue represent the full span of 1.4 Ga ranges (0.001-0.1 PAL) in darker blue we present a preferred range of 0.01-0.04 PAL.

Bibliography

Anbar, A.D. and Knoll, A.H., 2002. Proterozoic ocean chemistry and evolution: a bioinorganic bridge?. *science*, *297*(5584), pp.1137-1142.

Angert, A., Rachmilevitch, S., Barkan, E. and Luz, B., 2003. Effects of photorespiration, the cytochrome pathway, and the alternative pathway on the triple isotopic composition of atmospheric O2. *Global Biogeochemical Cycles*, *17*(1).

Antler, G., Turchyn, A.V., Rennie, V., Herut, B. and Sivan, O., 2013. Coupled sulfur and oxygen isotope insight into bacterial sulfate reduction in the natural environment. *Geochimica et Cosmochimica Acta*, *118*, pp.98-117.

Balci, N., Shanks, W.C., Mayer, B. and Mandernack, K.W., 2007. Oxygen and sulfur isotope systematics of sulfate produced by bacterial and abiotic oxidation of pyrite. *Geochimica et Cosmochimica Acta*, *71*(15), pp.3796-3811.

Bao, H., Lyons, J.R. and Zhou, C., 2008. Triple oxygen isotope evidence for elevated CO2 levels after a Neoproterozoic glaciation. *Nature*, *453*(7194), p.504.

Bao, H., Chen, Z.Q. and Zhou, C., 2012. An 17 O record of late Neoproterozoic glaciation in the Kimberley region, Western Australia. *Precambrian Research*, *216*, pp.152-161.

Bao, H., Fairchild, I.J., Wynn, P.M. and Spötl, C., 2009. Stretching the envelope of past surface environments: Neoproterozoic glacial lakes from Svalbard. *Science*, *323*(5910), pp.119-122.

Barkan, E. and Luz, B., 2011. The relationships among the three stable isotopes of oxygen in air, seawater and marine photosynthesis. *Rapid communications in mass spectrometry: RCM*, *25*(16), pp.2367-2369.

Bender, M., Sowers, T. and Labeyrie, L., 1994. The Dole effect and its variations during the last 130,000 years as measured in the Vostok ice core. *Global Biogeochemical Cycles*, *8*(3), pp.363-376.

Blunier, T., Barnett, B., Bender, M.L. and Hendricks, M.B., 2002. Biological oxygen productivity during the last 60,000 years from triple oxygen isotope measurements. *Global Biogeochemical Cycles*, *16*(3).

Brasier, M.D. and Lindsay, J.F., 1998. A billion years of environmental stability and the emergence of eukaryotes: New data from northern Australia. *Geology*, *26*(6), pp.555-558.

Buick, R., Des Marais, D.J. and Knoll, A.H., 1995. Stable isotopic compositions of carbonates from the Mesoproterozoic Bangemall Group, northwestern Australia. *Chemical Geology*, *123*(1-4), pp.153-171.

Canfield, D.E., 2005. The early history of atmospheric oxygen: homage to Robert M. Garrels. *Annu. Rev. Earth Planet. Sci.*, *33*, pp.1-36.

Canfield, D.E., Rosing, M.T. and Bjerrum, C., 2006. Early anaerobic metabolisms. *Philosophical Transactions of the Royal Society of London B: Biological Sciences*, *361*(1474), pp.1819-1836.

Cao, X. and Bao, H., 2013. Dynamic model constraints on oxygen-17 depletion in atmospheric O2 after a snowball Earth. *Proceedings of the National Academy of Sciences*, *110*(36), pp.14546-14550.

Cole, D.B., Reinhard, C.T., Wang, X., Gueguen, B., Halverson, G.P., Gibson, T., Hodgskiss, M.S., McKenzie, N.R., Lyons, T.W. and Planavsky, N.J., 2016. A shale-hosted Cr isotope record of low atmospheric oxygen during the Proterozoic. *Geology*, *44*(7), pp.555-558.

Cowie, B.R. and Johnston, D.T., 2016. High-precision measurement and standard calibration of triple oxygen isotopic compositions ($\delta^{18}O$, $\Delta'^{17}O$) of sulfate by F_2 laser fluorination. *Chemical Geology*, *440*, pp.50-59.

Cox, G.M., Jarrett, A., Edwards, D., Crockford, P.W., Halverson, G.P., Collins, A.S., Poirier, A. and Li, Z.X., 2016. Basin redox and primary productivity within the Mesoproterozoic Roper Seaway. *Chemical Geology*, *440*, pp.101-114.

Crockford, P.W., Cowie, B.R., Johnston, D.T., Hoffman, P.F., Sugiyama, I., Pellerin, A., Bui, T.H., Hayles, J., Halverson, G.P., Macdonald, F.A. and Wing, B.A., 2016. Triple oxygen and multiple sulfur isotope constraints on the evolution of the post-Marinoan sulfur cycle. *Earth and Planetary Science Letters*, *435*, pp.74-83.

Daines, S.J., Mills, B.J. and Lenton, T.M., 2017. Atmospheric oxygen regulation at low Proterozoic levels by incomplete oxidative weathering of sedimentary organic carbon. *Nature Communications*, *8*, p.14379.

Derry, L.A., 2015. Causes and consequences of mid-Proterozoic anoxia. *Geophysical Research Letters*, *42*(20), pp.8538-8546.

Hardie, L.A., 1968. The origin of the Recent non-marine evaporite deposit of Saline Valley, Inyo County, California. *Geochimica et Cosmochimica Acta*, *32*(12), pp.1279-1301.

Holland, H.D., Feakes, C.R. and Zbinden, E.A., 1989. The Flin Flon paleosol and the composition of the atmosphere 1.8 BYBP. *American Journal of Science*, *289*(4), pp.362-389.

Johnston, D.T., Wolfe-Simon, F., Pearson, A. and Knoll, A.H., 2009. Anoxygenic photosynthesis modulated Proterozoic oxygen and sustained Earth's middle age. *Proceedings of the National Academy of Sciences*, *106*(40), pp.16925-16929.

Kharecha, P., Kasting, J. and Siefert, J., 2005. A coupled atmosphere–ecosystem model of the early Archean Earth. *Geobiology*, *3*(2), pp.53-76.

Kirschvink, J.L., 1992. Late Proterozoic low-latitude global glaciation: the snowball Earth.

Kohl, I. and Bao, H., 2011. Triple-oxygen-isotope determination of molecular oxygen incorporation in sulfate produced during abiotic pyrite oxidation (pH= 2–11). *Geochimica et Cosmochimica Acta*, *75*(7), pp.1785-1798.

Kunzmann, M., Halverson, G.P., Sossi, P.A., Raub, T.D., Payne, J.L. and Kirby, J., 2013. Zn isotope evidence for immediate resumption of primary productivity after snowball Earth. *Geology*, *41*(1), pp.27-30.

Laakso, T.A. and Schrag, D.P., 2014. Regulation of atmospheric oxygen during the Proterozoic. *Earth and Planetary Science Letters*, *388*, pp.81-91.

Liu, X.M., Kah, L.C., Knoll, A.H., Cui, H., Kaufman, A.J., Shahar, A. and Hazen, R.M., 2015. Tracing Earth's O_2 evolution using Zn/Fe ratios in marine carbonates.

Luz, B., Barkan, E., Bender, M.L., Thiemens, M.H. and Boering, K.A., 1999. Triple-isotope composition of atmospheric oxygen as a tracer of biosphere productivity. *Nature*, *400*(6744), p.547.

Luz, B. and Barkan, E., 2010. Variations of 17 O/16 O and 18 O/16 O in meteoric waters. *Geochimica et Cosmochimica Acta*, *74*(22), pp.6276-6286.

Lyons, T.W., Reinhard, C.T. and Planavsky, N.J., 2014. The rise of oxygen in Earth's early ocean and atmosphere. *Nature*, *506*(7488), pp.307-315.

Miller, M.F., 2002. Isotopic fractionation and the quantification of 17 O anomalies in the oxygen three-isotope system: an appraisal and geochemical significance. *Geochimica et Cosmochimica Acta*, *66*(11), pp.1881-1889.

Mills, B., Lenton, T.M. and Watson, A.J., 2014. Proterozoic oxygen rise linked to shifting balance between seafloor and terrestrial weathering. *Proceedings of the National Academy of Sciences*, *111*(25), pp.9073-9078.

Olson, S.L., Reinhard, C.T. and Lyons, T.W., 2016. Limited role for methane in the mid-Proterozoic greenhouse. *Proceedings of the National Academy of Sciences*, *113*(41), pp.11447-11452.

Payne, J.L., McClain, C.R., Boyer, A.G., Brown, J.H., Finnegan, S., Kowalewski, M., Krause, R.A., Lyons, S.K., McShea, D.W., Novack-Gottshall, P.M. and Smith, F.A., 2011. The evolutionary consequences of oxygenic photosynthesis: a body size perspective. *Photosynthesis research*, *107*(1), pp.37-57.

Pellerin, A., Bui, T.H., Rough, M., Mucci, A., Canfield, D.E. and Wing, B.A., 2015. Mass-dependent sulfur isotope fractionation during reoxidative sulfur cycling: A case study from Mangrove Lake, Bermuda. *Geochimica et Cosmochimica Acta*, *149*, pp.152-164.

Percak-Dennett, E., He, S., Converse, B., Konishi, H., Xu, H., Corcoran, A., Noguera, D., Chan, C., Bhattacharyya, A., Borch, T. and Boyd, E., 2017. Microbial acceleration of aerobic pyrite oxidation at circumneutral pH. *Geobiology*.

Planavsky, N.J., Reinhard, C.T., Wang, X., Thomson, D., McGoldrick, P., Rainbird, R.H., Johnson, T., Fischer, W.W. and Lyons, T.W., 2014. Low Mid-Proterozoic atmospheric oxygen levels and the delayed rise of animals. *Science*, *346*(6209), pp.635-638.

Reinhard, C.T., Planavsky, N.J., Robbins, L.J., Partin, C.A., Gill, B.C., Lalonde, S.V., Bekker, A., Konhauser, K.O. and Lyons, T.W., 2013. Proterozoic ocean redox and biogeochemical stasis. *Proceedings of the National Academy of Sciences*, *110*(14), pp.5357-5362.

Reinhard, C.T., Planavsky, N.J., Gill, B.C., Ozaki, K., Robbins, L.J., Lyons, T.W., Fischer, W.W., Wang, C., Cole, D.B. and Konhauser, K.O., 2017. Evolution of the global phosphorus cycle. *Nature*, *541*(7637), pp.386-389.

Rogala, B., Fralick, P.W., Heaman, L.M. and Metsaranta, R., 2007. Lithostratigraphy and chemostratigraphy of the Mesoproterozoic Sibley Group, northwestern Ontario, Canada. *Canadian Journal of Earth Sciences*, *44*(8), pp.1131-1149.

Runnegar, B., 1991. Precambrian oxygen levels estimated from the biochemistry and physiology of early eukaryotes. *Global and Planetary Change*, *5*(1-2), pp. 97-111.

Ryu, J.H., Zierenberg, R.A., Dahlgren, R.A. and Gao, S., 2006. Sulfur biogeochemistry and isotopic fractionation in shallow groundwater and sediments of Owens Dry Lake, California. *Chemical geology*, *229*(4), pp.257-272.

Sánchez-Baracaldo, P., Ridgwell, A. and Raven, J.A., 2014. A neoproterozoic transition in the marine nitrogen cycle. *Current Biology*, *24*(6), pp.652-657.

Sheldon, N.D., 2013. Causes and consequences of low atmospheric pCO_2 in the Late Mesoproterozoic. *Chemical Geology*, *362*, pp.224-231.

Sperling, E.A., Halverson, G.P., Knoll, A.H., Macdonald, F.A. and Johnston, D.T., 2013. A basin redox transect at the dawn of animal life. *Earth and Planetary Science Letters*, *371*, pp.143-155.

Ward, L.M., Kirschvink, J.L. and Fischer, W.W., 2016. Timescales of oxygenation following the evolution of oxygenic photosynthesis. *Origins of Life and Evolution of Biospheres*, *46*(1), pp.51-65.

Wen, J. and Thiemens, M.H., 1993. Multi-isotope study of the O (1 D)+ CO2 exchange and stratospheric consequences. *Journal of Geophysical Research: Atmospheres*, *98*(D7), pp.12801-12808.

Wing, B.A., 2013. A cold, hard look at ancient oxygen. *Proceedings of the National Academy of Sciences*, *110*(36), pp.14514-14515.

Wolf, E.T. and Toon, O.B., 2014. Controls on the Archean climate system investigated with a global climate model. *Astrobiology*, *14*(3), pp.241-253.

Yung, Y.L., DeMore, W.B. and Pinto, J.P., 1991. Isotopic exchange between carbon dioxide and ozone via O (1D) in the stratosphere. *Geophysical Research Letters*, *18*(1), pp.13-16.

Young, E.D., Yeung, L.Y. and Kohl, I.E., 2014. On the Δ 17 O budget of atmospheric O 2. *Geochimica et Cosmochimica Acta*, *135*, pp.102-125.

Zhang, S., Wang, X., Wang, H., Bjerrum, C.J., Hammarlund, E.U., Costa, M.M., Connelly, J.N., Zhang, B., Su, J. and Canfield, D.E., 2016. Sufficient oxygen for animal respiration 1,400 million years ago. *Proceedings of the National Academy of Sciences*, *113*(7), pp.1731-1736.

4.2 Supplementary Information

Materials and Methods

Sample Location

Sediments of the Sibley Group were deposited over an ≈ 70,000 km^2 area that extends into northern Lake Superior, and to the margins of Lake Nipigon in Ontario, Canada (Fig. S4.1). While the surface expression of the Sibley Group is typically as subcrop, extensive mineral exploration in the area has provided kilometers of drill core, which this study is reliant upon. For this study 68 samples were collected from three different drill cores: NI-92-7 (located at (UTM) east 353850, north 5443000), NB-97-2 (east 426990 north 5416241), NB-97-4 (east 425430 north 5410540) and WP-07-03.

Age Constraints

Maximum age constraints for the entire Sibley Group are provided by rhyolites that unconformably underlie the Sibley Group with a U-Pb age of 1530.5 +/- 6.2 Ma (Davis and Sutcliffe, 1985). A minimum age is constrained by cross-cutting diabase sills dated at 1109.7 +/- 2 Ma (Davis and Sutcliffe, 1985). The only age measured on Sibley Group material is provided by a whole-rock Rb-Sr isochron that gave a calculated minimum age of 1339 +/- 33 Ma for the Kama Hill Formation shales (Franklin, 1978). Paleomagnetic pole positions for the Sibley Group (Robertson, 1973), however, place these units at the same location of the apparent wander path as the 1.4 Ga Belt Supergroup (Elston et al., 2002).

Depositional Setting

Gypsum nodules used in this study were taken from the Firehill member of the Rossport Formation, which was deposited between the fluvial to near shore lacustrine sandstones and conglomerates of the Pass Lake Formation and saline mud-flats of the Kama Hill Formation (Rogala, et al., 2007), of the Sibley Group. The Rossport Formation is subdivided into three members beginning with the Channel Island Member at the base (Cheadle, 1986). The Channel Island Member is characterized by cyclic siltstone-dolostone couplets with evaporite minerals preferentially being deposited in dolostone layers as nodules and bladed crystals (Metsaranta, 2006). The Channel Island Member contains massive beds of sandstone near its top and is overlain by the Middlebrun Bay Member (Cheadle, 1986). This 0.5-3m thick, stromatolitic dolostone-chert represents the shoreline of the saline lake (Rogala et al., 2007). The Middlebrun Bay Member is overlain by the Firehill Member, which consists of massive to finely laminated red siltstones with sporadic intraformational, mass-flow conglomerate beds. Deposition occurred on mud- and sand-flats with a near-surface, saline water table (Rogala et al., 2007; Metsaranta, 2006). Sulfate minerals throughout the Firehill Member have been observed to occur as nodules, bladed crystals, veins, cements and detrital grains, however this study's sample set only consisted of nodules. The Firehill Member is terminated by the appearance of ripple marks and hummocky cross-bedded sandstones and mudstones of the Kama Hill Formation marking transgression of a large water-mass. Together these observations have shaped the view that the Pass Lake and Rossport Formations of the Sibley Group were deposited in predominantly fluvio-lacustrine and sabkha settings.

Although, a sabkha setting has been inferred, additional work is needed to constrain the influence of marine waters on the system.

Δ^{17}O Measurements

For complete methods see Bao et al., (2008) and Crockford et al., (2016). Drill core samples with abundant gypsum nodules were selected for oxygen isotope analyses. After a thin layer of material was removed from the outer surface, samples were drilled to collect ≈30 mg for pre-treatment. Sulfate samples were first dissolved into a 0.1 M sodium hydroxide – 0.05 M diethylenetriaminepentaacetic acid (DTPA) solution to extract sulfate into solution and remove any non-sulfate oxygen-bearing species Bao, 2006). The extracted sulfate samples were then reprecipitated at 80˚C by acidifying with double distilled 6 M hydrochloric acid followed by the addition of drops of concentrated barium chloride solution. This dissolution and reprecipitation was repeated to further eliminate possible contaminations. Approximately 10 mg of each sample was then loaded onto a 316L stainless steel plate and placed under a bromine pentafluoride (BrF_5) atmosphere for 12 hours to eliminate any water from samples. Oxygen was generated from the samples using a CO_2-laser fluorination system. Approximately 25 µmol of O_2 gas was generated (25-35% yield) for each sample although this process is not observed to induce any isotopic fractionation for Δ^{17}O values due to the high temperatures of lazing. Although yields are comparatively low for BrF_5 fluorination/infrared lazing, compared to Ni-bomb fluorination, previous comparisons have found consistent isotopic results between theses methods (Bao and Thiemens, 2000). Samples of O_2 from the fluorination process were then taken through a number of cryo-focusing steps to remove condensable gases followed by collection onto 5A mol-seive at -196 ˚C. Triple oxygen isotope measurements were conducted on a Thermo MAT 253 in dual-inlet mode with a total estimated analytical uncertainty (1σ) of 0.05‰ on individual measurements of $\Delta^{17}O$ (Tables S4.1 and S4.2; Fig. S4.2).

Calculations of final $\Delta^{17}O$ values were conducted as follows:

$$\Delta^{17}O = \delta'^{17}O - 0.5305 \times \delta'^{18}O$$

where 0.5305 represents the high temperature limit of θ for oxygen isotope fractionation (Matsuhisa et al., 1978; Cao and Liu, 2011; Bao et al., 2016),

$$\delta'^{17,18}O = \ln({}^{17,18}R_{sample}/{}^{17,18}R_{SMOW})$$

where "R" = $^{17,18}O/^{16}O$.

The above equations can be rearranged forming:

$$\Delta^{17}O = ln(\delta^{17}O+1) - 0.5305 \times ln(\delta^{18}O+1)$$

calculations in this form are preferred to the common ($\Delta^{17}O = \delta^{17}O - 0.5305 \times \delta^{18}O$) definition that linearly approximates mass independent oxygen isotope fractionation and is highly dependent on the reference material used (Miller, 2002; Angert et al., 2003).

δ^{18}O Measurements

Since laser-fluorination techniques induce a fractionation in the δ^{18}O value of sulfates, we combusted samples and measured the major oxygen isotope composition as CO_2 (Cowie and Johnston, 2016). Measurements for δ^{18}O values were made on the same aliquots of sample used for Δ^{17}O analysis that underwent the DTPA – reprecipitation treatment. Analyses were performed using a Temperature Conversion Elemental Analyzer (TCEA) connected to a Conflo-III and measured the same MAT-253 as CO in continuous-flow mode. The estimated total analytical error for δ^{18}O analyses from repeated measurements of laboratory standards is 0.5‰ (Bao et al., 2009).

δ^{34}S Measurements

Sulfur isotope measurements were made on samples after they underwent DTPA – reprecipitation treatment for oxygen isotope analysis. Approximately 10 mg of barite powder was reacted with 15 mL of Thode reduction solution at 100˚ C for at least 2 hours (Thode et al., 1961). Powders reacted to produce H_2S that was carried through a condenser in a N_2 gas stream and bubbled into a 0.4 M zinc acetate solution converting H_2S into ZnS. Samples were then reacted with drops of 0.2 M $AgNO_3$ solution to covert ZnS to Ag_2S. Samples were then filtered, collected and dried for 12 hours. 3 mg aliquots of dried samples were then loaded into nickel bombs and heated to 250 ˚C for 12 hours under a fluorine gas atmosphere in order to generate SF_6 gas for analysis. Generated SF_6 gas was purified through a vacuum line, which included a gas chromatograph before analysis on a MAT-253 set in dual-inlet mode. Results were calculated with international reference material IAEA-S-1 that has a defined $\delta^{34}S$ value of -0.3‰ value. The estimated (1σ) total analytical uncertainty on the entire procedure is estimated to be better than 0.1‰ for $\delta^{34}S$ and 0.01‰ for $\Delta^{33}S$ (Table S1).

Calculations of final $\delta^{34}S$ values were conducted as follows:

$$\delta^{34}S = ([^{34}R_{sample}/^{34}R_{V\text{-}CDT}] - 1) \times 1000$$

where $^{34}R = ^{34}S/^{32}S$, and V-CDT represents the Vienna Canon Diablo Troilite scale. Calculations of final $\Delta^{33}S$ values were conducted as follows:

$$\Delta^{33}S = \delta^{34}S - 1000 \times ([1+ (\delta^{33}S/1000)]^{0.515} -1)$$

Covariation of isotopic data

In figure S4.2 we present cross plots of $\Delta^{17}O$-$\delta^{18}O$, $\delta^{18}O$-$\delta^{34}S$, and $\Delta^{17}O$-$\delta^{34}S$ data. Performing a linear regression analysis on these data sets it is observed that significant correlations are observed for $\Delta^{17}O$-$\delta^{18}O$ and $\Delta^{17}O$-$\delta^{34}S$ data but not for $\Delta^{17}O$-$\delta^{18}O$ and $\Delta^{33}S$- $\delta^{34}S$ data (Table S2). Although $\Delta^{17}O$-$\delta^{18}O$ and $\Delta^{17}O$-$\delta^{34}S$ pass a significance test (P value > 0.05), R^2 values are significantly less than correlations observed in $\Delta^{17}O$-$\delta^{34}S$ data from syn and post-Marinoan sulfates (Crockford et al., 2016; Bao et al., 2009; Table S4.2).

Comparison between Phanerozoic and Cryogenian datasets

In figure S4.3 we present histograms of $\Delta^{17}O$ values of sulfate from Phanerozoic samples (Bao et al., 2008), Marinoan-aged barites (Bao et al., 2008; Peng et al., 2011; Killingsworth et al., 2013; Crockford et al., 2016;, Marinoan-aged CAS (Bao et al., 2009; 2012), and results from this study.

Stratigraphic Variation

In order to assess secular variations in the isotopic composition of sulfate minerals from the Sibley Group we measured a set of samples from core NI-92-7 (Fig. S4.4). The abundance of sulfates within this core provided ≈10 m resolution to this sample set. Within this subset of samples there are not obvious coherent trends observed in isotopic systems measured. Such a stratigraphic distribution suggests competing processes in generating the isotopic values within sulfate minerals across the basin.

Model Description

Accounting for variations in primary production, pCO_2, pO_2, and O_2 residence time when interpreting $\Delta^{17}O$ data, requires consideration of important processes that may impact results under a wide range of possible Proterozoic atmospheric conditions (Cao and Bao, 2013). We applied a dynamic 4-box biosphere-atmosphere model put forward in ref. 32 at steady state. Under this framework, with $\Delta^{17}O$ results under different pO_2, pCO_2, and O_2 residence times, *GPP* solutions become achievable. Below we describe the accounting of parameters to calculate solutions consistent with $\Delta^{17}O$ results from this study.

First the difference in stratospheric $\Delta^{17}O$ values between O_2 and CO_2 ($\Delta^{17}O_{STR-CO2-O2}$) at steady state in the O_2-O_3-CO_2 photochemical reaction system, has been shown to vary with changing ratios of pO_2 to pCO_2. This $\Delta^{17}O_{CO2-O2}$ relationship has been determined experimentally and here we apply these results (Shaheen et al., 2007), following Cao and Bao, (2013). The ratio of pO_2 to pCO_2, will not only impact $\Delta^{17}O_{STR-CO2-O2}$ but also $\Delta^{17}O$ values of tropospheric O_2, as this variable will both dictate the magnitude of the stratospheric $\Delta^{17}O$ anomaly, but the expression and lifetime of this in the troposphere. Next we consider the proportion of total O_2 in the atmosphere that is exchanged between the stratosphere and the troposphere ($O_{2(STR-TROP)}$) and rely on studies of the modern atmosphere, and apply this as a constant (0.1321; Appenzeller et al., 1996; Trenberth and Smith, 2005). Finally we consider the mixing efficiency of the stratosphere ($O_{2(MIX)}$), where again this has been determined experimentally through reproducing the $\Delta^{17}O$ of modern atmospheric O_2 under modern atmospheric conditions providing a value of 0.017 (Cao and Bao, 2013). It is important to note that variables $O_{2(MIX)}$ and $O_{2(STR-TROP)}$, are strongly dependent on Brewer-Dobson circulation and it is far beyond the scope of this work to speculate how this may have changed under a Proterozoic atmospheric regime. It has been shown through sensitivity tests of $O_{2(MIX)}$ and $O_{2(STR-TROP)}$ by Cao and Bao, (2013) and earlier modeling work (Butchart et al., 2006) however that variations of $O_{2(MIX)}$ and $O_{2(STR-TROP)}$ in response to elevated pCO_2 conditions will only impact the Brewer-Dobson circulation within a factor of one and further concluded that elevated pCO_2 or reduced primary production remains the dominant driver of $\Delta^{17}O$ anomalies in the troposphere (Cao and Bao, 2013). We account for the above variables assuming steady state through Eq. 1 (Cao and Bao, 2013).

(1) $\Delta^{17}O_{O2} = -\Phi(\rho)\gamma\Theta\tau /1+\rho+ \gamma\Theta\tau$

Parameter Values

pCO_2:

Constraining *p*CO_2 levels beyond the ice-core record remains an enormous challenge. To date explorations into the Proterozoic have utilized both modeling and geochemical approaches to constrain *p*CO_2 levels (Fig. S4.5). Initial modeling work utilized 1-D radiative convective modeling and calculated required *p*CO_2 levels to maintain Earth surface temperatures of 273˚K and 288˚K. Under this approach broad upper and lower limits can be place on 1.4 Ga CO_2 levels of 1 and 100 PAL respectively (Fig. S4.5; von Paris, 2008). Given that modern mean surface temperature is substantially higher than 273˚K and includes large polar icesheets, such a lower limit seems unreasonable. A further accounting of transport process through extrapolation of results from the CAM3 GCM model refines these values considerably for 288˚K where a pure CO_2 atmosphere provides an upper bound of ≈ 30 PAL and an atmosphere including 1 PAL N_2 and 10^{-4} Bar of methane providing a lower bound of ≈ 5 PAL *p*CO_2 when extrapolated to 1.4 Ga (Fig. S4.5; Wolf and Toon, 2014). These ranges are consistent with results from the COPSE Earth System model that put forward a 1.4 Ga *p*CO_2 range of 8-20 PAL (Fig. S4.5; Mills et al., 2014) Geochemical approaches have also been burdened with a high degree of uncertainty in constraining Proterozoic CO_2 levels. A singular previous study attempted to constrain 1.4 Ga *p*CO_2 levels by relating isotopic fractionations between organic matter and carbonates in microfossils to extracellular CO_2 levels (Kaufman and Xiao, 2003). While theoretically possible, such estimates remain poorly calibrated in the laboratory, particularly at high CO_2 levels suggested through results. Further the fidelity of such archives remains under-explored, therefore we do not include the suggested 10-200 PAL range put forward. Further geochemical evidence has related the variation in silicate weathering in response to different pCO_2 levels in profiles of 1.8 (pCO_2 = 45 PAL) and 1.1 (pCO_2 = 1 PAL) Ga paleosols and suggests pCO_2 levels were between ≈ 2-20 PAL when extrapolated to 1.4 Ga (Sheldon, 2013). A lower bound of 2 PAL approximates the CO_2 threshold (350-550 ppm) thought to maintain an ice-sheet free Paleogene Earth (Fig. S4.5; Hansen et al., 2008). In concert Results from all of these works suggest 1.4 Ga CO_2 levels were likely less than 30 PAL using GCM results from a pure CO_2 atmosphere as an upper limit (Wolf and Toon, 2014), and that CO_2 levels were likely greater than 2 PAL utilizing lower paleosol estimates (Fig. S4.5; Sheldon, 2013).

pO_2:

Like pCO_2, estimates of Proterozoic pO_2 have been approached using very different methodologies and logic, but can broadly be placed into three categories: box model calculations, geochemical measurements, and O_2 requirements of hypothesized biospheres (Fig. S4.6). Initial biological constraints were provided by calculated O_2 requirements for *Grypiania Spiralis* and suggested to be between 0.01-0.1 PAL pO_2 (Runnegar, 1991). Lower estimates have been brought down considerably in recent years however, with calculations based on requirements of simple bilaterians, and minimum requirements of sponges grown in the laboratory to ≈ 0.0015 and 0.004 PAL respectively

(Fig. S4.6; Sperling et al., 2013; Mills et al., 2014b. Implicit in invoking these estimates is that O_2 levels greater than this would have permitted the evolution of these organisms and that their existence would be preserved in the geologic record, however it is important to note that this greatly over simplifies our understanding of the link between environmental oxygen concentrations and the evolution of metabolically active forms of life. Complementing these biologically based estimates, are various geochemical proxies with initial studies based on mineral stability within paleosols marked by Fe loss estimating mid-Proterozoic O_2 levels were greater than 0.01 PAL (Holland et al., 1989). Consistent with paleosol estimates is recent work however, exploiting the kinetics involved in oxidizing terrestrial Mn or Fe and tracking this through the isotopic composition of Cr through the mid-Proterozoic sedimentary record have provided a threshold estimate of mid-Proterozoic pO_2 at < 0.01-0.001 PAL, with evidence for pO_2 levels above this only appearing after 1.2 – 0.8 Ga (Fig. S4.6; Planavsky et al., 2014; Cole et al., 2016). Recently trace metal enrichments and biomarkers in 1.4 Ga shales have been used as evidence for pO_2 levels > 0.04 PAL (Zhang et al., 2016). However some have considered these results highly controversial raising concerns about the primary nature of reported biomarkers as well as trace element signatures falling within a range characteristic of modern detrital sediments Planavsky et al., 2016). These estimates are consistent with a broad estimate given through tracking Zn/Fe ratios of carbonates over the latter 3.5 billion years of Earth history that place pO_2 at less than 0.06 PAL over the mid-Proterozoic (Liu et al., 2016) although assumptions about several poorly constrained variables are embedded in these estimates. Modeling studies have added to this debate suggesting mid-Proterozoic pO_2 must be less than 0.1 PAL to be consistent with no evidence for persistent fully oxygenated oceans in preserved marine sediments (Canfield, 2005; Reinhard et al., 2013; Cox et al., 2016). While all of these studies in concert speak to reduced pO_2 in the mid-Proterozoic compared to later chapters in Earth history (Fig. S4.6). As there is yet to be a clear consensus on specific mid-Proterozoic pO_2 levels we remain largely agnostic to previous estimates, but feel confident in applying a 0.1 PAL upper limit, and treat pO_2 levels as a free parameter in exploring mid-Proterozoic *GPP*.

GPP:

For this study we approximate gross primary production (*GPP*) as the gross oxygen flux from the biosphere to the troposphere. Estimates of *GPP* through deep time have typically relied upon arguments suggesting earlier Earth's would be less hospitable to life. Archean estimates have relied upon identifying what metabolisms likely existed and calculating how much energy could be supplied to ecosystems based on them (Kharecha, et al., 2005; Canfield et al., 2006; Ward et al., 2016). While the Proterozoic may have indeed been significantly nutrient limited compared to the modern (Anbar and Knoll, 2002), providing empirical estimates has not yet been possible. Here we treat *GPP* as a free parameter and attempt to calculate potential *GPP* levels under hypothesized atmospheric regimes.

f_{O2}:

The amount of atmospheric oxygen that is incorporated into product sulfate during pyrite oxidation (f_{O2}) underlies much of the uncertainty when utilizing the $\Delta^{17}O$ to explore ancient environments. Two laboratory studies (Balci et al., 2007; Kohl and Bao, 2011) have attempted to quantify different pathways of pyrite oxidation and the proportion of O_2 incorporated into product sulfate. Initial experiments explored both biologically and abiologically mediated pyrite oxidation. In experiments with *A. Ferrooxidans* it was determined that between 8 and 15% of oxygen in product sulfate was from atmospheric oxygen (Balci et al., 2007). In abiotic experiments it was determined that 13% of oxygen in product sulfate was from atmospheric oxygen (Balci et al., 2007). Both experiments were conducted at low pH values between 2.2-3 (Balci et al., 2007). In a second study abiotic experiments were conducted over a much broader pH range and O_2 incorporation into sulfate during pyrite oxidation was determined utilizing both major ($\delta^{18}O$) and minor ($\Delta^{17}O$) oxygen isotopes (Kohl and Bao, 2011). In these experiments a broader pH range was explored with values between 2-11. In these experiments it was determined that between 21-34% of oxygen in sulfate was sourced from atmospheric oxygen (Kohl and Bao, 2011). While it remains difficult to determine the proportion of oxygen within sulfate that is sourced from H_2O and O_2 the range provided by these previous studies provides a conservative range of f_{O2} to explore ancient $\Delta^{17}O$ signals between 8-34%. This range can be refined however given the different kinetics involved in abiotic versus biologically mediated pyrite oxidation. Experiments and natural observations have shown that biologically mediated pyrite oxidation can dramatically increase reaction kinetics and therefore is more likely to dominate natural surface environments both at present and in the past (Nordstrom, 1982; Percak-Dennett et al., 2017). Plotting existing modern measurements of marine and terrestrial sulfate as well as Messinian-aged evaporites largely agrees with these previous observations with most modern marine sulfate (Bao et al., 2008; Cowie and Johnston, 2016; Bao and Thiemens, 2000) and most terrestrial sulfates plotting between -0.09 - -0.04‰ (Bao et al., 2008; Fig. S4.7). For terrestrial sulfates, which should be analogous to samples used in this study, only one location appears to have incorporated much more oxygen during pyrite oxidation. This sample however was taken from a volcanic environment however and is not analogous to an ancient terrestrial lake setting. Therefore in this study we assume 8-15% O_2 incorporation during pyrite oxidation when calculating $\Delta^{17}O_{O2}$. Any subsequent processes either abiological or biological will dilute atmospheric signals after initial oxidation, and therefore greatly reduce f_{O2} values and by consequence extrapolate to much more negative $\Delta^{17}O_{O2}$ values.

$\Phi(\rho)$:

Underlying the model utilized in this study is previously conducted photochemical experiments that calibrate the difference in the $\Delta^{17}O$ value of CO_2 from the $\Delta^{17}O$ value of O_2 (Shaheen et al., 2007). In these experiments pO_2/pCO_2 ratios were held between 0.2 and 100, and conducted within reactors between 0.2 – 2 L (Shaheen et al., 2007). Results from this study allow for the calculation of the difference in $\delta^{18}O$ of CO_2 from the $\delta^{18}O$ of O_2 through the following equation:

(2) $\delta^{18}O_{CO2-O2} = (X_l + X_h(\rho/\rho0))/(1+ \rho/\rho0)$

(3) $\delta^{18}O_{CO2-O2} = (64+146\ (\rho/1.23))/(1+ \rho/1.23)$

where ρ is the ratio of pO_2/pCO_2 and X_l and X_h represent the $\delta^{18}O$ composition of CO_2 at low and high O_2 concentrations respectively (Eq. 3). $\rho0$ characterizes when the high or low O_2 regime defines the system (Eq. 3). In Eq. 4 input values utilized in this study and from ref. 32 are displayed. In order to calculate Φ(ρ) we utilize Eq. 5:

$$(4)\ \Phi(\rho) = 0.5305(\delta^{18}O_{CO2\text{-}O2}) - 7.1738$$

Were 0.5305 represents the high temperature limit of for oxygen isotope (θ) fractionation and 7.1738 is the empirical relationship between $\delta^{18}O_{CO2\text{-}O2}$ and $\delta^{17}O_{CO2\text{-}O2}$ determined by previous photochemical experiments (Shaheen et al., 2007). It is important to note that previous studies utilizing this approach have used a θ value of 0.52, and for the present study we have recalculated these values with a θ value of 0.5305.

τ:

Without clear constraints on net oxygen production from the biosphere to the atmosphere and atmospheric oxygen levels makes estimating the residence time of oxygen in the atmosphere difficult to impossible. Some previous work has attempted to work around this unknown by assuming that τ would be constant through time and making interpretations of $\Delta^{17}O$ data under this assumption. Here we treat τ as a free parameter and vary it from 0.01-100 times modern (1244 years; Bender et al., 1994) as scaling *GPP* with pO_2 requires many assumptions through Earth history that are unwarranted.

ρ:

Please refer to above pO_2 and pCO_2 sections. Given the uncertainty in mid-Proterozoic pO_2 and pCO_2 levels allows for a range in possible values of ρ. Assuming pO_2 values at

1.4 Ga were between 0.001 – 0.1 PAL and that pCO_2 was between 5-30 PAL provides a range in ρ of 0.02 – 14. For calculations in this study we allow ρ to vary beyond this to allow for comparisons to the modern atmosphere (ρ ≈ 1000) and extreme end member scenarios with much higher pCO_2 estimates (eg. >100 PAL; ρ ≈ 0.01).

γ:

Mass transfer across the tropopause is an area of active research in the modern environment. This work has highlighted the dynamic nature of this interface with significant variation seasonally and spatially. Quantifying how the transfer of oxygen across the tropopause would change in response to different atmospheric chemistry requires further exploration however previous works have explored how Brewer-Dobson circulation may change with elevated pCO_2 levels that are predicted due to the anthropogenic emissions (Garcia and Randel, 2008). One study has predicted that increasing pCO_2 levels by a factor of two will only increase mass flux across the tropopause by ≈20% and a further increase in pCO_2 values only slightly increasing this stratosphere troposphere exchange (Butchart et al., 2006). It is important to note however that a full exploration into the diversity of estimates of the mid-Proterozoic environment has yet to be conducted therefore modifying values of γ away from modern may not be warranted even at predicted elevated pCO_2 levels. Therefore here we apply the modern value as a constant to remain consistent with initial modeling efforts from Cao and Bao, (2013) of 0.1321.

θ:

The mixing efficiency of the stratosphere with respect to oxygen would have likely been different under different atmospheric oxygen concentrations as well as different atmospheric chemistry and solar output across the mid-Proterozoic (Segura et al., 2003; Kasting and Donahue, 1980). In light of this uncertainty we apply the modern value as a constant 0.017 without a compelling reason to vary in either direction.

Model Sensitivity

Through a plethora of previous work it has been demonstrated that the greatest sensitivity of the $\Delta^{17}O$ value of atmospheric oxygen is the concentration of CO_2 in the atmosphere and the rate of oxygen production from the biosphere (*GPP*; Cao and Bao, 2013). As *GPP* is related to pO_2 and τ, we keep all of these variable along with CO_2 levels as free parameters in calculations. Constraints on pO_2 and pCO_2 levels are only brought in afterward to explore *GPP* levels under atmospheric conditions suggested by previous studies. Below we discuss the sensitivity of model calculations to other variables that underlie our results.

$\Phi(\rho)$:

Underlying model calculations in this work are photochemical experiments that provided constraints for the difference in $\Delta^{17}O$ of CO_2 and O_2 in the CO_2-O_2-O_3 reaction network (Shaheen et al., 2007) Results from this work come with associated uncertainties in values from eqn. (4). Below in figure S4.8 we show the uncertainty envelopes of these experiments in the grey fields for simulations performed at different residence times of 0.1, 1, and 10. We also plot the range in $\Delta^{17}O$ values utilized in this study. What is observed is that for the majority of τ values relevant for results from the Sibley Group ($\Delta^{17}O$ = -12.9 - -6.8), this uncertainty will have little effect on results in this work.

θ and γ:

Given the challenges in measuring the troposphere-stratosphere exchange rate (γ) and the amount of O_2 that is actually involved in photochemical reaction networks (θ) over meaningful timescales in modern settings it is only with great caution that one should speculate how these variable could change under different atmospheric conditions experienced at earlier times in Earth history. While previous work has calculated a weak relationship between pCO_2 levels and γ the relationship depicted is non-linear and not expected to vary beyond a factor (Butchart et al., 2006). Such extrapolations based on CO_2 levels may not be relevant however as a detailed exploration that takes into account other atmospheric species and variations in atmospheric circulation. Therefore in calculations in this work we utilized modern values of both θ and γ. Below we depict how the summed expression of these variables would impact results when raised by a factor, and show results at τ values of 0.1, 1 and 10 (Fig. S4.9). What is observed is that increasing θγ will slightly modify interpretations, with the largest impacts observed at progressively shorter τ values.

f_{O2}:

GPP results from this work are very sensitive to the amount of O_2 that is incorporated into SO_4 during pyrite oxidation. Below we display how changing f_{O2} values will change *GPP* values at varying pCO_2 levels for an initial $\Delta^{17}O$ value of -0.8‰ (Fig. S4.10). The general trend that is observed is smaller f_{O2} values lead to lower *GPP* estimates. Therefore experimentally calibrated ranges (Balci et al., 2007) utilized in this work can be thought of as conservative as it is not possible to have much more O_2 into product sulfate in a natural setting than those found in laboratory experiments.

Supplementary Tables

Table S4.1. Data table for samples used in this study. Associated errors on total laboratory procedures and analysis are presented in the above text.

Sample	$\Delta^{17}O$	$\delta^{18}O$	$\delta^{34}S$	$\Delta^{33}S$	Sample	$\Delta^{17}O$	$\delta^{18}O$	$\delta^{34}S$	$\Delta^{33}S$
PF-5	-0.62	6.9	6.2	-0.027	NI-92-7-15.4	-0.66	8.8	11.2	-0.044
PF-12	-0.67	8.8	10.6	-0.039	NI-92-7-15.95	-0.62	8.1	10.5	-0.029
PF-2	-0.53	9.8	12.3	-0.040	NI-92-7-26.8	-0.61	9.2	9.9	-0.018
PF-20	-0.56	1.0	9.4	-0.038	NI-92-7-32.58	-1.02	8.6	10.4	-0.017
PF-11	-0.63	8.3	12.4	-0.033	NI-92-7-35.75	-0.95	8.3		
PF-21	-0.59	10.9	10.6	-0.042	NI-92-7-51.45	-0.61	10.0	8.3	-0.033
PF-4	-0.61	7.9	11.6	-0.043	NI-92-7-52.3	-0.60	6.9		
PF-10	-0.50	10.9	11.4	-0.047	NI-92-7-54.25	-0.53	8.3	9.9	-0.044
PF-7	-0.53	8.3	11.6	-0.050	NI-92-7-57.3	-0.60	8.4	9.9	-0.048
PF-8	-0.47	8.4	10.1	-0.054	NI-92-7-78.3	-0.55	7.2	9.6	-0.054
PF-9	-0.88	6.9	8.9	-0.027	NI-92-7-88.5	-0.58	9.4	11.8	-0.062
PF-9 re-run	-0.70				NI-92-7-126.75	-0.56	10.2	9.7	-0.048
PF-6	-0.68	6.0	9.1	-0.036	NI-92-7-158.7	-0.77	7.7	5.3	-0.046
PF-6 re-run	-0.66				NI-92-7-164.7				
PF-15	-0.58	9.7	12.0	-0.053	WP-07-03-1	-0.69	6.5		
PF-13	-0.74	10.8	12.0	-0.037	WP-07-03-2	-0.84	6.9	5.6	-0.045
PF-13 re-run	-0.75				WP-07-03-3	-0.58	9.1		
PF-1	-0.59	11.1	12.0	-0.043	WP-07-03-4	-0.49	8.0		
PF17	-0.40	7.6	13.0	-0.039	WP-07-03-5	-0.79	7.3		
PF-3	-0.64	13.1	12.1	-0.048	WP-07-03-8	-0.70	6.6		
PF-3 re-run	-0.56				WP-07-03-10	-0.76	8.5		
PF-16	-0.35	9.6	13.5	-0.039	WP-07-03-10	-0.88	6.8	5.9	-0.22
PF-18	-0.67	8.3	9.8	-0.034	WP-07-03-11	-0.71	6.8		
PF-19	-0.57	10.9	10.7	0.044	WP-07-03-12	-0.74	6.6		
PF-18-	-0.59	13.3	11.9	-0.052	WP-07-03-12	-0.72	6.6		
03RM26	-0.51	12.9	9.3	-0.037	WP-07-03-13	-0.83	7.0		
03RM27	-0.75	3.3	10.6	-0.044	WP-07-03-15	-0.85	7.0		
03Rm62	-0.85	4.0	11.4	-0.039	WP-07-03-18	-0.84	8.1		
04Rm9	-0.84	2.9	8.8	-0.039	WP-07-03-19	-0.87	8.4	4.7	-0.41
04RM30	-0.74	5.9	5.3	-0.044	WP-07-03-20	-0.73	8.4		
04RM31	-0.72	9.8	5.4	-0.032	WP-07-03-21	-0.85	8.9	6.4	-0.24
NI-92-7-2.35	-0.79	8.6	12.4	-0.041	WP-07-03-23	-0.70	8.8		
NI-92-7-3.7	-0.76	9.1	12.2	-0.046	WP-07-03-216.6	-0.88	7.7		
NI-92-7-6.2	-0.65	7.8	12.0	-0.049	WP-07-03-217.6	-0.83	6.5		
NI-92-7-8.72	-0.62	7.9	10.8	-0.051					

Table S4.2. Regression analysis for $\Delta^{17}O$-$\delta^{18}O$, $\delta^{18}O$-$\delta^{34}S$ $\Delta^{17}O$-$\delta^{34}S$ and $\Delta^{33}S$- $\delta^{34}S$ data from this study along with results from previously published syn-Marinoan CAS (Bao et al., 2009), and post-Marinoan barite (Crockford et al., 2016). Correlations are deemed significant based slopes that are significantly non-zero if a P value is > 0.05.

Parameter	This Study				Marinoan Barite	Marinoan CAS
	$\Delta^{17}O$-$\delta^{18}O$	$\delta^{18}O$-$\delta^{34}S$	$\Delta^{17}O$-$\delta^{34}S$	$\Delta^{33}S$-$\delta^{34}S$	$\Delta^{17}O$-$\delta^{34}S$	$\Delta^{17}O$-$\delta^{34}S$
F	7.82	3.64	13.27	1.16	45.2	238.1
P value	0.007	0.063	0.0007	0.29	0.0003	<0.0001
R^2	0.11	0.076	0.23	0.025	0.87	0.96
Significant?	Yes	No	Yes	No	Yes	Yes

Table S4.3. Summary statistics of $\Delta^{17}O$ results (mean, number of values, percentiles, median, standard deviation, and confidence intervals (CI)) on samples from this study compared to post-Marinan barites (Bao et al., 2008; Peng et al., 2011; Killingsworth et al., 2013; Crockford et al., 2016), syn-Marinoan CAS (Bao et al., 2009), and Phanerozoic evaporites (Bao et al., 2008). Samples were binned with 0.1‰ increments.

Parameter	This Study	Phanerozoic Evaporites	Cryogenian Barites	Cryogenian CAS
Total number of values	68	51	200	25
Number of excluded values	0	0	2	0
Number of binned values	68	51	198	25
Minimum	-1.03	-0.34	-0.87	-1.64
25% Percentile	-0.77	-0.18	-0.54	-0.63
Median	-0.67	-0.12	-0.40	-0.36
75% Percentile	-0.58	-0.06	-0.25	-0.12
Maximum	-0.35	0.00	-0.02	-0.04
Mean	-0.68	-0.13	-0.41	-0.51
Std. Deviation	0.13	0.08	0.21	0.48
Std. Error of Mean	0.02	0.01	0.03	0.10
Lower 95% CI of mean	-0.71	-0.16	-0.44	-0.71
Upper 95% CI of mean	-0.65	-0.11	-0.38	-0.31

Table S4.4. Modern and recent $\Delta^{17}O$ measurements from natural samples (Bao and Thiemens, 2000; Bao et al., 2008; Cowie and Johnston, 2016).

Sample	$\Delta^{17}O$	f_{O2}	Description
Air	-0.513	100	
Seawater	0	0	
Seawater Sulfate			
Seamount	-0.05		
LJ-SW	-0.01		
Drp-LJ-SW	-0.04	7.8	
SW-BK	-0.09	17.6	
AT84-1	-0.14	27.4	
Terrestrial Sulfates			
PCMA-2	-0.185	36.3	
Akron-S	-0.06	11.8	
Akron Peck	-0.03	5.9	
Marcasite	-0.05	9.8	
Messinian			
PCMA-3	-0.112	22.0	
JMG	-0.057	11.2	

Table S4.5. Summary of input parameters into model calculations. Symbols in the input column refer to initial notation used by Cao and Bao, (2013) Input* represents terms utilized in this study. Modern τ = 1244 years (Bender et al., 1994).

Input	Input*	Definition	MaxRange	Value	Reference
$\Phi(\rho)$	$\Delta^{17}O_{STR\text{-}CO2\text{-}O2}$	$(\Delta^{17}O_{CO2}\text{-}\Delta^{17}O_{O2})_{strat}$	See Eqn. 5	See Eqn. 5	69
τ	O_2/GPP	O_2 residence time	-	-	-
ρ	O_2/CO_2	pO_2/pCO_2	0.01-1000	0.02-14	36-38, 39-47
γ	$O_{2(STR\text{-}TROP)}$	(exchange rate)$_{trop\text{-}strat}$	-	0.1321	74,75
θ	$O_{2(MIX)}$	(mixing efficiency)$_{strat}$	-	0.017	32
f_{O2}	$O_{2\text{-}incorp}$	$\Delta^{17}O_{SO4}/\Delta^{17}O_{O2}$	0.15-0.08	0.15-0.08	20
$\Delta^{17}O_{O2}$		$\Delta^{17}O_{SO4}/f_{O2}$	-6.8 - -12.9	-6.8 - -12.9	-
pCO_2	see ρ	-	1-100	5-30	36-38
pO_2	see ρ	-	0.001-1	0.001-0.1	39-47
GPP	-	-	-	-	-

Supplementary Figures

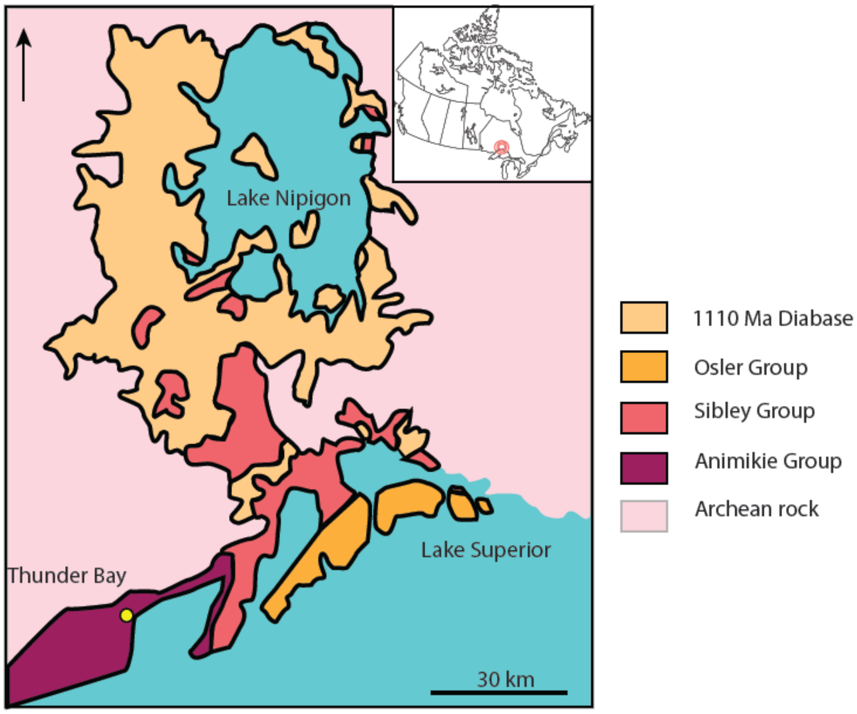

Figure S4.1. Geological map of the Lake Nipigon – northern Lake Superior region adapted from Rogala et al., (2007).

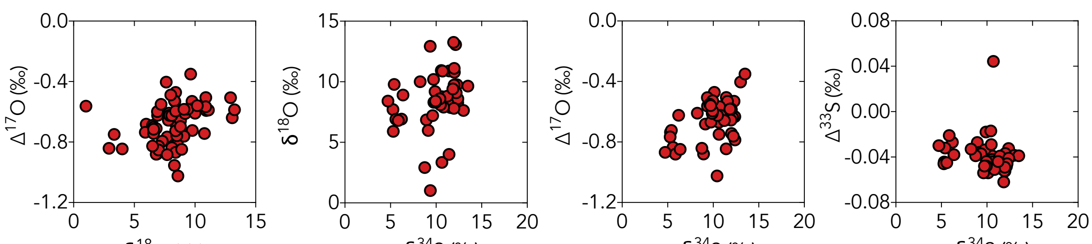

Figure S4.2. Cross plots of (from left to right) $\Delta^{17}O$-$\delta^{18}O$, $\delta^{18}O$-$\delta^{34}S$, $\Delta^{17}O$-$\delta^{34}S$ and $\Delta^{33}S$- $\delta^{34}S$ from data generated in this study.

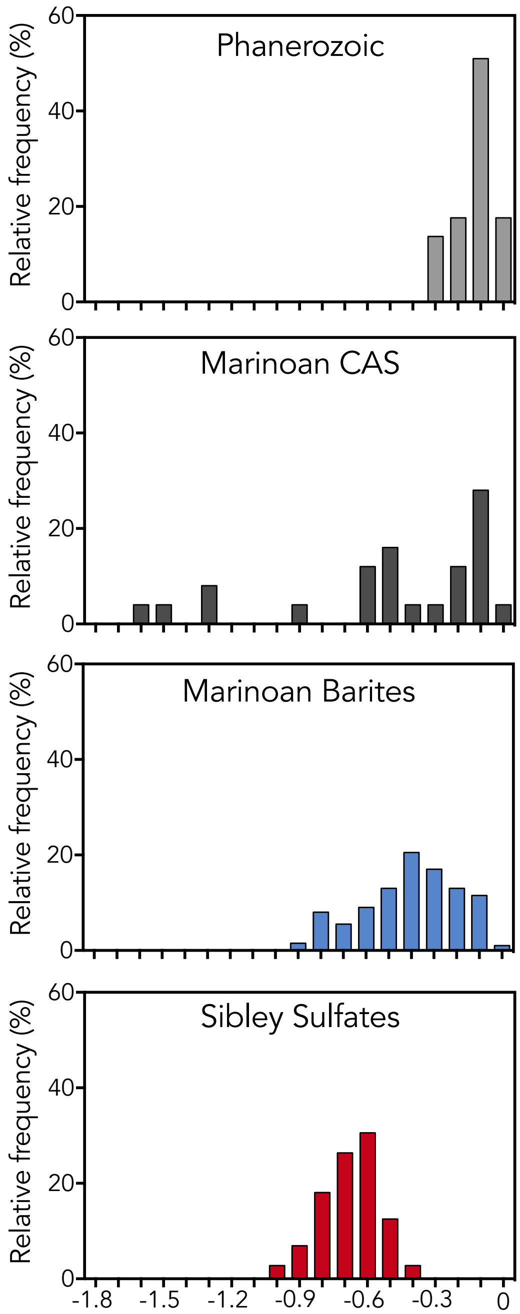

Figure S4.3. Histograms of existing $\Delta^{17}O$ data: Phanerozoic sulfates (Bao et al., 2008; light grey), Marinoan CAS (Bao et al., 2009; 2012; dark grey), Marinoan barite (Bao et al., 2008; Peng et al., 2011; Killingsworth et al., 2013; Crockford et al., 2016; blue), and this study (red).

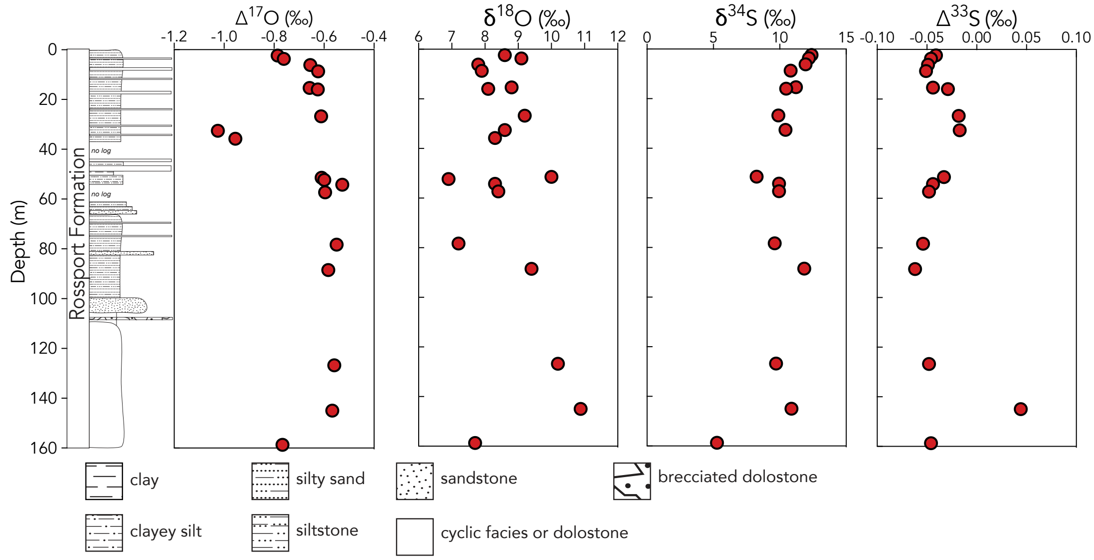

Figure S4.4: Isotopic values ($\Delta^{17}O$, $\delta^{18}O$, $\delta^{34}S$ and $\Delta^{33}S$) for a sub sample set taken from drill hole NI-92-7 plotted against stratigraphic height. Error on all analyses within this figure is less than the uncertainty represented by the sizes of the data points plotted.

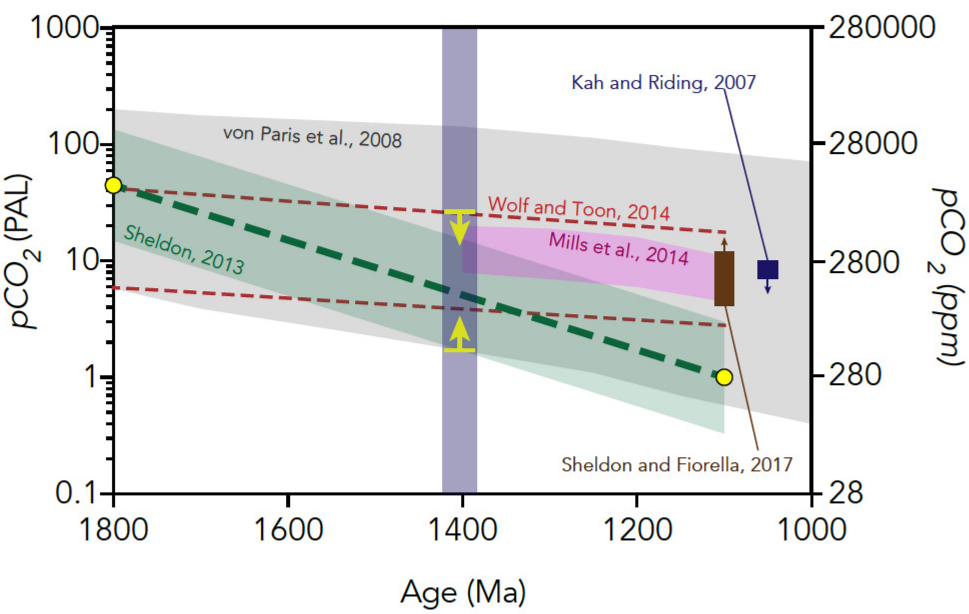

Figure S4.5: Compiled pCO_2 estimates (PAL, left y axis; ppm, right y axis) from 1800-1000 Ma. In grey outlines results from 1-D modeling (von Paris et al., 2008) with calculations based on temperature paths at 273˚K (bottom), and 288˚K (top) and changing solar luminosity. The red dotted lines represent extrapolated GCM modeling (Wolf and Toon, 2014) from Archean estimates. The green shaded region represents the uncertainty envelope of paleosol based estimates (Sheldon, 2013) with the green dotted lines tying calculated estimates at 1800 and 1100 Ma together. The pink shaded region represents estimates based on the COPSE Earth system model (Mills et al., 2014). In brown are modeling based estimates calculating CO_2 and CH_4 mixing ratios required to prevent a global glaciation at 1100 Ma (Fiorella and Sheldon, 2017). In dark blue are microfossil-based estimates at 1050 Ma setting maximum limits (Kah and Riding, 2007). The yellow arrows represent the upper and lower limits utilized in this work.

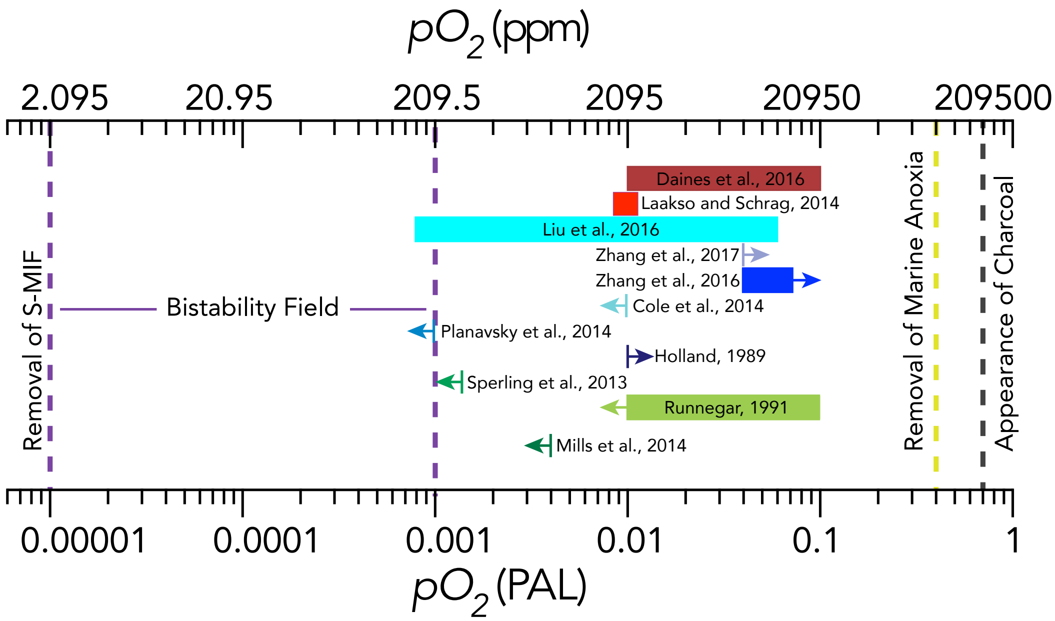

Figure S4.6: Compiled pO_2 estimates for 1.4 Ga. Shades of green represent biologically based estimates inferred from O_2 requirements of animals. Shades of blue represent geochemical estimates. Shades of red represent modeling based estimates. Purple dashed lines represent photochemical constraints for the removal of S-MIF (Farquhar et al., 2000; left) and the upper limit of a bi-stability field (Goldblatt et al., 2006; right). The grey dashed line to the far right represents O_2 levels in conjunction with the first appearance of charcoal (Belcher and McElwain, 2008), and the yellow dashed line represents calculations to remove persistent marine anoxia (Canfield, 1998).

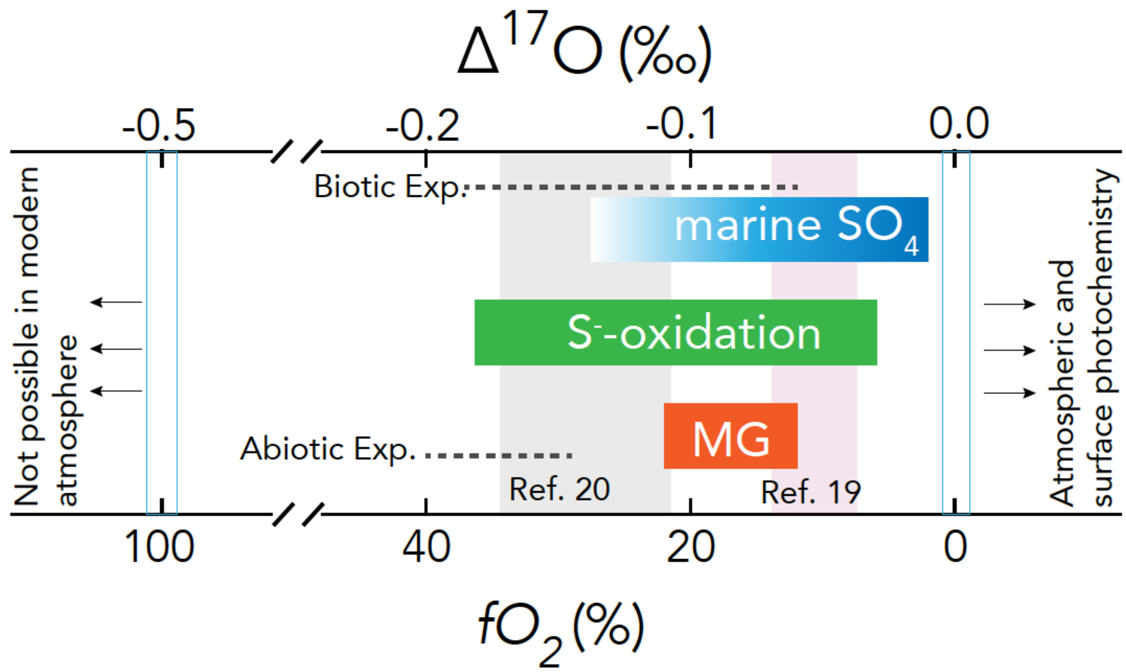

Figure S4.7. Oxygen incorporation percent (f_{O2}; upper x axis) during pyrite oxidation from experiments and natural samples and $\Delta^{17}O$ values (bottom x axis; Bao et al., 2008; Cowie and Johnston, 2016; Bao and Thiemens, 2000). At $\Delta^{17}O$ = -0.5‰ are upper f_{O2} limits of modern values of sulfate imposed by the value of modern atmospheric oxygen. At $\Delta^{17}O$ = 0‰ are lower limits of modern values of sulfate imposed by the value of modern seawater. In the blue bar are measurements of marine sulfate that favor less negative $\Delta^{17}O$ values. In green are $\Delta^{17}O$ measurements of modern-direct-oxidation samples. In orange are measurements on Messinian aged evaporites from Sicily (Cowie and Johnston, 2016) and Spain. The grey field represents f_{O2} results from abiotic experiments (Kohl and Bao, 2011), the pink field represents f_{O2} results from biologically mediated experiments (Balci et al., 2007).

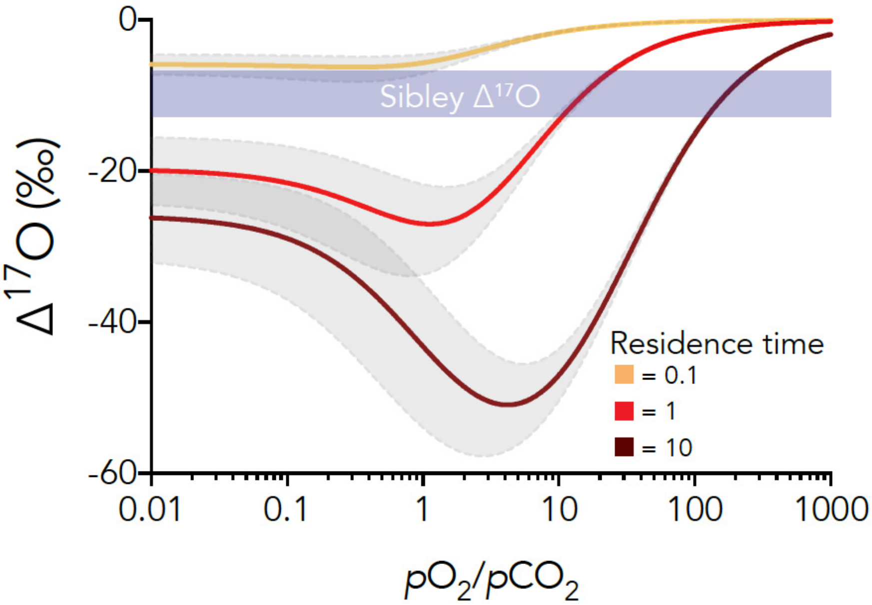

Figure S4.8. Sensitivity analysis of input values for Φ(ρ) from photochemical experiments (Shaheen et al., 2007). Grey fields represent uncertainty envelopes from inputting maximum uncertainties on variables in eqn 4. Coloured lines within uncertainty envelopes represent simulations under different values of τ. The blue bar represents $\Delta^{17}O_{O2}$ calculated from samples from this study for reference.

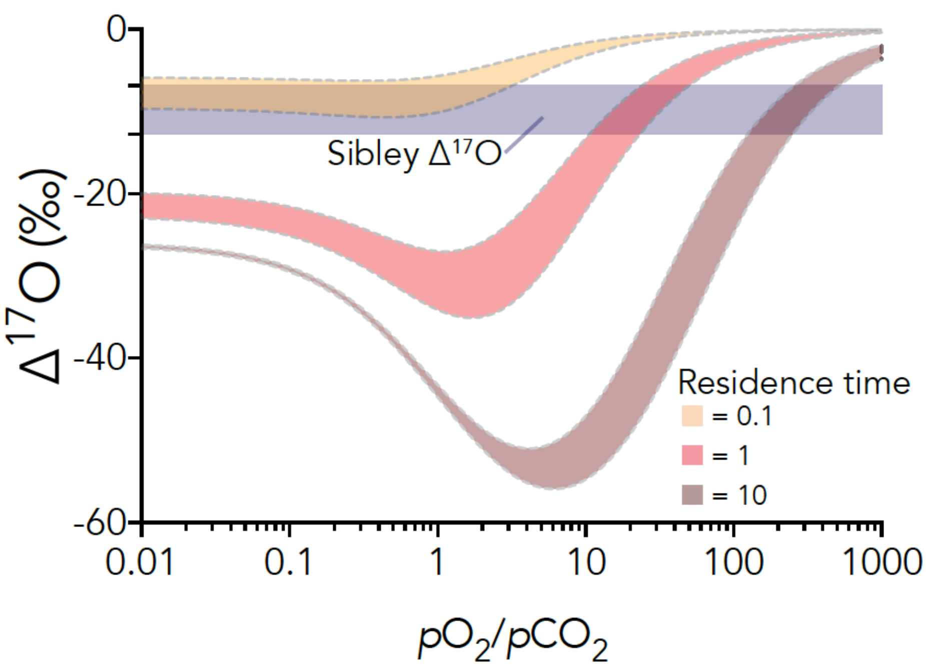

Figure S4.9. Sensitivity analysis of input values for θ and γ. Colored fields represent simulations under different values of τ (burgundy = 10; red = 1; yellow = 0.1). Lower bounds of these fields are calculated from a summed θγ value of twice modern values. Upper bounds of fields are calculated from modern values of θγ. The blue bar represents $\Delta^{17}O_{O2}$ calculated from samples from this study for reference.

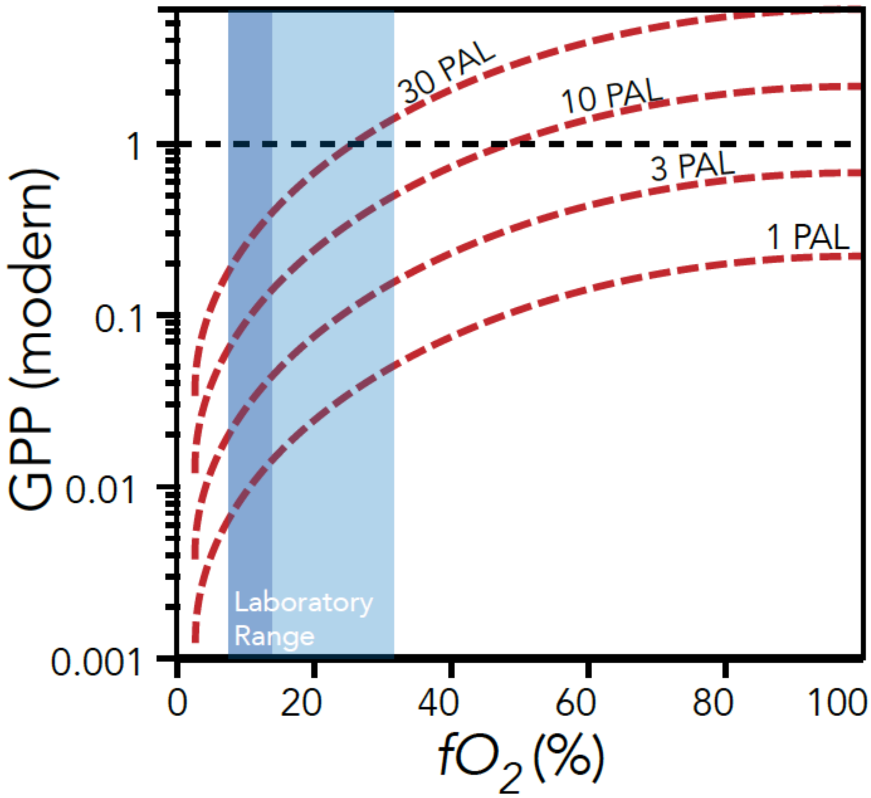

Figure S4.10. Sensitivity of model *GPP* results (y axis) to changing f_{O2} values (0-100%; x axis) at pCO$_2$ levels of 1, 3, 10 and 30 PAL (red dotted lines). The dark blue bar represents experimental constraints on f_{O2} from Balci et al., (2007) and the light blue bar represents experimental constraints from Kohl and Bao, (2011).

Bibliography

Anbar, A.D. and Knoll, A.H., 2002. Proterozoic ocean chemistry and evolution: a bioinorganic bridge?. *science*, *297*(5584), pp.1137-1142.

Angert, A., Rachmilevitch, S., Barkan, E. and Luz, B., 2003. Effects of photorespiration, the cytochrome pathway, and the alternative pathway on the triple isotopic composition of atmospheric O2. *Global Biogeochemical Cycles*, *17*(1).

Antler, G., Turchyn, A.V., Rennie, V., Herut, B. and Sivan, O., 2013. Coupled sulfur and oxygen isotope insight into bacterial sulfate reduction in the natural environment. *Geochimica et Cosmochimica Acta*, *118*, pp.98-117.

Appenzeller, C., Holton, J.R. and Rosenlof, K.H., 1996. Seasonal variation of mass transport across the tropopause. *Journal of Geophysical Research: Atmospheres*, *101*(D10), pp.15071-15078.

Balci, N., Shanks, W.C., Mayer, B. and Mandernack, K.W., 2007. Oxygen and sulfur isotope systematics of sulfate produced by bacterial and abiotic oxidation of pyrite. *Geochimica et Cosmochimica Acta*, *71*(15), pp.3796-3811.

Bao, H., Lyons, J.R. and Zhou, C., 2008. Triple oxygen isotope evidence for elevated CO2 levels after a Neoproterozoic glaciation. *Nature*, *453*(7194), p.504.

Bao, H., Chen, Z.Q. and Zhou, C., 2012. An 17 O record of late Neoproterozoic glaciation in the Kimberley region, Western Australia. *Precambrian Research*, *216*, pp.152-161.

Bao, H., Cao, X. and Hayles, J.A., 2016. Triple oxygen isotopes: fundamental relationships and applications. *Annual Review of Earth and Planetary Sciences*, *44*, pp.463-492.

Bao, H., Fairchild, I.J., Wynn, P.M. and Spötl, C., 2009. Stretching the envelope of past surface environments: Neoproterozoic glacial lakes from Svalbard. *Science*, *323*(5910), pp.119-122.

Bao, H., 2006. Purifying barite for oxygen isotope measurement by dissolution and reprecipitation in a chelating solution. *Analytical chemistry*, *78*(1), pp.304-309.

Bao, H. and Thiemens, M.H., 2000. Generation of O2 from BaSO4 using a CO2− laser fluorination system for simultaneous analysis of δ18O and δ17O. *Analytical chemistry*, *72*(17), pp.4029-4032.

Barkan, E. and Luz, B., 2011. The relationships among the three stable isotopes of oxygen in air, seawater and marine photosynthesis. *Rapid communications in mass spectrometry: RCM*, *25*(16), pp.2367-2369.

Belcher, C.M. and McElwain, J.C., 2008. Limits for combustion in low O2 redefine paleoatmospheric predictions for the Mesozoic. *Science*, *321*(5893), pp.1197-1200.

Bender, M., Sowers, T. and Labeyrie, L., 1994. The Dole effect and its variations during the last 130,000 years as measured in the Vostok ice core. *Global Biogeochemical Cycles*, *8*(3), pp.363-376.

Blunier, T., Barnett, B., Bender, M.L. and Hendricks, M.B., 2002. Biological oxygen productivity during the last 60,000 years from triple oxygen isotope measurements. *Global Biogeochemical Cycles*, *16*(3).

Brasier, M.D. and Lindsay, J.F., 1998. A billion years of environmental stability and the emergence of eukaryotes: New data from northern Australia. *Geology*, *26*(6), pp.555-558.

Buick, R., Des Marais, D.J. and Knoll, A.H., 1995. Stable isotopic compositions of carbonates from the Mesoproterozoic Bangemall Group, northwestern Australia. *Chemical Geology*, *123*(1-4), pp.153-171.

Butchart, N., Scaife, A.A., Bourqui, M., De Grandpré, J., Hare, S.H.E., Kettleborough, J., Langematz, U., Manzini, E., Sassi, F., Shibata, K. and Shindell, D., 2006. Simulations of anthropogenic change in the strength of the Brewer–Dobson circulation. *Climate Dynamics*, *27*(7-8), pp.727-741.

Canfield, D.E., 2005. The early history of atmospheric oxygen: homage to Robert M. Garrels. *Annu. Rev. Earth Planet. Sci.*, *33*, pp.1-36.

Canfield, D.E., Rosing, M.T. and Bjerrum, C., 2006. Early anaerobic metabolisms. *Philosophical Transactions of the Royal Society of London B: Biological Sciences*, *361*(1474), pp.1819-1836.

Canfield, D.E., 1998. A new model for Proterozoic ocean chemistry. *Nature*, *396*(6710), p.450.

Cao, X. and Liu, Y., 2011. Equilibrium mass-dependent fractionation relationships for triple oxygen isotopes. *Geochimica et Cosmochimica Acta*, *75*(23), pp.7435-7445.

Cao, X. and Bao, H., 2013. Dynamic model constraints on oxygen-17 depletion in atmospheric O2 after a snowball Earth. *Proceedings of the National Academy of Sciences*, *110*(36), pp.14546-14550.

Cheadle, B.A., 1986. Alluvial–playa sedimentation in the lower Keweenawan Sibley Group, Thunder Bay District, Ontario. *Canadian Journal of Earth Sciences*, *23*(4), pp.527-542.

Cole, D.B., Reinhard, C.T., Wang, X., Gueguen, B., Halverson, G.P., Gibson, T., Hodgskiss, M.S., McKenzie, N.R., Lyons, T.W. and Planavsky, N.J., 2016. A shale-hosted Cr isotope record of low atmospheric oxygen during the Proterozoic. *Geology*, *44*(7), pp.555-558.

Cowie, B.R. and Johnston, D.T., 2016. High-precision measurement and standard calibration of triple oxygen isotopic compositions ($\delta^{18}O$, $\Delta'^{17}O$) of sulfate by F_2 laser fluorination. *Chemical Geology*, *440*, pp.50-59.

Cox, G.M., Jarrett, A., Edwards, D., Crockford, P.W., Halverson, G.P., Collins, A.S., Poirier, A. and Li, Z.X., 2016. Basin redox and primary productivity within the Mesoproterozoic Roper Seaway. *Chemical Geology*, *440*, pp.101-114.

Crockford, P.W., Cowie, B.R., Johnston, D.T., Hoffman, P.F., Sugiyama, I., Pellerin, A., Bui, T.H., Hayles, J., Halverson, G.P., Macdonald, F.A. and Wing, B.A., 2016. Triple oxygen and multiple sulfur isotope constraints on the evolution of the post-Marinoan sulfur cycle. *Earth and Planetary Science Letters*, *435*, pp.74-83.

Daines, S.J., Mills, B.J. and Lenton, T.M., 2017. Atmospheric oxygen regulation at low Proterozoic levels by incomplete oxidative weathering of sedimentary organic carbon. *Nature Communications*, *8*, p.14379.

Davis, D.W. and Sutcliffe, R.H., 1985. U-Pb ages from the Nipigon plate and northern Lake Superior. *Geological Society of America Bulletin*, *96*(12), pp.1572-1579.

Derry, L.A., 2015. Causes and consequences of mid-Proterozoic anoxia. *Geophysical Research Letters*, *42*(20), pp.8538-8546.

Farquhar, J., Bao, H. and Thiemens, M., 2000. Atmospheric influence of Earth's earliest sulfur cycle. *Science*, *289*(5480), pp.756-758.

Fiorella, R.P. and Sheldon, N.D., 2017. Equable end Mesoproterozoic climate in the absence of high CO2. *Geology*, *45*(3), pp.231-234.

Franklin, J.M., 1978. The Sibley Group, Ontario. *Rubidium–strontium isotopic age studies, report*, *2*, pp.77-14.

Elston, D.P., Enkin, R.J., Baker, J. and Kisilevsky, D.K., 2002. Tightening the Belt: Paleomagnetic-stratigraphic constraints on deposition, correlation, and deformation of the Middle Proterozoic (ca. 1.4 Ga) Belt-Purcell Supergroup, United States and Canada. *Geological Society of America Bulletin*, *114*(5), pp.619-638.

Garcia, R.R. and Randel, W.J., 2008. Acceleration of the Brewer–Dobson circulation due to increases in greenhouse gases. *Journal of the Atmospheric Sciences*, *65*(8), pp.2731-2739.

Goldblatt, C., Lenton, T.M. and Watson, A.J., 2006. Bistability of atmospheric oxygen and the Great Oxidation. *Nature*, *443*(7112), p.683.

Hansen, J., Sato, M., Kharecha, P., Beerling, D., Berner, R., Masson-Delmotte, V., Pagani, M., Raymo, M., Royer, D.L. and Zachos, J.C., 2008. Target atmospheric CO_2: Where should humanity aim?. *arXiv preprint arXiv:0804.1126*.

Hardie, L.A., 1968. The origin of the Recent non-marine evaporite deposit of Saline Valley, Inyo County, California. *Geochimica et Cosmochimica Acta*, *32*(12), pp.1279-1301.

Holland, H.D., Feakes, C.R. and Zbinden, E.A., 1989. The Flin Flon paleosol and the composition of the atmosphere 1.8 BYBP. *American Journal of Science*, *289*(4), pp.362-389.

Johnston, D.T., Wolfe-Simon, F., Pearson, A. and Knoll, A.H., 2009. Anoxygenic photosynthesis modulated Proterozoic oxygen and sustained Earth's middle age. *Proceedings of the National Academy of Sciences*, *106*(40), pp.16925-16929.

Kah, L.C. and Riding, R., 2007. Mesoproterozoic carbon dioxide levels inferred from calcified cyanobacteria. *Geology*, *35*(9), pp.799-802.

Kasting, J.F. and Donahue, T.M., 1980. The evolution of atmospheric ozone. *Journal of Geophysical Research: Oceans*, *85*(C6), pp.3255-3263.

Kaufman, A.J. and Xiao, S., 2003. Hich CO2 levels in the Proterozoic atmosphere estimated from analyses of individual microfossils. *Nature*, *425*(6955), p.279.

Kharecha, P., Kasting, J. and Siefert, J., 2005. A coupled atmosphere–ecosystem model of the early Archean Earth. *Geobiology*, *3*(2), pp.53-76.

Killingsworth, B.A., Hayles, J.A., Zhou, C. and Bao, H., 2013. Sedimentary constraints on the duration of the Marinoan Oxygen-17 Depletion (MOSD) event. *Proceedings of the National Academy of Sciences*, *110*(44), pp.17686-17690.

Kirschvink, J.L., 1992. Late Proterozoic low-latitude global glaciation: the snowball Earth.

Kohl, I. and Bao, H., 2011. Triple-oxygen-isotope determination of molecular oxygen incorporation in sulfate produced during abiotic pyrite oxidation (pH= 2–11). *Geochimica et Cosmochimica Acta*, *75*(7), pp.1785-1798.

Kunzmann, M., Halverson, G.P., Sossi, P.A., Raub, T.D., Payne, J.L. and Kirby, J., 2013. Zn isotope evidence for immediate resumption of primary productivity after snowball Earth. *Geology*, *41*(1), pp.27-30.

Laakso, T.A. and Schrag, D.P., 2014. Regulation of atmospheric oxygen during the Proterozoic. *Earth and Planetary Science Letters*, *388*, pp.81-91.

Liu, X.M., Kah, L.C., Knoll, A.H., Cui, H., Kaufman, A.J., Shahar, A. and Hazen, R.M., 2015. Tracing Earth's O_2 evolution using Zn/Fe ratios in marine carbonates.

Luz, B., Barkan, E., Bender, M.L., Thiemens, M.H. and Boering, K.A., 1999. Triple-isotope composition of atmospheric oxygen as a tracer of biosphere productivity. *Nature*, *400*(6744), p.547.

Luz, B. and Barkan, E., 2010. Variations of 17 O/16 O and 18 O/16 O in meteoric waters. *Geochimica et Cosmochimica Acta*, *74*(22), pp.6276-6286.

Lyons, T.W., Reinhard, C.T. and Planavsky, N.J., 2014. The rise of oxygen in Earth's early ocean and atmosphere. *Nature*, *506*(7488), pp.307-315.

Metsaranta R. T., thesis, Lakehead University (2006).

Matsuhisa, Y., Goldsmith, J.R. and Clayton, R.N., 1978. Mechanisms of hydrothermal crystallization of quartz at 250 C and 15 kbar. *Geochimica et Cosmochimica Acta*, *42*(2), pp.173-182.

Miller, M.F., 2002. Isotopic fractionation and the quantification of 17 O anomalies in the oxygen three-isotope system: an appraisal and geochemical significance. *Geochimica et Cosmochimica Acta*, *66*(11), pp.1881-1889.

Mills, B., Lenton, T.M. and Watson, A.J., 2014. Proterozoic oxygen rise linked to shifting balance between seafloor and terrestrial weathering. *Proceedings of the National Academy of Sciences*, *111*(25), pp.9073-9078.

Mills, D.B., Ward, L.M., Jones, C., Sweeten, B., Forth, M., Treusch, A.H. and Canfield, D.E., 2014. Oxygen requirements of the earliest animals. *Proceedings of the National Academy of Sciences*, *111*(11), pp.4168-4172.

Nordstrom, D.K., 1982. *Aqueous pyrite oxidation and the consequent formation of secondary iron minerals* (No. acidsulfateweat, pp. 37-56). Soil Science Society of America.

Olson, S.L., Reinhard, C.T. and Lyons, T.W., 2016. Limited role for methane in the mid-Proterozoic greenhouse. *Proceedings of the National Academy of Sciences*, *113*(41), pp.11447-11452.

Payne, J.L., McClain, C.R., Boyer, A.G., Brown, J.H., Finnegan, S., Kowalewski, M., Krause, R.A., Lyons, S.K., McShea, D.W., Novack-Gottshall, P.M. and Smith, F.A., 2011. The evolutionary consequences of oxygenic photosynthesis: a body size perspective. *Photosynthesis research*, *107*(1), pp.37-57.

Pellerin, A., Bui, T.H., Rough, M., Mucci, A., Canfield, D.E. and Wing, B.A., 2015. Mass-dependent sulfur isotope fractionation during reoxidative sulfur cycling: A case study from Mangrove Lake, Bermuda. *Geochimica et Cosmochimica Acta*, *149*, pp.152-164.

Peng, Y., Bao, H., Zhou, C. and Yuan, X., 2011. 17 O-depleted barite from two Marinoan cap dolostone sections, south China. *Earth and Planetary Science Letters*, *305*(1), pp.21-31.

Percak-Dennett, E., He, S., Converse, B., Konishi, H., Xu, H., Corcoran, A., Noguera, D., Chan, C., Bhattacharyya, A., Borch, T. and Boyd, E., 2017. Microbial acceleration of aerobic pyrite oxidation at circumneutral pH. *Geobiology*.

Planavsky, N.J., Cole, D.B., Reinhard, C.T., Diamond, C., Love, G.D., Luo, G., Zhang, S., Konhauser, K.O. and Lyons, T.W., 2016. No evidence for high atmospheric oxygen levels 1,400 million years ago. *Proceedings of the National Academy of Sciences*, *113*(19), pp.E2550-E2551.

Planavsky, N.J., Reinhard, C.T., Wang, X., Thomson, D., McGoldrick, P., Rainbird, R.H., Johnson, T., Fischer, W.W. and Lyons, T.W., 2014. Low Mid-Proterozoic atmospheric oxygen levels and the delayed rise of animals. *Science*, *346*(6209), pp.635-638.

Reinhard, C.T., Planavsky, N.J., Robbins, L.J., Partin, C.A., Gill, B.C., Lalonde, S.V., Bekker, A., Konhauser, K.O. and Lyons, T.W., 2013. Proterozoic ocean redox and biogeochemical stasis. *Proceedings of the National Academy of Sciences*, *110*(14), pp.5357-5362.

Reinhard, C.T., Planavsky, N.J., Gill, B.C., Ozaki, K., Robbins, L.J., Lyons, T.W., Fischer, W.W., Wang, C., Cole, D.B. and Konhauser, K.O., 2017. Evolution of the global phosphorus cycle. *Nature*, *541*(7637), pp.386-389.

Robertson, W.A., 1973. Pole position from thermally cleaned Sibley Group sediments and its relevance to Proterozoic magnetic stratigraphy. *Canadian Journal of Earth Sciences*, *10*(2), pp.180-193.

Robinson, T.D. and Catling, D.C., 2013. Common 0.1 bar tropopause in thick atmospheres set by pressure-dependent infrared transparency. *arXiv preprint arXiv:1312.6859*.

Rogala, B., Fralick, P.W., Heaman, L.M. and Metsaranta, R., 2007. Lithostratigraphy and chemostratigraphy of the Mesoproterozoic Sibley Group, northwestern Ontario, Canada. *Canadian Journal of Earth Sciences*, *44*(8), pp.1131-1149.

Runnegar, B., 1991. Precambrian oxygen levels estimated from the biochemistry and physiology of early eukaryotes. *Global and Planetary Change*, *5*(1-2), pp. 97-111.

Ryu, J.H., Zierenberg, R.A., Dahlgren, R.A. and Gao, S., 2006. Sulfur biogeochemistry and isotopic fractionation in shallow groundwater and sediments of Owens Dry Lake, California. *Chemical geology*, *229*(4), pp.257-272.

Sánchez-Baracaldo, P., Ridgwell, A. and Raven, J.A., 2014. A neoproterozoic transition in the marine nitrogen cycle. *Current Biology*, *24*(6), pp.652-657.

Segura, A., Krelove, K., Kasting, J.F., Sommerlatt, D., Meadows, V., Crisp, D., Cohen, M. and Mlawer, E., 2003. Ozone concentrations and ultraviolet fluxes on Earth-like planets around other stars. *Astrobiology*, *3*(4), pp.689-708.

Shaheen, R., Janssen, C. and Röckmann, T., 2007. Investigations of the photochemical isotope equilibrium between O 2, CO 2 and O 3. *Atmospheric chemistry and physics*, *7*(2), pp.495-509.

Sheldon, N.D., 2013. Causes and consequences of low atmospheric pCO_2 in the Late Mesoproterozoic. *Chemical Geology*, *362*, pp.224-231.

Sperling, E.A., Halverson, G.P., Knoll, A.H., Macdonald, F.A. and Johnston, D.T., 2013. A basin redox transect at the dawn of animal life. *Earth and Planetary Science Letters*, *371*, pp.143-155.

Thode, H.G., Monster, J. and Dunford, H.B., 1961. Sulphur isotope geochemistry. *Geochimica et Cosmochimica Acta*, *25*(3), pp.159-174.

Trenberth, K.E. and Smith, L., 2005. The mass of the atmosphere: A constraint on global analyses. *Journal of Climate*, *18*(6), pp.864-875.

von Paris, P., Rauer, H., Grenfell, J.L., Patzer, B., Hedelt, P., Stracke, B., Trautmann, T. and Schreier, F., 2008. Warming the early Earth—CO 2 reconsidered. *Planetary and Space Science*, *56*(9), pp.1244-1259.

Ward, L.M., Kirschvink, J.L. and Fischer, W.W., 2016. Timescales of oxygenation following the evolution of oxygenic photosynthesis. *Origins of Life and Evolution of Biospheres*, *46*(1), pp.51-65.

Wen, J. and Thiemens, M.H., 1993. Multi-isotope study of the O (1 D)+ CO2 exchange and stratospheric consequences. *Journal of Geophysical Research: Atmospheres*, *98*(D7), pp.12801-12808.

Wing, B.A., 2013. A cold, hard look at ancient oxygen. *Proceedings of the National Academy of Sciences*, *110*(36), pp.14514-14515.

Wolf, E.T. and Toon, O.B., 2014. Controls on the Archean climate system investigated with a global climate model. *Astrobiology*, *14*(3), pp.241-253.

Yung, Y.L., DeMore, W.B. and Pinto, J.P., 1991. Isotopic exchange between carbon dioxide and ozone via O (1D) in the stratosphere. *Geophysical Research Letters*, *18*(1), pp.13-16.

Young, E.D., Yeung, L.Y. and Kohl, I.E., 2014. On the $\Delta^{17}O$ budget of atmospheric O_2. *Geochimica et Cosmochimica Acta*, *135*, pp.102-125.

Zhang, S., Wang, X., Wang, H., Bjerrum, C.J., Hammarlund, E.U., Costa, M.M., Connelly, J.N., Zhang, B., Su, J. and Canfield, D.E., 2016. Sufficient oxygen for animal respiration 1,400 million years ago. *Proceedings of the National Academy of Sciences*, *113*(7), pp.1731-1736.

Preface to Chapter 5

In 1980 Claypool et al., presented a comprehensive survey of the major isotopes of sulfur ($^{32,34}S$; $\delta^{34}S$) and oxygen ($^{16,18}O$; $\delta^{18}O$) within sulfate over the past billion years of Earth history (Claypool et al., 1980). This record has provided a foundation to evaluate how seawater sulfate concentrations have varied through time, and how the cycles of sulfur and oxygen have operated over this interval of Earth history. Since Claypool et al., 1980, further populating of the $\delta^{18}O$ and $\delta^{34}S$ records and extension to earlier times in Earth history has highlighted both connections and disconnections between these important geochemical records. Further advances in analytical capabilities over the past several decades have added a new dimension through the minor isotopes of sulfur ($^{33,36}S$; $\Delta^{33}S$) and oxygen (^{17}O; $\Delta^{17}O$). These additions are rapidly improving our understanding of both the cycling of oxygen and sulfur in the surface environment as well as other processes these isotopic tools track, thus holding enormous promise for further resolution of Earth's ancient biogeochemical environments. Despite this progress, the application of these tools to ancient records remains sparse. This is most notable in the Proterozoic where large gaps in data exist particularly with respect to oxygen ($\delta^{18}O$, $\Delta^{17}O$) and multiple sulfur isotopic data ($\Delta^{33}S$, $\Delta^{36}S$).

In this chapter we briefly review the progress made to date in understanding the Proterozoic sulfur and oxygen cycles viewed through the isotopic record of sedimentary sulfate minerals of evaporative origin. We compliment this review by extending $\delta^{34}S$ and $\delta^{18}O$ age curves of sulfate through to the early Paleoproterozoic and present results alongside minor isotopic $\Delta^{17}O$, $\Delta^{33}S$ and $\Delta^{36}S$ measurements. We further utilize this data set to explore secular variations and links in these systems highlighting potential causal mechanisms that may have driven revealed trends. Finally we attempt to take a birds-eye view of emerging models of the evolution of the Earth's surface and compare this to insights revealed through the isotopic record of Proterozoic sulfate.

5. An Isotopic Record of Proterozoic Sulfate

Abstract

The Proterozoic represents Earth's middle age where many important transitions in the evolution of the surface environment occurred. Such transitions include the oxygenation of the atmosphere, emergence of eukaryotic organisms and growth of continents. As the sulfur and oxygen cycles are have deep connections in most surface biogeochemical processes it is difficult to envisage such transitions without significant impacts on these cycles through changes to the isotopic composition of marine sulfate. Advances in analytical capabilities over the past few decades are opening new possibilities in the amount of information that can be extracted from the geochemical record through Earth history. For example the measurements of the minor isotopes of sulfur (^{33}S) and oxygen (^{17}O) are providing new insights into identifying microbial metabolisms in ancient sediments as well as estimates on the composition of the atmosphere and size of the biosphere through geologic time. Here we present a comprehensive isotopic record of Proterozoic sulfate through the measurement of over 300 samples for oxygen ($\Delta^{17}O$, $\delta^{18}O$) and sulfur ($\Delta^{33}S$, $\delta^{34}S$) isotopes in evaporite minerals from 32 different formations spanning the Earth's earliest evaporites at 2.35 Ga to Ediacaran aged samples. Results, when compiled with literature values, depict distinct intervals (*GOE*, mid-Proterozoic, late Proterozoic, Cryogenian, Ediacaran) with respect to expression of sulfate isotopes. The clearest example of this is the $\Delta^{17}O$ record that shows muted signatures only slightly more negative than modern values across the *GOE*, late Proterozoic and Ediacaran, with highly negative values across the mid-Proterozoic and Cryogenian. We interpret this

record along with estimates of atmospheric chemistry to produce a gross primary production (GPP) curve across the Proterozoic.

5.1 Introduction

Sulfate (SO_4^{2-}) is the second most abundant anion in modern marine environments and must have played a significant role in ancient biogeochemical cycles in remineralizing organic matter, albeit often at lower concentrations than the modern environment (Jørgensen, 1982; Kah et al., 2004; Johnston et al., 2008; Bekker and Holland, 2012, Luo et al., 2015). Through the isotopes within sulfate and reduced forms of sulfur such as sulfide, important information can be derived for much of the Earth System with signals preserved in the sedimentary record for billions of years. For example sulfur-based metabolisms are a key control on the amount of organic matter that gets deposited into sediments as well as the amount of sulfur buried as pyrite, linking the sulfur cycle to the cycles of carbon and oxygen (Bowles et al., 2014; Jørgensen et al., 2006). While it is clear that much of the Earth System has changed between 2.5 and 0.541 Ga (Fig. 5.1), it is difficult to envisage how this could have occurred without a significant impact on the sulfate isotope record. Importantly, the sensitivity of isotopic systems within marine sulfate to change depends on the size and capacity of the marine sulfate reservoir to buffer such perturbations. The marine sulfate concentration, in turn, is linked to atmospheric oxygen concentrations (Fig. 5.1) as sulfate is supplied to the ocean by oxidative weathering of crustal sulfide minerals (Figs 5.2-4). Further, the majority of sulfur cycling occurs within marine sediments on coastal margins, the distribution of which, has likely significantly changed throughout Earth history (Bradley, 2011; Fig. 5.1). Therefore, a first step in exploring these aspects of the Earth System is uncovering and expanding such archives that preserve ancient sulfate.

Claypool et al., (1980) presented a comprehensive survey of the major isotopes of sulfur ($\delta^{34}S$) and oxygen ($\delta^{18}O$) within sulfate over the last one billion years of Earth history (Claypool et al., 1980). This record has provided a foundation to evaluate how seawater sulfate concentrations have varied through time, and how the cycles of sulfur and oxygen have operated over this interval of Earth history. Since this pioneering work further populating of the $\delta^{18}O$ and $\delta^{34}S$ records and extending them to earlier times (e.g. Strauss, 1993) has highlighted both connections and disconnections between these important geochemical records (Kampshulte, 2004; Turchyn et al., 2009; Utrilla et al., 1992; Strauss, 1999; Wu et al., 2014). Further advances in analytical capabilities over the past several decades have added new dimensions through the ability to measure the minor isotopes of sulfur (^{33}S, ^{36}S; Farquhar et al., 2000; Farquhar and Wing, 2003; Johnston, 2011) and oxygen (^{17}O; Thiemens and Heidenreich, 1983; Luz et al., 1999; Thiemens, 2006; Bao, 2006). These new datasets are rapidly improving our understanding of both oxygen and sulfur cycling in the surface environment as well as other processes that these isotopic tools track such as the composition of the ancient atmosphere ($\Delta^{33}S$, $\Delta^{17}O$; Farquhar et al., 2000; Bao et al., 2008). Despite this progress, the application of these tools to ancient records remains sparse. This is most notable for the Proterozoic where large gaps in data exist particularly with respect to oxygen ($\delta^{18}O$, $\Delta^{17}O$) and multiple sulfur isotopic data ($\Delta^{33}S$, $\Delta^{36}S$).

Here we briefly review the progress made to date in understanding the Proterozoic sulfur and oxygen cycles viewed through the isotopic record of sedimentary sulfate minerals of evaporative origins. We compliment this review by extending $\delta^{34}S$ and $\delta^{18}O$ age curves of sulfate through to the early Paleoproterozoic and present results alongside minor isotope ($\Delta^{17}O$, and $\Delta^{33}S$) measurements. We further utilize this dataset to explore secular variations and links in these systems, highlighting potential causal mechanisms that may have driven the revealed trends. Finally, we attempt to take a birds-eye view of emerging models of the evolution of the Earth's surface (Bekker and Holland, 2012; Lyons et al., 2014; Payne et al., 2011; Planavsky et al., 2011; Sperling et al., 2015; 5.1) and compare this to insights revealed through the isotopic record of Proterozoic sulfate.

Box 1: Isotopic Notation

$\delta^{18}O$ and $\delta^{17}O$ values are expressed as:

(1) $\delta^{17,18}O = (((^{17,18}O/^{16}O)_{sample} / (^{17,18}O/^{16}O)_{V\text{-}SMOW}) - 1) \times 1000$

where V-SMOW refers to Standard Mean Ocean Water international reference scale.

$\delta^{33}S$, $\delta^{34}S$ and $\delta^{36}S$ values are expressed as:

(2) $\delta^{33,34,36}S = ((^{33,34,36}S/^{32}S)_{sample} / (^{33,34,36}S/^{32}S)_{V\text{-}CDT} - 1) \times 1000$

where V-CDT refers to the Vienna Canon Diablo Troilite international reference scale.

Isotopic differences between two different reservoirs has been signified by the Δ symbol, for example $\Delta^{34}S$ has been used to denote the difference in $\delta^{34}S$ values between sulfate and sulfide minerals. In biological systems however the ε is more commonly used.

Deviations from theoretically calculated equilibrium isotopic exchange at high temperatures for oxygen $\delta^{17}O$ vs. $\delta^{18}O$ space (0.5305; Cao and Liu, 2011) and equilibrium predictions at temperatures relevant for biogeochemical reactions for sulfur isotopes in $\delta^{33}S$ vs. $\delta^{34}S$ space (0.515; Johnston, 2011) are used as references when comparing $\delta^{17}O$ and $\delta^{33}S$ values relative to $\delta^{18}O$ and $\delta^{34}S$ values, respectively, and are presented as $\Delta^{17}O$ and $\Delta^{33}S$ on the ‰ scale. Although previous studies have used different mass laws when calculating the magnitude of $\Delta^{17}O$ values reflective of either the terrestrial fractionation line (0.52), or the meteoric water line (0.528), here we use the high temperature thermodynamic limit of 0.5305 as this has been argued for as a preferred datum in previous studies (Matsuhisa et al., 1978; Pack and Herwartz, 2014; Bao et al., 2016; Hayles et al., 2017). These coefficients are often denoted as λ or θ values.

$\Delta^{17}O$ values were calculated as:
(3) $\Delta^{17}O = \delta'^{17}O - (0.5305)\delta'^{18}O$

where $\delta'^{17}O$ and $\delta'^{18}O$ are calculated as:

(4) $\delta'^{17}O$ or $\delta'^{18}O = \ln(^{17,18}R_{sample}/^{17,18}R_{standard}) \times 1000$

$\Delta^{33}S$ and $\Delta^{36}S$ values were calculated as:

(5) $\Delta^{33,36}S = \delta^{34}S - 1000 \times ([1+ (\delta^{33,36}S/1000)]0.515 - 1)$

5.2 Fidelity of sulfate-bearing archives

Central to all geochemical studies investigating the evolution of Earth's surface environment through deep time is the fidelity of archives that preserve isotopic signatures. While a great deal of work has been conducted to identify primary isotopic signatures of marine, microbial, and atmospheric reservoirs, reliably screening such measurements from those that have been subjected to post-depositional processes remains a challenge and this is especially poignant over much of the Proterozoic. Given that the expression of primary isotopic signals is a reflection of environmental conditions that include atmospheric chemistry, marine sulfate levels, and the composition and rate of microbial sulfur cycling, the high degree of uncertainty on these factors over the Proterozoic allow for a wide range of plausible isotopic signatures that can be interpreted to be of potentially primary origin. Below we summarize processes that may cause sedimentary archives (e.g. gypsum, anhydrite, barite and carbonate associated sulfate (CAS)) to deviate in their initial seawater isotopic compositions and present possible isotopic patterns and trajectories that such processes may manifest. Such processes inform how these data sets must be viewed with respect to confidence in interpretations.

Barite

Sedimentary barite has been widely relied upon as an archive of both the Archean biosphere (Shen et al., 2001; Ueno et al., 2006), as well as the Phanerozoic sulfur cycle (Turchyn and Schrag, 2006; Paytan et al., 1998), however its utility in providing insight into the Proterozoic surface environment is much less explored than other sulfate archives (e.g., Strauss and Schieber, 1990; Deb et al., 1991; Clark et al., 2004). In the modern environment barites can precipitate in diagenetic, hydrothermal, and pelagic, environments even under incredibly low ambient sulfate concentrations (Horner et al., 2017). Each mode of deposition goes with diagnostic isotopic signatures. While pelagic barites have been relied upon in more recent Earth history for records of seawater sulfate

(Paytan et al., 1998; 2004), their utility in deep time is less explored as their depositional settings have poor preservation potential. Moreover, recent work has demonstrated that preparation of samples for analysis can significantly impact observed trends (Markovic et al., 2016; Turchyn and Schrag, 2006) with a fractionation of up to 2.5‰, between pelagic barite and coeval sulfate that is likely due to small kinetic isotope effects (Turchyn and Schrag, 2006). Diagenetic barites in environments where dissolution of sulfate minerals followed by reprecipitation as barite at the sulfate-methane transition zone will typically produce much heavier $\delta^{18}O$ and $\delta^{34}S$ values than that of ambient sulfate (Sakai, 1971; Antler et al., 2015). Isotopic signatures such as $\Delta^{17}O$ values of sulfates formed in diagenetic environments may not provide insight into atmospheric chemistry, where even ancient hydrothermal deposits appear to bear distinct microbial signatures and clues to how the ancient sulfur cycle operated (Shen et al., 2001; 2009). While Proterozoic barite occurrences have been documented (e.g., Strauss and Schieber, 1990; Deb et al., 1991; Clark et al., 2004), most are interpreted as stratiform barites of hydrothermal origins, disconnected from the surface environment. Therefore, we reserve barite isotopic data for future interpretation and publication.

Carbonate Associated Sulfate (CAS)

Due to the sparse distribution of evaporite minerals through much of the Proterozoic, as well as the difficulty in dating such deposits, many have focused on sulfate bound within carbonates for an isotopic record of ancient seawater sulfate (e.g. Hurtgen et al., 2002; Jones and Fike, 2013; Guo et al., 2009; Luo et al., 2015). Caution is need with CAS samples however as the incorporation of sulfate into the carbonate lattice remains incompletely understood particularly with respect to effects on its isotopic composition. For example it is difficult to disentangle the influence of pore-water processes versus original seawater sulfate on the isotopic value of CAS (Fike et al., 2015). Therefore the degree to which diagenetic alteration, and dolomitization overprint original isotopic signatures is poorly constrained (Kampshulte and Strauss 2004). Beyond isotopic values, CAS records have been used to reconstruct seawater sulfate concentrations as the amount of sulfate incorporated into carbonates during deposition is thought to be proportional to ambient sulfate concentrations. However, post-depositional processes such as dolomitization or meteoric diagenesis may significantly alter the abundance of carbonate-bound sulfate, raising concerns about the reliability of this proxy. Recent work testing the susceptibility of primary $\delta^{34}S$ and $\delta^{18}O$ value to post depositional processes has highlighted that $\delta^{18}O$ values show less resilience to post-depositional alteration than coeval $\delta^{34}S$ values (Gill et al., 2008; Fichtner et al., 2017). Furthermore, low CAS concentrations have led to analytical challenges as small concentrations of sulfate are prone to contamination through oxidation of trace pyrite within samples (Marenco et al., 2008). Finally it has also been shown that surface weathered samples can be contaminated by atmospheric sulfate thereby shifting their $\Delta^{17}O$ isotopic compositions (Peng et al., 2014). Nonetheless, direct comparisons between CAS- and evaporite-generated sulfur isotope records agree well with each other (Kah et al., 2004), encouraging the use of CAS as an archive of the isotopic composition of seawater sulfate (e.g. Luo et al., 2015; Fike et al., 2006; Tostevin et al., 2017).

Evaporites

Sulfate evaporites have likely been a feature of the sedimentary record since the Great Oxidation Event (*GOE;* Holland, 2002), and possibly even earlier (Chandler, 1988). While the majority of evaporite deposits are precipitated from seawater-derived brines, significant terrestrial sulfate deposits are not uncommon, at least in more recent Earth history (e.g. Cenozoic; Palmer et al., 2004). As basin restriction and evaporative conditions are a requirement for the precipitation of sulfate salts, the obvious challenge in utilizing this archive in reconstructing ancient seawater sulfate compositions is to decipher local (restricted basin) from global signatures (Claypool et al., 1980 Van Stempvoort and Krouse, 1994; Lu et al., 2001). That is, while evaporative basins are by definition restricted, they preserve some of the best samples of seawater chemistry in the sedimentary record, provided significant local sulfate inputs do not overprint the seawater isotopic signature. While some extensive evaporative sequences are utilized in this study (e.g. Ten Stone Formation (NW Canada), Angmaat Formation (N. Canada)), many samples are from much more limited evaporite occurrences as veins and nodules (e.g. Juderina, West Australia). Beyond identifying the degree to which basins are restricted or influenced from the marine reservoir, is their immunity to local effects such as microbial sulfur cycling, or influence from locally weathered evaporites. This is true of Messinian aged deposits from southern Spain recording the closure of the Mediterranean Sea and subsequent deposition of large sulfate deposits that display variability of up to 2‰ for $\delta^{34}S$ and 5‰ for $\delta^{18}O$ (Lu et al., 2001). This variation in $\delta^{34}S$ is a possible consequence of reservoir effects coupled to fractionations of up to +1.6‰ in $\delta^{34}S$ and 3.7‰ for $\delta^{18}O$ for fractionations between sulfate bearing fluids and sulfate precipitates (Thode and Monster, 1965; Lloyd, 1968; Raab and Spiro, 1991). Evidence for local factors is also observed in the Red Sea where hydrothermal brines have been shown to depress the $\delta^{18}O$ value of sulfate in this setting (Longinelli and Craig 1967). Interpreting evaporite records can become increasingly complicated due to post-depositional factors that can not only influence isotopic values but also the distribution of preserved evaporite deposits in the sedimentary record. Given the ease at which gypsum is weathered it is unclear if the temporal distribution of preserved evaporite deposits reflects secular changes in sulfate and calcium concentrations in the ocean, the nature of continental margins (i.e. basin architecture), or the preservation of such deposits (Mackenzie and Garrels, 1971). Factors such as metamorphic equilibration or thermochemical sulfate reduction are also important factors to consider that may shift $\delta^{18}O$ more positive, and dilute primary signatures of original sulfate (Alonso-Azcárate et al., 2006). Despite these considerations, evaporite minerals remain among the best archives in the sedimentary record of ancient seawater chemistry, and thus are an important archive of the ancient sulfur and oxygen cycles.

In sum, all sulfate bearing phases can offer important insights into Earth's surface environments. Provided that the depositional setting can be identified, seawater isotope curves can be constructed, the primary nature of such archives can be further bolstered by combining isotopic records from geographically disparate but temporally equivalent, archives. What is apparent is that most post-depositional and post-sulfide-oxidation processes tend to push highly negative $\Delta^{17}O$ values and isotopically light $\delta^{34}S$ values of sulfate toward more positive values (e.g. Luz et al., 1999; Antler et al., 2013). This observation suggests that within sample sets from individual formations, the lightest $\Delta^{17}O$ and $\delta^{34}S$ values may be the most reflective of initial seawater compositions. General rules however are difficult to apply to $\Delta^{33}S$ and $\delta^{18}O$ values. However, poor age constraints and age-models make such efforts potentially perilous where true interformational variation could be lost. Given the above considerations herein we take a largely agnostic approach with isotopic data generated and compiled, and are cautious to discard extraneous values.

5.3 Isotopes of Sulfate

The concentration of seawater sulfate through Earth history is thought to increase with increasing atmospheric oxygen levels (e.g. Canfield and Raiswell, 1999; Canfield, 2005; Fig. 5.1). Further, sulfate is critical in the remineralization of organic carbon (Jørgensen, 1982) (and by extension, the fraction of organic carbon that is buried; f_{org}), making it a critical piece of a feedback loop controlling the degree of oxidation of Earth's surface environment. The sulfur and oxygen within sulfate that is ultimately preserved in the geologic record within sulfate-bearing minerals, records the history of redox shuttling between many reservoirs by both biological and abiological pathways. Importantly, kinetic (i.e. non-reversible) processes most commonly favor lighter products than their precursors. In the cases of sulfur and oxygen these fractionations are on the order of a few per mil, and provided that many of these processes are not completely reversible allows for the preservation of signals both between reservoirs in the modern environment and within sedimentary rocks in the geologic past. What has become apparent over the past decades is that both major isotopes of sulfur and oxygen within sulfate record different processes, most noticeably observed through the non-parallel trajectory of $\delta^{18}O$ and $\delta^{34}S$ records over much of the Phanerozoic (Bottrell and Newton, 2006). More recently however, it has been demonstrated that monitoring the minor isotopic values adds a new layer of information and insight into atmospheric chemistry (e.g. Farquhar et al., 2001; Bao et al., 2008), diagenetic processes (Pellerin et al., 2015a; Crémière et al., 2017) and sulfur based microbial metabolisms (Leavitt et al., 2013; Pellerin et al., 2015b; Bradley et al., 2016; Antler et al., 2017). Therefore a great deal of information is extractable from the minor isotopes of sulfate that can provide insights from both planetary to cellular scale processes.

$\Delta^{17}O$

An example of this new dimension is the information contained within the ratio of ^{17}O to ^{16}O relative to the ratio of ^{18}O to ^{16}O in oxygen-bearing species such as sulfate. Upon reaching sufficient levels of atmospheric oxygen to establish an ozone (O_3) layer, O_2 becomes imprinted with a mass-independent signature imparted through the formation and destruction of ozone (Fig. 5.2). During photolysis O_3 will dissociate into a single oxygen atom and one O_2 molecule. Symmetry effects during recombination of ozone as well as reactions with other atmospheric species that temporarily sequester heavy isotopes, has a net effect on the O_2 molecules retaining ^{16}O-^{16}O bonds resulting in tropospheric oxygen being mass independently depleted in heavy isotopes (Thiemens and Heidenrich, 1983; Heidenrich and Thiemens, 1986; Thiemens, 2006; Fig. 5.2). This process is so active that even in the modern environment depletions in ^{17}O are observed in tropospheric oxygen with an isotopic signature with five less ^{17}O atoms per ten thousand atoms ($\Delta^{17}O$ = -0.5‰) than is predicted (Barkan and Luz, 2011). Since initial experiments that explored the photochemical dissociation of ozone it has been observed that the magnitude of this $\Delta^{17}O$ signal in atmospheric oxygen is also dependent upon reactions involving the spalled off oxygen atom and other stratospheric species (Blunier et al., 2002; Bao et al., 2008). Reactions with these species preserve the negative $\Delta^{17}O$ signature of residual O_2 from photochemical reactions by temporarily sequestering the positive isotopic anomaly, thus making the magnitude of $\Delta^{17}O$ depletions proportional to the concentrations of these species. The main atmospheric constituent that governs the expression of $\Delta^{17}O$ values of atmospheric oxygen is thought to be CO_2 and importantly its concentration has likely varied significantly throughout Earth history (Gamo et al., 1989; Wen and Thiemens, 1993; Yung et al., 1991; 1997; Blunier et al., 2002; Figs. 5.1 and 5.2). This stratospheric flux is counteracted in the troposphere through photosynthetically produced oxygen from the biosphere that bears a $\Delta^{17}O$ value of seawater (0‰; Luz et al., 1999). Therefore, the $\Delta^{17}O$ signature of atmospheric oxygen represents a balance between the amount of CO_2 available to sequester the positive $\Delta^{17}O$ anomaly, the rate of oxygen produced from the biosphere (Gross Primary Productivity (*GPP)*), and the size of the O_2 reservoir (Cao and Bao, 2013; Fig. 5.2). The clearest example of the CO_2-$\Delta^{17}O$ relationship is observed through the ice core record over the past 60,000 years where increases in CO_2 from the last glacial period to the present are paralleled by decreasing $\Delta^{17}O$ values (Blunier et al., 2002). Given that atmospheric oxygen archives do not extend beyond the ice-core record (<1 Myrs; Barnola et al., 1987; Petit et al., 1999; Stolper et al., 2016) other oxygen bearing archives that can maintain a portion of the atmospheric signal are required for explorations into earlier times in Earth history. Sulfate is one such example that is much more resilient to isotopic exchange than many other oxy-anions (Hall and Alexander, 1940; Gamsjager and Murmann, 1983; Bao, 2015) and through the oxidation of sulfide minerals a predictable portion of the $\Delta^{17}O$

atmospheric oxygen signature is incorporated into product sulfate (8-30%; Balci et al., 2007; Kohl and Bao 2011; Fig. 5.2). This allows for the preservation of $\Delta^{17}O$ signals for billions of years in depositional environments where limited sulfur cycling occurs that would otherwise erase initial $\Delta^{17}O$ signals. Importantly all subsequent processes following sulfide oxidation will remove anomalous $\Delta^{17}O$ values and cannot impart them, therefore interpreting minimum values provides conservative estimates of original $\Delta^{17}O_{O2}$ values. Despite this potential utility in probing the geologic record for new information on pCO_2 and *GPP* levels that have likely varied significantly through Earth history (Fig. 5.1), the current $\Delta^{17}O$ record of sulfate only extends slightly beyond the Cryogenian (717-635; Bao et al., 2008; Bao, 2015).

$\delta^{18}O$

The $\delta^{18}O$ composition of modern marine sulfate (9.3‰; Lloyd, 1968) sits between the two large biologically accessible reservoirs: atmospheric oxygen at 22.9‰ (Nier, 1950) and seawater at 0‰ (Fig. 5.3). If allowed to reach equilibrium with seawater, sulfate would be enriched in ^{18}O by ≈23‰ relative to seawater at 25˚C (Zeebe, 2010), however the slow kinetics of isotope exchange at low temperatures and moderate pH values allow for various processes to modify its isotopic composition away from this equilibrium value (Zak et al., 1980; Turchyn and Schrag, 2006). Both abiological and biologically mediated isotopic exchange between these reservoirs is central to governing the $\delta^{18}O$ isotopic composition of sulfate in the modern environment and likely also dictated the isotopic composition of marine sulfate in the past. Sulfate is cycled through many metabolic pathways where biological selection, or rapid equilibration of reaction intermediates (e.g.

sulfite and thiosulfate) with oxygen-bearing species (typically H_2O), sequestering light oxygen isotopes and enriching residual sulfate in heavy isotopes (Mizutani and Rafter, 1973; Fritz et al., 1989). Another mechanism identified to shift the $\delta^{18}O$ of seawater sulfate to more positive values is dissolution of evaporite deposits, provided that earlier oceans contained isotopically heavier sulfate (Tostevin et al., 2014; Fig. 5.3). This mechanism however, while valid for modern environments, may not be relevant for earlier times in Earth history where evaporites would be deposited under different pH, CO_2 and marine sulfate conditions (Fig. 5.1). Finally the production of dimethyl sulfide (DMS) through the degradation of dimethylsulfonium propionate in marine algae ultimately leads to the rapid exchange of isotopes between SO_2 and other oxy-anions that can enrich product sulfate by up to 20‰ in $\delta^{18}O$ (Kumar et al., 2002; Holt et al., 1983), and this flux has been estimated to be up to one third of the flux of modern riverine sulfate (Turchyn and Schrag, 2006), thus tying isotopic records to the emergence of such metabolisms (Figs. 5.1 and 5.3). Direct sulfide oxidation on the continents and reoxidation in sediments are the primary processes driving the $\delta^{18}O$ composition to values typically lower than initial marine sulfate values (Van Stempvoort and Krouse, 1994) and the influence of reoxidative sulfur cycling has likely varied significantly through Earth history (Canfield and Farquhar, 2009; Tarhan et al., 2015; Kunzmann et al., 2017; Fig. 5.1).

$\delta^{34}S$

Sulfate primarily enters the ocean via riverine input, which has a $\delta^{34}S$ composition reflective of the lithology being weathered in the provenance (dominated either by sulfate evaporites or organic matter-rich, sulfidic shales; Fig. 5.4). In the modern environment, and in Proterozoic time as well, a large portion of sulfur removed from the ocean is done so as pyrite (≈10-99%) due to most evaporite deposits being rapidly recycled back into the marine reservoir via riverine input (Canfield et al., 2004; Halevy et al., 2012; Canfield, 2013; Tostevin et al., 2014; Fig. 5.4). Additional fluxes of sulfate into and out of the marine reservoir include biologically and abiologically mediated sulfide oxidation (source), volcanic inputs (source) and hydrothermal alteration of oceanic crust (sink; Wolery and Sleep, 1976; Alt, 1995; Fig. 5.4). Pyrite burial is typically biologically mediated through dissimilitory sulfate reduction where sulfate is effectively respired to produce H_2S/HS^- which then reacts with iron to produce iron sulfide minerals and eventually pyrite (Jørgensen, 1982). Since the isotopic difference between pyrite and sulfate minerals from the existing geochemical record approximates sulfur isotopic fractionations associated with dissimilatory sulfate reduction, it seems that this metabolism has been a dominant control on pyrite burial for much of Earth history (Shen et al., 2001; Butler et al., 2004; Johnston, 2011; Fig. 4). Another metabolic pathway that imparts a $\delta^{34}S$ signature to marine sulfur involves inorganic fermentation without phosphorylation, termed sulfur disproportionation, where intermediate sulfur species (e.g. elemental sulfur, thiosulfate, sulfite) are disproportionated to produce H_2S and sulfate (Bak and Cypionka, 1987; Jørgensen, 1990; Thamdrup et al., 1993; Canfield et al., 1998; Finster, 2008). Initially sulfur disproportionation reactions were thought to be the only pathway capable of producing large, $\delta^{34}S$ >46‰ differences between sulfate and H_2S (ultimately preserved as pyrite) (Canfield and Thamdrup, 1994; Böttcher et al., 2001) and previous work dated the emergence of this metabolism to as early as the Paleoarchean and inferred it to be an important pathway in the Mesoproterozoic sulfur cycle (Philippot et al., 2007; Detmers et al., 2001; Johnston et al., 2005b). Both interpretations identifying this metabolism based on isotopic results have been challenged with recent works demonstrating large sulfur isotope fractionation during dissimilatory sulfate reduction up to -70‰ (Canfield et al., 2010; Sim et al., 2011; Wing and Halevy, 2015), and subsequent publications exploring the Precambrian sulfur cycle suggest that this metabolism only rose to prominence in the Ediacaran (Johnston et al., 2005b; Ueno et al., 2008; Shen et al., 2009; Kunzmann et al., 2017). However, the intensity of dissimilatory sulfate reduction is one of the dominant controls on the $\delta^{34}S$ composition of marine sulfate with increased dissimilatory sulfate reduction leading to a progressively isotopically heavier marine sulfate reservoir due to organisms preferential uptake of light isotopes (Thode et al., 1951; Harrison and Thode, 1958; Fig. 5.4). Therefore both the nature of the biosphere, intensity of its ability to cycle sulfur, and relative strength of abiological processes such as weathering and hydrothermal reactions control the $\delta^{34}S$ isotopic composition of the marine sulfate reservoir (Bottrel and Newton, 2006; Tostevin et al., 2014; Fig. 5.4. The sensitivity of these factors to atmospheric and marine chemistry likely make further revealing such records informative in pursuit of understanding the evolution of the surface Earth (Fig. 5.1).

$\Delta^{33}S$

The near disappearance of mass independent sulfur isotope anomalies from the geologic record in the earliest Paleoproterozoic has arguably been the most convincing observation for a rise in atmospheric oxygen over this interval of Earth history (Farquhar et al., 2000).

In the absence of an ozone layer, UV radiation is permitted to penetrate into the lower atmosphere and drive photochemistry that imparts a large mass independent fractionations into sulfur species that remain in sulfur species cycling in the surface environment (Fig. 5.4). Beyond a litmus test for the presence of atmospheric oxygen, the utilization of multiple sulfur isotopes within the mass-dependent range of fractionation has brought invaluable information to the geochemical record, particularly in identifying different metabolisms that obey different mass laws ($^{33}\lambda$ or $^{33}\theta$; cf. Johnston, 2011) in governing their diagnostic fractionations in $\Delta^{33}S$-$\delta^{34}S$ fields (Farquhar et al., 2003; Johnston et al., 2005a; Johnston et al., 2011; Zerkle et al., 2009). Differences in mass laws are due to different metabolisms allowing for different degrees of isotopic exchange between sulfur-bearing species during respective metabolic processes, potentially a result of different capacities for kinetic isotope effects to modify isotopic values (Wing and Halevy, 2014). For example sulfur disproportionators have been found to have a slightly higher affinity for taking up ^{33}S versus ^{34}S during metabolic processes compared to dissimilatory sulfate reducers, resulting in a slightly larger (> 0.515) mass law (Johnston et al., 2005a). Beyond metabolic processes the utilization of minor sulfur isotopes can also aid in a more accurate accounting for processes within sediments (e.g. diffusion; Pellerin et al., 2015a). However, similar to $\Delta^{17}O$ records, the Proterozoic Eon is far from replete with $\Delta^{33}S$ data of sulfates, leaving models based on the $\Delta^{33}S$ values of sulfides reliant upon assumptions about initial marine sulfate isotopic values (Scott et al., 2014; Kunzmann et al., 2017). Again this highlights the need for expanded records as $\Delta^{33}S$ values are predicted to vary in response to evolving surface conditions over the Proterozoic (Fig. 5.1)

Links and Gaps

While much progress has been made toward identifying the controls on the isotopic composition of modern marine sulfate, additional work is needed to fully understand the cycles of its embedded isotopic systems both in modern and ancient environments. This is not to say that great strides have not been made in aforementioned isotopic systems. For example the disappearance of large S-MIF signatures from sulfates and sulfides across the *GOE* is largely credited with ending the debate as to when free oxygen initially accumulated in the atmosphere (Farquhar et al., 2000). Furthermore, the use of multiple sulfur isotopes have also been implemented to develop isotopic tools to exploit measured and calculated mass laws to isotopically distinguish different metabolisms, providing evolutionary calibration points to explore the geologic record (Johnston et al., 2005b; Ono et al., 2006; Sim et al., 2011; Kunzmann et al., 2017). Critically, in the case of sulfur disproportionation, ties have been made to atmospheric oxygen level being causally linked to the rise to prominence of this metabolism, thus suggesting oxygenation of the marine realm across the Ediacaran (Canfield and Teske, 1996; Kunzmann et al., 2017). Progress has also been made through utilizing $\delta^{34}S$ values of coeval sulfate and pyrite to reconstruct marine sulfate concentrations (Harrison and Thode, 1958; Habicht et al., 2002; Hurtgen et al., 2005; Gomes and Hurtgen, 2013; Luo et al., 2015). The $\Delta^{17}O$ signal of sedimentary sulfates has been an important tool in providing evidence for the Snowball Earth hypothesis with large $\Delta^{17}O$ anomalies reported on five paleo-continents providing strong support for large syn-glacial CO_2 buildup on an ice-covered planet (Bao et al., 2008; Bao et al., 2009; Crockford et al., 2016; Cao and Bao, 2013) as well as evidence for a significantly smaller mid-Proterozoic biosphere (Crockford et al., *in review*). Despite these efforts the current isotopic record is sparse with the most notable gap in data spanning the majority of the Proterozoic Eon.

While each of the above isotopic systems is sensitive to various controls, they contain key linkages that permit some degree of cross-calibration. For example microbial metabolisms will preferentially utilize light isotopes (^{16}O and ^{32}S), leaving residual seawater relatively isotopically heavy (i.e. enriched in ^{18}O, ^{17}O and ^{34}S, ^{33}S, ^{36}S). The different residence times between $\delta^{34}S$ and $\delta^{18}O$ as well as differences in processes that modify their isotopic values, make them powerful in constraining possible scenarios that could have generated observed isotopic trends. For example, a lack of covariation likely suggests processes in operation that are independent of changes in oxidative weathering and riverine input (Turchyn et al., 2009). The size of the atmospheric oxygen reservoir modifies the $\Delta^{17}O$ composition of atmospheric oxygen which given sufficient fluxes into the marine environment, can impart a signature into marine sulfate that ultimately gets cycled by the biosphere. Changing atmospheric oxygen levels however will impact reoxidative sulfur cycling and metabolisms in operation that bear isotopic consequences for $\delta^{18}O$, $\delta^{34}S$ and $\Delta^{33}S$ values (Canfield and Teske, 1996; Kunzmann et al., 2017). These linkages along with others provide a framework for interpretation where signals in one system make predictions for others, making their combined use advantageous in seeking drivers of isotopic variability (Bao et al., 2007; Antler et al., 2013; Crockford et al., 2016).

As seawater chemistry has changed through Earth history (Fig. 5.1), the speciation of biologically essential nutrients may have also shifted though the impact of these changes to metabolisms is unclear (Dupont et al., 2010; Robbins et al., 2017). Laboratory cultures have identified diagnostic fractionation factors for different species of both dissimilatory sulfate reducers as well as disproportionators and it is unclear what species may have dominated in the distant geologic past. Recent work has also identified that microbial fitness is an evolutionarily modifiable trait, and it remains unclear if ancestors were as efficient as their modern descendants (Pellerin et al., 2015b). Furthermore, explorations into intercellular oxygen isotope effects particularly those involving ^{17}O are virtually non-existent in the literature, which limits the interpretation of such data. A critical first step in drawing meaning from modern calibrations into ancient systems however, is developing a record to frame the range in values uncovered through Earth history. To do this, an important next step is to expand isotopic records of sulfate through Earth history that will provide the ability to further test laboratory-based studies, and test existing hypotheses.

5.4 Methods

Samples

For this study we analyzed over 300 samples from 32 different locations on every continent with the exceptions of South America and Antarctica (Fig. 5.5; Table 5.1). We rely on the most current literature estimates of ages for formations and summarize this along with sample locations, and formation names in figure 5.1 and Table 5.1, respectively. This sample suite covers the oldest known sulfate-evaporite occurrences from North America (Gordon Lake Formation) and from South Africa (Duitschland Formation) to Ediacaran aged samples from southern Iran and Siberia. The majority of samples were deposited as sulfate evaporite minerals with a few exceptions where carbonate associated sulfate (CAS) was measured.

Sample Preparation

Sulfate evaporites were micro-drilled from thin beds, veins and bladed crystal forms, or hand crushed using an agate mortar and pestle in the case of massively bedded deposits and nodules. For CAS samples, 50 to 500 g of carbonate were crushed in a steel ring mill and resulting powders were then placed into a 1 L Pyrex Erlenmeyer flask. Powdered carbonates were first placed in a 5% sodium chloride (NaCl) solution for 12 hours and then subject to multiple rinses with deionized water to remove any non-CAS sulfate. Next, samples were placed in a weak (5%) hydrogen peroxide (H_2O_2) solution for 12 hours in order to oxidize pyrite and subsequently precipitate and remove it from solution as sulfate. Samples were then dissolved into a 4 N hydrochloric acid (HCl) – 5% tin chloride ($SnCl_2$) solution over a 12-hour period. Samples were then decanted and filtered through a 0.45 μm filter and mixed with a concentrated barium chloride ($BaCl_2$) solution to precipitate liberated sulfate as barite over a 72-hour period. Finally, barite precipitates were collected onto a 0.2 μm filter, lightly rinsed with 4 N HCl, and dried in an oven at 80˚C. Although HCl and acetic acids have been shown to oxidize sulfides, and thus potentially affect samples in both oxygen and sulfur isotope values in CAS (e.g. Marenco et al., 2008), calculated modal pyrite abundances within a subset of analyzed evaporite samples of less than 0.3% pyrite-sulfur likely renders such isotopic contamination insignificant.

Oxygen Isotopes

Oxygen isotope measurements ($\Delta^{17}O$ and $\delta^{18}O$) were made at the Louisiana State University OASIC laboratory. Samples were taken through a series of dissolution and precipitation steps (Bao et al., 2006) in order to remove all non-sulfate oxygen-bearing contaminants such as nitrate. Samples of evaporites were first dissolved into a 0.05 N Diethylenetriaminepentaacic acid (DTPA) – 1.0 M sodium hydroxide (NaOH) solution. Upon dissolution samples were filtered through a 0.2 µm filter to remove silicates or non-soluble residues in samples. After filtering, samples were precipitated by driving saturation up, and pH down by adding double-distilled 6 N HCl at 80˚C followed by $BaCl_2$, thus preventing witherite ($BaCO_3$) formation. This full procedure was then repeated and final products were dried in an oven at 80˚C.

Oxygen was generated from sulfates to measure $\Delta^{17}O$ values using a laser fluorination system. Approximately 10 mg sample powders were loaded onto a stainless steel (SS316) plate and placed into a SS316 chamber capped with a BaF_2 window. The chamber was then exposed to a bromine pentafluoride (BrF_5) atmosphere of >100 mbar for three minutes, cleaned, and followed by another BrF_5 injection at 20 mbar for 12 hours. The sample chamber was then evacuated and the atmosphere replaced with a fresh injection of BrF_5. Samples were heated with a CO_2 laser which liberated oxygen from sulfate. Upon lazing, analyte gas was passed through five cold traps at -196˚C to remove any condensable gases. Purified oxygen was then collected onto 5A mol-seive immersed in a cold-trap for seven minutes. Samples were then analyzed on a Thermo MAT-253 in dual inlet mode. Analyses were conducted over 3 acquisitions consisting of 8 standard-sample brackets. Error on the total analytical procedure including analyses is estimated to be ≈ 0.03‰ for $\Delta^{17}O$ with a maximum 1σ error of 0.05‰ on individual analyses.

Measurements of $\delta^{18}O$ values were performed on the same samples that had been through the barite cleaning procedure described above. Between ≈ 180 and 220 μg of sample was weighed out and wrapped in silver foil before loading samples into a thermal conversion elemental analyzer (TC/EA) coupled to the same Thermo MAT-253 isotope ratio mass spectrometer set in continuous flow mode. Samples were analyzed in duplicate and the total error on analyses is estimated from replicate analyses of in house standards to be below 0.3‰.

Sulfur Isotopes

In order to liberate sulfur from sulfate minerals, samples were placed into Thode solution (HI, H_3PO_2 and HCl; Thode et al., 1961; Pepkowitz and Shirley 1951) and boiled at 100˚C. In this solution sulfate was converted to hydrogen sulfide (H_2S) and carried through a chilled column in a nitrogen gas stream. H_2S was bubbled through deionized water followed by a zinc acetate trap to convert H_2S to zinc sulfide (ZnS). Solutions containing ZnS were then reacted with 0.2 M silver nitrate ($AgNO_3$) to precipitate silver sulfide (Ag_2S). Samples containing Ag_2S precipitates were then collected onto a 0.45 μm membrane and dried in an oven at 80˚C. Once dried, approximately 3 mg of Ag_2S was weighed into a cleaned aluminum foil and placed into a nickel bomb under a fluorine gas (F_2) atmosphere at 250˚C and allowed to react for 12 hours. Within nickel bombs F_2 reacts with Ag_2S to produce sulfur hexafluoride gas (SF_6). SF_6 gas was purified through multiple cold-traps under vacuum, followed by gas chromatography. Once purified, samples were analyzed as SF_5^+ on a Thermo MAT-253 in dual inlet mode. Results were measured against international standard reference material IAEA-S1. Estimated maximum errors (1σ) on measurements and the entire analytical procedure are 0.1‰ for $\delta^{34}S$ measurements and 0.01‰ for $\Delta^{33}S$ measurements.

5.5 The Isotopic Record of Proterozoic Sulfate

We explore the isotopic record of Proterozoic sulfate through new data generated in this study (Figs. 5.6-8) along with compiled literature data through five Proterozoic Intervals. Given that large age uncertainties are endemic to evaporite deposits (i.e. no organics for Re-Os dating, or zircons for U-Pb dating) together with significant gaps in the sulfate evaporite record, allows for a large degree of freedom in setting boundaries between such intervals. Beyond the sulfate isotope record, we rely upon other geochemical records tracking Earth's surface evolution such as changes in the $\delta^{13}C$ of carbonates and organic matter that indicate variations in the fraction of carbon buried as organic matter through time (f_{org}; Krissansen-Totten et al., 2015). These boundaries are broadly consistent with previously suggested changes in the redox state of the Earth's atmosphere and oceans (Holland, 2006; Lyons et al., 2014).

First, we isolate the Great Oxidation Event (*GOE*; ca. 2.45 – 2.0 Ga) that some have argued should be designated as its own geological period termed the Eoproterozoic (Havig et al., 2017) which includes the disappearance of S-MIF signatures ($\Delta^{33}S > 0.2‰$) in both reduced and oxidized forms of sulfur, as well as including the Lomagundi-Jatuli positive carbon isotope excursion (Gumsley et al., 2017; Bekker et al., 2004, Bekker 2014a, b). Next, the mid-Proterozoic (2.0 – 1.1 Ga) encompasses most of the colloquially named ‘boring billion’ that defines what is thought of as ‘typical’ Proterozoic conditions with higher atmospheric CO_2, lower oxygen and no evidence of glaciation (Kasting and Ono, 2006, Laakso and Schrag, 2014). The late Proterozoic (1.1 – 0.72 Ga) marks a gradual increase in the carbon isotope composition of the DIC reservoir possibly a result of increased atmospheric oxygen levels (Gilleaudeau et al., 2016; Kah et al., 2004) in response to either a diversification in primary producers in the biosphere and increasing proportions of carbon buried as organic matter (Krissansen-Totton et al., 2015) or tectonic drivers related to the assembly and breakup of Rodinia (e.g., Li et al., 2013; Kuznetsov et al., 2017). In contrast to previous studies outlining broad secular trends in the evolution of the Earth’s surface environment we isolate the Cryogenian period (0.72-0.635 Ga) as it is becoming apparent that this interval is climatologically and geochemically distinct from times before or after (Hoffman et al. *in press*). Finally, we discuss the Ediacaran (0.635-0.541 Ga) that bridges the Proterozoic and Phanerozoic Earth surface environment. With all of these isotopic systems within sulfate it is difficult to discuss the Proterozoic in complete isolation from the preceding Archean and the following Phanerozoic, therefore we use these eons as end member examples of how sulfur and oxygen cycles operated under different surface conditions when exploring the Proterozoic record.

The Archean

The isotopic composition of Archean sulfate depicts near zero $\Delta^{17}O$ values (Farquhar et al., 2000; Bao et al., 2007), which is contrasted by a large amount of variation in $\Delta^{33}S$ values with the maximum expression of this near the Archean-Proterozoic transition

(Johnston, 2011). Major isotopic compositions show limited variation in $\delta^{18}O$ and $\delta^{34}S$ values compared to later times in Earth history (Canfield and Farquhar, 2009), however, in the case of $\delta^{34}S$ values, sufficient deviations from the pyrite record have been used to suggest the advent of microbial sulfate reduction as early as 3.5 Ga (Shen et al., 2001). These isotopic records are consistent with much lower sulfate inventories (e.g. <200 μM; Habicht et al., 2002; ≈80 μM Jamieson et al., 2012; <2.5 μM Crowe et al., 2014) than Proterozoic or Phanerozoic Eons largely driven by a much different atmospheric and biospheric composition than later times in Earth history. Reduced sulfate levels were a likely consequence of extremely low atmospheric oxygen, throttling many of the dominant input pathways that maintain the 28 mM sulfate level in the modern ocean. Provided atmospheric oxygen and marine sulfate reached the low levels predicted by many studies, distinct isotopic signatures in the minor isotopes of sulfate should reflect these conditions. Although some similar major isotope signatures of sulfate between modern, post-GOE and Archean samples have been observed (Shen et al., 2001), the relatively large atmospheric flux at this time prevents direct calibrations and comparisons of pre-*GOE* with post-*GOE* sulfur isotopic signatures.

In a low oxygen pre-*GOE* atmosphere, UV radiation would have been permitted to reach the lower atmosphere and drive sulfur photochemical reactions imparting large S-MIF signatures to product sulfur species (Farquhar et al., 2000; Farquhar and Wing, 2003; Endo et al., 2016; Ono, 2017). Critically, the existence and expression of large S-MIF provides a suite of constraints on the Archean atmosphere. Pavlov and Kasting, 2002 calculated that the S-MIF signature would likely only exist between pO_2 levels of 10^{-5} and 10^{-13} PAL. Under such conditions, mechanisms invoked to explain modern mass independent oxygen isotope fractionation would not be permitted as they rely on the creation and destruction of ozone and subsequent reactions with other atmospheric species such as CO_2 (Thiemens and Heidenreich, 1983; Wen and Thiemens, 1993). Although the record of Archean sulfate deposits is sparse (possibly a consequence of near-permanently undersaturated with respect to gypsum and barite due to low levels of sulfate in seawater (Horner et al., 2017)), existing Δ^{17}O data for ca. 3.5 Ga barites from Western Australia and 3.2 Ga barites from South Africa appear consistent with the scenario outlined by Δ^{33}S values, with Δ^{17}O values falling within a mass-dependent-near-zero range (Farquhar et al., 2000; Bao et al., 2007). Although the Archean atmosphere is thought to have held much larger inventories of greenhouse gases, the existence of S-MIF can only exist provided that shielding from organic hazes (Domagal-Goldman et al., 2008; Zerkle et al., 2012), or atmospheric species, did not exceed levels that shield UV radiation from penetrating the stratosphere, therefore placing upper limits on such gases (e.g. $pCO_2 < 0.5$ bar; Farquhar et al., 2001).

While Archean atmospheric chemistry drove large mass-independent isotopic signatures of sulfur, but not oxygen (Farquhar et al., 2000; Bao et al., 2007), surface mass dependent processes isotopically fingerprinted sulfur pools and these signals have been preserved within the sedimentary record (Halevy et al., 2010). Large δ^{34}S fractionations between barite and associated sulfide with similarly negative Δ^{33}S values in 3.5 Ga rocks have been argued as strong evidence that dissimilatory sulfate reduction was an important metabolism driving the sulfur cycle at this time (Shen et al., 2001; Ueno et al., 2008; Shen et al., 2009). While many major metabolisms that characterize the modern Earth may have originated in Archean environments (Hug et al., 2016), the degree to which they operated would likely have been far different. These factors make the Archean sulfur and oxygen cycles geochemically distinct from any later time in Earth history and thus they can serve as a baseline in interpreting later records.

GOE (2.4 – 2.0 Ga)

Results from sulfate data generated here, together with compiled data from previous studies show muted variations in $\Delta^{33}S$ values compared to the Archean and earliest Proterozoic with all data falling within a mass-dependent range (Farquhar and Wing, 2003). Triple oxygen values display the opposite behavior with the first mass independent oxygen isotope signals observed in the earliest evaporite deposits from South Africa (Duitschland Formation) and Canada (Gordon Lake Formation; Table 1; Figs. 5.5 and 5.6) displaying $\Delta^{17}O$ values down to -0.34 and -0.36‰ respectively (Fig. 5.6). Major sulfur isotopic ($\delta^{34}S$) data displays a wide range between 4 and 42‰, however most values fall near an average of 16‰ (Fig. 5.7). Major oxygen isotopes ($\delta^{18}O$) display values that are slightly heavier than modern seawater with an average value of 13‰ (Fig. 5.7).

Minor isotope records are consistent with characterizations of the Archean-Proterozoic transition with an increase in the oxidative capacity of the atmosphere (Lyons et al., 2014; Fig. 5.1) indicated by mirrored trends in $\Delta^{33}S$ and $\Delta^{17}O$ values within sulfate. Specifically at 2.35 Ga there is a disappearance in S-MIF with $\Delta^{33}S$ values falling to within +/- 0.2‰ from the over 12‰ variation observed over the latest Archean which is coincident with an increase in the magnitude of O-MIF with $\Delta^{17}O$ values reaching down to < -0.3‰ (Fig. 5.7). Whether a result of an increase in organic carbon burial due to the advent of oxygenic photosynthesis (Soo et al., 2017), a rise to dominance of this metabolism millions of years after its evolution (Castresana and Saraste, 1995; Pereira et al., 2001; Crowe et al., 2013; Planavsky et al., 2014b), tectonomagmatic evolution linked to the assembly and breakup of supercontinents/supercratons (Gumsley et al., 2017), or a sharp decrease in reductant fluxes to the surface environments (Ebelmen, 1845; Berner and Maasch, 1996; Canil, 1997; Kump et al., 2001), the disappearance of S-MIF signatures from the sedimentary record indicate an increase in atmospheric oxygen levels above predicted thresholds (Farquhar et al., 2000; Pavlov and Kasting, 2002; Guo et al., 2009). This increase in pO_2 across the *GOE,* however, was likely even higher than that required to remove S-MIF signatures with previous studies highlighting the inherent instability of Earth's climate with pO_2 levels between 10^{-5}-10^{-3} PAL (Goldblatt et al., 2006). An increase in atmospheric oxygen levels can also be observed in macroscale features of the sedimentary record with a disappearance of detrital pyrites and uraninites (Rasmussen et al., 1999), large manganese deposits (Laznicka, 1992; Kirschvink et al., 2000; Kunzmann et al., 2014), the appearance of redbeds, and perhaps most notably the first appearance of sulfate evaporites at <2.4 Ga (Wood, 1973; Bekker et al., 2006; Schröder et al., 2008), that are also suggestive of a rise in marine sulfate concentrations above ≈ 2.5 mM (Schröder et al., 2008). While mechanisms exist for a more complicated record of the disappearance of S-MIF either from crustal recycling of Archean terranes (Selvaraja et al., 2017) or initial oxidative terrestrial pulses bearing S-MIF signatures, masking a rise in atmospheric oxygen (Reinhard et al., 2013a), the lack of S-MIF in Earth's earliest sulfate evaporite deposits suggest that such processes were not able to exert a measureable influence on marine sulfate as of 2.43-2.35 Ga (Fig. 5.6). That is, the marine sulfate $\Delta^{33}S$ record preserved within sulfate evaporites lends credence to suggestions that the accumulation of oxygen in the atmosphere and subsequent increase in the intensity of sulfur cycling was relatively rapid upon the destruction of S-MIF (Bekker and Kaufman, 2007; Gumsley et al., 2017; Luo et al., 2016). Moreover analysis of over 80 samples from seven different formations on three different continents all yielding $\Delta^{33}S$ values with no mass-independent signature suggests that any recycling of Archean sulfur, or a protracted history of atmospheric oxygen was not preserved within the sulfate evaporite record and was therefore likely never sufficient to have been of global significance.

Beyond suggesting a growth of the marine sulfate reservoir through their existence, these earliest sulfate evaporite deposits bear negative $\Delta^{17}O$ values that not only confirm inferences made from $\Delta^{33}S$ data, but also add new layers of information. The existence of such negative $\Delta^{17}O$ values requires sufficient atmospheric oxygen to establish an ozone layer and by consequence a predicted mirrored trend between $\Delta^{33}S$ and $\Delta^{17}O$ values across this interval. Mirrored mass independent $\Delta^{33}S$ - $\Delta^{17}O$ records have been posited across the *GOE* and results from this study support such a prediction (Bao, 2015; Figs. 5.6 and 5.9). Minimum $\Delta^{17}O$ values measured in *GOE*-aged formations between -0.4 to -0.3‰ must have been deposited under different pCO_2-pO_2-*GPP* conditions than experienced in the modern environment, as present day O_2 with a $\Delta^{17}O$ value of ≈ -0.5‰ cannot impart more than ≈30% of its signature into product sulfate (Kohl and Bao, 2011). While large uncertainties exist when extending atmospheric models to the Archean-Proterozoic transition (particularly with respect to atmospheric oxygen levels), multiple lines of evidence support much higher pCO_2 levels than the modern (von Paris et al., 2008; Kanzaki and Murakami, 2014; Wolf and Toon; 2014; Blättler et al., 2017). Such inferences can be considered conservative as multiple processes can drive $\Delta^{17}O$ signatures more positive but only photochemical reactions in the stratosphere and a less productive biosphere appear to drive values more negative (Cao and Bao, 2013). Under the assumption that atmospheric O_2 reached somewhere between half and double modern levels (Bachan and Kump, 2014) in conjunction with existing CO_2 estimates that are nearly unanimous in arguing for elevated concentrations from modern levels (von Paris et al., 2008; Rosing et al., 2010; Sheldon, 2006; Blättler et al., 2017; Table 5.2) suggest that the *GOE* may have been characterized with the highest levels of primary production experienced over all of Earth history (Fig. 5.10).

With these considerations however, when considering previous estimates of atmospheric inventories of CO_2 and O_2, it is important to note that these estimates do not capture the likely dynamic nature of atmospheric chemistry across the *GOE* as extensive glaciations (Young et al., 1991), possibly of global nature (Evans et al., 1997; Kirschvink et al., 2000; Kopp et al., 2005; Bekker 2014) engulfed the Earth, and inferred oxygen "overshoots" dramatically changed the Earth surface environment at this time (Bekker and Holland, 2012; Partin et al., 2013; Bachan and Kump, 2015). These possible Snowball Earth glaciations must have induced large perturbations to the Earth system (cf. Bekker et al., 2005; Bekker and Kaufman, 2007; Zahnle, 2006; Konhauser et al., 2009) that may not have been captured in the preserved marine sulfate record as their existence, like Cryogenian glaciations, would cause extremely low sedimentation rates (Partin and Sadler, 2016). Furthermore the *GOE* record of sulfate within evaporite minerals is only present between ~2.35 and 2.05 Ga, upon which it has been suggested that O_2 levels in the atmosphere dropped dramatically coincident with the end of the Lomagundi-Jatuli positive carbon isotope excursion (Bekker and Holland, 2012; Planavsky et al., 2012; Scott et al., 2014). A likely outcome of a drop in atmospheric oxygen levels after the *GOE* would be a contraction of the marine sulfate reservoir and by consequence a gap in evaporite deposition over this interval.

Inferences into the Earth System across the *GOE* based on the minor isotopes of sulfate are largely borne out in its major isotope ratios ($\delta^{18}O$ and $\delta^{34}S$) (Figs. 5.6 and 5.7). Unlike the $\Delta^{17}O$ system, the $\delta^{18}O$ values of sulfate primarily reflect the balance between sulfate reduction and reoxidation (Turchyn et al., 2009). The most positive $\delta^{18}O$ values observed over the Proterozoic are across the *GOE* with a maximum value of 36.1‰ and an average value over this interval of 14.5‰ (approximately 6‰ heavier than modern seawater sulfate; Fig. 5.7; Table 5.1.). Highly positive values are also observed across the late-Proterozoic with values reaching 30.6‰, and an average value of 15.0‰ (Fig. 5.7). These highly positive values are achievable provided sulfate and ambient seawater are able to reach equilibrium with one another, however such conditions are only possible over 10^{7}-10^{9} year timescales, or at pH and temperature conditions far outside of likely *GOE* seawater conditions (Lloyd, 1968; Halevy and Bachan, 2017; Crockford et al., 2014). Generating such positive values could be achieved through increases in reoxidative sulfur cycling by sulfur disproportionating bacteria, however as mentioned previously, this metabolism did not likely rise to prominence until the Ediacaran (Kunzmann et al., 2017). Other mechanisms include large-scale evaporite weathering or atmospheric inputs via dimethyl sulfide (DMS) production, however the earliest Proterozoic lacks a record of massive, bedded evaporite deposits with the exception of the Tulomozero Formation in Karelia, Russia (Morozov et al., 2010), and significant DMS production is unlikely to occur until the emergence or diversification of marine algae. (Knoll et al., 2006; Parfrey et al., 2011). Therefore a likely explanation for such positive $\delta^{18}O$ values observed from the Lomagundi and Fedorovka Formations is possibly a result of post-depositional metamorphism. The expansion of euxinic coastal environments could also potentially drive positive $\delta^{18}O$ and $\delta^{34}S$ values through a reduction in sulfide reoxidation rates, however increases to atmospheric oxygen levels and likely transient increases to marine sulfate are predicted to dilute such a signal (Poulton et al., 2010; Gomes and Johnston, 2017). Plausible global mechanisms to drive such positive $\delta^{18}O$ and $\delta^{34}S$ values could be vigorous dissimilatory sulfate reduction, which would leave residual sulfate isotopically heavy through enzymatic processes. This mechanism requires a large supply of organic substrate to fuel such sulfur cycling, however this would need to occur with moderate levels of f_{org} to drive the Lomagundi carbon isotope excursion (Bekker and Holland, 2012; Bekker, 2014).

Deducing clear trends from $\delta^{34}S$ values is tenuous over the *GOE*, however it is worth noting that the amplitude of variation compared to the mid-Proterozoic appears to be significantly lower (Fig. 5.6). Less variation in $\delta^{34}S$ across the *GOE* compared to the mid-Proterozoic is consistent with a larger marine sulfate reservoir during the *GOE* due to higher atmospheric oxygen concentrations. It is also apparent that most values cluster toward a decreasing trend over the *GOE,* possibly as a result of a shifting degree of pyrite burial that may have ultimately controlled the growth of the marine sulfate reservoir and its subsequent crash (Planavsky et al., 2012; Scott et al., 2014). While broadly consistent with suggested trajectories in the redox state of the surface Earth, additional details over this interval are required to fully flush out its complexity.

In sum, the *GOE* saw an irreversible increase in pO_2 levels borne out in the disappearance and appearance of $\Delta^{33}S$ and $\Delta^{17}O$ anomalies, respectively, and the deposition of Earth's first evaporite deposits that preserve these signatures. However, such records do not fully capture the dynamic nature of this interval of Earth history that is suggested through evidence for Paleoproterozoic Snowball Earth glaciations (Evans et al., 1997; Kirschvink et al., 2000; Gumsley et al., 2017) and dramatic shifts in the stable carbon isotope record within carbonates and atmospheric oxygen levels (Bekker and Holland, 2012; Bekker, 2014). While incomplete, the distribution of preserved sulfate evaporite minerals along with their major and minor isotope signatures supports a model of seawater sulfate evolution reaching relatively high concentrations during the Lomagundi-Jatuli positive carbon isotope excursion (>5 mM; Planavsky et al., 2012) but dramatically falling at ~ 2.05 Ga (<500 μM, Scott et al., 2014; Bekker and Holland, 2012; Karhu and Holland, 1996). Although many of the changes to the Earth System over the *GOE* may have often been transient with respect to expansions and contractions of the marine sulfate reservoir and shifting atmospheric chemistry, it is clear that this interval of Earth history introduced some irreversible changes to the surface environment through increases to the oxidative capacity of the atmosphere and size of the biosphere that remain a critical part of biogeochemical cycles to present day (Catling et al, 2005).

The mid-Proterozoic 2.0 – 1.1 Ga

The mid-Proterozoic stands out from other times in Earth history with respect to sulfate isotope records with consistently negative $\Delta^{17}O$ values, and the lowest $\Delta^{33}S$ and $\delta^{18}O$ values of all other intervals. At the same time major sulfur isotopes ($\delta^{34}S$) show the greatest variation, distinguishing the mid-Proterozoic Earth from earlier or later times across the Proterozoic. Notably these signatures are only preserved within a limited number of basins that were likely highly restricted and never deposited as massive evaporites such as some occurrences across the *GOE*.

While initially regarded as “rather boring” (Buick et al., 1995; Brasier and Lindsay, 1998; Holland, 2006) the mid-Proterozoic has recently seen an uptick in controversy surrounding atmospheric oxygen levels with estimates spanning orders of magnitude across this critical interval where important biological innovations are suggested to have occurred (Planavsky et al., 2014; Cole et al., 2016; Zhang et al., 2016; 2017; Planavsky et al., 2016; Canfield, 2005; Daines et al., 2017). Despite an apparent lack of significant variation in the stable carbon isotope record (e.g., Bekker et al., 2016), the mid-Proterozoic Earth System likely served as an important incubator for some of the most important biological innovations through Earth history such as the emergence and diversification of eukaryotic organisms (Butterfield, 2000; Peng et al., 2009; Knoll, 2014). Therefore it is remarkable that the characterization of this near billion-year apparent stable plateau is still met with so much uncertainty with respect to the composition of the atmosphere, timing of evolutionary events, and chemistry of the marine environment. Further constraining these conditions over the mid-Proterozoic is at least as critical as understanding major perturbations that precede and follow it.

The isotopic record of mid-Proterozoic sulfate displays many features that are distinct from other times in Earth history. For example this interval consistently records relatively low $\Delta^{33}S$, $\delta^{18}O$, and $\Delta^{17}O$ isotopic values (Figs. 5.6 and 5.7). Low $\Delta^{33}S$ values together with a large observed range in $\delta^{34}S$ values suggest that dissimilatory sulfate reduction dominated the sulfur cycle over the mid-Proterozoic (Fig. 5.8). Notably low to negative $\Delta^{33}S$ values suggest either a weaker sulfur cycle, or a larger role of certain sinks compared to earlier or later times, possibly reflecting low seawater sulfate concentrations (Johnston et al., 2006). For example the mid-Proterozoic is where the majority of Earth's largest sedimentary-exhalative (SEDEX) deposits are found within the sedimentary record (Lyons et al., 2009). Moreover less microbial sulfur cycling may also explain isotopically light $\delta^{18}O$ with limited opportunities for exchange with other oxygen bearing species, which potentially drove the more positive values observed over the *GOE.*

Expanding the mid-Proterozoic $\Delta^{17}O$ record of sulfate from a singular previous study (Crockford et al., *in review*) highlights some of the most negative $\Delta^{17}O$ values outside of the Cryogenian. Three formations from India, Australia, and previously published results from Canada, all display highly negative minimum values of -0.59‰, -0.78‰ and -1.03‰, respectively (Fig. 5.6). Such negative $\Delta^{17}O$ values in conjunction with existing pCO_2, and pO_2 estimates have been argued as evidence for a less productive mid-Proterozoic biosphere, that would have throttled oxygen export from surface waters to the troposphere (Crockford et al., *in review*). Results here, suggest that this finding is robust (Fig. 5.10). Beyond this, minimum values from these deposits, may indicate a secular trend in the size of the biosphere and composition of the atmosphere and therefore possibly a reflection of changing nutrient dynamics over this interval of time (Canfield et al., 1998; Anbar and Knoll, 2002; Koehler et al., 2017; Crockford et al., *in review*). Nutrient limitation over the Proterozoic has been suggested as a mechanism to both temper and galvanize the biosphere through multiple mechanisms (e.g. crustal growth Fig. 5.1) that typically involve nitrogen and phosphorus cycles (Laakso and Schrag, 2013; Reinhard et al., 2013b; Derry, 2015; Sánchez-Baracaldo, 2014; Cox et al., 2016a; 16b; Reinhard et al., 2016; Kuznetsov et al., in press; Koehler et al., 2017). With studies suggesting decreasing pCO_2 levels over the Proterozoic, one would predict a concomitant increase in $\Delta^{17}O$ values (Cao and Bao, 2013; von Paris et al., 2008, Sheldon, 2013). With the opposite trend observed between ca. 1.9 – 1.4 Ga, however, (i.e. progressively more negative $\Delta^{17}O$ values) another process must be considered to generate such signatures (Fig 5.6.). The most likely culprit is a reduction in *GPP* that induced a much stronger effect on $\Delta^{17}O$ values than that of decreasing atmospheric pCO_2 levels. Maximum $\Delta^{17}O$ values also provide interesting insights into the mid-Proterozoic marine sulfate reservoir. Provided some portion of sulfate within deposits from India, Australia and Canada was of marine origin, low maximum values of -0.21‰, -0.54‰ and -0.35‰ possibly indicate a much larger influence of continental runoff influencing the isotopic composition of the marine sulfate reservoir (Figs. 5.2, 5.6 and 5.7). Under the assumption that the $\Delta^{17}O$ composition for seawater has not changed through Earth history the above suggestion is consistent with a much smaller mid-Proterozoic marine sulfate reservoir with a much shorter residence time that only allowed for highly restricted settings sampled in this study to be preserved in the sedimentary record (Richter and Turekian, 1991; Shen et al., 2002).

It stands to reason that a weak biosphere would ultimately drive lower atmospheric oxygen concentrations, assuming relatively constant reductant fluxes to the surface environment as well as f_{org} values within previously suggested ranges (Sleep and Zahnle, 2001; Krissansen-Totton et al., 2015). Low oxygen export from the biosphere over this interval is consistent with low mid-Proterozoic atmospheric oxygen levels that have been inferred in previous studies (Planavsky et al., 2014; Cole et al., 2016; Zhang et al., 2016; Liu et al., 2016; Daines et al., 2017; Holland et al., 1989; Runnegar, 1991; Mills et al., 2014). Low oxygen concentrations may have led to a decrease in the size of the marine sulfate reservoir that is supported by two observations from the sedimentary record and the $\delta^{34}S$ record presented above (Fig 5.6). The majority of the mid-Proterozoic has relatively few sulfate occurrences compared to earlier or later times in Earth history (e.g., Scott et al., 2014). While preservational bias and secular variations in basin architecture are entirely plausible, the observation that so few locations preserve sulfate evaporite deposits is most consistent with lower marine sulfate concentrations over this interval. Low sulfate levels would potentially create a more dynamic system with respect to $\delta^{34}S$ values, as the residence time of sulfate in the ocean would be considerably shorter compared to the modern environment (Johnston et al., 2006). A smaller sulfate reservoir would have more variable $\delta^{34}S$ values with shorter periods and higher amplitudes than times before or after (Richter and Turekian, 1991). Data presented and compiled here supports such a model with a wider range in mid-Proterozoic $\delta^{34}S$ values than across the *GOE* and the majority of the late-Proterozoic that is also consistent with highly negative $\Delta^{17}O$ values over this interval. These observations as well as the potential for $\delta^{34}S$ values to reach such isotopically light $\delta^{34}S$ values over the mid-Proterozoic is consistent with it being a period of enhanced pyrite burial relative to organic carbon burial compared to earlier or later times in Earth history (Canfield, 2005; Figs. 5.4, 5.6 and 5.7).

Late-Proterozoic (1.1 – 0.72 Ga)

Minor sulfate isotopes over the late-Proterozoic display similarities to values observed over the *GOE* however these were likely produced under different conditions. $\Delta^{17}O$ values beginning at ≈1.05 Ga (Gibson et al., *in review*) from Baffin Island display minimum values down to -0.38‰ and younger units from Northwest Canada reaching values of -0.44‰. $\Delta^{33}S$ values show a slight increase in average values compared to mid-Proterozoic samples (0.018‰). This increase is also observed in $\delta^{18}O$ and $\delta^{34}S$ values with averages of 15‰ and 23‰ respectively. These signatures are often preserved within massively bedded evaporites that make a reappearance in the sedimentary record over this interval, potentially speaking to a growth in the size of the marine sulfate reservoir (Jackson and Cumming, 1981; Aitken, 1981).

Studies on the oldest formations across the late-Proterozoic have suggested that it witnessed a decrease in the dissolved inorganic carbon reservoir (DIC) and an increase in atmospheric oxygen levels (Gilleaudeau et al., 2016; Kah et al., 2004; Blamey et al., 2016). Decreasing the DIC reservoir may have been a consequence of a progressive increase in solar luminosity requiring reduced pCO_2 levels to maintain clement surface conditions (Walker et al., 1980; Gough, 1981). Consistent with a decrease in the marine DIC reservoir are high amplitude shifts in its carbon isotopic composition beginning in the Angmaat Formation in the Bylot Supergroup and continuing into the Bitter Springs negative carbon isotope anomaly at ca. 810 to 790 Ma (Kah et al., 1999; Halverson et al., 2005; Macdonald et al., 2010; Swanson-Hysell et al., 2015). Factors that may have contributed to a rise in atmospheric oxygen levels include a diversification of the biosphere with evidence for Earth's earliest sexually reproducing eukaryotes (Butterfield, 2000). These evolutionary steps may have increased the ratio of organic carbon to total carbon that is buried (f_{org}), consistent with previously inferred $\delta^{13}C$ trends over this interval (Sleep and Zhanle, 2001; Krissanen-Totton et al., 2015).

Consistent with the picture described above is the first appearance of massively bedded evaporite deposits in the sedimentary record (Jackson and Cumming, 1981; Scott et al., 2014). Within these and other evaporites sampled over the late-Proterozoic are minimum $\Delta^{17}O$ values of ≈ -0.41‰ that lie between the less negative values measured for the Phanerozoic but not reaching the large depletions recorded across the mid-Proterozoic or the Cryogenian (Fig. 5.6, 5.7). Although similar in magnitude to the $\Delta^{17}O$ signatures during the *GOE*, changes in atmospheric composition as well as in the biosphere likely produced these similar results under much different geochemical conditions. Over the late-Proterozoic reduced oxygen export from the biosphere to the troposphere coupled to a reduction in pCO_2 levels would have potentially generated similar $\Delta^{17}O$ values to *GOE*-aged samples (Cao and Bao, 2013; Wing, 2013). Therefore the likely lower pCO_2 levels experienced over the late-Proterozoic compared to the *GOE* infer that the capacity of the biosphere to dilute negative $\Delta^{17}O$ values was also lower than the *GOE* consistent with suggestions of high levels of primary production potentially leading to an oxygen overshoot (Bekker and Holland, 2012; Fig. 5.10). These results also lend support to models suggesting that high marine sulfate levels present during the *GOE* did not see a return until the mid-Neoproterozoic.

Major sulfur isotopes ($\delta^{34}S$) of late-Proterozoic sulfate also show a slight departure from mid-Proterozoic values with a decrease in the amplitude of scatter for the majority of formations measured (Fig. 5.6). This is also a possible consequence of a growth in the marine sulfate reservoir, making it less prone to isotopic modification from changes in input and output fluxes (Kah et al., 2004). Such an increase in seawater sulfate appears consistent with a notable increase in the deposition of bedded gypsum and anhydrite deposits beginning at ~1.05 Ga in the Bylot Supergroup of Baffin Island and continuing on with examples of hundreds of meters of bedded gypsum over hundreds of kilometers along strike in the Ten Stone Formation in northwestern Canada (Aitken, 1981; Turner and Bekker, 2016; Jackson and Cumming, 1981; Scott et al., 2014; Gibson et al., *in review*). A shift to more positive $\Delta^{33}S$ values across the late-Proterozoic with respect to the mid-Proterozoic may also be a direct result of this growth in marine sulfate concentrations coupled to more active microbial sulfur cycling (Figs. 5.6 and 5.7).

Results for $\delta^{18}O$ values within sulfate display a similar symmetric pattern observed in $\Delta^{17}O$ and $\Delta^{33}S$ values with maximum values during the *GOE* and the late-Proterozoic and lowest values over the mid-Proterozoic (Figs. 5.6 and 5.7). High $\delta^{18}O$ values over the late-Proterozoic are a possible consequence of increased dissimilatory sulfate reduction. An increase in microbial sulfur cycling is a potential consequence of increased atmospheric oxygen levels resulting from increased primary production that would have provided organic substrate and increased sulfate levels to fuel the microbial sulfate reduction (Fig. 5.10). Further raising $\delta^{18}O$ may have been an increased opportunity for isotopic exchange in the atmosphere of sulfur species due to enhanced DMS production from algae that experienced a major diversification over this interval of

Earth history and likely contributed to the enhanced primary production of the biosphere inferred from $\Delta^{17}O$ results (Kumar et al., 2002; Parfrey et al., 2011; Fig. 5.3). In sum, the late-Proterozoic saw an apparent increase in marine sulfate, atmospheric oxygen and the size of the biosphere that distinguish it from the preceding mid-Proterozoic. Importantly, some combination of these and other factors likely created conditions prone to climatic instability and contributed to events that ultimately plunged the Earth into the Cryogenian (Hoffman et al., 1998; Feulner et al., 2017; Cox et al., 2016; Mckenzie et al., 2016; Macdonald and Wordsworth, 2017; Schmid, 2017; Kuznetsov et al., in press).

The Cryogenian (0.72-0.635 Ga)

Due to the unique climatic and geochemical conditions both during and in the immediate aftermath of two Snowball Earth glaciations, we segregate the Cryogenian even though data is relatively sparse over this interval of Earth history (Hoffman et al., 2017). $\Delta^{17}O$ data over this interval has only been generated from syn-glacial and immediately post-glacial Marinoan CAS and barite that both display highly negative values (Bao et al., 2008; Bao et al., 2009; Bao et al., 2012; Peng et al., 2011; Killingsworth et al., 2013; Crockford et al., 2016). These isotopic signatures are now reported from five paleo-continents and have been interpreted as evidence for high syn-glacial pCO_2 levels in the atmosphere that would have ultimately terminated the Marinoan glaciation (Bao et al., 2008; Cao and Bao, 2013). While similar atmospheric conditions experienced during the Marinoan glaciation are predicted for the Sturtian glaciation, no deposits bearing such signals have been uncovered from the sedimentary record. This observation potentially suggests much different geochemical dynamics operating over the Sturtian, which may be a consequence of its much longer duration than the Marinoan (4 Ma vs 55 Ma; Prave et al., 2016; Macdonald et al., 2010; Rooney et al, 2014; 2015; Hoffman et al., 2017). A clear example of such differences between Marinoan and Sturtian glaciations is the deposition of Sturtian aged Fe-formations. Such chemical sediments must have been deposited under ferruginous conditions, potentially indicating a larger hydrothermal or continental iron supply to the ocean and/or significant decrease in the size of marine sulfate reservoir with declined oxidative continental weathering of sulfides with respect to earlier Earth history (Cox et al., 2013). It is predicted that sulfate inputs in a sub-glacial ocean would be severely attenuated, however many outputs would also be affected, namely microbial sulfate reduction due to limited organic substrates. The net effect of such conditions would be the draw down of marine sulfate levels, which is consistent with arguments based on $\Delta^{17}O$ and $\delta^{34}S$ data from post-Marinoan sequences (Hurtgen et al., 2006; Crockford et al., 2016). Therefore, the Sturtian's long duration may have drawn down sulfate levels too low to capture transient post-glacial signatures reflective of syn-glacial conditions, or the consistent lack of transgressive sequences in Sturtian aged sequences that are where Marinoan anomalies are recorded further raises the possibility of fundamentally different post-glacial dynamics operating between the two Cryogenain glaciations. While it is clear that the Cryogenian Earth was distinct from earlier or later times, its relationship to the evolution of the biosphere remains enigmatic, with life confined to specific niche environments (Hoffman, 2016) potentially serving as either an evolutionary "activated complex" or as a temporary bottle neck for the dramatic evolutionary changes observed in the biosphere over this interval (Javaux, 2007). Therefore while one can envisage dramatic changes to the sulfur and oxygen cycles over this interval of Earth history, the geochemical record is too sparse to fully explore it and its relationship with the evolution of life.

The Ediacaran (0.635-0.542 Ga)

The Ediacaran sulfur and oxygen cycles appear to have been different to any earlier time in Earth history. Across the Ediacaran major evaporite deposits reappear in the sedimentary record potentially speaking to a growth in the size in the marine sulfate reservoir from post-Cryogenain levels (Hurtgen et al., 2002; Crockford et al., 2016). Minor isotopic values within sulfate display limited variations with values comparable to the *GOE* but with much less variability (e.g. minimum $\Delta^{17}O$ = -0.29‰ and average $\Delta^{33}S$ = 0.02‰). Major oxygen isotopes show similarity to late-Proterozoic samples with an average value slightly higher than modern marine sulfate at 13.6‰. Major sulfur isotopes show some of the most positive $\delta^{34}S$ values up to 34‰ (Figs. 5.6 and 5.7) however these notably heavy values are also concomitant with the emergence of some coherent structure to this record.

These isotopic similarities to other times in Earth history however are done with under a backdrop of dramatic changes to the nature of the biosphere with the emergence of the Ediacaran fauna and flora (Erwin et al., 2011) and changes to the sulfur cycle (Kunzmann et al., 2017) over the Cryogenian that have been well documented through well preserved fossil assemblages and isotopic signatures recorded in sediments. An apparent growth in the marine sulfate reservoir (Crockford et al., 2016; Hurtgen et al., 2002; 2006; Halverson and Hurtgen, 2007), as well as increased atmospheric oxygen levels inferred from trace element and Fe-speciation data (Sahoo et al., 2012), provide evidence that changes in the biosphere appeared in conjunction with changes in atmospheric chemistry. While transient oxygenation (Sahoo et al., 2016) or disparate local records (Sahoo et al., 2012; Miller et al., 2017) may suggest a complicated history of oxygenation over this interval, broad trends of an increased inventory of oxygen, possibly above critical thresholds in the atmosphere (Ozaki and Tajika, 2013; Sperling et al., 2015) appear to be borne out in the sulfur and oxygen isotopes of sulfate evaporites.

$\Delta^{17}O$ values within post-Marinoan barites and CAS all display a trend to less negative values than those deposited earlier in the Proterozoic (Figs. 5.6 and 5.7) implying a transition from anomalous conditions brought on through Cryogenian glaciations, to conditions with potentially higher atmospheric oxygen levels and *GPP* but lower pCO_2 than any other time over the Proterozoic. The record of this transition in sulfate evaporites implies an initial small post-Cryogenian marine sulfate reservoir, highly vulnerable to fluctuations due to post-glacial input fluxes. These earliest Ediacaran pCO_2, pO_2, and *GPP* conditions however appear to have continued later into the Ediacaran with evaporites from Siberia and Iran as well as CAS from northern Australia displaying isotopically normal $\Delta^{17}O$ values with the most negative values only reaching -0.29‰ (Figs. 5.6 and 5.7). The environmental conditions inferred above, together with the observation of large evaporite occurrences over the Ediacaran (most notably in Oman; Schröder et al., 2003) appear to support this inference of increased oxygen levels and by consequence a growth in the marine sulfate reservoir. Indeed evidence of ≈16 mM sulfate has been suggested from fluid inclusions from the Ara Group of Oman (Brennan et al., 2004). Although not as anomalous as post-Marinoan values, they are more negative than is likely possible in the modern environment (Figs. 5.6 and 5.7). Such values could suggest higher pCO_2 levels possibly resulting from a slightly dimmer Ediacaran sun and reduced weathering rates before the colonization of land plants (Berner, 2006; Berner, 1997). An alternative possibility is a less productive biosphere due to a throttled phosphorous release from sediments under more oxic bottom water conditions (Lenton et al., 2014; Sahoo et al., 2016), which seems to contradict recent studies of phosphorous cycling in the Precambrian (e.g. Reinhard et al., 2016).

While atmospheric and biospheric conditions recorded in $\Delta^{17}O$ values tell a consistent story, sulfur isotope signatures bare a closer resemblance to complicated trace metal records (Johnston et al., 2013; Kunzmann et al., 2015; Sahoo et al., 2016; Miller et al., 2017). Samples from Iran and Russia span the range in $\delta^{34}S$ experienced by post-Marinoan barites from values of ~18 to 46‰ (Figs. 5.6 and 5.7). Such variation suggests a dynamic sulfur cycle over this interval with periods of intense microbial sulfur cycling and potential expansions and contractions of euxinic environments leaving an isotopically heavy marine reservoir observed in Russian samples (Fig. 5.6; Gomes and Johnston, 2017). $\Delta^{33}S$ values appear similar to modern values with averages of 0.022 and 0.015‰ for Iranian and Russian samples, respectively. These records do however provide a foundation for modeling efforts attempting to explore the role of sulfur disproportionating bacteria through pyrite records rising to global significance over this interval of Earth history (Kunzmann et al., 2017).

The $\delta^{18}O$ record over the Ediacaran is similar to other isotopic records, with a large range of initial variation that settles into more coherent trends toward the Cambrian boundary (Fig. 5.6). While initial post-Marinoan values across multiple paleo-continents appear to be constrained to ~10 and 25‰, variation grows into ~600 Ma South China sections with extremely light values near 0‰. This large variation has been interpreted as a result of both an increased proportion of water-oxygen incorporated into sulfate during sulfide oxidation generating isotopically light values, as well as increased euxinia driving values heavier toward the Cambrian-Precambrian boundary (Goldberg et al., 2005). Another possibility that is consistent with the expansion of euxinic environments is enhanced microbial sulfur cycling in sediments. Such cycling would progressively drive isotopic values of both $\delta^{18}O$ and $\delta^{34}S$ more positive through intercellular isotopic exchange, and biological selection of light isotopes into respired products and organic matter (Fike et al., 2008).

In sum, the transition between Proterozoic and Phanerozoic environments revealed through Ediacaran records appears to be complicated, but likely a consequence of the progressive oxygenation of the marine environment. While $\Delta^{17}O$ results speak to intermediate conditions between typical Proterozoic and Phanerozoic values, a further populating of this record is needed to tie marine records to atmospheric conditions. Further, changes in global temperatures most notably signified through the Gaskiers glaciation, and dramatic shifts in the carbon cycle observed through the Shuram excursion as well as large shifts into the Cambrian-Ediacaran transition are likely coeval with important changes to the Earth system, which the evaporite record is unable to capture. The existing isotopic record of sulfate evaporites appears to be consistent with an increase in microbial sulfur cycling progressively driving major isotopic values ($\delta^{18}O$ and $\delta^{34}S$) of sulfate more positive, possibly in response to increased organic matter loading through enhanced primary organic productivity driving $\Delta^{17}O$ values further towards 0‰ than in earlier times in Earth history.

Phanerozoic

Phanerozoic sulfate isotope records (Claypool et al., 1980; Payton et al., 1998; 2004; Masterson et al., 2016; Bao et al., 2008) contrast sharply from the majority of the Proterozoic, with significantly less negative $\Delta^{17}O$ values (< -0.32‰), coherent trends in $\delta^{34}S$, and $\delta^{18}O$ values and slightly more positive $\Delta^{33}S$ values than the majority of the Proterozoic (Fig. 5.6). These isotopic patterns and characteristics are a likely consequence of the progressive rise in atmospheric oxygen through the latest Proterozoic that appears to have continued into the Phanerozoic (Sperling et al., 2015), potentially reaching modern levels with the colonization of land plants in the late Silurian-early Devonian (Lenton et al., 2016). Redox conditions in the marine environment inferred from a rise in atmospheric oxygen have largely been borne out in multiple lines of evidence, one of which being a growth in size of the marine sulfate reservoir, possibly a consequence of the advent of bioturbation that galvanized reoxidative sulfur cycling (Canfield and Farquhar, 2009; Tarhan et al., 2015). Here we add another line of contrast between the Proterozoic and Phanerozoic by suggesting that an increase in atmospheric oxygen is in conjunction with a growth of the biosphere (Fig. 5.10; Wing, 2013). Higher Phanerozoic productivity together with lower pCO_2 levels (von Paris et al., 2008; Berner, 2006) predict less negative $\Delta^{17}O$ values that is borne out in the record produced here. The impacts of this growth and diversification of the biosphere likely had consequences for the sulfur cycle that extended all the way to the mantle (Canil and Fellows, 2017), such as a growth in the size of the marine sulfate reservoir, with coherent $\delta^{34}S$ trends suggesting that geographically disparate records are truly sampling a homogenous global reservoir.

This observation coupled to near uniform positive $\Delta^{33}S$ values also speaks to an increase in microbial sulfur cycling across the Proterozoic – Phanerozoic transition (Fig. 5.6).

6.6 A Speculative Synthesis

Here we have put forward a comprehensive isotopic record of Proterozoic sulfate from over 300 hundred samples from 32 different formations. We construct the first GPP curve across the Proterozoic (Fig. 5.10) based on empirical atmospheric constraints and argue that changes in the productivity in the biosphere likely underlie many of the biogeochemical transformations witnessed over this eon. Importantly, these changes in the biosphere appear to be borne out in other isotopic systems within sulfate and below we summarize highlights by Proterozoic interval.

GOE (2.4 - 2.0 Ga): Mirrored mass independent isotopic trends in $\Delta^{17}O$ and $\Delta^{33}S$ across this interval suggest the establishment of an ozone layer well in advance of Earth's earliest evaporites. Further, a lack of any S-MIF in evaporite records suggests that oxygenation of Earth's surface over this interval was not protracted but rather uni-directional and possibly reaching levels comparable or even greater than the modern atmosphere. This oxygenation was likely in conjunction with potentially the most productive biosphere ever in Earth history.

Mid-Proterozoic (2.0 - 1.1 Ga): Extremely depleted $\Delta^{17}O$ values when coupled to existing pCO_2 and pO_2 estimates suggest lower primary production values compared to any post-Archean time with the exceptions of Snowball Earth and major extinctions. Decreasing minimum $\Delta^{17}O$ values over the mid-Proterozoic between the three formations measured possibly suggest that *GPP* levels steadily declined over this interval. These results are consistent with a weaker sulfur cycle in a small marine sulfate reservoir that is borne out through depressed $\Delta^{33}S$ and $\delta^{18}O$ values and highly variable $\delta^{34}S$ values.

Late-Proterozoic (1.1 – 0.72 Ga): Less variation in $\delta^{34}S$ values compared to mid-Proterozoic coupled to widespread large evaporite occurrences suggests a rise in marine sulfate levels and/or a rise in the propensity for evaporative environments over this interval. $\Delta^{17}O$ values down to -0.44‰ suggest that the late-Proterozoic environment was characterized by both higher $p\mathrm{CO_2}$ levels than Ediacaran or Phanerozoic times as well as a lower *GPP* levels. Elevated $\delta^{18}O$ values potentially reflect enhanced DMSO production due to a diversification of marine algae (Knoll et al., 2006; Feulner et al., 2015), or vigorous sulfur cycling leaving marine sulfate isotopically heavy.

Cryogenian (0.72 – 0.635 Ga): Highly negative $\Delta^{17}O$ values within Marinoan aged strata indicate extremely high $p\mathrm{CO_2}$ levels due to a Snowball Earth glaciation. Other aspects of the sulfur cycle however remain unknown due to incomplete isotopic records. Future work is needed over the Cryogenian to both better characterize the conditions immediately preceding each glaciation, the interglacial, as well as the dynamics of the sulfur and oxygen cycles in the subglacial oceans.

Ediacaran (0.635 – 0.542 Ga): The Ediacaran continues the trend from the mid-Proterozoic through the late-Proterozoic of increased oxygenation of the surface environment, growth of the marine sulfate reservoir and growth of the biosphere. Isotopic records suggest vigorous sulfur cycling pushing $\delta^{34}S$ values of marine sulfate very heavy. $\Delta^{17}O$ suggest however that the Ediacaran was distinct from times before or after, and acted as a true transition between the Proterozoic and Phanerozoic Earth surface environment.

Acknowledgements

Funding for the duration of this work was provided by the NSERC CREATE, CATP, NSERC PGS-D, McGill McGregor Fellowship, McGill Mobility program, McGill GREAT program, Canadian Polar Continental Shelf Program, Northern Science Training Program, Mineralogical Association of Canada Foundation Scholarship and Travel Grant.

Tables

Table 1: Formations sampled for isotopic analysis.

Map #	*Region*	*Area*	*Unit*	*Age (Ga)*	*Lith.*	*References*
Modern/Cenozoic						
1	N. Canada	Axel Heiberg I.	N/A	0	Evap	
2	SW. USA	California	N/A	0	Evap	
3	SW. USA	California	N/A	0	Evap	
4	SW. USA	Nevada	N/A	0	Evap	
5	S. Australia	Flinders R.	N/A	0	Evap	
6	Spain	Sorbas B.	N/A	0.006	Evap	
7	N. Canada	Devon I.	N/A	0.014	Evap	
Ediacaran >635 Ma						
8	Siberia		Oskoba	0.56	Evap	
9	Iran			0.545	Evap	
10	N. Australia	Kimberley	Egan	0.58	CAS	
Cryogenian 635 - 717 Ma						
11	N. Australia	Kimberley	Landrigan	0.635	CAS	Condon et al., 2005
Late-Proterozoic 717 - 1100 Ma						
12	NW. Canada	Mackenzie Mts	Redstone R.	0.75	Evap	Jefferson and Parish, 1989
13	N. Canada	Victoria I.	Kilian Fm.	0.795	Evap	Rayner and Rainbird, 2013
14	N. Canada	Brock Inlier	Kilian Fm.	0.795	Evap	Rayner and Rainbird, 2013
15	S. Australia	Flinders R.	Skillogollee	0.8	CAS	
16	C. Australia	Amadeus B.	Bitter Springs	0.8	Evap	
17	NW. Canada	Mackenzie Mts	Ten Stone	0.815	Evap	Macdonald et al., 2010
18	W. Australia	Officer B.	Browne	0.83	Evap	Hill and Walter, 2000; Preiss, 2000
19	Zambia		Roan	0.883 (0.893-0.873)	Evap	Armstrong et al., 2005
20	D. R. Congo		Mbuji/Mayi	0.883*	Evap	Cahen et al., 1984; Delpomdor et al., 2013
21	N. Canada	Victoria I.	Minto Inlent	0.89	Evap	Van Acken et al., 2013
22	N. Canada	Baffin I.	Angmaat	1.05	Evap	Gibson et al., subimitted
Mid-Proterozoic II 1100 - 2000 Ma						
23	N. Australia	McArthur B.	Myrtle Shale	1.7	Evap	Muir, 1987; Walker et al., 1977
24	E. India	Cuddapah	Tadpatri	1.89	Evap	Collins et al., 2015
GOE 2000 - 2350 Ma						
25	N.W. Russia	Karelia	Tulomozero	2.09 (2.16-2.02)	Evap	Ovchinnikova et al., 2007; Kuznetsov et al., 2010
26	Siberia, Russia	Aldan Shield	Fedorovka	2.1	Evap	Vinogradov et al., 1976; Zolotarev et al., 1989; Velikoslavinsky et al., 2003
27	S. Africa	Griqualand West Basin	Lucknow	2.16 (1.86-2.46)	Evap	Schröder et al., 2008
28	Zimbabwe	Magondi Basin	Lomagundi	2.15 (2.1-2.2)	Evap	Schidlowski and Todt, 1998; Master et al., 2010
29	W. Australia	Yerrida	Juderina	2.173 (2.237-2.109)	Evap	Woodhead and Hergt, 1997; Sheppard et al., 2016
30	Zimbabwe	Deweras	Norah	2.262	Evap	Manyeruke et al., 2004; Master et al., 2010
31	S. Canada	Ontario	Gordon Lake	2.308 (2.3 – 2.316)	Evap	Rasmussen et al., 2013
32	S. Africa	Transvaal basin	Duitschland	2.35	Evap	Bekker et al., 2001; Gumsley et al., 2017

Table 2: Input parameters for *GPP* calculations for Fig. 5.10. CO_2 and O_2 values are given as PAL (CO_2 1 PAL = 280 ppm; O_2 1 PAL = 209500 ppm)

Age (Ma)	$\Delta^{17}O$	O_2 max	O_2 min	CO_2 max*	CO_2 max	CO_2 avg.	CO_2 min	CO_2 min*
2325	-0.36	4	0.1	83.2	63.8	40.4	16.9	10.7
2150	-0.32	4	0.1	100	56.5	49.5	42.4	8.6
1890	-0.59	0.1	0.001	50	43.5	38.5	33.2	6.6
1700	-0.76	0.1	0.001	37.2	37.2	21.3	5.3	5.3
1400	-1.03	0.1	0.001	-	30	-	2	-
1050	-0.38	0.1	0.001	16.6	8.7	6.3	4.1	1
880	-0.44	0.1	0.001	13.8	10.4	6.4	2.4	2.3
810	-0.44	0.5	0.001	12.2	8.6	5.3	2	2
750	-0.37	0.5	0.001	11.5	7.9	4.8	1.6	1.3
560	-0.29	0.5	0.001	20	10.3	3.5	1.4	1.2

Figures

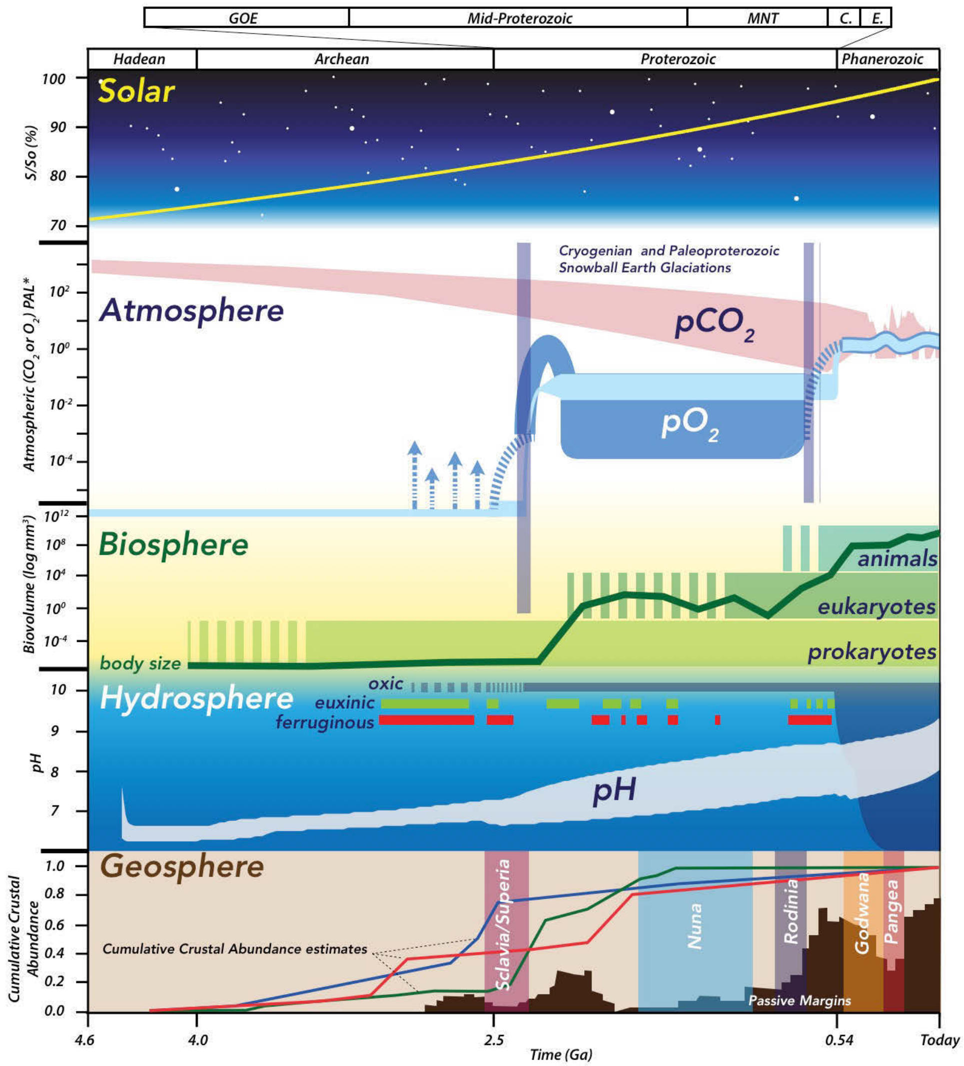

Figure 5.1: Schematic of Changes to the Earth System over geologic time. Estimates for major changes to the Earth System are outlined for Solar, Atmosphere, Biosphere, Hydrosphere and Geosphere presented from top to bottom, respectively. At the top we track changes in solar output relative to present levels calculated from Gough et al., 1981. Below we track proposed trajectories of atmospheric CO_2 and O_2 levels presented relative to Present Atmospheric Levels (PAL; 280 ppm CO_2; 209,500 ppm O_2). The CO_2 field is taken from the 1D model of von Paris et al., 2008 from 4.6-0.6 Ga, and using estimates from Franks et al., 2014 and Berner, 2006. The O_2 field is based on combined proxy data compiled by Lyons et al., 2014 with average estimates in light blue, and a broader range presented in purple/dark blue?. Overlaying atmospheric estimates are panglacial intervals so called Snowball Earth events in blue lines (Hoffman et al., 1998; Kirschvink et al., 2000). Below the biosphere panel depicts changes in maximum body sizes of organisms over Earth history, as summarized by Payne et al., 2011, and overlain with the diversity of the biosphere separated into prokaryote, eukaryote and animals with dashed bars representing uncertainty in origin. Below in the hydrosphere panel we plot marine redox conditions (Hardisty et al., 2017; Anbar et al., 2007; Planavsky et al., 2011) together with a predicted evolution of seawater pH values (Halevy and Bachan, 2017). Finally at the base of the figure in the geosphere panel we plot the distribution of passive margins through time (dark brown; Bradley, 2011), supercontinents (and cratonic amalgamations e.g. Sclavia/Superia) through Earth history, and crustal growth curves from Jacobsen, 1988 (red), Ying, 2011 (green) and Taylor and Mclennan, 1985 (blue).

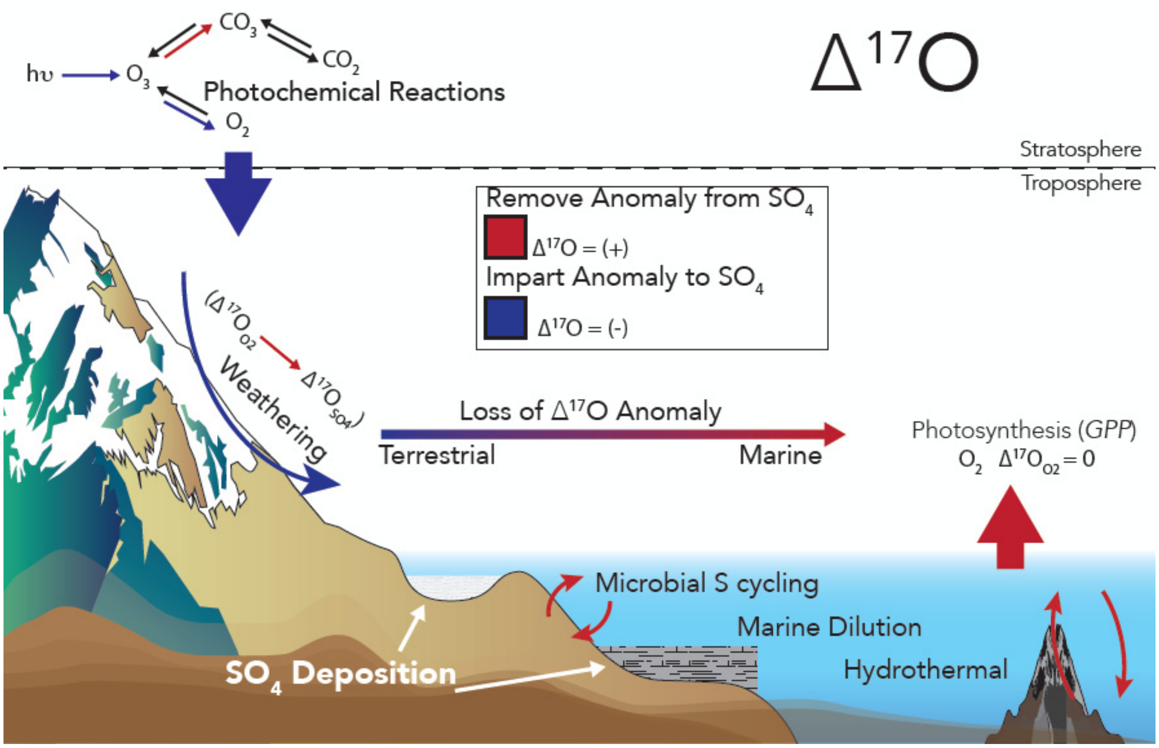

Figure 5.2: A simplified schematic of the controls on the $\Delta^{17}O$ composition of sulfate atmospheric O_2 for the Earth surface environment.

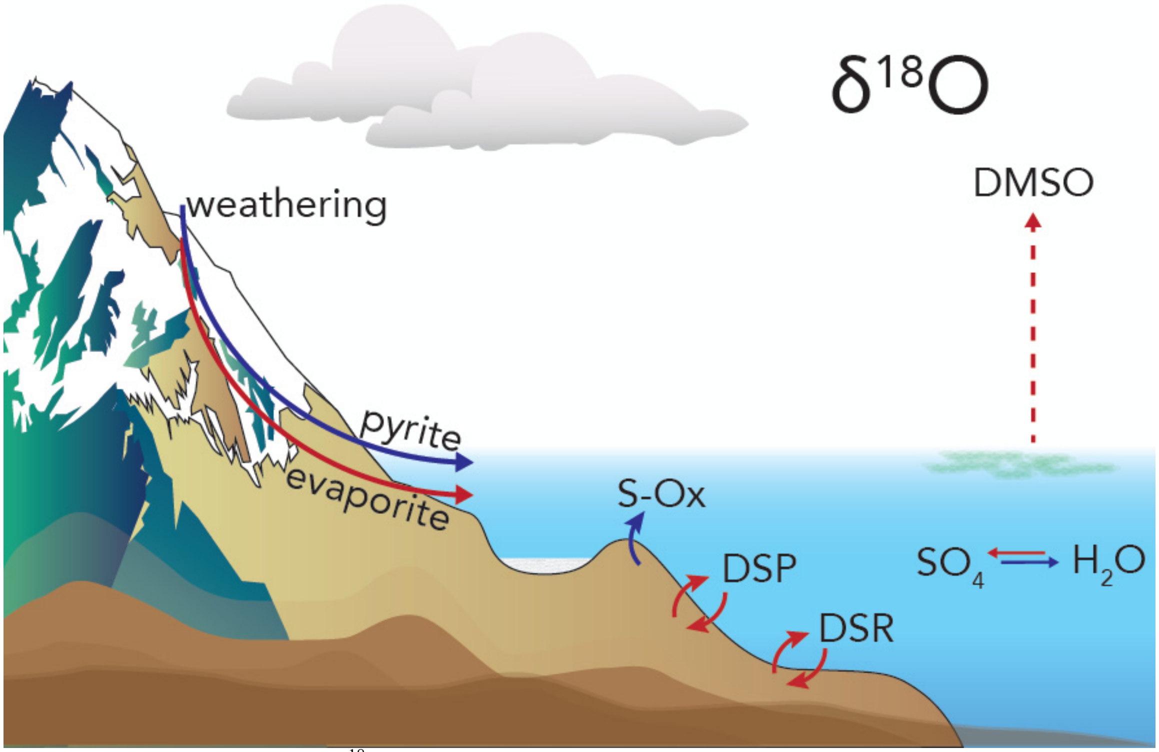

Figure 5.3: Schematic of the $\delta^{18}O$ system and its interpretation within sulfate. We outline the dominant controls on marine sulfate being following Turchyn and Schrag, (2006). Dissimilatory sulfate reduction (DSR); sulfur disproportionation (DSP); sulfide oxidation (S-Ox); dimethyl sulfoxide (DMSO).

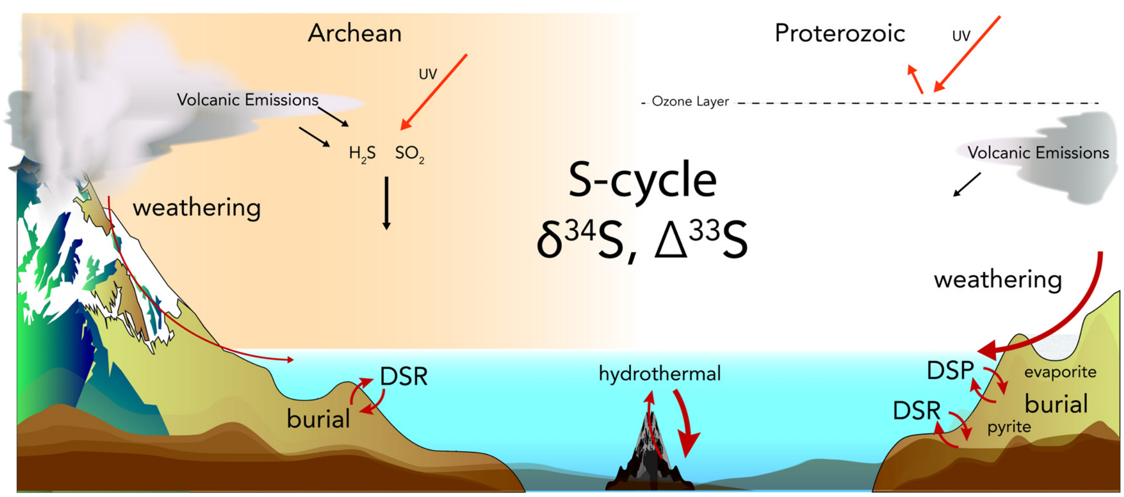

Figure 5.4: Schematic of the $\delta^{34}S$ and $\Delta^{33}S$ systems and its interpretation within sulfate. We outline the dominant controls on marine sulfate along with how this may have changed across the Archean-Proterozoic transition. We show how dissimilatory sulfate reduction (DSP) may have been prominent in the Archean and the Proterozoic, but sulfur disproportionation (DSP) likely did not reach importance until the Ediacaran (Kunzmann et al., 2017).

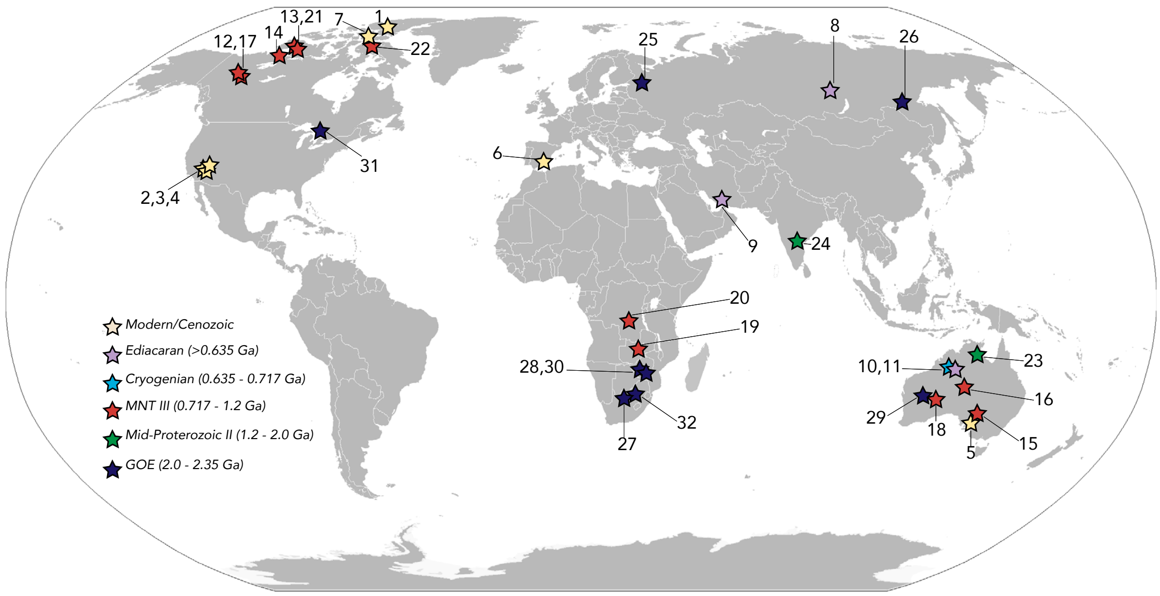

Figure 5.5: Map of Sulfate evaporites sampled. Locations of samples analyzed in this study are presented as different colored stars separated into different time intervals and labeled with numbers corresponding to information in Table 1. *GOE* locations are in dark blue; mid-Proterozoic locations are in green; late-Proterozoic locations are in red; Cryogenian locations are in light blue; Ediacaran locations in purple; and modern/Cenozoic samples in cream.

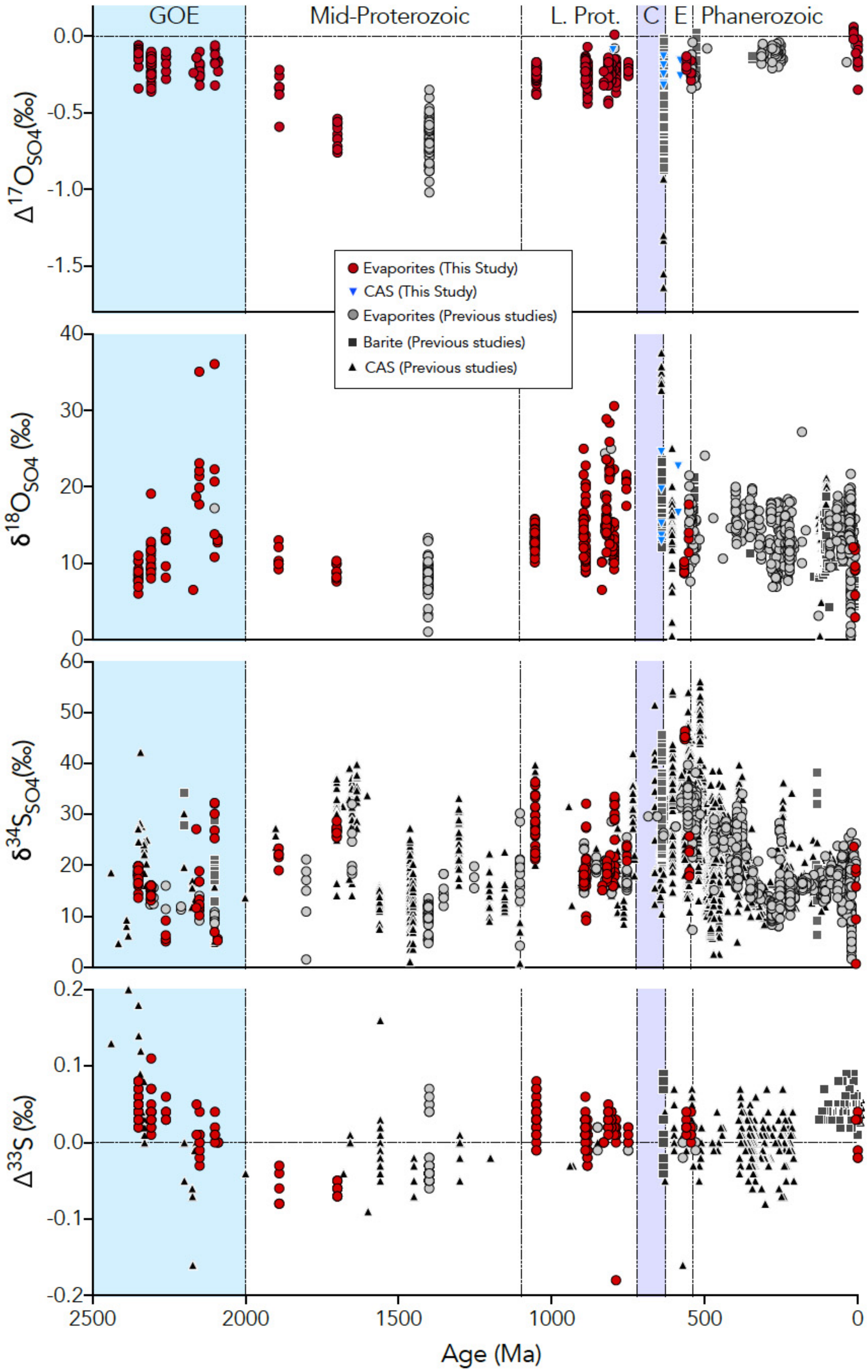
GOE
Mid-Proterozoic
L. Prot.
C
E
Phanerozoic
Δ17OSO4(‰)
δ18OSO4 (‰)
δ34SSO4(‰)
Δ33S (‰)
Evaporites (This Study)
CAS (This Study)
Evaporites (Previous studies)
Barite (Previous studies)
CAS (Previous studies)
Age (Ma)

Figure 5.6: Isotopic record of Proterozoic Sulfate. New results from this study (red circles = evaporites; blue triangles = CAS) compiled with previously published $\delta^{34}S$, $\delta^{18}O$, $\Delta^{33}S$, and $\Delta^{17}O$ data (maroon circles = evaporites; blue squares = barites; grey triangles = CAS) in panels A), B), C) and D). Data is compiled from: Bao et al., 2008; 2009; 2012; Killingsworth et al., 2013; Peng et al., 2011; Kah et al., 2004; Claypool et al., 1980; Ueda et al., 1987; Reuschel et al., 2012; Ueda et al., 1990; Gellatly and Lyons, 2004; Luo et al., 2010; 2015; Li et al., 2015; Strauss et al., 1993; Azmy et al., 2001; Hurtgen et al., 2004; Gill et al., 2007; Goldberg et al., 2005; Hough et al., 2006; Peryt et al., 2005; Hurtgen et al., 2002; Williams et al., 2006; Strauss et al., 2001; Misi and Veizer, 1998; Mazumdar and Strauss; Deb et al., 1991; Master et al., 1993; Grinenko et al., 1989; Taylor et al., 1970; Cameron et al., 1983; Guo et al., 2009; Johnston et al., 2005; Wu et al., 2010; Cowie and Johnston, 2016; Paytan et al., 1998; Kamschulte et al., 1998; 2004; Turchyn and Schrag, 2004; Turchyn et al., 2009; Turchyn and Schrag, 2006; Masterson et al., 2016; Sim et al., 2015; Markovic et al., 2016; Fike et al., 2008; Utrilla et al., 1992; Fox and Videtich, 1997; Holser and Kaplan, 1966; Strauss et al., 1999; Das et al., 1990; Worden et al., 1997; Kesler and Jones, 1981; Schröder et al., 2008; Sakai, 1972; Wu et al., 2014; Kah et al., 2016; Thomson et al., 2012; Wotte et al., 2012; Cortecci et al., 1981; Longinelli and Flora, 2007; Orti et al., 2010; Tostevin et al., 2017; Krupenik et al., 2011; Pierre and Rouchy, 1986; Rick, 1990; Thompson and Kah, 2012; Sim et al., 2015; Tostevin et al., 2014; Wotte et al., 2012; and new data from this study. Please refer to individual studies for associated errors on analysis and refer to the methods section of this paper for errors on newly generated data.

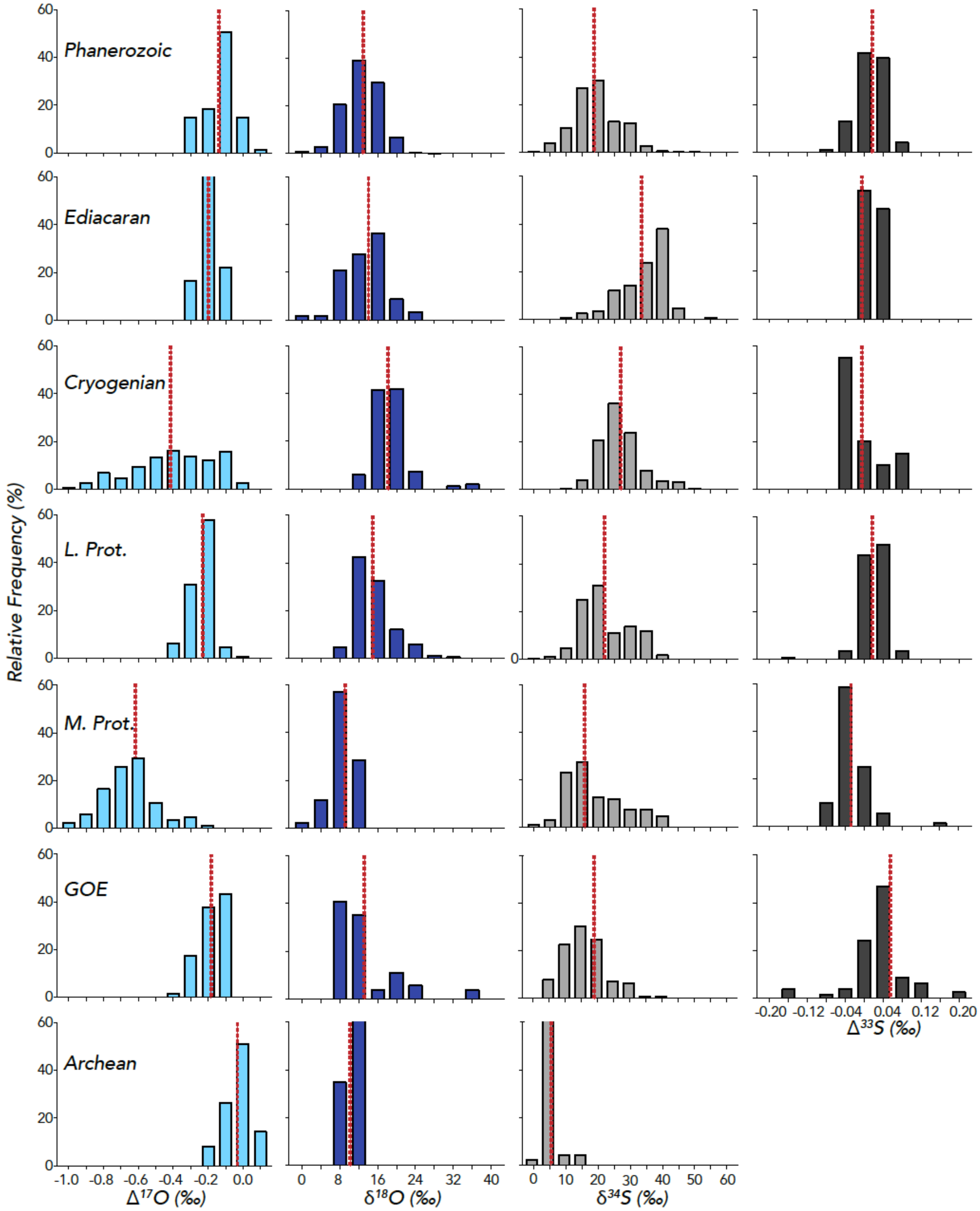

Figure 5.7: Histograms of isotopic values of sulfate. From top to bottom histograms are plotted for Archean, Proterozoic, and Phanerozoic values. From left to right $\Delta^{17}O$ values (light blue), $\delta^{18}O$ (white), $\delta^{34}S$ (light grey), and $\Delta^{33}S$ (dark grey) are presented respectively. Red bars represent average values different time intervals.

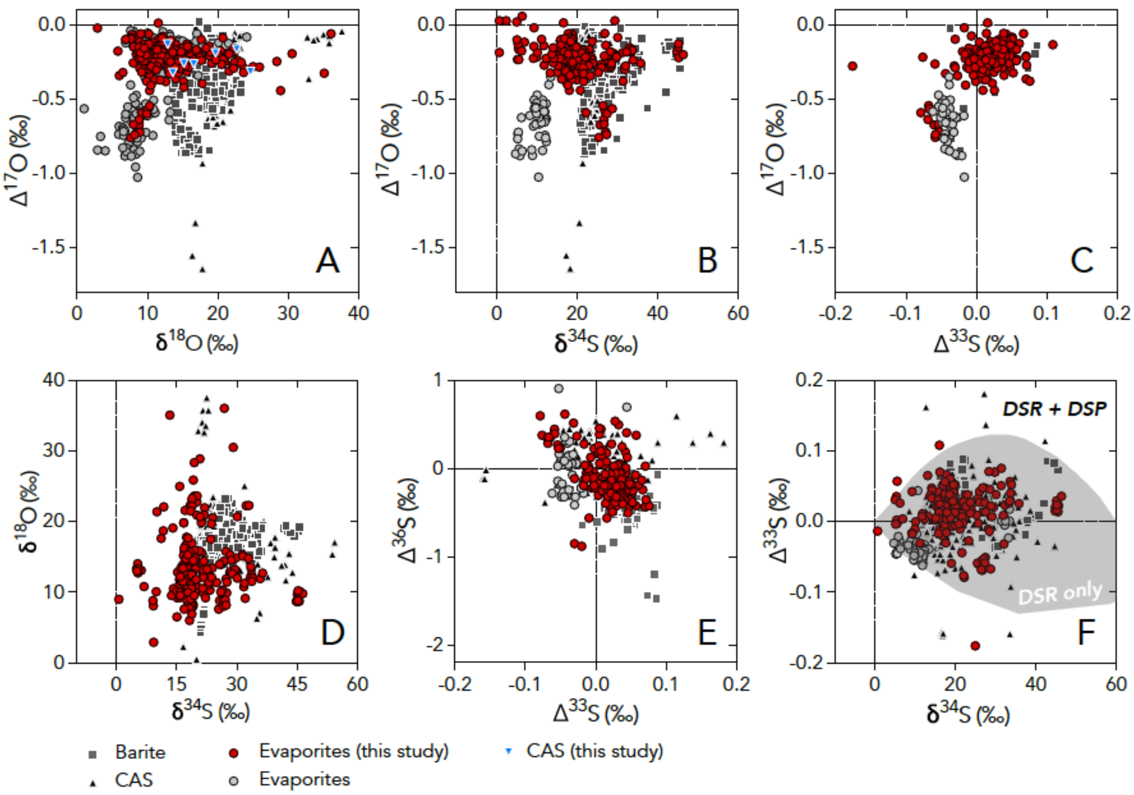

Figure 5.8: Cross plots of isotopic measurements (A $\Delta^{17}O$-$\delta^{18}O$; B $\Delta^{17}O$-$\delta^{34}S$; C $\Delta^{17}O$-$\Delta^{33}S$; D $\delta^{18}O$-$\delta^{34}S$; E $\Delta^{33}S$-$\Delta^{36}S$; F $\Delta^{33}S$-$\delta^{34}S$) from this and previous studies. The field outlined in grey which almost all data falls within, represents the predicted range of possible values from a steady state global sulfur cycle model (Johnston et al., 2005) augmented to include an expanded range of possible $^{34}\varepsilon$ (or $^{34}\alpha$ and $^{33}\lambda$ (or $^{33}\theta$) from Sim et al., 2015.

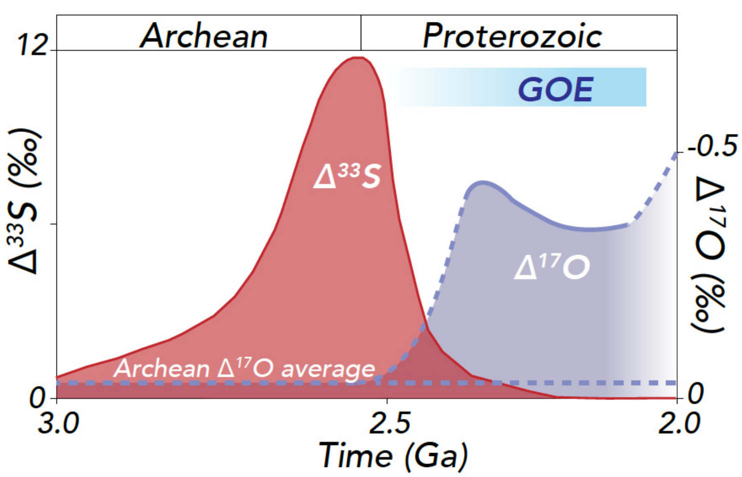

Figure 5.9: Schematics of mirrored $\Delta^{17}O$ and $\Delta^{33}S$ trends across the *GOE*. In red is an outline of compiled $\Delta^{33}S$ values between 3.0 – 2.0 Ga. In blue is an outline of $\Delta^{17}O$ values from this study, with dotted lines representing inferred trends and on the bottom Archean average $\Delta^{17}O$ values from Bao et al., 2007 and Farquhar et al., 2000.

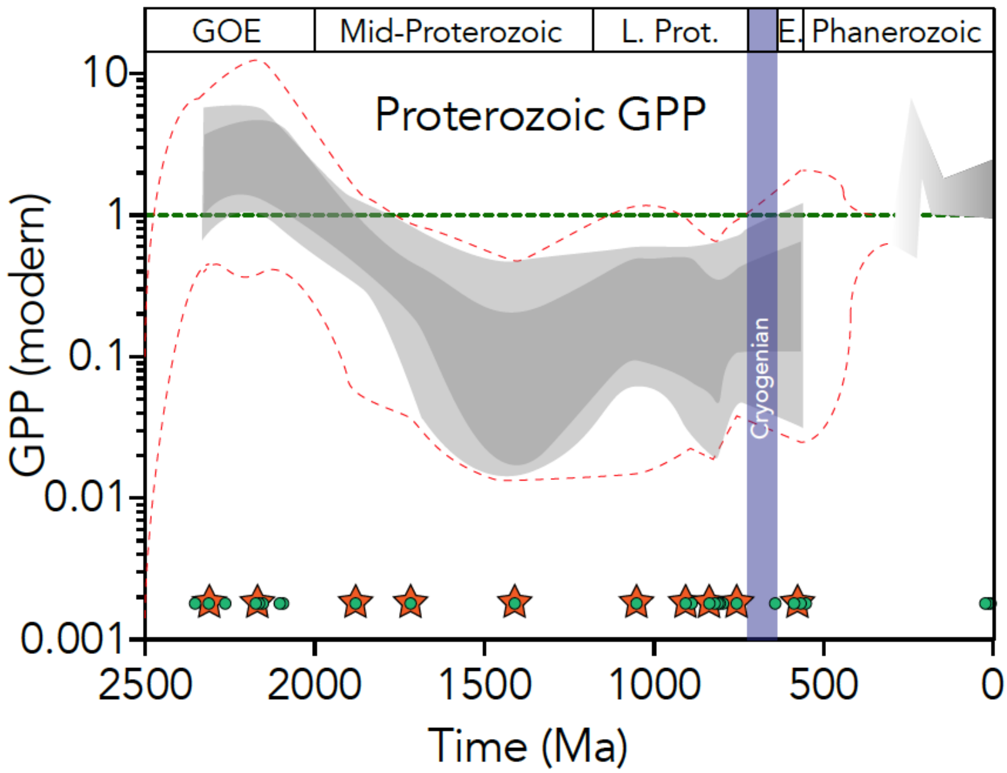

Figure 5.10: A calculated record of gross primary production (*GPP*) across the Proterozoic eon. Calculations are based upon Proterozoic pCO_2, and pO_2 estimates together with $\Delta^{17}O$ values of sulfate calculated through the model of Cao and Bao, 2013. The dark grey field represents *GPP* estimates based on average pCO_2 levels. The light grey field represents, averaged upper and lower pCO_2 estimates, and the red dotted lines represent calculated *GPP* values based on end-member pCO_2 estimates. Green circles represent ages of measured evaporites. Orange stars represent time points for calculated *GPP* estimates.

Bibliography

Aitken, J.D., 1981. Stratigraphy and sedimentology of the Upper Proterozoic Little Dal Group, Mackenzie Mountains, Northwest Territories. *Proterozoic basins of Canada. Edited by FHA Campbell. Geological Survey of Canada, Paper*, *8*, pp.1-10.

Alonso-Azcárate, J., Bottrell, S.H. and Mas, J.R., 2006. Synsedimentary versus metamorphic control of S, O and Sr isotopic compositions in gypsum evaporites from the Cameros Basin, Spain. *Chemical Geology*, *234*(1), pp.46-57.

Alt, J.C., 1995. Sulfur isotopic profile through the oceanic crust: Sulfur mobility and seawater-crustal sulfur exchange during hydrothermal alteration. *Geology*, *23*(7), pp.585-588.

Anbar, A.D. and Knoll, A.H., 2002. Proterozoic ocean chemistry and evolution: a bioinorganic bridge?. *Science*, *297*(5584), pp.1137-1142.

Anbar, A.D., Duan, Y., Lyons, T.W., Arnold, G.L., Kendall, B., Creaser, R.A., Kaufman, A.J., Gordon, G.W., Scott, C., Garvin, J. and Buick, R., 2007. A whiff of oxygen before the great oxidation event?. *Science*, *317*(5846), pp.1903-1906.

Antler, G., Turchyn, A.V., Rennie, V., Herut, B. and Sivan, O., 2013. Coupled sulfur and oxygen isotope insight into bacterial sulfate reduction in the natural environment. *Geochimica et Cosmochimica Acta*, *118*, pp.98-117.

Antler, G., Turchyn, A.V., Herut, B. and Sivan, O., 2015. A unique isotopic fingerprint of sulfate-driven anaerobic oxidation of methane. *Geology*, *43*(7), pp.619-622.

Antler, G., Turchyn, A.V., Ono, S., Sivan, O. and Bosak, T., 2017. Combined 34 S, 33 S and 18 O isotope fractionations record different intracellular steps of microbial sulfate reduction. *Geochimica et Cosmochimica Acta*, *203*, pp.364-380.

Armstrong, R.A., Master, S. and Robb, L.J., 2005. Geochronology of the Nchanga Granite, and constraints on the maximum age of the Katanga Supergroup, Zambian Copperbelt. *Journal of African Earth Sciences*, *42*(1), pp.32-40.

Bachan, A. and Kump, L.R., 2015. The rise of oxygen and siderite oxidation during the Lomagundi Event. *Proceedings of the National Academy of Sciences*, *112*(21), pp.6562-6567.

Bak, F. and Cypionka, H., 1987. A novel type of energy metabolism involving fermentation of inorganic sulphur compounds. *Nature*, *326*(6116), pp.891-892.

Balci, N., Shanks, W.C., Mayer, B. and Mandernack, K.W., 2007. Oxygen and sulfur isotope systematics of sulfate produced by bacterial and abiotic oxidation of pyrite. *Geochimica et Cosmochimica Acta*, *71*(15), pp.3796-3811.

Bao, H., Chen, Z.Q. and Zhou, C., 2012. An 17 O record of late Neoproterozoic glaciation in the Kimberley region, Western Australia. *Precambrian Research*, *216*, pp.152-161.

Bao, H., Rumble, D. and Lowe, D.R., 2007. The five stable isotope compositions of Fig Tree barites: Implications on sulfur cycle in ca. 3.2 Ga oceans. *Geochimica et Cosmochimica Acta*, *71*(20), pp.4868-4879.

Bao, H., Lyons, J.R. and Zhou, C., 2008. Triple oxygen isotope evidence for elevated CO2 levels after a Neoproterozoic glaciation. *Nature*, *453*(7194), pp.504-506.

Bao, H., Cao, X. and Hayles, J.A., 2016. Triple oxygen isotopes: fundamental relationships and applications. *Annual Review of Earth and Planetary Sciences*, *44*, pp.463-492.

Bao, H., 2015. Sulfate: A time capsule for Earth's O_2, O_3, and H_2O. *Chemical Geology*, *395*, pp.108-118

Bao, H., 2006. Purifying barite for oxygen isotope measurement by dissolution and reprecipitation in a chelating solution. *Analytical chemistry*, *78*(1), pp.304-309.

Bao, H., Fairchild, I.J., Wynn, P.M. and Spötl, C., 2009. Stretching the envelope of past surface environments: Neoproterozoic glacial lakes from Svalbard. *Science*, *323*(5910), pp.119-122.

Barkan, E. and Luz, B., 2011. The relationships among the three stable isotopes of oxygen in air, seawater and marine photosynthesis. *Rapid communications in mass spectrometry: RCM*, *25*(16), pp.2367-2369.

Barnola, J.M., Raynaud, D.Y.S.N., Korotkevich, Y.S. and Lorius, C., 1987. Vostok ice core provides 160,000-year record of atmospheric CO2. *Nature*, *329*(6138), pp.408-414.

Bekker, A., Kaufman, A.J., Karhu, J.A., Beukes, N.J., Swart, Q.D., Coetzee, L.L. and Eriksson, K.A., 2001. Chemostratigraphy of the Paleoproterozoic Duitschland Formation, South Africa: implications for coupled climate change and carbon cycling. *American Journal of Science*, *301*(3), pp.261-285.

Bekker, A., Holland, H.D., Wang, P.L. Rumble III, D., Stein, H.J., Hannah, J.L., Coetzee, L.L. Beukes, N.J., 2004. Dating the rise of atmospheric oxygen. *Nature*, *427*(6970), p.117.

Bekker, A., Karhu, J.A. and Kaufman, A.J., 2006. Carbon isotope record for the onset of the Lomagundi carbon isotope excursion in the Great Lakes area, North America. *Precambrian Research*, *148*(1), pp.145-180.

Bekker, A., Kaufman, A.J., Karhu, J.A. and Eriksson, K.A., 2005. Evidence for Paleoproterozoic cap carbonates in North America. *Precambrian Research*, *137*(3), pp.167-206.

Bekker, A. and Holland, H.D., 2012. Oxygen overshoot and recovery during the early Paleoproterozoic. *Earth and Planetary Science Letters*, *317*, pp.295-304.

Bekker, A., 2014, Lomagundi Carbon Isotope Excursion, In: Encyclopedia of Astrobiology, Springer-Verlag, p. 1-6.

Bekker, A., 2014. Great oxygenation event. *Encyclopedia of Astrobiology, eds R. Amils, M. Gargaud, J. Cernicharo Quintanilla, JH Cleaves, MW Irvine, D. Pinti, et al.(Berlin: Springer)*, pp.1-9.

Bekker, A. and Kaufman, A.J., 2007. Oxidative forcing of global climate change: a biogeochemical record across the oldest Paleoproterozoic ice age in North America. *Earth and Planetary Science Letters*, *258*(3), pp.486-499.

Bekker, A., Krapež, B., Müller, S., Karhu, J.A., 2016, A short-term, post-Lomagundi positive C isotope excursion at ~2.03 Ga recorded by the Wooly Dolomite, Western Australia, Journal of the Geological Society of London, v. 173, p. 689-700.

Berner, R.A., 2006. GEOCARBSULF: a combined model for Phanerozoic atmospheric O_2 and CO_2. *Geochimica et Cosmochimica Acta*, *70*(23), pp.5653-5664.

Berner, R.A., 1997. The rise of plants and their effect on weathering and atmospheric CO_2. *Science*, *276*(5312), pp.544-546.

Berner, R.A. and Maasch, K.A., 1996. Chemical weathering and controls on atmospheric O_2 and CO_2: fundamental principles were enunciated by JJ Ebelmen in 1845. *Geochimica et Cosmochimica Acta*, *60*(9), pp.1633-1637.

Blättler, C.L., Kump, L.R., Fischer, W.W., Paris, G., Kasbohm, J.J. and Higgins, J.A., 2017. Constraints on ocean carbonate chemistry and pCO_2 in the Archaean and Palaeoproterozoic. *Nature Geoscience*, *10*(1), pp.41-45.

Blunier, T., Barnett, B., Bender, M.L. and Hendricks, M.B., 2002. Biological oxygen productivity during the last 60,000 years from triple oxygen isotope measurements. *Global Biogeochemical Cycles*, *16*(3).

Böttcher, M.E., Thamdrup, B. and Vennemann, T.W., 2001. Oxygen and sulfur isotope fractionation during anaerobic bacterial disproportionation of elemental sulfur. *Geochimica et Cosmochimica Acta*, *65*(10), pp.1601-1609.

Bottrell, S.H. and Newton, R.J., 2006. Reconstruction of changes in global sulfur cycling from marine sulfate isotopes. *Earth-Science Reviews*, *75*(1), pp.59-83.

Bowles, M.W., Mogollón, J.M., Kasten, S., Zabel, M. and Hinrichs, K.U., 2014. Global rates of marine sulfate reduction and implications for sub–sea-floor metabolic activities. *Science*, *344*(6186), pp.889-891.

Bradley, D.C., 2011. Secular trends in the geologic record and the supercontinent cycle. *Earth-Science Reviews*, *108*(1), pp.16-33.

Bradley, A.S., Leavitt, W.D., Schmidt, M., Knoll, A.H., Girguis, P.R. and Johnston, D.T., 2016. Patterns of sulfur isotope fractionation during microbial sulfate reduction. *Geobiology*, *14*(1), pp.91-101.

Brasier, M.D. and Lindsay, J.F., 1998. A billion years of environmental stability and the emergence of eukaryotes: New data from northern Australia. *Geology*, *26*(6), pp.555-558.

Brennan, S.T., Lowenstein, T.K. and Horita, J., 2004. Seawater chemistry and the advent of biocalcification. *Geology*, *32*(6), pp.473-476.

Buick, R., Des Marais, D.J. and Knoll, A.H., 1995. Stable isotopic compositions of carbonates from the Mesoproterozoic Bangemall Group, northwestern Australia. *Chemical Geology*, *123*(1-4), pp.153-171.

Butler, I.B., Böttcher, M.E., Rickard, D. and Oldroyd, A., 2004. Sulfur isotope partitioning during experimental formation of pyrite via the polysulfide and hydrogen sulfide pathways: implications for the interpretation of sedimentary and hydrothermal pyrite isotope records. *Earth and Planetary Science Letters*, *228*(3), pp.495-509.

Butterfield, N.J., 2000. Bangiomorpha pubescens n. gen., n. sp.: implications for the evolution of sex, multicellularity, and the Mesoproterozoic/Neoproterozoic radiation of eukaryotes. *Paleobiology*, *26*(3), pp.386-404.

Cahen, L., 1982. Geochronological correlation of the Late Precambrian sequences on and around the stable zones of Equatorial Africa. *Precambrian Research*, *18*(1-2), pp.73-86.

Cameron, E.M., 1983. Evidence from early Proterozoic anhydrite for sulphur isotopic partitioning in Precambrian oceans. *Nature*, *304*(5921), pp.54-56.

Canfield, D.E., 1998. A new model for Proterozoic ocean chemistry. *Nature*, *396*(6710), pp.450-453.

Canfield, D.E., Thamdrup, B., Fleischer, S., 1998. Isotope fractionation and sulfur metabolism by pure and enrichment cultures of elemental sulfur-disproportionating bacteria. *Limnology and Oceanography, 43(2)*, 253-264.

Canfield, D.E. and Raiswell, R., 1999. The evolution of the sulfur cycle. *American Journal of Science*, *299*(7-9), pp.697-723.

Canfield, D.E., 2005. The early history of atmospheric oxygen: homage to Robert M. Garrels
Annu. Rev. Earth Planet. Sci., *33*, pp.1-36.

Canfield, D.E. and Thamdrup, B., 1994. The production of ^{34}S-depleted sulfide during bacterial disproportionation of elemental sulfur. *Science*, *266*(5193), p.1973.

Canfield, D.E., 2004. The evolution of the Earth surface sulfur reservoir. *American Journal of Science*, *304*(10), pp.839-861.

Canfield, D.E. and Farquhar, J., 2009. Animal evolution, bioturbation, and the sulfate concentration of the oceans. *Proceedings of the National Academy of Sciences*, *106*(20), pp.8123-8127.

Canfield, D.E., Farquhar, J. and Zerkle, A.L., 2010. High isotope fractionations during sulfate reduction in a low-sulfate euxinic ocean analog. *Geology*, *38*(5), pp.415-418.

Canfield, D.E., 2013. Sulfur isotopes in coal constrain the evolution of the Phanerozoic sulfur cycle. *Proceedings of the National Academy of Sciences*, *110*(21), pp.8443-8446.

Canfield, D.E. and Teske, A., 1996. Late Proterozoic rise in atmospheric oxygen concentration inferred from phylogenetic and sulphur-isotope studies. *Nature*, *382*(6587), p.127.

Canil, D., 1997. Vanadium partitioning and the oxidation state of Archaean komatiite magmas. *Nature*, *389*(6653), pp.842-845.

Canil, D. and Fellows, S.A., 2017. Sulphide–sulphate stability and melting in subducted sediment and its role in arc mantle redox and chalcophile cycling in space and time. *Earth and Planetary Science Letters*, *470*, pp.73-86.

Cao, X. and Liu, Y., 2011. Equilibrium mass-dependent fractionation relationships for triple oxygen isotopes. *Geochimica et Cosmochimica Acta*, *75*(23), pp.7435-7445.

Cao, X. and Bao, H., 2013. Dynamic model constraints on oxygen-17 depletion in atmospheric O2 after a snowball Earth. *Proceedings of the National Academy of Sciences*, *110*(36), pp.14546-14550.

Castresana, J. and Saraste, M., 1995. Evolution of energetic metabolism: the respiration-early hypothesis. *Trends in biochemical sciences*, *20*(11), pp.443-448.

Catling, D.C., Glein, C.R., Zahnle, K.J. and McKay, C.P., 2005. Why O_2 Is Required by Complex Life on Habitable Planets and the Concept of Planetary" Oxygenation Time". *Astrobiology*, *5*(3), pp.415-438.

Chandler, F.W., 1988. Diagenesis of sabkha-related, sulphate nodules in the early Proterozoic Gordon Lake Formation, Ontario, Canada. *Carbonates and Evaporites*, *3*(1), pp.75-94.

Clark, S.H., Poole, F.G. and Wang, Z., 2004. Comparison of some sediment-hosted, stratiform barite deposits in China, the United States, and India. *Ore Geology Reviews*, *24*(1), pp.85-101.

Claypool, G.E., Holser, W.T., Kaplan, I.R., Sakai, H. and Zak, I., 1980. The age curves of sulfur and oxygen isotopes in marine sulfate and their mutual interpretation. *Chemical Geology*, *28*, pp.199-260.

Cole, D.B., Reinhard, C.T., Wang, X., Gueguen, B., Halverson, G.P., Gibson, T., Hodgskiss, M.S., McKenzie, N.R., Lyons, T.W. and Planavsky, N.J., 2016. A shale-hosted Cr isotope record of low atmospheric oxygen during the Proterozoic. *Geology*, *44*(7), pp.555-558.

Collins, A.S., Patranabis-Deb, S., Alexander, E., Bertram, C.N., Falster, G.M., Gore, R.J., Mackintosh, J., Dhang, P.C., Saha, D., Payne, J.L. and Jourdan, F., 2015. Detrital mineral age, radiogenic isotopic stratigraphy and tectonic significance of the Cuddapah Basin, India. *Gondwana Research*, *28*(4), pp.1294-1309.

Condon, D., Zhu, M., Bowring, S., Wang, W., Yang, A. and Jin, Y., 2005. U-Pb ages from the neoproterozoic Doushantuo Formation, China. *Science*, *308*(5718), pp.95-98.

Cowie, B.R. and Johnston, D.T., 2016. High-precision measurement and standard calibration of triple oxygen isotopic compositions ($\delta^{18}O$, $\Delta'^{17}O$) of sulfate by F_2 laser fluorination. *Chemical Geology*, *440*, pp.50-59.

Cox, G.M., Halverson, G.P., Minarik, W.G., Le Heron, D.P., Macdonald, F.A., Bellefroid, E.J. and Strauss, J.V., 2013. Neoproterozoic iron formation: An evaluation of its temporal, environmental and tectonic significance. *Chemical Geology*, *362*, pp.232-249.

Cox, G.M., Halverson, G.P., Stevenson, R.K., Vokaty, M., Poirier, A., Kunzmann, M., Li, Z.X., Denyszyn, S.W., Strauss, J.V. and Macdonald, F.A., 2016. Continental flood basalt weathering as a trigger for Neoproterozoic Snowball Earth. *Earth and Planetary Science Letters*, *446*, pp.89-99.

Cox, G.M., Jarrett, A., Edwards, D., Crockford, P.W., Halverson, G.P., Collins, A.S., Poirier, A. and Li, Z.X., 2016. Basin redox and primary productivity within the Mesoproterozoic Roper Seaway. *Chemical Geology*, *440*, pp.101-114.

Crémière, A., Strauss, H., Sebilo, M., Hong, W.L., Gros, O., Schmidt, S., Tocny, J., Henry, F., Gontharet, S. and Laverman, A.M., 2017. Sulfur diagenesis under rapid accumulation of organic-rich sediments in a marine mangrove from Guadeloupe (French West Indies). *Chemical Geology*, *454*, pp.67-79.

Crockford, P.W., Hayles, J.A., Bao, H., Planavsky, N.J., Bekker, A., Bui, T.H., Halverson, G.P., Frallick, P., Wing, B.A., (XXXX) Limited primary production sustained low mid-Proterozoic oxygen levels *Nature in review*

Crockford, P.W., Cowie, B.R., Johnston, D.T., Hoffman, P.F., Sugiyama, I., Pellerin, A., Bui, T.H., Hayles, J., Halverson, G.P., Macdonald, F.A. and Wing, B.A., 2016. Triple oxygen and multiple sulfur isotope constraints on the evolution of the post-Marinoan sulfur cycle. *Earth and Planetary Science Letters*, *435*, pp.74-83.

Crockford, P., Telmer, K. and Best, M., 2014. Dissolution kinetics of Devonian carbonates at circum-neutral pH, 50bar pCO 2, 105° C, and 0.4 M: The importance of complex brine chemistry on reaction rates. *Applied Geochemistry*, *41*, pp.128-134.

Crowe, S.A., Døssing, L.N., Beukes, N.J., Bau, M., Kruger, S.J., Frei, R. and Canfield, D.E., 2013. Atmospheric oxygenation three billion years ago. *Nature*, *501*(7468), pp.535-538.

Crowe, S.A., Paris, G., Katsev, S., Jones, C., Kim, S.-T., Zerkle, A.L., Nomosatryo, S., Fowle, D.A., Adkins, J.F., Sessions, A.L., Farquhar, J., Canfield, D.E., 2014. Sulfate was a trace constituent of Archean seawater. *Science, 346*, 735-739.

Daines, S.J., Mills, B.J. and Lenton, T.M., 2017. Atmospheric oxygen regulation at low Proterozoic levels by incomplete oxidative weathering of sedimentary organic carbon. *Nature Communications*, *8*.

Das, N., Horita, J. and Holland, H.D., 1990. Chemistry of fluid inclusions in halite from the Salina Group of the Michigan Basin: Implications for Late Silurian seawater and the origin of sedimentary brines. *Geochimica et Cosmochimica Acta*, *54*(2), pp.319-327.

Deb, M., Hoefs, J. and Bauman, A., 1991. Isotopic composition of two Precambrian stratiform barite deposits from the Indian shield. *Geochimica et Cosmochimica Acta*, *55*(1), pp.303-308.

Delpomdor, F., Linnemann, U., Boven, A., Gärtner, A., Travin, A., Blanpied, C., Virgone, A., Jelsma, H. and Preat, A., 2013. Depositional age, provenance, and tectonic and paleoclimatic settings of the late Mesoproterozoic–middle Neoproterozoic Mbuji-Mayi Supergroup, Democratic Republic of Congo. *Palaeogeography, palaeoclimatology, palaeoecology*, *389*, pp.4-34.

Derry, L.A., 2015. Causes and consequences of mid‐Proterozoic anoxia. *Geophysical Research Letters*, *42*(20), pp.8538-8546.

Detmers, J., Brüchert, V., Habicht, K.S. and Kuever, J., 2001. Diversity of sulfur isotope fractionations by sulfate-reducing prokaryotes. *Applied and Environmental Microbiology*, *67*(2), pp.888-894.

Domagal-Goldman, S.D., Kasting, J.F., Johnston, D.T. and Farquhar, J., 2008. Organic haze, glaciations and multiple sulfur isotopes in the Mid-Archean Era. *Earth and Planetary Science Letters*, *269*(1), pp.29-40.

Dupont, C.L., Butcher, A., Valas, R.E., Bourne, P.E. and Caetano-Anollés, G., 2010. History of biological metal utilization inferred through phylogenomic analysis of protein structures. *Proceedings of the National Academy of Sciences*, *107*(23), pp.10567-10572.

Ebelmen, J.J., 1845. Sur les produits de la décomposition des espèces minérales de la famille des silicates. In *Annales des Mines* (Vol. 7, No. 3, p. 66).

Endo, Y., Ueno, Y., Aoyama, S. and Danielache, S.O., 2016. Sulfur isotope fractionation by broadband UV radiation to optically thin SO 2 under reducing atmosphere. *Earth and Planetary Science Letters*, *453*, pp.9-22.

Erwin, D.H., Laflamme, M., Tweedt, S.M., Sperling, E.A., Pisani, D. and Peterson, K.J., 2011. The Cambrian conundrum: early divergence and later ecological success in the early history of animals. *Science*, *334*(6059), pp.1091-1097.

Evans, D.A.D., Beukes, N.J., Kirschvink, J.L., 1997. Low-latitude glaciation in the Paleoproterozoic era. *Nature, 386*, 262-266.

Farquhar, J., Bao, H. and Thiemens, M., 2000. Atmospheric influence of Earth's earliest sulfur cycle. *Science*, *289*(5480), pp.756-758.

Farquhar, J. and Wing, B.A., 2003. Multiple sulfur isotopes and the evolution of the atmosphere. *Earth and Planetary Science Letters*, *213*(1), pp.1-13.

Farquhar, J., Johnston, D.T., Wing, B.A., Habicht, K.S., Canfield, D.E., Airieau, S. and Thiemens, M.H., 2003. Multiple sulphur isotopic interpretations of biosynthetic pathways: implications for biological signatures in the sulphur isotope record. *Geobiology*, *1*(1), pp.27-36.

Farquhar, J., Savarino, J., Airieau, S. and Thiemens, M.H., 2001. Observation of wavelength‐sensitive mass‐independent sulfur isotope effects during SO2 photolysis: Implications for the early atmosphere. *Journal of Geophysical Research: Planets*, *106*(E12), pp.32829-32839.

Feulner, G., Hallmann, C., Kienert, H., 2015. Snowball cooling after algal rise. *Nature Geoscience, 8*, 659-662.

Fichtner, V., Strauss, H., Immenhauser, A., Buhl, D., Neuser, R.D. and Niedermayr, A., 2017. Diagenesis of carbonate associated sulfate. *Chemical Geology*, *463*, pp.61-75.

Fike, D.A., Grotzinger, J.P., Pratt, L.M. and Summons, R.E., 2006. Oxidation of the Ediacaran ocean. *Nature*, *444*(7120), pp.744-747.

Fike, D.A. and Grotzinger, J.P., 2008. A paired sulfate–pyrite $\delta^{34}S$ approach to understanding the evolution of the Ediacaran–Cambrian sulfur cycle. *Geochimica et Cosmochimica Acta*, *72*(11), pp.2636-2648.

Fike, D.A., Bradley, A.S. and Rose, C.V., 2015. Rethinking the ancient sulfur cycle. *Annual Review of Earth and Planetary Sciences*, *43*, pp.593-622.

Finster, K., 2008. Microbiological disproportionation of inorganic sulfur compounds. *Journal of Sulfur Chemistry*, *29*(3-4), pp.281-292.

Fox, J.S. and Videtich, P.E., 1997. Revised estimate of δ34S for marine sulfates from the Upper Ordovician: data from the Williston Basin, North Dakota, USA. *Applied geochemistry*, *12*(1), pp.97-103.

Franks, P.J., Royer, D.L., Beerling, D.J., Van de Water, P.K., Cantrill, D.J., Barbour, M.M. and Berry, J.A., 2014. New constraints on atmospheric CO2 concentration for the Phanerozoic. *Geophysical Research Letters*, *41*(13), pp.4685-4694.

Fritz, P., Basharmal, G.M., Drimmie, R.J., Ibsen, J. and Qureshi, R.M., 1989. Oxygen isotope exchange between sulphate and water during bacterial reduction of sulphate. *Chemical Geology: Isotope Geoscience Section*, *79*(2), pp.99-105.

Gamo, T., Tsutsumi, M., Sakai, H., Nakazawa, T., Tanaka, M., Honda, H., Kubo, H. and Itoh, T., 1989. Carbon and oxygen isotopic ratios of carbon dioxide of a stratospheric profile over Japan. *Tellus B*, *41*(2), pp.127-133.

Gamsjager, H. and Murmann, R.K., 1983. Advances in Inorganic and Bioinorganic Mechanisms. *Sykes, AG, Ed*, pp.317-381.

Gellatly, A.M. and Lyons, T.W., 2005. Trace sulfate in mid-Proterozoic carbonates and the sulfur isotope record of biospheric evolution. *Geochimica et Cosmochimica Acta*, *69*(15), pp.3813-3829.

Gibson et al., *Nature Geoscience Submitted*

Gill, B.C., Lyons, T.W. and Saltzman, M.R., 2007. Parallel, high-resolution carbon and sulfur isotope records of the evolving Paleozoic marine sulfur reservoir. *Palaeogeography, Palaeoclimatology, Palaeoecology*, *256*(3), pp.156-173.

Gill, B.C., Lyons, T.W. and Frank, T.D., 2008. Behavior of carbonate-associated sulfate during meteoric diagenesis and implications for the sulfur isotope paleoproxy. *Geochimica et Cosmochimica Acta*, *72*(19), pp.4699-4711.

Gilleaudeau, G.J., Frei, R., Kaufman, A.J., Kah, L.C., Azmy, K., Bartley, J.K., Chernyavskiy, P. and Knoll, A.H., 2016. Oxygenation of the mid-Proterozoic atmosphere: clues from chromium isotopes in carbonates. *Geochemical Perspectives Letters*, *2*, pp.178-187.

Goldberg, T., Poulton, S.W. and Strauss, H., 2005. Sulphur and oxygen isotope signatures of late Neoproterozoic to early Cambrian sulphate, Yangtze Platform, China: diagenetic constraints and seawater evolution. *Precambrian Research*, *137*(3), pp.223-241.

Goldblatt, C., Lenton, T.M. and Watson, A.J., 2006. Bistability of atmospheric oxygen and the Great Oxidation. *Nature*, *443*(7112), pp.683-686.

Gomes, M.L. and Johnston, D.T., 2017. Oxygen and sulfur isotopes in sulfate in modern euxinic systems with implications for evaluating the extent of euxinia in ancient oceans. *Geochimica et Cosmochimica Acta*, *205*, pp.331-359.

Gomes, M.L. and Hurtgen, M.T., 2013. Sulfur isotope systematics of a euxinic, low-sulfate lake: evaluating the importance of the reservoir effect in modern and ancient oceans. *Geology*, *41*(6), pp.663-666.

Gough, D.O., 1981. Solar interior structure and luminosity variations. *Solar Physics*, *74*(1), pp.21-34.

Grinenko, L.N., Melezhik, V.A. and Feti- sova, O.A., 1989. First discovery of barites in the Precambrian sedimentary deposits of Baltic Shield. Dokl. Akad. Nauk, 304, 1453–1455 (in Russian)

Gumsley, A.P., Chamberlain, K.R., Bleeker, W., Söderlund, U., de Kock, M.O., Larsson, E.R. and Bekker, A., 2017. Timing and tempo of the Great Oxidation Event. *Proceedings of the National Academy of Sciences*, *114*(8), pp.1811-1816.

Guo, Q., Strauss, H., Kaufman, A.J., Schröder, S., Gutzmer, J., Wing, B., Baker, M.A., Bekker, A., Jin, Q., Kim, S.T. and Farquhar, J., 2009. Reconstructing Earth's surface oxidation across the Archean-Proterozoic transition. *Geology*, *37*(5), pp.399-402.

Habicht, K.S., Gade, M., Thamdrup, B., Berg, P. and Canfield, D.E., 2002. Calibration of sulfate levels in the Archean ocean. *Science*, *298*(5602), pp.2372-2374.

Halevy, I., Peters, S.E. and Fischer, W.W., 2012. Sulfate burial constraints on the Phanerozoic sulfur cycle. *Science*, *337*(6092), pp.331-334.

Halevy, I. and Bachan, A., 2017. The geologic history of seawater pH. *Science*, *355*(6329), pp.1069-1071.

Halevy, I., Johnston, D.T. and Schrag, D.P., 2010. Explaining the structure of the Archean mass-independent sulfur isotope record. *Science*, *329*(5988), pp.204-207.

Hall, N.F. and Alexander, O.R., 1940. Oxygen exchange between anions and water. *Journal of the American Chemical Society*, *62*(12), pp.3455-3462.

Halverson, G.P., Hoffman, P.F., Schrag, D.P., Maloof, A.C. and Rice, A.H.N., 2005. Toward a Neoproterozoic composite carbon-isotope record. *Geological Society of America Bulletin*, *117*(9-10), pp.1181-1207.

Halverson, G.P. and Hurtgen, M.T., 2007. Ediacaran growth of the marine sulfate reservoir. *Earth and Planetary Science Letters*, *263*(1), pp.32-44.

Hardisty, D.S., Lu, Z., Bekker, A., Diamond, C.W., Gill, B.C., Jiang, G., Kah, L.C., Knoll, A.H., Loyd, S.J., Osburn, M.R. and Planavsky, N.J., 2017. Perspectives on Proterozoic surface ocean redox from iodine contents in ancient and recent carbonate. *Earth and Planetary Science Letters*, *463*, pp.159-170.

Harrison, A.G. and Thode, H.G., 1958. Mechanism of the bacterial reduction of sulphate from isotope fractionation studies. *Transactions of the Faraday Society*, *54*, pp.84-92.

Havig, J.R., Hamilton, T.L., Bachan, A. and Kump, L.R., 2017. Sulfur and carbon isotopic evidence for metabolic pathway evolution and a four-stepped Earth system progression across the Archean and Paleoproterozoic. *Earth-Science Reviews*.

Hayles, J.A., Cao, X. and Bao, H., 2017. The statistical mechanical basis of the triple isotope fractionation relationship. *GEOCHEMICAL PERSPECTIVES LETTERS*, *3*(1), pp.1-11.

Heidenreich III, J.E. and Thiemens, M.H., 1986. A non‐mass‐dependent oxygen isotope effect in the production of ozone from molecular oxygen: The role of molecular symmetry in isotope chemistry. *The Journal of chemical physics*, *84*(4), pp.2129-2136.

Hill, A.C. and Walter, M.R., 2000. Mid-Neoproterozoic (∼ 830–750 Ma) isotope stratigraphy of Australia and global correlation. *Precambrian Research*, *100*(1), pp.181-211.

Hoffman, P.F., 2016. Cryoconite pans on Snowball Earth: supraglacial oases for Cryogenian eukaryotes?. *Geobiology*, *14*(6), pp.531-542.

Hoffman, P.F., Kaufman, A.J., Halverson, G.P. and Schrag, D.P., 1998. A Neoproterozoic snowball earth. *Science*, *281*(5381), pp.1342-1346.

Hoffman et al., *Sci Adv accepted*

Holland, H.D., Feakes, C.R. and Zbinden, E.A., 1989. The Flin Flon paleosol and the composition of the atmosphere 1.8 BYBP. *American Journal of Science*, *289*(4), pp.362-389.

Holland, H.D., 2002. Volcanic gases, black smokers, and the Great Oxidation Event. *Geochimica et Cosmochimica Acta*, *66*(21), pp.3811-3826.

Holland, H.D., 2006. The oxygenation of the atmosphere and oceans. *Philosophical Transactions of the Royal Society of London B: Biological Sciences*, *361*(1470), pp.903-915.

Holser, W.T. and Kaplan, I.R., 1966. Isotope geochemistry of sedimentary sulfates. *Chemical Geology*, *1*, pp.93-135.

Holt, B.D., Cunningham, P.T., Engelkemeir, A.G., Graczyk, D.G. and Kumar, R., 1983. Oxygen-18 study of nonaqueous-phase oxidation of sulfur dioxide. *Atmospheric Environment (1967)*, *17*(3), pp.625-632.

Horner, T.J., Pryer, H.V., Nielsen, S.G., Crockford, P.W., Gauglitz, J.M., Wing, B.A., Ricketts, R.D., (XXXX) Pelagic barite precipitation at micromolar ambient sulphate. *Nature Communications. In review*

Hough, M.L., Shields, G.A., Evins, L.Z., Strauss, H., Henderson, R.A. and Mackenzie, S., 2006. A major sulphur isotope event at c. 510 Ma: a possible anoxia–

extinction–volcanism connection during the Early–Middle Cambrian transition?. *Terra Nova*, *18*(4), pp.257-263.

Hug, L.A., Baker, B.J., Anantharaman, K., Brown, C.T., Probst, A.J., Castelle, C.J., Butterfield, C.N., Hernsdorf, A.W., Amano, Y., Ise, K. and Suzuki, Y., 2016. A new view of the tree of life. *Nature Microbiology*, *1*, p.16048.

Hurtgen, M.T., Arthur, M.A., Suits, N.S. and Kaufman, A.J., 2002. The sulfur isotopic composition of Neoproterozoic seawater sulfate: implications for a snowball Earth?. *Earth and Planetary Science Letters*, *203*(1), pp.413-429.

Hurtgen, M.T., Halverson, G.P., Arthur, M.A. and Hoffman, P.F., 2006. Sulfur cycling in the aftermath of a 635-Ma snowball glaciation: evidence for a syn-glacial sulfidic deep ocean. *Earth and Planetary Science Letters*, *245*(3), pp.551-570.

Hurtgen, M.T., Arthur, M.A. and Prave, A.R., 2004. The sulfur isotope composition of carbonate-associated sulfate in Mesoproterozoic to Neoproterozoic carbonates from Death Valley, California. *Geological Society of America Special Papers*, *379*, pp.177-194.

Jackson, G.D. and Cumming, L.M., 1981. Evaporites and folding in the Neohelikian Society Cliffs Formation, northeastern Bylot Island, Arctic Canada. *Geological Survey of Canada, Current Research, part C, Paper*, pp.35-44.

Jacobsen, S.B., 1988. Isotopic constraints on crustal growth and recycling. *Earth and Planetary Science Letters*, *90*(3), pp.315-329.

Jamieson, J.W., Wing, B.A., Farquhar, J. and Hannington, M.D., 2013. Neoarchaean seawater sulphate concentrations from sulphur isotopes in massive sulphide ore. *Nature Geoscience*, *6*(1), pp.61-64.

Javaux, E.J., 2007. The early eukaryotic fossil record. *Eukaryotic Membranes and Cytoskeleton*, pp.1-19.

Jefferson, C.W. and Parrish, R.R., 1989. Late Proterozoic stratigraphy, U–Pb zircon ages, and rift tectonics, Mackenzie Mountains, northwestern Canada. *Canadian Journal of Earth Sciences*, *26*(9), pp.1784-1801.

Johnston, D.T., Farquhar, J., Wing, B.A., Kaufman, A.J., Canfield, D.E. and Habicht, K.S., 2005. Multiple sulfur isotope fractionations in biological systems: a case study with sulfate reducers and sulfur disproportionators. *American Journal of Science*, *305*(6-8), pp.645-660.

Johnston, D.T., 2011. Multiple sulfur isotopes and the evolution of Earth's surface sulfur cycle. *Earth-Science Reviews*, *106*(1), pp.161-183.

Johnston, D.T., Wing, B.A., Farquhar, J., Kaufman, A.J., Strauss, H., Lyons, T.W., Kah, L.C. and Canfield, D.E., 2005. Active microbial sulfur disproportionation in the Mesoproterozoic. *Science*, *310*(5753), pp.1477-1479.

Johnston, D.T., Poulton, S.W., Fralick, P.W., Wing, B.A., Canfield, D.E. and Farquhar, J., 2006. Evolution of the oceanic sulfur cycle at the end of the Paleoproterozoic. *Geochimica et Cosmochimica Acta*, *70*(23), pp.5723-5739.

Johnston, D.T., Farquhar, J., Summons, R.E., Shen, Y., Kaufman, A.J., Masterson, A.L. and Canfield, D.E., 2008. Sulfur isotope biogeochemistry of the Proterozoic McArthur Basin. *Geochimica et Cosmochimica Acta*, *72*(17), pp.4278-4290.

Johnston, D.T., Poulton, S.W., Tosca, N.J., O'Brian, T., Halverson, G.P., Schrag, D.P., Macdonald, F.A., 2013. Searching for an oxygenation event in the fossiliferous Ediacaran of northwestern Canada. *Chemical Geology, 326*, 273-286.

Jones, D.S. and Fike, D.A., 2013. Dynamic sulfur and carbon cycling through the end-Ordovician extinction revealed by paired sulfate–pyrite δ 34 S. *Earth and Planetary Science Letters*, *363*, pp.144-155.

Jørgensen, B.B. and Kasten, S., 2006. Sulfur cycling and methane oxidation. In *Marine geochemistry* (pp. 271-309). Springer Berlin Heidelberg.

Jørgensen, B.B., 1982. Mineralization of organic matter in the sea bed—the role of sulphate reduction. Nature, 296, pp. 643-645

Jørgensen, B.B., 1990. A thiosulfate shunt in the sulfur cycle of marine sediments. *Science*, *249*(4965), pp.152-155.

Kah, L.C., Lyons, T.W. and Frank, T.D., 2004. Low marine sulphate and protracted oxygenation of the Proterozoic biosphere. *Nature*, *431*(7010), pp.834-838.

Kah, L.C., Sherman, A.G., Narbonne, G.M., Knoll, A.H. and Kaufman, A.J., 1999. δ13C stratigraphy of the Proterozoic Bylot Supergroup, Baffin Island, Canada: implications for regional lithostratigraphic correlations. *Canadian Journal of Earth Sciences*, *36*(3), pp.313-332.

Kah, L.C., Thompson, C.K., Henderson, M.A. and Zhan, R., 2016. Behavior of marine sulfur in the Ordovician. *Palaeogeography, Palaeoclimatology, Palaeoecology*, *458*, pp.133-153.

Kampschulte, A., Buhl, D. and Strauss, H., 1998. The sulfur and strontium isotopic compositions of Permian evaporites from the Zechstein basin, northern Germany. *Geologische Rundschau*, *87*(2), pp.192-199.

Kampschulte, A. and Strauss, H., 2004. The sulfur isotopic evolution of Phanerozoic seawater based on the analysis of structurally substituted sulfate in carbonates. *Chemical Geology*, *204*(3), pp.255-286.

Kanzaki, Y. and Murakami, T., 2016. Estimates of atmospheric O_2 in the Paleoproterozoic from paleosols. *Geochimica et Cosmochimica Acta*, *174*, pp.263-290.

Kasting, J.F. and Ono, S., 2006. Palaeoclimates: the first two billion years. *Philosophical Transactions of the Royal Society of London B: Biological Sciences*, *361*(1470), pp.917-929.

Killingsworth, B.A., Hayles, J.A., Zhou, C. and Bao, H., 2013. Sedimentary constraints on the duration of the Marinoan Oxygen-17 Depletion (MOSD) event. *Proceedings of the National Academy of Sciences*, *110*(44), pp.17686-17690.

Kirschvink, J.L., Gaidos, E.J., Bertani, L.E., Beukes, N.J., Gutzmer, J., Maepa, L.N. and Steinberger, R.E., 2000. Paleoproterozoic snowball Earth: Extreme climatic and geochemical global change and its biological consequences. *Proceedings of the National Academy of Sciences*, *97*(4), pp.1400-1405.

Knoll, A.H., Javaux, E.J., Hewitt, D. and Cohen, P., 2006. Eukaryotic organisms in Proterozoic oceans. *Philosophical Transactions of the Royal Society of London B: Biological Sciences*, *361*(1470), pp.1023-1038.

Knoll, A.H., 2014. Paleobiological perspectives on early eukaryotic evolution. *Cold Spring Harbor Perspectives in Biology*, *6*(1), p.a016121.

Koehler, M.C., Stüeken, E.E., Kipp, M.A., Buick, R. and Knoll, A.H., 2017. Spatial and temporal trends in Precambrian nitrogen cycling: a Mesoproterozoic offshore nitrate minimum. *Geochimica et Cosmochimica Acta*, *198*, pp.315-337.

Kohl, I. and Bao, H., 2011. Triple-oxygen-isotope determination of molecular oxygen incorporation in sulfate produced during abiotic pyrite oxidation (pH = 2–11). *Geochimica et Cosmochimica Acta*, *75*(7), pp.1785-1798.

Kopp, R.E., Kirschvink, J.L., Hilburn, I.A. and Nash, C.Z., 2005. The Paleoproterozoic snowball Earth: a climate disaster triggered by the evolution of oxygenic photosynthesis. *Proceedings of the National Academy of Sciences of the United States of America*, *102*(32), pp.11131-11136.

Krissansen-Totton, J., Buick, R. and Catling, D.C., 2015. A statistical analysis of the carbon isotope record from the Archean to Phanerozoic and implications for the rise of oxygen. *American Journal of Science*, *315*(4), pp.275-316.

Krupenik, V.A., Akhmedov, A.M. and Sveshnikova, K.Y., 2011. Isotopic composition of carbon, oxygen and sulphur in the Ludicovian and Jatulian rocks. *The Onega*

Palaeoproterozoic structure (Geology, tectonics, deep structure and minerageny). Karelian Research Centre, Petrozavodsk, pp.250-255.

Kumar, M.D., Shenoy, D.M., Sarma, V.V.S.S., George, M.D. and Dandekar, M., 2002. Export fluxes of dimethylsulfoniopropionate and its break down gases at the air‐sea interface. *Geophysical Research Letters*, *29*(2).

Kump, L.R., Kasting, J.F. and Barley, M.E., 2001. Rise of atmospheric oxygen and the "upside‐down" Archean mantle. *Geochemistry, Geophysics, Geosystems*, *2*(1).

Kunzmann, M., Gutzmer, J., Beukes, N.J. and Halverson, G.P., 2014. Depositional environment and lithostratigraphy of the Paleoproterozoic Mooidraai Formation, Kalahari Manganese Field, South Africa. *South African Journal of Geology*, *117*(2), pp.173-192.

Kunzmann, M., Halverson, G.P., Scott, C., Minarik, W.G., Wing, B.A., 2015. Geochemistry of Neoproterozoic black shales from Svalbard: implications for oceanic redox conditions spanning Cryogenian glaciations. *Chemical Geology, 417*, 383-393.

Kunzmann, M., Bui, T.H., Crockford, P.W., Halverson, G.P., Scott, C., Lyons, T.W. and Wing, B.A., 2017. Bacterial sulfur disproportionation constrains timing of Neoproterozoic oxygenation. *Geology*, 45 (3), pp. 207-210.

Kuznetsov, A.B., Melezhik, V.A., Gorokhov, I.M., Melnikov, N.N., Konstantinova, G.V., Kutyavin, E.P., Turchenko, T.L., 2010. Sr isotopic composition of Paleoproterozoic C-13-rich carbonate rocks The Tulomozero Formation, SE Fennoscandian Shield. Precambrian Research, 182(4), pp. 300-312.

Kuznetsov, A.B., Bekker, A., Ovchinnikova, G.V., Gorokhov, I.M. and Vasilyeva, I.M., 2017. Unradiogenic strontium and moderate-amplitude carbon isotope variations in early Tonian seawater after the assembly of Rodinia and before the Bitter Springs Excursion. *Precambrian Research*.

Laakso, T.A. and Schrag, D.P., 2014. Regulation of atmospheric oxygen during the Proterozoic. *Earth and Planetary Science Letters*, *388*, pp.81-91.

Laznicka, P., 1992. Manganese deposits in the global lithogenetic system: Quantitative approach. *Ore Geology Reviews*, *7*(4), pp.279-356.

Leavitt, W.D., Halevy, I., Bradley, A.S. and Johnston, D.T., 2013. Influence of sulfate reduction rates on the Phanerozoic sulfur isotope record. *Proceedings of the National Academy of Sciences*, *110*(28), pp.11244-11249.

Lenton, T.M., Boyle, R.A., Poulton, S.W., Shields-Zhou, G.A. and Butterfield, N.J., 2014. Co-evolution of eukaryotes and ocean oxygenation in the Neoproterozoic era. *Nature Geoscience*, *7*(4), pp.257-265.

Lenton, T.M., Dahl, T.W., Daines, S.J., Mills, B.J., Ozaki, K., Saltzman, M.R. and Porada, P., 2016. Earliest land plants created modern levels of atmospheric oxygen. *Proceedings of the National Academy of Sciences*, p.201604787.

Li, C., Planavsky, N.J., Love, G.D., Reinhard, C.T., Hardisty, D., Feng, L., Bates, S.M., Huang, J., Zhang, Q., Chu, X. and Lyons, T.W., 2015. Marine redox conditions in the middle Proterozoic ocean and isotopic constraints on authigenic carbonate formation: Insights from the Chuanlinggou Formation, Yanshan Basin, North China. *Geochimica et Cosmochimica Acta*, *150*, pp.90-105

Li, Z.X., Evans, D.A. and Halverson, G.P., 2013. Neoproterozoic glaciations in a revised global palaeogeography from the breakup of Rodinia to the assembly of Gondwanaland. *Sedimentary Geology*, *294*, pp.219-232.

Liu, X.M., Kah, L.C., Knoll, A.H., Cui, H., Kaufman, A.J., Shahar, A. and Hazen, R.M., 2016. Tracing Earth's O_2 evolution using Zn/Fe ratios in marine carbonates. *GEOCHEMICAL PERSPECTIVES LETTERS.* 2(1), pp. 24-34

Lloyd, R.M., 1968. Oxygen isotope behavior in the sulfate-water system. *Journal of Geophysical Research*, *73*(18), pp.6099-6110.

Longinelli, A. and Craig, H., 1967. Oxygen-18 variations in sulfate ions in sea water and saline lakes. *Science*, *156*(3771), pp.56-59.

Longinelli, A. and Flora, O., 2007. Isotopic composition of gypsum samples of Permian and Triassic age from the north-eastern Italian Alps: Palaeoenvironmental implications. *Chemical Geology*, *245*(3), pp.275-284.

Lu, F.H., Meyers, W.J. and Schoonen, M.A., 2001. S and O (SO 4) isotopes, simultaneous modeling, and environmental significance of the Nijar Messinian gypsum, Spain. *Geochimica et Cosmochimica Acta*, *65*(18), pp.3081-3092.

Luo, G., Ono, S., Beukes, N.J., Wang, D.T., Xie, S. and Summons, R.E., 2016. Rapid oxygenation of Earth's atmosphere 2.33 billion years ago. *Science Advances*, *2*(5), p.e1600134.

Luo, G., Ono, S., Huang, J., Algeo, T.J., Li, C., Zhou, L., Robinson, A., Lyons, T.W. and Xie, S., 2015. Decline in oceanic sulfate levels during the early Mesoproterozoic. *Precambrian Research*, *258*, pp.36-47.

Luo, G., Kump, L.R., Wang, Y., Tong, J., Arthur, M.A., Yang, H., Huang, J., Yin, H. and Xie, S., 2010. Isotopic evidence for an anomalously low oceanic sulfate concentration following end-Permian mass extinction. *Earth and Planetary Science Letters*, *300*(1), pp.101-111.

Luz, B. and Barkan, E., 2010. Variations of 17 O/16 O and 18 O/16 O in meteoric waters. *Geochimica et Cosmochimica Acta*, *74*(22), pp.6276-6286.

Luz, B., Barkan, E., Bender, M.L., Thiemens, M.H. and Boering, K.A., 1999. Triple-isotope composition of atmospheric oxygen as a tracer of biosphere productivity. *Nature*, *400*(6744), pp.547-550.

Lyons, T.W., Anbar, A.D., Severmann, S., Scott, C. and Gill, B.C., 2009. Tracking euxinia in the ancient ocean: a multiproxy perspective and Proterozoic case study. *Annual Review of Earth and Planetary Sciences*, *37*, pp.507-534.

Lyons, T.W., Reinhard, C.T. and Planavsky, N.J., 2014. The rise of oxygen in Earth/'s early ocean and atmosphere. *Nature*, *506*(7488), pp.307-315.

Macdonald, F.A., Schmitz, M.D., Crowley, J.L., Roots, C.F., Jones, D.S., Maloof, A.C., Strauss, J.V., Cohen, P.A., Johnston, D.T. and Schrag, D.P., 2010. Calibrating the Cryogenian. *Science*, *327*(5970), pp.1241-1243.

Macdonald, F.A. and Wordsworth, R., 2017. Initiation of Snowball Earth with volcanic sulfur aerosol emissions. *Geophysical Research Letters*, *44*(4), pp.1938-1946.

Mackenzie, F.T. and Garrels, R.M., 1971. *Evolution of sedimentary rocks*. Norton.

Manyeruke, T.D., Blenkinsop, T.G., Buchholz, P., Love, D., Oberthür, T., Vetter, U.K. and Davis, D.W., 2004. The age and petrology of the Chimbadzi Hill Intrusion, NW Zimbabwe: first evidence for early Paleoproterozoic magmatism in Zimbabwe. *Journal of African Earth Sciences*, *40*(5), pp.281-292.

Marenco, P.J., Corsetti, F.A., Hammond, D.E., Kaufman, A.J. and Bottjer, D.J., 2008. Oxidation of pyrite during extraction of carbonate associated sulfate. *Chemical Geology*, *247*(1), pp.124-132.

Markovic, S., Paytan, A., Li, H. and Wortmann, U.G., 2016. A revised seawater sulfate oxygen isotope record for the last 4Myr. *Geochimica et Cosmochimica Acta*, *175*, pp.239-251.

Master, S., Verhagen, B.T., Bassot, J.P., Beukes, N.J. and Lemoine, S., 1993. Stable isotopic signatures of Paleopro- terozoic carbonates from Guinea, Sene- gal, South Africa and Zimbabwe: constraints on the timing of the ca. 2 Ga Lomagundi d13C excursion. In: Interna- tional Symposium Early Proterozoic, Geochemical and Structural Constraints – Metallogeny (D.I.A. Abdoulaye, ed), pp. 38–41. Centre international pour la for- mation et les e ́ changes ge ́ ologiques, Da- kar.

Masterson, A.L., Wing, B.A., Payton, A., Farquhar, J., Johnston, D.T., 2016. The minor sulfur isotope composition of Cretaceous and Cenozoic seawater sulfate. Paleoceanography, 31 (6), 779-788.

Matsuhisa, Y., Goldsmith, J.R. and Clayton, R.N., 1978. Mechanisms of hydrothermal crystallization of quartz at 250 C and 15 kbar. *Geochimica et Cosmochimica Acta*, *42*(2), pp.173-182.

Mazumdar, A. and Strauss, H., 2006. Sulfur and strontium isotopic compositions of carbonate and evaporite rocks from the late Neoproterozoic–early Cambrian Bilara Group (Nagaur-Ganganagar Basin, India): Constraints on intrabasinal correlation and global sulfur cycle. *Precambrian Research*, *149*(3), pp.217-230

McKenzie, N.R., Horton, B.K., Loomis, S.E., Stockli, D.F., Planavsky, N.J. and Lee, C.T.A., 2016. Continental arc volcanism as the principal driver of icehouse-greenhouse variability. *Science*, *352*(6284), pp.444-447.

Miller, A.J., Strauss, J.V., Halverson, G.P., Macdonald, F.A., Johnston, D.T. and Sperling, E.A., 2017. Tracking the onset of Phanerozoic-style redox-sensitive trace metal enrichments: New results from basal Ediacaran post-glacial strata in NW Canada. *Chemical Geology*. *447,* 24-37.

Mills, D.B., Ward, L.M., Jones, C., Sweeten, B., Forth, M., Treusch, A.H. and Canfield, D.E., 2014. Oxygen requirements of the earliest animals. *Proceedings of the National Academy of Sciences*, *111*(11), pp.4168-4172.

Mizutani, Y. and Rafter, T.A., 1973. Isotopic behaviour of sulphate oxygen in the bacterial reduction of sulphate. *Geochemical Journal*, *6*(4), pp.183-191.

Morozov, A.F., Hakhaev, B.N., Petrov, O.V., Gorbachev, V.I., Tarkhanov, G.B., Tsvetkov, L.D., Erinchek, Y., Akhmedov, A.M., Krupenik, V.A. and Sveshnikova, K., 2010. Rock-salts in Palaeoproterozoic strata of the Onega depression of Karelia (based on data from the Onega parametric drillhole). *Trans Acad Sci*, *435*(2), pp.230-233.

Muir, M., 1987. Facies models for Australian Precambrian evaporites. *Evaporite basins*, pp.5-21.

Nier, A.O., 1950. A redetermination of the relative abundances of the isotopes of carbon, nitrogen, oxygen, argon, and potassium. *Physical Review*, *77*(6), p.789.

Ono, S., 2017. Photochemistry of Sulfur Dioxide and the Origin of Mass-Independent Isotope Fractionation in Earth's Atmosphere. *Annual Review of Earth and Planetary Sciences*, *45*(1).

Ono, S., Wing, B., Johnston, D., Farquhar, J. and Rumble, D., 2006. Mass-dependent fractionation of quadruple stable sulfur isotope system as a new tracer of sulfur biogeochemical cycles. *Geochimica et Cosmochimica Acta*, *70*(9), pp.2238-2252.

Ortí, F., Rosell, L. and Anadón, P., 2010. Diagenetic gypsum related to sulfur deposits in evaporites (Libros Gypsum, Miocene, NE Spain). *Sedimentary Geology*, *228*(3), pp.304-318.

Ovchinnikova, G.V., Kuznetsov, A.B., Melezhik, V.A., Gorokhov, I.M., Vasil'eva, I.M. and Gorokhovskii, B.M., 2007. Pb-Pb age of Jatulian carbonate rocks: the Tulomozero Formation of southeast Karelia. *Stratigraphy and Geological Correlation*, *15*(4), pp.359-372.

Ozaki, K. and Tajika, E., 2013. Biogeochemical effects of atmospheric oxygen concentration, phosphorus weathering, and sea-level stand on oceanic redox chemistry: Implications for greenhouse climates. *Earth and Planetary Science Letters*, *373*, pp.129-139.

Pack, A., and Herwartz, D., 2014, The triple oxygen isotope composition of the Earth mantle and understanding $\delta^{17}O$ variations in terrestrial rocks and minerals: Earth and Planetary Science Letters, v. 390, p. 138–145

Palmer, M.R., Helvací, C. and Fallick, A.E., 2004. Sulphur, sulphate oxygen and strontium isotope composition of Cenozoic Turkish evaporites. *Chemical Geology*, *209*(3), pp.341-356.

Parfrey, L.W., Lahr, D.J., Knoll, A.H. and Katz, L.A., 2011. Estimating the timing of early eukaryotic diversification with multigene molecular clocks. *Proceedings of the National Academy of Sciences*, *108*(33), pp.13624-13629.

Partin, C.A., Bekker, A., Planavsky, N.J., Scott, C.T., Gill, B.C., Li, C., Podkovyrov, V., Maslov, A., Konhauser, K.O., Lalonde, S.V. and Love, G.D., 2013. Large-scale fluctuations in Precambrian atmospheric and oceanic oxygen levels from the record of U in shales. *Earth and Planetary Science Letters*, *369*, pp.284-293.

Partin, C.A. and Sadler, P.M., 2016. Slow net sediment accumulation sets snowball Earth apart from all younger glacial episodes. *Geology*, *44*(12), pp.1019-1022.

Pavlov, A.A. and Kasting, J.F., 2002. Mass-independent fractionation of sulfur isotopes in Archean sediments: strong evidence for an anoxic Archean atmosphere. *Astrobiology*, *2*(1), pp.27-41.

Payne, J.L., McClain, C.R., Boyer, A.G., Brown, J.H., Finnegan, S., Kowalewski, M., Krause, R.A., Lyons, S.K., McShea, D.W., Novack-Gottshall, P.M. and Smith, F.A., 2011. The evolutionary consequences of oxygenic photosynthesis: a body size perspective. *Photosynthesis Research*, *107*(1), pp.37-57.

Paytan, A., Kastner, M., Campbell, D. and Thiemens, M.H., 1998. Sulfur isotopic composition of Cenozoic seawater sulfate. *Science*, *282*(5393), pp.1459-1462.

Paytan, A., Kastner, M., Campbell, D. and Thiemens, M.H., 2004. Seawater sulfur isotope fluctuations in the Cretaceous. *science*, *304*(5677), pp.1663-1665.

Pellerin, A., Bui, T.H., Rough, M., Mucci, A., Canfield, D.E. and Wing, B.A., 2015. Mass-dependent sulfur isotope fractionation during reoxidative sulfur cycling: A case study from Mangrove Lake, Bermuda. *Geochimica et Cosmochimica Acta*, *149*, pp.152-164.

Pellerin, A., Anderson-Trocmé, L., Whyte, L.G., Zane, G.M., Wall, J.D. and Wing, B.A., 2015. Sulfur isotope fractionation during the evolutionary adaptation of a sulfate-reducing bacterium. *Applied and environmental microbiology*, *81*(8), pp.2676-2689.

Peng, Y., Bao, H. and Yuan, X., 2009. New morphological observations for Paleoproterozoic acritarchs from the Chuanlinggou Formation, North China. *Precambrian Research*, *168*(3), pp.223-232.

Peng, Y., Bao, H., Zhou, C. and Yuan, X., 2011. 17 O-depleted barite from two Marinoan cap dolostone sections, south China. *Earth and Planetary Science Letters*, *305*(1), pp.21-31.

Peng, Y., Bao, H., Pratt, L.M., Kaufman, A.J., Jiang, G., Boyd, D., Wang, Q., Zhou, C., Yuan, X., Xiao, S. and Loyd, S., 2014. Widespread contamination of carbonate-associated sulfate by present-day secondary atmospheric sulfate: Evidence from triple oxygen isotopes. *Geology*, *42*(9), pp.815-818.

Pepkowitz, L. and Shirley, E., 1951. Microdetection of sulfur. *Analytical Chemistry*, *23*(11), pp.1709-1710.

Pereira, M.M., Santana, M. and Teixeira, M., 2001. A novel scenario for the evolution of haem–copper oxygen reductases. *Biochimica et Biophysica Acta (BBA)-Bioenergetics*, *1505*(2), pp.185-208.

Peryt, T.M., Hałas, S., Kovalevych, V.M., Petrychenko, Y. and Dzhinoridze, N.M., 2010. The sulphur and oxygen isotopic composition of Lower Cambrian anhydrites in East Siberia. *Geological Quarterly*, *49*(2), pp.235-242.

Petit, J.R., Jouzel, J., Raynaud, D., Barkov, N.I., Barnola, J.M., Basile, I., Bender, M., Chappellaz, J., Davis, M., Delaygue, G. and Delmotte, M., 1999. Climate and atmospheric history of the past 420,000 years from the Vostok ice core, Antarctica. *Nature*, *399*(6735), pp.429-436.

Philippot, P., Van Zuilen, M., Lepot, K., Thomazo, C., Farquhar, J. and Van Kranendonk, M.J., 2007. Early Archaean microorganisms preferred elemental sulfur, not sulfate. *Science*, *317*(5844), pp.1534-1537.

Pierre, C. and Rouchy, J.M., 1986. Oxygen and sulfur isotopes in anhydrites from Givetian and Visean evaporites of Northern France and Belgium. *Chemical Geology: Isotope Geoscience section*, *58*(3), pp.245-252

Planavsky, N.J., Cole, D.B., Reinhard, C.T., Diamond, C., Love, G.D., Luo, G., Zhang, Konhauser, K.O. and Lyons, T.W., 2016. Comment: No evidence for high atmospheric oxygen levels 1,400 million years ago. *Proceedings of the National Academy of Sciences*, *113*(19), pp.E2550-E2551.

Planavsky, N.J., Reinhard, C.T., Wang, X., Thomson, D., McGoldrick, P., Rainbird, R.H., Johnson, T., Fischer, W.W. and Lyons, T.W., 2014. Low Mid-Proterozoic atmospheric oxygen levels and the delayed rise of animals. *Science*, *346*(6209), pp.635-638.

Planavsky, N.J., McGoldrick, P., Scott, C.T., Li, C., Reinhard, C.T., Kelly, A.E., Chu, X., Bekker, A., Love, G.D. and Lyons, T.W., 2011. Widespread iron-rich conditions in the mid-Proterozoic ocean. *Nature*, *477*(7365), pp.448-451.

Planavsky, N.J., Bekker, A., Hofmann, A., Owens, J.D. and Lyons, T.W., 2012. Sulfur record of rising and falling marine oxygen and sulfate levels during the Lomagundi event. *Proceedings of the National Academy of Sciences*, *109*(45), pp.18300-18305.

Poulton, S.W., Fralick, P.W. and Canfield, D.E., 2010. Spatial variability in oceanic redox structure 1.8 billion years ago. *Nature Geoscience*, *3*(7), pp.486-490.

Prave, A.R., Condon, D.J., Hoffmann, K.H., Tapster, S. and Fallick, A.E., 2016. Duration and nature of the end-Cryogenian (Marinoan) glaciation. *Geology*, *44*(8), pp.631-634.

Preiss, W.V., 2000. The Adelaide Geosyncline of South Australia and its significance in Neoproterozoic continental reconstruction. *Precambrian Research*, *100*(1), pp.21-63.

Raab, M. and Spiro, B., 1991. Sulfur isotopic variations during seawater evaporation with fractional crystallization. *Chemical Geology: Isotope Geoscience section*, *86*(4), pp.323-333.

Rasmussen, B. and Buick, R., 1999. Redox state of the Archean atmosphere: evidence from detrital heavy minerals in ca. 3250–2750 Ma sandstones from the Pilbara Craton, Australia. *Geology*, *27*(2), pp.115-118.

Rasmussen, B., Bekker, A. and Fletcher, I.R., 2013. Correlation of Paleoproterozoic glaciations based on U–Pb zircon ages for tuff beds in the Transvaal and Huronian Supergroups. *Earth and Planetary Science Letters*, *382*, pp.173-180.

Rayner, N.M. and Rainbird, R.H., 2013. U-Pb Geochronology of the Shaler Supergroup, Victoria Island, Northwest Canada: 2009–2013. *Geological Survey of Canada Open File 7419*, p.62.

Reinhard, C.T., Planavsky, N.J. and Lyons, T.W., 2013. Long-term sedimentary recycling of rare sulphur isotope anomalies. *Nature*, *497*(7447), pp.100-103.

Reinhard, C.T., Planavsky, N.J., Robbins, L.J., Partin, C.A., Gill, B.C., Lalonde, S.V., Bekker, A., Konhauser, K.O. and Lyons, T.W., 2013. Proterozoic ocean redox and biogeochemical stasis. *Proceedings of the National Academy of Sciences*, *110*(14), pp.5357-5362.

Reinhard, C.T., Planavsky, N.J., Gill, B.C., Ozaki, K., Robbins, L.J., Lyons, T.W., Fischer, W.W., Wang, C., Cole, D.B. and Konhauser, K.O., 2016. Evolution of the global phosphorus cycle. *Nature*. 541 (7637), pp. 386-389.

Reuschel, M., Melezhik, V.A., Whitehouse, M.J., Lepland, A., Fallick, A.E. and Strauss, H., 2012. Isotopic evidence for a sizeable seawater sulfate reservoir at 2.1 Ga. *Precambrian Research*, *192*, pp.78-88.

Richter, F.M. and Turekian, K.K., 1993. Simple models for the geochemical response of the ocean to climatic and tectonic forcing. *Earth and Planetary Science Letters*, *119*(1), pp.121-131.

Rick, B., 1990. Sulphur and oxygen isotopic composition of Swiss Gipskeuper (Upper Triassic). *Chemical Geology: Isotope Geoscience section*, *80*(3), pp.243-250

Ries, J.B., Fike, D.A., Pratt, L.M., Lyons, T.W. and Grotzinger, J.P., 2009. Superheavy pyrite (δ34Spyr> δ34SCAS) in the terminal Proterozoic Nama Group, southern Namibia: A consequence of low seawater sulfate at the dawn of animal life. *Geology*, *37*(8), pp.743-746.

Robbins, L.J., Lalonde, S.V., Planavsky, N.J., Partin, C.A., Reinhard, C.T., Kendall, B., Scott, C., Hardisty, D.S., Gill, B.C., Alessi, D.S. and Dupont, C.L., 2016. Trace elements at the intersection of marine biological and geochemical evolution. *Earth-Science Reviews*, *163*, pp.323-348.

Rooney, A.D., Macdonald, F.A., Strauss, J.V., Dudás, F.Ö., Hallmann, C. and Selby, D., 2014. Re-Os geochronology and coupled Os-Sr isotope constraints on the Sturtian snowball Earth. *Proceedings of the National Academy of Sciences*, *111*(1), pp.51-56.

Rooney, A.D., Strauss, J.V., Brandon, A.D. and Macdonald, F.A., 2015. A Cryogenian chronology: Two long-lasting synchronous Neoproterozoic glaciations. *Geology*, *43*(5), pp.459-462.

Rosing, M.T., Bird, D.K., Sleep, N.H. and Bjerrum, C.J., 2010. No climate paradox under the faint early Sun. *Nature*, *464*(7289), pp.744-747.

Runnegar, B., 1991. Precambrian oxygen levels estimated from the biochemistry and physiology of early eukaryotes. *Global and Planetary Change*, *5*(1-2), pp.97-111.

Sánchez-Baracaldo, P., Ridgwell, A. and Raven, J.A., 2014. A neoproterozoic transition in the marine nitrogen cycle. *Current Biology*, *24*(6), pp.652-657.

Sahoo, S.K., Planavsky, N.J., Kendall, B., Wang, X., Shi, X., Scott, C., Anbar, A.D., Lyons, T.W. and Jiang, G., 2012. Ocean oxygenation in the wake of the Marinoan glaciation. *Nature*, *489*(7417), pp.546-549.

Sahoo, S.K., Planavsky, N.J., Jiang, G., Kendall, B., Owens, J.D., Wang, X., Shi, X., Anbar, A.D. and Lyons, T.W., 2016. Oceanic oxygenation events in the anoxic Ediacaran ocean. *Geobiology*, *14*(5), pp.457-468.

Sakai, H., 1972. Oxygen isotopic ratios of some evaporites from Precambrian to Recent ages. *Earth and Planetary Science Letters*, *15*(2), pp.201-205.

Sakai, H., 1971. Sulfur and oxygen isotopic study of barite concretions from banks in the Japan Sea off the Northeast Honshu, Japan. *Geochemical Journal*, *5*(2), pp.79-93.

Schidlowski, M. and Todt, W., 1998. The Proterozoic Lomagundi carbonate province as paragon of a13C-enriched carbonate facies: Geology, radiometric age and geochemical significance. *Chinese Science Bulletin*, *43*(1), pp.114-114.

Schmid, S., 2017, Neoproterozoic evaporites and their role in carbon isotope chemostratigraphy (Amadeus Basin, Australia). Precambrian Research, 290, 16-31.

Schröder, S., Bekker, A., Beukes, N.J., Strauss, H. and Van Niekerk, H.S., 2008. Rise in seawater sulphate concentration associated with the Paleoproterozoic positive carbon isotope excursion: evidence from sulphate evaporites in the~ 2.2–2.1 Gyr shallow‐marine Lucknow Formation, South Africa. *Terra Nova*, *20*(2), pp.108-117.

Schröder, S., Schreiber, B.C., Amthor, J.E. and Matter, A., 2003. A depositional model for the terminal Neoproterozoic–Early Cambrian Ara Group evaporites in south Oman. *Sedimentology*, *50*(5), pp.879-898.

Scott, C., Wing, B.A., Bekker, A., Planavsky, N.J., Medvedev, P., Bates, S.M., Yun, M. and Lyons, T.W., 2014. Pyrite multiple-sulfur isotope evidence for rapid expansion and contraction of the early Paleoproterozoic seawater sulfate reservoir. *Earth and Planetary Science Letters*, *389*, pp.95-104.

Selvaraja, V., Fiorentini, M.L., LaFlamme, C.K., Wing, B.A. and Bui, T.H., 2017. Anomalous sulfur isotopes trace volatile pathways in magmatic arcs. *Geology*, *45*(5), pp.419-422.

Shaheen, R., Janssen, C. and Röckmann, T., 2007. Investigations of the photochemical isotope equilibrium between O 2, CO 2 and O 3. *Atmospheric chemistry and physics*, *7*(2), pp.495-509.

Shields, G., Kimura, H., Yang, J. and Gammon, P., 2004. Sulphur isotopic evolution of Neoproterozoic-Cambrian seawater: new francolite-bound sulphate δ 34 S data and a critical appraisal of the existing record. *Chemical Geology*, *204*(1), pp.163-182

Sheldon, N.D., 2006. Precambrian paleosols and atmospheric CO 2 levels. *Precambrian Research*, *147*(1), pp.148-155.

Sheldon, N.D., 2013. Causes and consequences of low atmospheric pCO_2 in the Late Mesoproterozoic. *Chemical Geology*, *362*, pp.224-231.

Shen, Y., Farquhar, J., Masterson, A., Kaufman, A.J. and Buick, R., 2009. Evaluating the role of microbial sulfate reduction in the early Archean using quadruple isotope systematics. *Earth and Planetary Science Letters*, *279*(3), pp.383-391.

Shen, Y., Canfield, D.E. and Knoll, A.H., 2002. Middle Proterozoic ocean chemistry: evidence from the McArthur Basin, northern Australia. *American Journal of Science*, *302*(2), pp.81-109.

Shen, Y., Buick, R. and Canfield, D.E., 2001. Isotopic evidence for microbial sulphate reduction in the early Archaean era. *Nature*, *410*(6824), pp.77-81.

Sim, M.S., Bosak, T. and Ono, S., 2011. Large sulfur isotope fractionation does not require disproportionation. *Science*, *333*(6038), pp.74-77.

Sim, M.S., Ono, S. and Hurtgen, M.T., 2015. Sulfur isotope evidence for low and fluctuating sulfate levels in the Late Devonian ocean and the potential link with the mass extinction event. *Earth and Planetary Science Letters*, *419*, pp.52-62

Sleep, N.H. and Zahnle, K., 2001. Carbon dioxide cycling and implications for climate on ancient Earth. *Journal of Geophysical Research: Planets*, *106*(E1), pp.1373-1399.

Soo, R.M., Hemp, J., Parks, D.H., Fischer, W.W. and Hugenholtz, P., 2017. On the origins of oxygenic photosynthesis and aerobic respiration in Cyanobacteria. *Science*, *355*(6332), pp.1436-1440.

Sperling, E.A., Wolock, C.J., Morgan, A.S., Gill, B.C., Kunzmann, M., Halverson, G.P., Macdonald, F.A., Knoll, A.H. and Johnston, D.T., 2015. Statistical analysis of iron geochemical data suggests limited late Proterozoic oxygenation. *Nature*, *523*(7561), pp.451-454.

Stolper, D.A., Bender, M.L., Dreyfus, G.B., Yan, Y. and Higgins, J.A., 2016. A Pleistocene ice core record of atmospheric O2 concentrations. *Science*, *353*(6306), pp.1427-1430.

Strauss, H., 1999. Geological evolution from isotope proxy signals—sulfur. *Chemical Geology*, *161*(1), pp.89-101.

Strauss, H., 1993. The sulfur isotopic record of Precambrian sulfates: new data and a critical evaluation of the existing record. *Precambrian research*, *63*(3-4), pp.225-246.

Strauss, H., Banerjee, D.M. and Kumar, V., 2001. The sulfur isotopic composition of Neoproterozoic to early Cambrian seawater—evidence from the cyclic Hanseran evaporites, NW India. *Chemical Geology*, *175*(1), pp.17-28.

Strauss, H. and Schieber, J., 1990. A sulfur isotope study of pyrite genesis: the Mid-Proterozoic Newland Formation, Belt Supergroup, Montana. *Geochimica et Cosmochimica Acta*, *54*(1), pp.197-204.

Swanson-Hysell, N.L., Maloof, A.C., Condon, D.J., Jenkin, G.R.T., Alene, M., Tremblay, M.M., Tesema, T., Rooney, A.D., Haileab, B., 2015, Stratigraphy and geochronology of the Tambien Group, Ethiopia: Evidence for globally synchronous carbon isotope change in the Neoproterozoic. *Geology, 43(4)*, 323-326.

Tarhan, L.G., Droser, M.L., Planavsky, N.J. and Johnston, D.T., 2015. Protracted development of bioturbation through the early Palaeozoic Era. *Nature Geoscience*, *8*(11), pp.865-869.

Taylor, S.R. and McLennan, S.M., 1985. The continental crust: its composition and evolution.

Thamdrup, B.O., Finster, K., Hansen, J.W. and Bak, F., 1993. Bacterial disproportionation of elemental sulfur coupled to chemical reduction of iron or manganese. *Applied and environmental microbiology*, *59*(1), pp.101-108.

Thiemens, M.H. and Heidenreich, J.E., 1983. The mass-independent fractionation of oxygen: A novel isotope effect and its possible cosmochemical implications. *Science*, *219*(4588), pp.1073-1075.

Thiemens, M.H., 2006. History and applications of mass-independent isotope effects. *Annu. Rev. Earth Planet. Sci.*, *34*, pp.217-262.

Thode, H.G., Kleerekoper, H. and McElcheran, D., 1951. Isotope fractionation in the bacterial reduction of sulphate. *Research*, *4*(12), p.581.

Thode, H.G., Monster, J. and Dunford, H.B., 1958. Sulphur isotope abundances in petroleum and associated materials. *AAPG Bulletin*, *42*(11), pp.2619-2641.

Thode, H.G., Monster, J. and Dunford, H.B., 1961. Sulphur isotope geochemistry. *Geochimica et Cosmochimica Acta*, *25*(3), pp.159-174.

Thode, H.G. and Monster, J., 1965. Sulfur-isotope geochemistry of petroleum, evaporites, and ancient seas.

Thompson, C.K. and Kah, L.C., 2012. Sulfur isotope evidence for widespread euxinia and a fluctuating oxycline in Early to Middle Ordovician greenhouse oceans. *Palaeogeography, Palaeoclimatology, Palaeoecology*, *313*, pp.189-214.

Tostevin, R., Turchyn, A.V., Farquhar, J., Johnston, D.T., Eldridge, D.L., Bishop, J.K. and McIlvin, M., 2014. Multiple sulfur isotope constraints on the modern sulfur cycle. *Earth and planetary science letters*, *396*, pp.14-21.

Tostevin, R., He, T., Turchyn, A.V., Wood, R.A., Penny, A.M., Bowyer, F., Antler, G. and Shields, G.A., 2017. Constraints on the late Ediacaran sulfur cycle from carbonate associated sulfate. *Precambrian Research*, *290*, pp.113-125.

Turchyn, A.V. and Schrag, D.P., 2004. Oxygen isotope constraints on the sulfur cycle over the past 10 million years. *Science*, *303*(5666).

Turchyn, A.V. and Schrag, D.P., 2006. Cenozoic evolution of the sulfur cycle: insight from oxygen isotopes in marine sulfate. *Earth and Planetary Science Letters*, *241*(3), pp.763-779.

Turchyn, A.V., Schrag, D.P., Coccioni, R. and Montanari, A., 2009. Stable isotope analysis of the Cretaceous sulfur cycle. *Earth and Planetary Science Letters*, *285*(1), pp.115-123.

Turner, E.C. and Bekker, A., 2016. Thick sulfate evaporite accumulations marking a mid-Neoproterozoic oxygenation event (Ten Stone Formation, Northwest Territories, Canada). *Geological Society of America Bulletin*, *128*(1-2), pp.203-222.

Ueda, A., Campbell, F.A., Krouse, H.R. and Spencer, R.J., 1987. 34S/32S variations in trace sulphide and sulphate in carbonate rocks of a Devonian reef, Alberta, Canada, and the Precambrian Siyeh Formation, Montana, USA. *Chemical Geology: Isotope Geoscience section*, *65*(3-4), pp.383-390

Ueno, Y., Yamada, K., Yoshida, N., Maruyama, S. and Isozaki, Y., 2006. Evidence from fluid inclusions for microbial methanogenesis in the early Archaean era. *Nature*, *440*(7083), pp.516-519.

Ueno, Y., Ono, S., Rumble, D. and Maruyama, S., 2008. Quadruple sulfur isotope analysis of ca. 3.5 Ga Dresser Formation: New evidence for microbial sulfate reduction in the early Archean. *Geochimica et Cosmochimica Acta*, *72*(23), pp.5675-5691.

Utrilla, R., Pierre, C., Orti, F. and Pueyo, J.J., 1992. Oxygen and sulphur isotope compositions as indicators of the origin of Mesozoic and Cenozoic evaporites from Spain. *Chemical Geology*, *102*(1-4), pp.229-244.

van Acken, D., Thomson, D., Rainbird, R.H. and Creaser, R.A., 2013. Constraining the depositional history of the Neoproterozoic Shaler Supergroup, Amundsen Basin, NW Canada: Rhenium-osmium dating of black shales from the Wynniatt and Boot Inlet Formations. *Precambrian Research*, *236*, pp.124-131.

Van Stempvoort, D. R., and Krouse. H. R. (1994) Controls of δ18O in sulfate: review of experimental data and application to specific environments. *ACS Symp. Ser. 550,* 446-480

Vinogradov, V.I., Reimer, T.O., Leites, A.M. and Smelov, S.B., 1976. The oldest sulfates in the Archean Formations of the South African and the Aldan Shields, and the evolution of the Earth's oxygen atmosphere. Lithol. Mineral Resour., 11, p. 407–420.

Velikoslavinsky, S.D., Kotov, A.B., Salnikova, E.B., Glebovitsky, V.A., Kovach, V.P., Zagarnaya, N.Y., Belyaevsky, N.A., Yakovleva, S.Z. and Fedoseenko, A.M., 2003. The U–Pb age of the Fedorov Sequence of the Aldan granulite–gneiss megacomplex, the Aldan Shield. Dokl. Earth Sci., 393, 1151–1155.

von Paris, P., Rauer, H., Grenfell, J.L., Patzer, B., Hedelt, P., Stracke, B., Trautmann, T. and Schreier, F., 2008. Warming the early Earth—CO_2 reconsidered. *Planetary and Space Science*, *56*(9), pp.1244-1259.

Walker, R.N., 1977. Evidence of major sulphate evaporite deposits in the Proterozoic McArthur Group, Northern Territory, Australia. *Nature*, *265*, pp.526-529.

Walker, J.C., Hays, P.B. and Kasting, J.F., 1981. A negative feedback mechanism for the long‐term stabilization of Earth's surface temperature. *Journal of Geophysical Research: Oceans*, *86*(C10), pp.9776-9782.

Wen, J. and Thiemens, M.H., 1993. Multi‐isotope study of the O (1 D)+ CO_2 exchange and stratospheric consequences. *Journal of Geophysical Research: Atmospheres*, *98*(D7), pp.12801-12808.

Wing, B.A., 2013. A cold, hard look at ancient oxygen. *Proceedings of the National Academy of Sciences*, *110*(36), pp.14514-14515.

Wing, B.A. and Halevy, I., 2014. Intracellular metabolite levels shape sulfur isotope fractionation during microbial sulfate respiration. *Proceedings of the National Academy of Sciences*, *111*(51), pp.18116-18125.

Wolery, T.J. and Sleep, N.H., 1976. Hydrothermal circulation and geochemical flux at mid-ocean ridges. *The Journal of Geology*, *84*(3), pp.249-275.

Wolf, E.T. and Toon, O.B., 2014. Controls on the Archean climate system investigated with a global climate model. *Astrobiology*, *14*(3), pp.241-253.

Wood, J., 1973. Stratigraphy and depositional environments of upper Huronian rocks of the Rawhide Lake-Flack Lake area, Ontario. *Huronian stratigraphy and sedimentation*, *12*, pp.73-95.

Woodhead, J.D. and Hergt, J.M., 1997. Application of thedouble spike technique to Pb-isotope geochronology. *Chemical Geology*, *138*(3), pp.311-321.

Worden, R.H., Smalley, P.C. and Fallick, A.E., 1997. Sulfur cycle in buried evaporites. *Geology*, *25*(7), pp.643-646.

Wotte, T., Strauss, H., Fugmann, A. and Garbe-Schönberg, D., 2012. Paired δ 34 S data from carbonate-associated sulfate and chromium-reducible sulfur across the traditional Lower–Middle Cambrian boundary of W-Gondwana. *Geochimica et Cosmochimica Acta*, *85*, pp.228-253

Wu, N., Farquhar, J., Strauss, H., Kim, S.T. and Canfield, D.E., 2010. Evaluating the S-isotope fractionation associated with Phanerozoic pyrite burial. *Geochimica et Cosmochimica Acta*, *74*(7), pp.2053-2071.

Wu, N., Farquhar, J. and Strauss, H., 2014. δ 34 S and Δ 33 S records of Paleozoic seawater sulfate based on the analysis of carbonate associated sulfate. *Earth and Planetary Science Letters*, *399*, pp.44-51.

Wu, N., Farquhar, J. and Fike, D.A., 2015. Ediacaran sulfur cycle: Insights from sulfur isotope measurements (Δ 33 S and δ 34 S) on paired sulfate–pyrite in the Huqf Supergroup of Oman. *Geochimica et Cosmochimica Acta*, *164*, pp.352-364

Ying, J.F., Zhou, X.H., Su, B.X. and Tang, Y.J., 2011. Continental growth and secular evolution: Constraints from U-Pb ages and Hf isotope of detrital zircons in Proterozoic Jixian sedimentary section (1.8–0.8 Ga), North China Craton. *Precambrian Research*, *189*(3), pp.229-238.

Young, G.M., 1991. The geologic record of glaciation: relevance to the climatic history of Earth. *Geoscience Canada*, *18*(3).

Yung, Y.L., DeMore, W.B. and Pinto, J.P., 1991. Isotopic exchange between carbon dioxide and ozone via O (1D) in the stratosphere. *Geophysical Research Letters*, *18*(1), pp.13-16.

Yung, Y.L., Lee, A.Y., Irion, F.W., DeMore, W.B. and Wen, J., 1997. Carbon dioxide in the atmosphere: Isotopic exchange with ozone and its use as a tracer in the middle atmosphere. *Journal of Geophysical Research: Atmospheres*, *102*(D9), pp.10857-10866.

Zak, I., Sakai, H. and Kaplan, I.R., 1980. Factors controlling the 18O/16O and 34S/32S isotope ratios of ocean sulfates, evaporites and interstitial sulfates from modern deep sea sediments. *Isotope marine chemistry*, pp.339-373.

Zeebe, R.E., 2010. A new value for the stable oxygen isotope fractionation between dissolved sulfate ion and water. *Geochimica et Cosmochimica Acta*, *74*(3), pp.818-828.

Zerkle, A.L., Farquhar, J., Johnston, D.T., Cox, R.P. and Canfield, D.E., 2009. Fractionation of multiple sulfur isotopes during phototrophic oxidation of sulfide and elemental sulfur by a green sulfur bacterium. *Geochimica et Cosmochimica Acta*, *73*(2), pp.291-306.

Zerkle, A.L., Claire, M.W., Domagal-Goldman, S.D., Farquhar, J. and Poulton, S.W., 2012. A bistable organic-rich atmosphere on the Neoarchaean Earth. *Nature Geoscience*, *5*(5), pp.359-363.

Zhang, S., Wang, X., Wang, H., Hammarlund, E.U., Su, J., Wang, Y. and Canfield, D.E., 2017. The oxic degradation of sedimentary organic matter 1400 Ma constrains atmospheric oxygen levels. *Biogeosciences*, *14*(8), pp.2133-2149.

Zhang, S., Wang, X., Wang, H., Bjerrum, C.J., Hammarlund, E.U., Dahl, T.W. and Canfield, D.E., 2016. Reply to Planavsky et al.: Strong evidence for high atmospheric oxygen levels 1,400 million years ago. *Proceedings of the National Academy of Sciences*, *113*(19), pp.E2552-E2553.

Zolotarev, A.A., Efremov, G.M., Brotigam, B. and Ivanova, T.V., 1989. Isotopic composition of sulfur in sulfates of Seligdar apatite deposit (Central Aldan). Geokhimiya, 11, 1656–1659.

Supplementary Table

	Oxygen			Sulfur			
Age (Ma)	$\delta^{18}O$	$\Delta^{17}O$	$\delta^{34}S$	$\Delta^{33}S$	$\Delta^{36}S$	Lithology	Reference
0	2.9	-0.02	9.4	-0.02	-0.19	Gypsum	This Study: Crockford et al.,
0	9.0	-0.19	0.7	-0.01	-0.11	Gypsum	This Study: Crockford et al.,
0		-0.20	15.8	-0.02	0.28	Gypsum	This Study: Crockford et al.,
0	9.1	-0.06	18.6	0.04	-0.40	Gypsum	This Study: Crockford et al.,
0	9.6	-0.15	19.4	0.03	-0.32	Gypsum	This Study: Crockford et al.,
0	12.1	-0.09				Gypsum	This Study: Crockford et al.,
0	5.8	-0.17				Gypsum	This Study: Crockford et al.,
0	11.7	-0.35				Gypsum	This Study: Crockford et al.,
6	12.1	-0.11	23.7	0.03	-0.38	Gypsum	This Study: Crockford et al.,
14	-19.7	0.06	6.4			Terrestrial Sulfates	This Study: Crockford et al.,
14	-14.3	0.03	2.4			Terrestrial Sulfates	This Study: Crockford et al.,
14	-14.6	0.03	0.7			Terrestrial Sulfates	This Study: Crockford et al.,
14	-12.2	0.03	29.4			Terrestrial Sulfates	This Study: Crockford et al.,
14	-13.1	0.02	5.0			Terrestrial Sulfates	This Study: Crockford et al.,
14	-14.5	-0.02	-18.9			Terrestrial Sulfates	This Study: Crockford et al.,
545		-0.26	18.8	0.01	0.06	Gypsum	This Study: Crockford et al.,
545	11.4	-0.16	23.0	0.04	-0.39	Gypsum	This Study: Crockford et al.,
545	13.2	-0.25	22.6	0.02	-0.28	Gypsum	This Study: Crockford et al.,
545	14.0	-0.29	25.7	0.00	-0.19	Gypsum	This Study: Crockford et al.,
545	17.7	-0.24	17.9	0.01	-0.06	Gypsum	This Study: Crockford et al.,
560	9.7		45.0	0.02	-0.32	Gypsum	This Study: Crockford et al.,
560	8.7		44.8	0.02	-0.44	Gypsum	This Study: Crockford et al.,
560	10.1		45.7	0.02	-0.42	Gypsum	This Study: Crockford et al.,
560	8.7		45.5	0.01	-0.39	Gypsum	This Study: Crockford et al.,
560	8.7	-0.18	44.8	0.02	0.08	Gypsum	This Study: Crockford et al.,
560	9.1	-0.22	45.2	0.02	-0.31	Gypsum	This Study: Crockford et al.,
560	8.8	-0.15	45.2	0.03	-0.42	Gypsum	This Study: Crockford et al.,
560	9.8	-0.20	46.4	0.04	-0.36	Gypsum	This Study: Crockford et al.,
560	10.2	-0.13	45.2	0.02	-0.49	Gypsum	This Study: Crockford et al.,
580	16.6	-0.26				CAS	This Study: Crockford et al.,
580	22.7	-0.16				CAS	This Study: Crockford et al.,
635	24.6	-0.31				CAS	This Study: Crockford et al.,
635	13.6	-0.32				CAS	This Study: Crockford et al.,
635	15.2	-0.25				CAS	This Study: Crockford et al.,
635	19.7	-0.19				CAS	This Study: Crockford et al.,
635	12.9	-0.13				CAS	This Study: Crockford et al.,
750	21.0	-0.24	21.9	0.00	-0.22	Gypsum	This Study: Crockford et al.,
750	21.6	-0.19				Gypsum	This Study: Crockford et al.,
750	20.7	-0.23	20.9	0.00	-0.10	Gypsum	This Study: Crockford et al.,
750		-0.17				Gypsum	This Study: Crockford et al.,
750	17.5	-0.21	23.5	0.02	-0.23	Gypsum	This Study: Crockford et al.,
750	20.6	-0.26	24.0	0.02	-0.19	Gypsum	This Study: Crockford et al.,
750	19.7	-0.23	23.7	0.01	-0.19	Gypsum	This Study: Crockford et al.,
790	13.2	-0.22	29.5	0.02	-0.20	Gypsum	This Study: Crockford et al.,
790	12.1	-0.18	21.7	0.01	-0.27	Gypsum	This Study: Crockford et al.,
790	12.7	-0.22	28.9	0.02	-0.13	Gypsum	This Study: Crockford et al.,
790	12.0	-0.21	30.1			Gypsum	This Study: Crockford et al.,
790	14.8	-0.18	32.9			Gypsum	This Study: Crockford et al.,
790	22.3	-0.15	33.0			Gypsum	This Study: Crockford et al.,
790	13.6	-0.18	33.5	0.03	-0.20	Gypsum	This Study: Crockford et al.,
790	30.6	-0.19	29.1	0.01	-0.17	Gypsum	This Study: Crockford et al.,
790	10.8	-0.29	31.7			Gypsum	This Study: Crockford et al.,
790	15.3	-0.24	17.9	0.00	-0.17	Gypsum	This Study: Crockford et al.,
790	11.7	-0.25	20.0			Gypsum	This Study: Crockford et al.,
790	11.4	-0.28	25.0	-0.18	-1.75	Gypsum	This Study: Crockford et al.,
790	9.2	-0.31	18.4	0.01	-0.19	Gypsum	This Study: Crockford et al.,
790	11.8	-0.37	19.9	0.01	-0.19	Gypsum	This Study: Crockford et al.,
790	13.1	-0.33	21.7	0.01	0.20	Gypsum	This Study: Crockford et al.,
790	10.5	-0.28	18.7			Gypsum	This Study: Crockford et al.,
790	10.0	-0.19	17.9			Gypsum	This Study: Crockford et al.,
790	11.3	-0.30	31.9	0.01	-0.25	Gypsum	This Study: Crockford et al.,
795	11.2	-0.16	15.8	0.02	-0.36	Gypsum	This Study: Crockford et al.,
795	11.5	-0.15	16.2	0.02	-0.18	Gypsum	This Study: Crockford et al.,
795	11.6	0.01	16.6	0.02	-0.56	Gypsum	This Study: Crockford et al.,

795	12.2	-0.22	15.9	0.01	-0.18	Gypsum	This Study: Crockford et al.,
800		-0.09				CAS	This Study: Crockford et al.,
805	21.4					Gypsum	This Study: Crockford et al.,
805	22.4	-0.25	18.4	0.03	-0.23	Gypsum	This Study: Crockford et al.,
805	13.3	-0.22	19.7	0.03	-0.34	Gypsum	This Study: Crockford et al.,
805	22.3	-0.29	18.9	0.04	-0.12	Gypsum	This Study: Crockford et al.,
805	12.6	-0.22	19.1	0.03	-0.31	Gypsum	This Study: Crockford et al.,
805	23.3	-0.25	18.9	0.04	-0.19	Gypsum	This Study: Crockford et al.,
805	21.5	-0.19	18.6	0.02	0.18	Gypsum	This Study: Crockford et al.,
805	12.5	-0.22	18.8	0.02	-0.29	Gypsum	This Study: Crockford et al.,
805	25.9	-0.28	19.2	0.03	-0.28	Gypsum	This Study: Crockford et al.,
805	28.4	-0.24	19.5	0.04	-0.19	Gypsum	This Study: Crockford et al.,
805	14.5	-0.29	19.2	0.03	-0.35	Gypsum	This Study: Crockford et al.,
805	21.0	-0.25	20.1	0.02	-0.24	Gypsum	This Study: Crockford et al.,
805	22.0	-0.18	22.0	0.03	-0.34	Gypsum	This Study: Crockford et al.,
815	14.7	-0.16	17.8	0.03	-0.18	Gypsum	This Study: Crockford et al.,
815	14.8	-0.24	17.3	0.02	-0.25	Gypsum	This Study: Crockford et al.,
815						Gypsum	This Study: Crockford et al.,
815	17.3	-0.20				Gypsum	This Study: Crockford et al.,
815	16.4	-0.17				Gypsum	This Study: Crockford et al.,
815	13.7	-0.18				Gypsum	This Study: Crockford et al.,
815		-0.20				Gypsum	This Study: Crockford et al.,
815	14.9	-0.20	17.5	0.03	-0.26	Gypsum	This Study: Crockford et al.,
815	16.3	-0.18	16.9	0.02	-0.20	Gypsum	This Study: Crockford et al.,
815						Gypsum	This Study: Crockford et al.,
815	18.9	-0.18				Gypsum	This Study: Crockford et al.,
815		-0.26				Gypsum	This Study: Crockford et al.,
815	11.4	-0.17				Gypsum	This Study: Crockford et al.,
815	15.0	-0.18				Gypsum	This Study: Crockford et al.,
815	16.0	-0.19	19.4	0.02	-0.25	Gypsum	This Study: Crockford et al.,
815	14.7	-0.31				Gypsum	This Study: Crockford et al.,
815		-0.27				Gypsum	This Study: Crockford et al.,
815	17.0	-0.16	18.8	0.03	-0.23	Gypsum	This Study: Crockford et al.,
815	15.5					Gypsum	This Study: Crockford et al.,
815	15.5					Gypsum	This Study: Crockford et al.,
815	18.4	-0.15				Gypsum	This Study: Crockford et al.,
815	23.6	-0.28	19.5	0.03	-0.21	Gypsum	This Study: Crockford et al.,
815	14.2	-0.25				Gypsum	This Study: Crockford et al.,
815	14.5	-0.32	19.6	0.05	-0.38	Gypsum	This Study: Crockford et al.,
815	15.2	-0.42				Gypsum	This Study: Crockford et al.,
815	15.4	-0.28				Gypsum	This Study: Crockford et al.,
815		-0.22				Gypsum	This Study: Crockford et al.,
815	23.6	-0.32	20.1	0.02	-0.31	Gypsum	This Study: Crockford et al.,
815	13.9	-0.18				Gypsum	This Study: Crockford et al.,
815	15.1	-0.18				Gypsum	This Study: Crockford et al.,
815	28.9	-0.44	20.8	0.03	-0.31	Gypsum	This Study: Crockford et al.,
815	15.8	-0.16				Gypsum	This Study: Crockford et al.,
815	14.8	-0.18	17.4	0.04	-0.33	Gypsum	This Study: Crockford et al.,
815		-0.27				Gypsum	This Study: Crockford et al.,
815	15.4	-0.16				Gypsum	This Study: Crockford et al.,
815	15.0	-0.15				Gypsum	This Study: Crockford et al.,
815	14.8	-0.21	19.7	0.04	-0.36	Gypsum	This Study: Crockford et al.,
815	15.7	-0.14	18.3	0.01	0.21	Gypsum	This Study: Crockford et al.,
815	14.0	-0.17				Gypsum	This Study: Crockford et al.,
830	10.2	-0.23	15.1	0.00	-0.09	Gypsum	This Study: Crockford et al.,
830	10.1	-0.30	16.0	0.00	-0.22	Gypsum	This Study: Crockford et al.,
830	6.5	-0.32	15.1	0.00	0.46	Gypsum	This Study: Crockford et al.,
883	17.8	-0.39	17.5	0.02	-0.22	Gypsum	This Study: Crockford et al.,
883	10.1	-0.22	10.0	-0.01	-0.02	Gypsum	This Study: Crockford et al.,
883	8.8	-0.22	9.2	-0.02	-0.12	Gypsum	This Study: Crockford et al.,
883	9.2	-0.28	32.1	-0.03	0.52	Gypsum	This Study: Crockford et al.,
883	8.9	-0.29	17.6	-0.03	-0.11	Gypsum	This Study: Crockford et al.,
883	9.6	-0.24	16.0	0.01	-0.14	Gypsum	This Study: Crockford et al.,
883	11.9					Gypsum	This Study: Crockford et al.,
883	13.0	-0.31				Gypsum	This Study: Crockford et al.,
883	10.3	-0.44	18.1	0.01	-0.11	Gypsum	This Study: Crockford et al.,
883	9.5	-0.30				Gypsum	This Study: Crockford et al.,
883	11.1	-0.37	18.7	0.01	0.15	Gypsum	This Study: Crockford et al.,
883	11.9	-0.26	27.4	0.03	-0.23	Gypsum	This Study: Crockford et al.,
883	11.5	-0.20	27.6	0.01	-0.18	Gypsum	This Study: Crockford et al.,
883	10.2	-0.30	17.6	-0.01	-0.05	Gypsum	This Study: Crockford et al.,
883	10.4	-0.28				Gypsum	This Study: Crockford et al.,

883	10.9	-0.25	17.0	-0.01	0.00	Gypsum	This Study: Crockford et al.,
883		-0.34	17.4	0.00	-0.12	Gypsum	This Study: Crockford et al.,
883	10.5	-0.41	17.7	-0.02	0.04	Gypsum	This Study: Crockford et al.,
883		-0.34				Gypsum	This Study: Crockford et al.,
883	12.2	-0.07	18.8	-0.01	0.13	Gypsum	This Study: Crockford et al.,
883	20.4	-0.24				Gypsum	This Study: Crockford et al.,
883	22.8	-0.24	20.1	-0.01	-0.22	Gypsum	This Study: Crockford et al.,
883	15.9	-0.28	20.7	0.01	-0.13	Gypsum	This Study: Crockford et al.,
883	20.4	-0.17	21.4	0.01	-0.17	Gypsum	This Study: Crockford et al.,
883	18.8	-0.20				Gypsum	This Study: Crockford et al.,
883	18.0					Gypsum	This Study: Crockford et al.,
883	19.9	-0.19	21.2	-0.01	0.00	Gypsum	This Study: Crockford et al.,
883	13.7	-0.17				Gypsum	This Study: Crockford et al.,
883	19.9	-0.19				Gypsum	This Study: Crockford et al.,
890	15.5	-0.24	17.4	0.06	-0.07	Gypsum	This Study: Crockford et al.,
890	16.6	-0.23	17.2	0.03	-0.07	Gypsum	This Study: Crockford et al.,
890	14.8					Gypsum	This Study: Crockford et al.,
890	14.2		17.0	0.03	-0.06	Gypsum	This Study: Crockford et al.,
890	15.8	-0.23	17.0	0.02	0.02	Gypsum	This Study: Crockford et al.,
890	12.5	-0.20	17.5	0.03	0.03	Gypsum	This Study: Crockford et al.,
890	15.7	-0.20	19.4	0.01	-0.27	Gypsum	This Study: Crockford et al.,
890	15.6	-0.13	17.5	0.04	-0.04	Gypsum	This Study: Crockford et al.,
890	15.7	-0.18	17.5	0.00	-0.17	Gypsum	This Study: Crockford et al.,
890	10.8	-0.14	17.4	0.02	-0.34	Gypsum	This Study: Crockford et al.,
890	15.2	-0.23	16.7	0.01	0.04	Gypsum	This Study: Crockford et al.,
890	21.6	-0.31	17.1	0.01	-0.11	Gypsum	This Study: Crockford et al.,
890	25.0	-0.28	15.8	0.03	-0.22	Gypsum	This Study: Crockford et al.,
890	13.8	-0.18	17.4	0.03	-0.05	Gypsum	This Study: Crockford et al.,
890	12.0	-0.15	18.0	0.01	-0.14	Gypsum	This Study: Crockford et al.,
890	13.7	-0.16	17.7	0.03	-0.05	Gypsum	This Study: Crockford et al.,
890	13.4	-0.16	16.0	-0.01	-0.07	Gypsum	This Study: Crockford et al.,
890	13.4	-0.20	16.6	0.01	-0.09	Gypsum	This Study: Crockford et al.,
890	14.4	-0.23	18.2	0.02	-0.06	Gypsum	This Study: Crockford et al.,
1050		-0.26				Gypsum	This Study: Crockford et al.,
1050		-0.27	25.8	0.03	-0.32	Gypsum	This Study: Crockford et al.,
1050	15.8	-0.29	27.3	0.05	-0.43	Gypsum	This Study: Crockford et al.,
1050	11.9	-0.26	35.8	0.03	-0.35	Gypsum	This Study: Crockford et al.,
1050	15.4	-0.19	31.4	0.05	-0.36	Gypsum	This Study: Crockford et al.,
1050	13.4	-0.17	33.6	0.06	-0.42	Gypsum	This Study: Crockford et al.,
1050	14.9	-0.21	29.8	0.07	-0.43	Gypsum	This Study: Crockford et al.,
1050	12.5		33.7	0.03	-0.31	Gypsum	This Study: Crockford et al.,
1050	12.8	-0.18	28.2	-0.01	0.03	Gypsum	This Study: Crockford et al.,
1050	13.4	-0.26	23.9	0.02	-0.20	Gypsum	This Study: Crockford et al.,
1050	13.1	-0.22	29.8	0.07	-0.43	Gypsum	This Study: Crockford et al.,
1050	10.1	-0.27	26.1	0.04	-0.36	Gypsum	This Study: Crockford et al.,
1050	13.6	-0.20				Gypsum	This Study: Crockford et al.,
1050	12.9	-0.19				Gypsum	This Study: Crockford et al.,
1050	14.1	-0.21				Gypsum	This Study: Crockford et al.,
1050	14.0	-0.36	21.5	0.02	-0.11	Gypsum	This Study: Crockford et al.,
1050	12.6	-0.38	21.7	0.00	-0.12	Gypsum	This Study: Crockford et al.,
1050	12.6	-0.23	22.4	0.04	-0.27	Gypsum	This Study: Crockford et al.,
1050	15.7	-0.31	21.2	0.01	-0.20	Gypsum	This Study: Crockford et al.,
1050	14.4	-0.26	21.8	0.03	-0.29	Gypsum	This Study: Crockford et al.,
1050	11.1	-0.28	22.9	0.02	-0.24	Gypsum	This Study: Crockford et al.,
1050	10.6	-0.29	21.5	0.01	0.39	Gypsum	This Study: Crockford et al.,
1050	12.1		33.4	0.03	-0.34	Gypsum	This Study: Crockford et al.,
1050	15.1	-0.38	31.5	0.08	-0.42	Gypsum	This Study: Crockford et al.,
1050	12.5	-0.21				Gypsum	This Study: Crockford et al.,
1050	13.9	-0.29	26.0	0.03	0.54	Gypsum	This Study: Crockford et al.,
1050	12.9	-0.28	28.5	-0.01	-0.05	Gypsum	This Study: Crockford et al.,
1050	12.0	-0.24	33.9	0.05	-0.39	Gypsum	This Study: Crockford et al.,
1050	15.3	-0.27	28.3	0.07	-0.35	Gypsum	This Study: Crockford et al.,
1050	14.5	-0.26	28.6	0.05	-0.50	Gypsum	This Study: Crockford et al.,
1050	12.5	-0.21	22.4	0.01	-0.22	Gypsum	This Study: Crockford et al.,
1050	14.4	-0.21	26.8	0.05	-0.35	Gypsum	This Study: Crockford et al.,
1050	11.6	-0.17	33.7	0.04	-0.31	Gypsum	This Study: Crockford et al.,
1050	14.0	-0.23				Gypsum	This Study: Crockford et al.,
1050	12.7		36.4	0.03	-0.20	Gypsum	This Study: Crockford et al.,
1700	8.8	-0.67	25.7	-0.06	1.02	Gypsum	This Study: Crockford et al.,
1700	7.6	-0.76	25.5	-0.06	0.45	Gypsum	This Study: Crockford et al.,
1700	8.8	-0.64	26.7	-0.07	0.35	Gypsum	This Study: Crockford et al.,
1700	9.9	-0.57	26.8	-0.06	0.35	Gypsum	This Study: Crockford et al.,

1700	8.0	-0.67	26.7	-0.05	0.27	Gypsum	This Study: Crockford et al.,
1700	9.9	-0.60	27.5	-0.05	0.23	Gypsum	This Study: Crockford et al.,
1700	8.9	-0.72	27.1	-0.05	0.23	Gypsum	This Study: Crockford et al.,
1700	8.2	-0.74	27.4	-0.06	0.40	Gypsum	This Study: Crockford et al.,
1700	10.3	-0.54	26.4	-0.07	0.29	Gypsum	This Study: Crockford et al.,
1700		-0.56	28.7	-0.07	0.36	Gypsum	This Study: Crockford et al.,
1890	9.9	-0.33	21.6	-0.04	0.62	Gypsum	This Study: Crockford et al.,
1890	10.3	-0.34	23.3	-0.03	0.37	Gypsum	This Study: Crockford et al.,
1890		-0.33				Gypsum	This Study: Crockford et al.,
1890	13.0	-0.26	19.0	-0.06	0.43	Gypsum	This Study: Crockford et al.,
1890	9.2	-0.59	22.2	-0.08	0.60	Gypsum	This Study: Crockford et al.,
1890	9.9	-0.38				Gypsum	This Study: Crockford et al.,
1890	12.1	-0.22	22.1	-0.08	0.38	Gypsum	This Study: Crockford et al.,
2090	12.7	-0.16	5.4	0.00	0.19	Gypsum	This Study: Crockford et al.,
2090	13.3	-0.17	5.6	0.00	0.23	Gypsum	This Study: Crockford et al.,
2090	13.0	-0.23	5.2	0.00	-0.03	Gypsum	This Study: Crockford et al.,
2100	13.8	-0.17				Gypsum	This Study: Crockford et al.,
2100	20.7	-0.08	30.1	0.04	-0.21	Gypsum	This Study: Crockford et al.,
2100	10.8	-0.12	6.9	0.00	0.26	Gypsum	This Study: Crockford et al.,
2100	22.3	-0.18	32.3	0.02	-0.23	Gypsum	This Study: Crockford et al.,
2100	36.1	-0.06	26.9	0.01	-0.09	Gypsum	This Study: Crockford et al.,
2100		-0.32	25.3	0.01	0.14	Gypsum	This Study: Crockford et al.,
2150	17.7	-0.10	11.2	-0.03	-0.85	Gypsum	This Study: Crockford et al.,
2150	21.4	-0.19	10.2	0.00	-0.13	Gypsum	This Study: Crockford et al.,
2150	22.1	-0.27	11.8	0.01	0.05	Gypsum	This Study: Crockford et al.,
2150		-0.20				Gypsum	This Study: Crockford et al.,
2150		-0.25				Gypsum	This Study: Crockford et al.,
2150	35.1	-0.32	13.3	0.01	0.45	Gypsum	This Study: Crockford et al.,
2150	19.9	-0.18	16.8	-0.02	-0.88	Gypsum	This Study: Crockford et al.,
2150	19.9	-0.18	16.8	-0.01	-0.56	Gypsum	This Study: Crockford et al.,
2150	23.1	-0.25	18.9	0.04	0.41	Gypsum	This Study: Crockford et al.,
2150		-0.23	12.3	0.00	-0.30	Gypsum	This Study: Crockford et al.,
2150		-0.26				Gypsum	This Study: Crockford et al.,
2160	18.7	-0.14	11.7	0.01	-0.18	Gypsum	This Study: Crockford et al.,
2160		-0.14	27.1	0.05	-0.17	Gypsum	This Study: Crockford et al.,
2170	6.5					Gypsum	This Study: Crockford et al.,
2170		-0.24				Gypsum	This Study: Crockford et al.,
2260		-0.28				Gypsum	This Study: Crockford et al.,
2260	8.1	-0.14	9.2	0.04	-0.26	Gypsum	This Study: Crockford et al.,
2260	14.1	-0.13	5.3	0.04	-0.05	Gypsum	This Study: Crockford et al.,
2260	9.6	-0.13				Gypsum	This Study: Crockford et al.,
2260	13.3	-0.10	5.1	0.03	0.04	Gypsum	This Study: Crockford et al.,
2260	13.0	-0.23	5.6	0.06	0.38	Gypsum	This Study: Crockford et al.,
2260	13.1	-0.18	6.3	0.03	-0.15	Gypsum	This Study: Crockford et al.,
2308		-0.18				Gypsum	This Study: Crockford et al.,
2308	10.5	-0.20				Gypsum	This Study: Crockford et al.,
2308		-0.11	15.8	0.04	-0.13	Gypsum	This Study: Crockford et al.,
2308	9.3	-0.13				Gypsum	This Study: Crockford et al.,
2308			15.9	0.01	-0.16	Gypsum	This Study: Crockford et al.,
2308		-0.13				Gypsum	This Study: Crockford et al.,
2308		-0.13				Gypsum	This Study: Crockford et al.,
2308	9.2		15.1	0.02	0.28	Gypsum	This Study: Crockford et al.,
2308		-0.12				Gypsum	This Study: Crockford et al.,
2308		-0.14				Gypsum	This Study: Crockford et al.,
2308	11.8		15.8	0.04	-0.11	Gypsum	This Study: Crockford et al.,
2308		-0.11				Gypsum	This Study: Crockford et al.,
2308	9.3		15.9	0.02	-0.06	Gypsum	This Study: Crockford et al.,
2308		-0.30				Gypsum	This Study: Crockford et al.,
2308		-0.16				Gypsum	This Study: Crockford et al.,
2308	11.5	-0.10	16.0	0.04	-0.05	Gypsum	This Study: Crockford et al.,
2308	12.4	-0.18				Gypsum	This Study: Crockford et al.,
2308		-0.14				Gypsum	This Study: Crockford et al.,
2308	12.8	-0.27	15.3	0.03	0.50	Gypsum	This Study: Crockford et al.,
2308		-0.16				Gypsum	This Study: Crockford et al.,
2308			15.8	0.03	0.06	Gypsum	This Study: Crockford et al.,
2308	9.9	-0.32				Gypsum	This Study: Crockford et al.,
2308		-0.23	15.7	0.04	0.01	Gypsum	This Study: Crockford et al.,
2308			13.1	0.07	-0.13	Gypsum	This Study: Crockford et al.,
2308	11.1	-0.36	16.1	0.07	0.03	Gypsum	This Study: Crockford et al.,
2308		-0.34				Gypsum	This Study: Crockford et al.,
2308	19.1	-0.26	14.2	0.05	-0.14	Gypsum	This Study: Crockford et al.,
2308	10.5	-0.23	14.2	0.04	0.13	Gypsum	This Study: Crockford et al.,

2308	9.5	-0.20	13.8	0.04	0.25	Gypsum	This Study: Crockford et al.,
2308		-0.19				Gypsum	This Study: Crockford et al.,
2308	11.7	-0.27				Gypsum	This Study: Crockford et al.,
2308		-0.13	16.0	0.11	2.36	Gypsum	This Study: Crockford et al.,
2308	8.5	-0.17				Gypsum	This Study: Crockford et al.,
2308	8.8	-0.24				Gypsum	This Study: Crockford et al.,
2308		-0.15	14.0	0.03	-0.16	Gypsum	This Study: Crockford et al.,
2308	8.0	-0.25				Gypsum	This Study: Crockford et al.,
2350	8.0	-0.14	19.1	0.05	-0.21	Gypsum	This Study: Crockford et al.,
2350	7.8	-0.06	18.7	0.04	-0.23	Gypsum	This Study: Crockford et al.,
2350	6.0	-0.34	18.3	0.04	-0.25	Gypsum	This Study: Crockford et al.,
2350	8.4	-0.20	17.8	0.04	-0.20	Gypsum	This Study: Crockford et al.,
2350	8.6	-0.13	18.8	0.04	0.19	Gypsum	This Study: Crockford et al.,
2350	10.2	-0.06	17.8	0.03	-0.22	Gypsum	This Study: Crockford et al.,
2350	7.7	-0.08	18.2	0.07	-0.24	Gypsum	This Study: Crockford et al.,
2350	7.6	-0.09	16.9	0.05	-0.17	Gypsum	This Study: Crockford et al.,
2350	9.2	-0.12	18.7	0.05	-0.29	Gypsum	This Study: Crockford et al.,
2350	10.3	-0.15	19.9	0.06	-0.18	Gypsum	This Study: Crockford et al.,
2350	11.0	-0.15	19.8	0.05	-0.25	Gypsum	This Study: Crockford et al.,
2350	6.9	-0.10	18.8	0.05	-0.18	Gypsum	This Study: Crockford et al.,
2350	8.9	-0.11	18.4	0.05	-0.18	Gypsum	This Study: Crockford et al.,
2350			19.7	0.02	-0.24	Gypsum	This Study: Crockford et al.,
2350			14.4	0.04	-0.24	Gypsum	This Study: Crockford et al.,
2350			19.6	0.04	-0.19	Gypsum	This Study: Crockford et al.,
2350			17.5	0.06	-0.30	Gypsum	This Study: Crockford et al.,
2350			18.2	0.04	-0.27	Gypsum	This Study: Crockford et al.,
2350			19.9	0.04	-0.14	Gypsum	This Study: Crockford et al.,
2350			18.0	0.05	-0.31	Gypsum	This Study: Crockford et al.,
2350			18.2	0.02	-0.08	Gypsum	This Study: Crockford et al.,
2350			18.0	0.03	-0.25	Gypsum	This Study: Crockford et al.,
2350			16.0	0.07	-0.35	Gypsum	This Study: Crockford et al.,
2350			19.8	0.05	-0.23	Gypsum	This Study: Crockford et al.,
2350			16.4	0.08	-0.43	Gypsum	This Study: Crockford et al.,
2350			19.0	0.03	-0.11	Gypsum	This Study: Crockford et al.,
2350			17.4	0.08	-0.44	Gypsum	This Study: Crockford et al.,
2350			16.5	0.08	-0.32	Gypsum	This Study: Crockford et al.,
2350			13.6	0.05	-0.20	Gypsum	This Study: Crockford et al.,
760			8.5			CAS	Azmy et al., 2001
760			9.9			CAS	Azmy et al., 2001
780			10.8			CAS	Azmy et al., 2001
760			10.8			CAS	Azmy et al., 2001
760			11.9			CAS	Azmy et al., 2001
780			12.3			CAS	Azmy et al., 2001
760			13.1			CAS	Azmy et al., 2001
760			13.2			CAS	Azmy et al., 2001
800			14.2			CAS	Azmy et al., 2001
780			16.5			CAS	Azmy et al., 2001
800			16.9			CAS	Azmy et al., 2001
725			18.0			CAS	Azmy et al., 2001
725			21.3			CAS	Azmy et al., 2001
725			22.0			CAS	Azmy et al., 2001
0	9.0	-0.10				Seawater	Bao et al., 2008
0	9.2	-0.09				Seawater	Bao et al., 2008
0	8.9	-0.15				Seawater	Bao et al., 2008
36	11.2	-0.17				gypsum	Bao et al., 2008
245	10.6	-0.15				gypsum	Bao et al., 2008
251	17.6	-0.17				gypsum	Bao et al., 2008
251	18.0	-0.15				gypsum	Bao et al., 2008
251	16.8	-0.15				gypsum	Bao et al., 2008
251	17.8	-0.13				gypsum	Bao et al., 2008
251	14.4	-0.10				gypsum	Bao et al., 2008
251	17.0	-0.06				gypsum	Bao et al., 2008
257	7.7	-0.06				gypsum	Bao et al., 2008
257	6.9	-0.12				gypsum	Bao et al., 2008
257	8.0	-0.08				gypsum	Bao et al., 2008
257	8.0	-0.04				gypsum	Bao et al., 2008
260	9.8	-0.12				gypsum	Bao et al., 2008
260	10.6	-0.11				gypsum	Bao et al., 2008
260	13.0	-0.20				gypsum	Bao et al., 2008
261		-0.10				gypsum	Bao et al., 2008
265	9.3	-0.11				gypsum	Bao et al., 2008

265	11.8	-0.13	gypsum	Bao et al., 2008
265	10.0	-0.05	gypsum	Bao et al., 2008
265	10.8	-0.08	gypsum	Bao et al., 2008
270	8.9	-0.12	gypsum	Bao et al., 2008
270	6.9	-0.10	gypsum	Bao et al., 2008
270	8.7	-0.07	gypsum	Bao et al., 2008
270	12.2	-0.09	gypsum	Bao et al., 2008
280	12.1	-0.21	gypsum	Bao et al., 2008
280	13.1	-0.06	gypsum	Bao et al., 2008
280	11.8	-0.08	gypsum	Bao et al., 2008
280	12.6	-0.17	gypsum	Bao et al., 2008
307.5	10.5	-0.15	gypsum	Bao et al., 2008
307.5	11.0	-0.12	gypsum	Bao et al., 2008
307.5	12.5	-0.08	gypsum	Bao et al., 2008
307.5	14.5	-0.11	gypsum	Bao et al., 2008
310.7	13.2	-0.07	gypsum	Bao et al., 2008
310.7	12.2	-0.05	gypsum	Bao et al., 2008
315	15.0	-0.11	gypsum	Bao et al., 2008
315	16.9	-0.11	gypsum	Bao et al., 2008
315	12.0	-0.15	gypsum	Bao et al., 2008
315	12.4	-0.18	gypsum	Bao et al., 2008
315	15.7	-0.13	gypsum	Bao et al., 2008
345	11.3	-0.15	barite	Bao et al., 2008
345	13.7	-0.13	barite	Bao et al., 2008
492	24.1	-0.08	gypsum	Bao et al., 2008
527	18.5	-0.02	Barite	Bao et al., 2008
527	17.3	0.02	Barite	Bao et al., 2008
527	19.4	-0.13	Barite	Bao et al., 2008
527	18.5	-0.02	Barite	Bao et al., 2008
527	20.7	-0.07	Barite	Bao et al., 2008
527	19.1	-0.15	Barite	Bao et al., 2008
527	19.6	-0.25	Barite	Bao et al., 2008
527	16.0	-0.23	Barite	Bao et al., 2008
527	16.5	-0.22	Barite	Bao et al., 2008
527	19.5	-0.16	Barite	Bao et al., 2008
527	17.0	-0.27	Barite	Bao et al., 2008
527	18.6	-0.27	Barite	Bao et al., 2008
527	21.3	-0.29	Barite	Bao et al., 2008
528	12.1	-0.32	gypsum	Bao et al., 2008
528	14.2	-0.32	gypsum	Bao et al., 2008
530	11.9	-0.26	gypsum	Bao et al., 2008
530	12.4	-0.26	gypsum	Bao et al., 2008
533	13.1	-0.27	gypsum	Bao et al., 2008
536	15.7	-0.28	gypsum	Bao et al., 2008
540	7.6	-0.04	gypsum	Bao et al., 2008
540	15.7	-0.19	gypsum	Bao et al., 2008
543	17.2	-0.34	gypsum	Bao et al., 2008
543	18.4	-0.16	gypsum	Bao et al., 2008
543	14.9	-0.17	gypsum	Bao et al., 2008
543	16.8	-0.18	gypsum	Bao et al., 2008
543	21.5	-0.12	gypsum	Bao et al., 2008
543	20.1	-0.12	gypsum	Bao et al., 2008
543	15.4	-0.21	gypsum	Bao et al., 2008
543	9.3	-0.24	gypsum	Bao et al., 2008
635	18.4	-0.13	Barite	Bao et al., 2008
635	14.6	-0.43	Barite	Bao et al., 2008
635	12.1	-0.25	Barite	Bao et al., 2008
635	15.8	-0.23	Barite	Bao et al., 2008
635	16.6	-0.25	Barite	Bao et al., 2008
635	18.3	-0.51	Barite	Bao et al., 2008
635	18.4	-0.68	Barite	Bao et al., 2008
635	16.8	-0.24	Barite	Bao et al., 2008
635	17.8	-0.35	Barite	Bao et al., 2008
635	18.9	-0.54	Barite	Bao et al., 2008
635	18.0	-0.57	Barite	Bao et al., 2008
635	18.4	-0.54	Barite	Bao et al., 2008
635	18.2	-0.23	Barite	Bao et al., 2008
635	18.5	-0.40	Barite	Bao et al., 2008
635	16.3	-0.51	Barite	Bao et al., 2008
635	13.6	-0.57	Barite	Bao et al., 2008
635	14.7	-0.75	Barite	Bao et al., 2008
635	17.2	-0.39	Barite	Bao et al., 2008

635	13.8	-0.11		Barite	Bao et al., 2008
635	14.3	-0.16		Barite	Bao et al., 2008
795	10.2	-0.26		Gypsum	Bao et al., 2008
795	15.4	-0.22		Gypsum	Bao et al., 2008
795	12.1	-0.08		Gypsum	Bao et al., 2008
635	35.0	-0.06		CAS	Bao et al., 2009
635	32.9	-0.36	20.4	CAS	Bao et al., 2009
635	21.8	-0.57	24.8	CAS	Bao et al., 2009
635	20.7	-0.65	23.4	CAS	Bao et al., 2009
635	19.4	-0.54	24.4	CAS	Bao et al., 2009
635	21.2	-0.52	23.8	CAS	Bao et al., 2009
635	16.3	-0.19	18.4	CAS	Bao et al., 2009
635	14.1	-0.14	15.8	CAS	Bao et al., 2009
635	21.4	-0.53	24.7	CAS	Bao et al., 2009
635	32.7	-0.08	21.9	CAS	Bao et al., 2009
635	21.9	-0.51	25.1	CAS	Bao et al., 2009
635	19.9	-0.61	24.4	CAS	Bao et al., 2009
635	17.9	-0.23	23.4	CAS	Bao et al., 2009
635	19.9	-0.26	23.4	CAS	Bao et al., 2009
635	37.6	-0.04	22.5	CAS	Bao et al., 2009
635	16.8	-1.33	20.6	CAS	Bao et al., 2009
635	17.8	-0.93	21.4	CAS	Bao et al., 2009
635	17.8	-1.64	18.3	CAS	Bao et al., 2009
635	16.4	-0.12	28.2	CAS	Bao et al., 2009
635	15.0	-0.20	26.6	CAS	Bao et al., 2009
635	35.8	-0.12	21.6	CAS	Bao et al., 2009
635	34.1	-0.09	21.4	CAS	Bao et al., 2009
635	33.6	-0.10	22.3	CAS	Bao et al., 2009
635	35.8	-0.07	22.9	CAS	Bao et al., 2009
635	16.4	-1.55	17.3	CAS	Bao et al., 2009
635		-1.30		CAS	Bao et al., 2009
635	20.7	-0.44	22.1	CAS	Bao et al., 2012
635	19.6	-0.35	21.9	CAS	Bao et al., 2012
635	19.5	-0.47	22.5	CAS	Bao et al., 2012
635	18.0	-0.47	21.9	CAS	Bao et al., 2012
635	19.5	-0.46	21.9	CAS	Bao et al., 2012
635	19.8	-0.51	22.0	CAS	Bao et al., 2012
635	19.8	-0.49	22.6	CAS	Bao et al., 2012
635				CAS	Bao et al., 2012
635	19.7	-0.61	21.5	CAS	Bao et al., 2012
635	19.0	-0.58	21.2	CAS	Bao et al., 2012
635	18.6	-0.62	22.2	CAS	Bao et al., 2012
635	18.6	-0.63	21.2	CAS	Bao et al., 2012
635				CAS	Bao et al., 2012
635	19.5	-0.68	21.9	CAS	Bao et al., 2012
635	19.5	-0.56	21.8	CAS	Bao et al., 2012
635	19.9	-0.66	20.9	CAS	Bao et al., 2012
635	19.3	-0.62	21.3	CAS	Bao et al., 2012
635	19.3	-0.57	21.8	CAS	Bao et al., 2012
635	19.6	-0.15	21.1	CAS	Bao et al., 2012
635	17.1	-0.18	21.4	CAS	Bao et al., 2012
635	16.9	-0.01	22.0	CAS	Bao et al., 2012
635	17.5	-0.05	19.7	CAS	Bao et al., 2012
635	17.8	-0.26	20.8	CAS	Bao et al., 2012
635	18.1	-0.12	20.9	CAS	Bao et al., 2012
635	17.0	-0.09	21.5	CAS	Bao et al., 2012
635	23.6	-0.07	26.7	CAS	Bao et al., 2012
635	22.4	-0.15	23.3	CAS	Bao et al., 2012
635	23.2	-0.15	23.9	CAS	Bao et al., 2012
635	22.0	-0.16	23.7	CAS	Bao et al., 2012
635	22.7	-0.14	24.0	CAS	Bao et al., 2012
635	22.6	-0.09	24.3	CAS	Bao et al., 2012
635	22.4	-0.05	23.5	CAS	Bao et al., 2012
635	23.5		23.9	CAS	Bao et al., 2012
635	23.5	-0.07	24.1	CAS	Bao et al., 2012
635	22.3	-0.10	24.5	CAS	Bao et al., 2012
635	22.3	-0.09	25.3	CAS	Bao et al., 2012
635	23.1	-0.07	26.3	CAS	Bao et al., 2012
635	18.0	-0.52	21.6	CAS	Bao et al., 2012
635	19.3	-0.37	22.4	CAS	Bao et al., 2012
635	18.2	-0.44	22.1	CAS	Bao et al., 2012

635	18.5	-0.46	22.7	CAS	Bao et al., 2012
2310			15.1	Anhydrite	Cameron, 1983
2310			15.6	Anhydrite	Cameron, 1983
2310			12.4	Anhydrite	Cameron, 1983
2310			12.3	Anhydrite	Cameron, 1983
2310			13.3	Anhydrite	Cameron, 1983
4	14.1		18.3	Gypsum	Claypool et al., 1980
4	12.1		17.4	Gypsum	Claypool et al., 1980
4			20.5	Gypsum	Claypool et al., 1980
8	12.9		21.8	Gypsum	Claypool et al., 1980
8	10.8		21.9	Gypsum	Claypool et al., 1980
8	12.9		21.6	Gypsum	Claypool et al., 1980
15			22.6	Anhydrite	Claypool et al., 1980
15			22.9	Anhydrite	Claypool et al., 1980
15			22.9	Anhydrite	Claypool et al., 1980
15			21.7	Anhydrite	Claypool et al., 1980
45			10.9	Gypsum	Claypool et al., 1980
45			16.9	Anhydrite	Claypool et al., 1980
45			18.0	Gypsum	Claypool et al., 1980
23			25.5	Gypsum	Claypool et al., 1980
61			17.1	Gypsum	Claypool et al., 1980
61			19.3	Anhydrite	Claypool et al., 1980
80			20.0	Anhydrite	Claypool et al., 1980
50			17.8	Anhydrite	Claypool et al., 1980
90			18.3	Anhydrite	Claypool et al., 1980
56			17.5	Anhydrite	Claypool et al., 1980
75			15.5	Anhydrite	Claypool et al., 1980
91			17.0	Anhydrite	Claypool et al., 1980
91			16.3	Anhydrite	Claypool et al., 1980
97			16.0	Anhydrite	Claypool et al., 1980
56			17.7	Anhydrite	Claypool et al., 1980
100			17.7	Anhydrite	Claypool et al., 1980
45			18.0	Anhydrite	Claypool et al., 1980
66			16.5	Anhydrite	Claypool et al., 1980
56			16.5	Anhydrite	Claypool et al., 1980
97			13.7	Anhydrite	Claypool et al., 1980
113			13.9	Anhydrite	Claypool et al., 1980
113			14.1	Anhydrite	Claypool et al., 1980
44			19.9	Anhydrite	Claypool et al., 1980
97			14.1	Anhydrite	Claypool et al., 1980
97			13.3	Anhydrite	Claypool et al., 1980
113			13.9	Anhydrite	Claypool et al., 1980
113			18.6	Anhydrite	Claypool et al., 1980
113			14.2	Anhydrite	Claypool et al., 1980
106			16.0	Anhydrite	Claypool et al., 1980
106			15.9	Anhydrite	Claypool et al., 1980
106			14.0	Anhydrite	Claypool et al., 1980
106			14.0	Anhydrite	Claypool et al., 1980
97			16.2	Anhydrite	Claypool et al., 1980
106			14.7	Anhydrite	Claypool et al., 1980
106			14.0	Anhydrite	Claypool et al., 1980
106			12.8	Anhydrite	Claypool et al., 1980
106			16.1	Anhydrite	Claypool et al., 1980
106			14.7	Anhydrite	Claypool et al., 1980
97			14.1	Anhydrite	Claypool et al., 1980
113			14.6	Anhydrite	Claypool et al., 1980
106			15.2	Anhydrite	Claypool et al., 1980
106			14.4	Anhydrite	Claypool et al., 1980
106			14.7	Anhydrite	Claypool et al., 1980
106			13.9	Anhydrite	Claypool et al., 1980
106			16.4	Anhydrite	Claypool et al., 1980
137			16.3	Anhydrite	Claypool et al., 1980
137			15.1	Anhydrite	Claypool et al., 1980
137			18.1	Anhydrite	Claypool et al., 1980
137			18.1	Anhydrite	Claypool et al., 1980
105			16.1	Anhydrite	Claypool et al., 1980
105			16.4	Anhydrite	Claypool et al., 1980
105			16.7	Anhydrite	Claypool et al., 1980
105			17.1	Anhydrite	Claypool et al., 1980
105			16.3	Gypsum	Claypool et al., 1980
105			16.2	Gypsum	Claypool et al., 1980

91	15.4	18.5	Gypsum	Claypool et al., 1980
91	15.4	16.8	Gypsum	Claypool et al., 1980
106		14.5	Anhydrite	Claypool et al., 1980
106		14.1	Anhydrite	Claypool et al., 1980
106		14.9	Anhydrite	Claypool et al., 1980
106		15.1	Anhydrite	Claypool et al., 1980
145		16.0	Anhydrite	Claypool et al., 1980
152		16.7	Anhydrite	Claypool et al., 1980
161		17.5	Anhydrite	Claypool et al., 1980
161		15.4	Anhydrite	Claypool et al., 1980
161		17.1	Anhydrite	Claypool et al., 1980
161		15.8	Anhydrite	Claypool et al., 1980
161		17.5	Anhydrite	Claypool et al., 1980
161	14.3	16.6	Anhydrite	Claypool et al., 1980
161	12.8	16.2	Anhydrite	Claypool et al., 1980
174		17.0	Gypsum	Claypool et al., 1980
174		16.5	Gypsum	Claypool et al., 1980
174		15.5	Gypsum	Claypool et al., 1980
174		15.8	Gypsum	Claypool et al., 1980
174	10.0	16.1	Gypsum	Claypool et al., 1980
174	27.2	15.1	Gypsum	Claypool et al., 1980
174		16.7	Gypsum	Claypool et al., 1980
174		15.5	Gypsum	Claypool et al., 1980
174		15.6	Anhydrite	Claypool et al., 1980
200		14.3	Anhydrite	Claypool et al., 1980
200	11.9	14.8	Anhydrite	Claypool et al., 1980
200	12.5	14.3	Anhydrite	Claypool et al., 1980
200		13.7	Anhydrite	Claypool et al., 1980
200		13.4	Anhydrite	Claypool et al., 1980
200		14.0	Anhydrite	Claypool et al., 1980
200		13.7	Anhydrite	Claypool et al., 1980
200		13.7	Anhydrite	Claypool et al., 1980
200		15.7	Gypsum	Claypool et al., 1980
233		16.4	Anhydrite	Claypool et al., 1980
233	13.8	15.7	Gypsum	Claypool et al., 1980
233	13.1	17.2	Gypsum	Claypool et al., 1980
233		17.8	Gypsum	Claypool et al., 1980
233		17.4	Gypsum	Claypool et al., 1980
233	9.6	16.0	Gypsum	Claypool et al., 1980
233		16.5	Anhydrite	Claypool et al., 1980
233	13.1	17.2	Anhydrite	Claypool et al., 1980
233	13.8	15.7	Gypsum	Claypool et al., 1980
250		28.2	Gypsum	Claypool et al., 1980
250		28.3	Gypsum	Claypool et al., 1980
253	9.1	11.9	Anhydrite	Claypool et al., 1980
253	11.4	12.0	Anhydrite	Claypool et al., 1980
253	8.7	11.3	Anhydrite	Claypool et al., 1980
253	8.4	11.3	Anhydrite	Claypool et al., 1980
253	9.0	11.8	Anhydrite	Claypool et al., 1980
253	9.5	11.3	Anhydrite	Claypool et al., 1980
253	8.4	11.3	Anhydrite	Claypool et al., 1980
253	9.6	12.3	Anhydrite	Claypool et al., 1980
253	12.2	13.8	Anhydrite	Claypool et al., 1980
253	10.8	12.3	Anhydrite	Claypool et al., 1980
253		11.4	Anhydrite	Claypool et al., 1980
253	12.3	11.9	Anhydrite	Claypool et al., 1980
253	11.3	12.1	Anhydrite	Claypool et al., 1980
253		8.0	Anhydrite	Claypool et al., 1980
253	11.5	12.1	Anhydrite	Claypool et al., 1980
253		12.1	Anhydrite	Claypool et al., 1980
253		12.2	Anhydrite	Claypool et al., 1980
253		8.1	Anhydrite	Claypool et al., 1980
257		10.5	Gypsum	Claypool et al., 1980
257		11.0	Anhydrite	Claypool et al., 1980
257		13.1	Anhydrite	Claypool et al., 1980
257		11.5	Anhydrite	Claypool et al., 1980
257		12.2	Anhydrite	Claypool et al., 1980
257		12.7	Anhydrite	Claypool et al., 1980
257		13.4	Anhydrite	Claypool et al., 1980
257		12.0	Gypsum	Claypool et al., 1980
285		13.9	Anhydrite	Claypool et al., 1980
285		12.9	Anhydrite	Claypool et al., 1980

285		13.2	Anhydrite	Claypool et al., 1980
285		13.0	Anhydrite	Claypool et al., 1980
307		14.2	Anhydrite	Claypool et al., 1980
307		14.2	Anhydrite	Claypool et al., 1980
307		13.9	Anhydrite	Claypool et al., 1980
315		14.8	Anhydrite	Claypool et al., 1980
315		14.8	Anhydrite	Claypool et al., 1980
315		15.1	Anhydrite	Claypool et al., 1980
319		15.8	Anhydrite	Claypool et al., 1980
319		15.9	Anhydrite	Claypool et al., 1980
319		16.2	Anhydrite	Claypool et al., 1980
319		15.3	Anhydrite	Claypool et al., 1980
319		13.4	Anhydrite	Claypool et al., 1980
319		14.4	Anhydrite	Claypool et al., 1980
311		13.3	Anhydrite	Claypool et al., 1980
311		15.4	Anhydrite	Claypool et al., 1980
311		15.6	Anhydrite	Claypool et al., 1980
320		14.4	Anhydrite	Claypool et al., 1980
320		20.8	Anhydrite	Claypool et al., 1980
359	17.8	22.7	Anhydrite	Claypool et al., 1980
359	17.1	21.8	Anhydrite	Claypool et al., 1980
371		27.0	Anhydrite	Claypool et al., 1980
371		28.2	Anhydrite	Claypool et al., 1980
371		27.5	Anhydrite	Claypool et al., 1980
371		26.3	Anhydrite	Claypool et al., 1980
371		24.2	Anhydrite	Claypool et al., 1980
371		24.0	Anhydrite	Claypool et al., 1980
371		24.6	Anhydrite	Claypool et al., 1980
371		24.6	Anhydrite	Claypool et al., 1980
371	12.9	24.2	Anhydrite	Claypool et al., 1980
371	14.0	25.7	Anhydrite	Claypool et al., 1980
371		30.5	Anhydrite	Claypool et al., 1980
371		34.0	Anhydrite	Claypool et al., 1980
389		30.1	Anhydrite	Claypool et al., 1980
389	15.7	31.6	Anhydrite	Claypool et al., 1980
389		30.0	Anhydrite	Claypool et al., 1980
389	15.4	30.5	Anhydrite	Claypool et al., 1980
389		28.5	Anhydrite	Claypool et al., 1980
389		29.2	Anhydrite	Claypool et al., 1980
389		28.9	Anhydrite	Claypool et al., 1980
389	16.6	28.5	Anhydrite	Claypool et al., 1980
389		28.5	Anhydrite	Claypool et al., 1980
389		28.5	Anhydrite	Claypool et al., 1980
389	15.3	29.1	Anhydrite	Claypool et al., 1980
389		25.1	Anhydrite	Claypool et al., 1980
389		28.0	Anhydrite	Claypool et al., 1980
389		29.3	Anhydrite	Claypool et al., 1980
389	14.0	28.4	Anhydrite	Claypool et al., 1980
389		27.9	Anhydrite	Claypool et al., 1980
389		27.6	Anhydrite	Claypool et al., 1980
389	17.3	28.2	Anhydrite	Claypool et al., 1980
389		28.5	Anhydrite	Claypool et al., 1980
389		24.0	Anhydrite	Claypool et al., 1980
389		28.6	Anhydrite	Claypool et al., 1980
389		28.5	Anhydrite	Claypool et al., 1980
389		28.6	Anhydrite	Claypool et al., 1980
389		27.7	Anhydrite	Claypool et al., 1980
389		26.8	Anhydrite	Claypool et al., 1980
389		28.1	Anhydrite	Claypool et al., 1980
389		28.2	Anhydrite	Claypool et al., 1980
389		28.1	Anhydrite	Claypool et al., 1980
389		25.5	Anhydrite	Claypool et al., 1980
388		18.8	Anhydrite	Claypool et al., 1980
388	14.5	21.8	Anhydrite	Claypool et al., 1980
388	15.5	20.5	Anhydrite	Claypool et al., 1980
388	14.7	21.3	Anhydrite	Claypool et al., 1980
388	14.3	19.4	Anhydrite	Claypool et al., 1980
388		17.1	Anhydrite	Claypool et al., 1980
384		18.7	Gypsum	Claypool et al., 1980
384		18.5	Gypsum	Claypool et al., 1980
384		18.5	Gypsum	Claypool et al., 1980
388	13.0	18.0	Anhydrite	Claypool et al., 1980

388		18.3	Anhydrite	Claypool et al., 1980
388	12.5	19.3	Anhydrite	Claypool et al., 1980
388	14.6	19.3	Anhydrite	Claypool et al., 1980
388		19.0	Gypsum	Claypool et al., 1980
388		16.7	Gypsum	Claypool et al., 1980
388		16.5	Gypsum	Claypool et al., 1980
388		16.6	Gypsum	Claypool et al., 1980
388		15.7	Gypsum	Claypool et al., 1980
388		17.4	Gypsum	Claypool et al., 1980
388		16.6	Gypsum	Claypool et al., 1980
388		17.5	Gypsum	Claypool et al., 1980
408		24.6	Anhydrite	Claypool et al., 1980
408		21.0	Anhydrite	Claypool et al., 1980
408		18.6	Anhydrite	Claypool et al., 1980
408		19.2	Anhydrite	Claypool et al., 1980
408		19.9	Anhydrite	Claypool et al., 1980
408		18.7	Anhydrite	Claypool et al., 1980
391		17.0	Gypsum	Claypool et al., 1980
391		15.6	Gypsum	Claypool et al., 1980
391		15.9	Gypsum	Claypool et al., 1980
391		16.1	Gypsum	Claypool et al., 1980
464		22.6	Gypsum	Claypool et al., 1980
464		15.1	Gypsum	Claypool et al., 1980
464		28.0	Gypsum	Claypool et al., 1980
464		29.0	Gypsum	Claypool et al., 1980
464		25.6	Gypsum	Claypool et al., 1980
431		28.2	Gypsum	Claypool et al., 1980
525		28.4	Anhydrite	Claypool et al., 1980
525		28.6	Anhydrite	Claypool et al., 1980
525		27.4	Anhydrite	Claypool et al., 1980
525		26.7	Anhydrite	Claypool et al., 1980
525		29.7	Anhydrite	Claypool et al., 1980
525		31.5	Anhydrite	Claypool et al., 1980
525		33.3	Anhydrite	Claypool et al., 1980
525		29.4	Anhydrite	Claypool et al., 1980
525		30.1	Anhydrite	Claypool et al., 1980
521		27.6	Anhydrite	Claypool et al., 1980
521		33.8	Anhydrite	Claypool et al., 1980
521	12.0	30.8	Anhydrite	Claypool et al., 1980
521	12.2	30.8	Anhydrite	Claypool et al., 1980
521	10.7	30.8	Anhydrite	Claypool et al., 1980
525		26.4	Gypsum	Claypool et al., 1980
525		27.9	Gypsum	Claypool et al., 1980
525		28.6	Anhydrite	Claypool et al., 1980
525		29.4	Gypsum	Claypool et al., 1980
525		29.1	Gypsum	Claypool et al., 1980
525		29.2	Gypsum	Claypool et al., 1980
525		28.6	Anhydrite	Claypool et al., 1980
525		28.6	Gypsum	Claypool et al., 1980
525		31.3	Gypsum	Claypool et al., 1980
525		30.7	Anhydrite	Claypool et al., 1980
521		30.0	Gypsum	Claypool et al., 1980
521		29.0	Anhydrite	Claypool et al., 1980
521		32.4	Gypsum	Claypool et al., 1980
521		30.1	Gypsum	Claypool et al., 1980
521		29.1	Gypsum	Claypool et al., 1980
521		33.4	Gypsum	Claypool et al., 1980
521		33.7	Gypsum	Claypool et al., 1980
521	15.5	33.4	Anhydrite	Claypool et al., 1980
521	15.7	34.2	Anhydrite	Claypool et al., 1980
521	13.8	34.4	Anhydrite	Claypool et al., 1980
525		26.4	Gypsum	Claypool et al., 1980
525		29.2	Anhydrite	Claypool et al., 1980
525		27.6	Gypsum	Claypool et al., 1980
525		29.7	Gypsum	Claypool et al., 1980
525		28.8	Gypsum	Claypool et al., 1980
525		29.8	Gypsum	Claypool et al., 1980
525		28.8	Gypsum	Claypool et al., 1980
525		28.5	Gypsum	Claypool et al., 1980
525		28.9	Anhydrite	Claypool et al., 1980
525		28.6	Gypsum	Claypool et al., 1980
525		28.4	Gypsum	Claypool et al., 1980

525			28.9	Gypsum	Claypool et al., 1980
525			27.9	Gypsum	Claypool et al., 1980
525			27.0	Gypsum	Claypool et al., 1980
540			28.4	Gypsum	Claypool et al., 1980
540			35.5	Anhydrite	Claypool et al., 1980
540			31.7	Anhydrite	Claypool et al., 1980
540			33.0	Anhydrite	Claypool et al., 1980
540			34.1	Anhydrite	Claypool et al., 1980
540			32.4	Anhydrite	Claypool et al., 1980
540			30.7	Anhydrite	Claypool et al., 1980
540			31.4	Anhydrite	Claypool et al., 1980
540			32.4	Anhydrite	Claypool et al., 1980
540			35.0	Anhydrite	Claypool et al., 1980
540			33.1	Anhydrite	Claypool et al., 1980
540			33.6	Anhydrite	Claypool et al., 1980
540			33.0	Anhydrite	Claypool et al., 1980
540			26.8	Anhydrite	Claypool et al., 1980
540			32.0	Anhydrite	Claypool et al., 1980
890			15.9	Gypsum	Claypool et al., 1980
890			24.3	Gypsum	Claypool et al., 1980
890			23.4	Gypsum	Claypool et al., 1980
890			23.1	Gypsum	Claypool et al., 1980
890	15.9		16.4	Gypsum	Claypool et al., 1980
890			14.7	Gypsum	Claypool et al., 1980
890			15.1	Gypsum	Claypool et al., 1980
890			16.7	Gypsum	Claypool et al., 1980
890			17.2	Gypsum	Claypool et al., 1980
890			15.1	Gypsum	Claypool et al., 1980
890			16.4	Gypsum	Claypool et al., 1980
890			18.5	Gypsum	Claypool et al., 1980
890			18.0	Gypsum	Claypool et al., 1980
890			14.6	Gypsum	Claypool et al., 1980
820	14.2		21.0	Anhydrite	Claypool et al., 1980
820	14.9		20.9	Anhydrite	Claypool et al., 1980
820	18.8		20.5	Anhydrite	Claypool et al., 1980
820	18.9		19.9	Anhydrite	Claypool et al., 1980
820			15.8	Anhydrite	Claypool et al., 1980
820	24.4		17.1	Anhydrite	Claypool et al., 1980
820			16.7	Anhydrite	Claypool et al., 1980
820	10.0		17.2	Anhydrite	Claypool et al., 1980
258	12.0		10.9	Gypsum	Cortecci et al., 1981
258	10.8		9.3	Gypsum	Cortecci et al., 1981
258	12.2		10.2	Gypsum	Cortecci et al., 1981
258	15.2		12.1	Gypsum	Cortecci et al., 1981
258	17.9		13.8	Gypsum	Cortecci et al., 1981
258	15.3		12.0	Gypsum	Cortecci et al., 1981
258	15.1		12.2	Gypsum	Cortecci et al., 1981
258	16.1		11.7	Gypsum	Cortecci et al., 1981
249	14.2		26.5	Gypsum	Cortecci et al., 1981
249	16.1		27.1	Gypsum	Cortecci et al., 1981
249	15.6		26.9	Gypsum	Cortecci et al., 1981
248	11.8		16.9	Gypsum	Cortecci et al., 1981
248	12.7		17.2	Gypsum	Cortecci et al., 1981
243	14.2		25.4	Gypsum	Cortecci et al., 1981
243	13.7		24.7	Gypsum	Cortecci et al., 1981
220	12.7		16.8	Gypsum	Cortecci et al., 1981
220	12.9		16.5	Gypsum	Cortecci et al., 1981
220	16.0		17.4	Gypsum	Cortecci et al., 1981
220	15.4		16.9	Gypsum	Cortecci et al., 1981
220	13.4		16.5	Gypsum	Cortecci et al., 1981
220	15.9		16.9	Gypsum	Cortecci et al., 1981
220	18.4		15.8	Gypsum	Cortecci et al., 1981
220	17.0		16.0	Gypsum	Cortecci et al., 1981
220	15.6		16.1	Gypsum	Cortecci et al., 1981
208	11.2		15.4	Gypsum	Cortecci et al., 1981
208	10.6		15.0	Gypsum	Cortecci et al., 1981
208	16.7		17.4	Gypsum	Cortecci et al., 1981
208	18.1		17.0	Gypsum	Cortecci et al., 1981
208	12.2		16.0	Gypsum	Cortecci et al., 1981
208	13.1		16.0	Gypsum	Cortecci et al., 1981
6	11.2	-0.06		Gypsum	Cowie and Johnston, 2016

635	18.8	-0.84	26.7	-0.02	-0.22	Barite	Crockford et al., 2016
635	17.1	-0.77	29.9	-0.04	-0.24	Barite	Crockford et al., 2016
635		-0.02	30.8	-0.04	0.02	Barite	Crockford et al., 2016
635		-0.63	30.7	-0.03	-0.31	Barite	Crockford et al., 2016
635	18.3	-0.29	45.5	0.07	-1.44	Barite	Crockford et al., 2016
635	19.0	-0.14	43.0	0.09	-1.47	Barite	Crockford et al., 2016
635		-0.20	44.5	0.08	-1.20	Barite	Crockford et al., 2016
635			40.7	0.01	-0.91	Barite	Crockford et al., 2016
635	19.5	-0.45	42.0	0.03	-0.83	Barite	Crockford et al., 2016
635	19.8		38.0	0.00	-0.60	Barite	Crockford et al., 2016
635	19.3	-0.56	37.4	-0.02	-0.64	Barite	Crockford et al., 2016
635		-0.51				Barite	Crockford et al., 2016
1400	6.9	-0.62	6.2	-0.03	0.05	Gypsum	Crockford et al., in review
1400	8.8	-0.67	10.6	-0.04	0.05	Gypsum	Crockford et al., in review
1400	9.8	-0.53	12.3	-0.04	0.29	Gypsum	Crockford et al., in review
1400	1.0	-0.56	9.4	-0.04	0.03	Gypsum	Crockford et al., in review
1400	8.3	-0.63	12.4	-0.03	0.14	Gypsum	Crockford et al., in review
1400	10.9	-0.59	10.6	-0.04	0.07	Gypsum	Crockford et al., in review
1400	7.9	-0.61	11.6	-0.04	0.32	Gypsum	Crockford et al., in review
1400	10.9	-0.50	11.4	-0.05	0.11	Gypsum	Crockford et al., in review
1400	8.3	-0.53	11.6	-0.05	0.08	Gypsum	Crockford et al., in review
1400	8.4	-0.47	10.1	-0.05	0.03	Gypsum	Crockford et al., in review
1400	6.9	-0.88	8.9	-0.03	0.06	Gypsum	Crockford et al., in review
1400		-0.70				Gypsum	Crockford et al., in review
1400	6.0	-0.68	9.1	-0.04	0.05	Gypsum	Crockford et al., in review
1400		-0.66				Gypsum	Crockford et al., in review
1400	9.7	-0.58	12.0	-0.05	0.91	Gypsum	Crockford et al., in review
1400	10.8	-0.74	12.0	-0.04	0.11	Gypsum	Crockford et al., in review
1400		-0.75				Gypsum	Crockford et al., in review
1400	11.1	-0.59	12.0	-0.04	0.11	Gypsum	Crockford et al., in review
1400	7.6	-0.40	13.0	-0.04	0.12	Gypsum	Crockford et al., in review
1400	13.1	-0.64	12.1	-0.05	0.12	Gypsum	Crockford et al., in review
1400		-0.56				Gypsum	Crockford et al., in review
1400	9.6	-0.35	13.5	-0.04	0.15	Gypsum	Crockford et al., in review
1400	8.3	-0.67	9.8	-0.03	0.06	Gypsum	Crockford et al., in review
1400	10.9	-0.57	10.7	0.04	0.70	Gypsum	Crockford et al., in review
1400	13.3	-0.59	11.9	-0.05	0.17	Gypsum	Crockford et al., in review
1400	12.9	-0.51	9.3	-0.04	0.31	Gypsum	Crockford et al., in review
1400	3.3	-0.75	10.6	-0.04	0.36	Gypsum	Crockford et al., in review
1400	4.0	-0.85	11.4	-0.04	0.14	Gypsum	Crockford et al., in review
1400	2.9	-0.84	8.8	-0.04	0.05	Gypsum	Crockford et al., in review
1400	5.9	-0.74	5.3	-0.04	0.09	Gypsum	Crockford et al., in review
1400	9.8	-0.72	5.4	-0.03	0.16	Gypsum	Crockford et al., in review
1400	8.6	-0.79	12.4	-0.04	-0.30	Gypsum	Crockford et al., in review
1400	9.1	-0.76	12.2	-0.05	-0.29	Gypsum	Crockford et al., in review
1400	7.8	-0.65	11.9	-0.05	-0.32	Gypsum	Crockford et al., in review
1400	7.9	-0.62	10.8	-0.05	-0.18	Gypsum	Crockford et al., in review
1400	8.8	-0.66	11.2	-0.04	-0.24	Gypsum	Crockford et al., in review
1400	8.1	-0.62	10.5	-0.03	-0.32	Gypsum	Crockford et al., in review
1400	9.2	-0.61	9.9	9.56	11.05	Gypsum	Crockford et al., in review
1400	8.6	-1.02	10.4	-0.02	-0.28	Gypsum	Crockford et al., in review
1400	8.3	-0.95	-5.3	0.05	-0.93	Gypsum	Crockford et al., in review
1400	10.0	-0.61	8.3	10.36	9.42	Gypsum	Crockford et al., in review
1400	6.9	-0.60				Gypsum	Crockford et al., in review
1400	8.3	-0.53	9.9	-0.04	-0.26	Gypsum	Crockford et al., in review
1400	8.4	-0.60	9.9	-0.05	-0.29	Gypsum	Crockford et al., in review
1400	7.2	-0.55	9.6	-0.05	-0.14	Gypsum	Crockford et al., in review
1400	9.4	-0.58	11.8	-0.06	-0.28	Gypsum	Crockford et al., in review
1400	10.2	-0.56	9.7	-0.05	-0.17	Gypsum	Crockford et al., in review
1400	7.7	-0.77	5.3	-0.05	-0.26	Gypsum	Crockford et al., in review
1400						Gypsum	Crockford et al., in review
1400	6.5	-0.69				Gypsum	Crockford et al., in review
1400	6.9	-0.84	5.6	-0.05	-0.32	Gypsum	Crockford et al., in review
1400	9.1	-0.58	-9.4	0.05	-0.81	Gypsum	Crockford et al., in review
1400	8.0	-0.49	-9.0	0.07	-0.89	Gypsum	Crockford et al., in review
1400	7.3	-0.79				Gypsum	Crockford et al., in review
1400	6.6	-0.70				Gypsum	Crockford et al., in review
1400	8.5	-0.76	-8.3	0.06	-0.72	Gypsum	Crockford et al., in review
1400	6.8	-0.88	5.9	-0.02	-0.22	Gypsum	Crockford et al., in review
1400	6.8	-0.71				Gypsum	Crockford et al., in review
1400	6.6	-0.74				Gypsum	Crockford et al., in review

1400	6.6	-0.72				Gypsum	Crockford et al., in review
1400	7.0	-0.83				Gypsum	Crockford et al., in review
1400	7.0	-0.85				Gypsum	Crockford et al., in review
1400	8.1	-0.84				Gypsum	Crockford et al., in review
1400	8.4	-0.87	4.7	-0.03	-0.41	Gypsum	Crockford et al., in review
1400	8.4	-0.73				Gypsum	Crockford et al., in review
1400	8.9	-0.85	6.4	-0.04	-0.24	Gypsum	Crockford et al., in review
1400	8.8	-0.70				Gypsum	Crockford et al., in review
1400	7.7	-0.88	-8.0	0.04	-0.80	Gypsum	Crockford et al., in review
1400	6.5	-0.83				Gypsum	Crockford et al., in review
425			28.6			Halite	Das et al., 1990
425			27.0			Halite	Das et al., 1990
425			27.5			Halite	Das et al., 1990
425			27.6			Halite	Das et al., 1990
425			26.9			Halite	Das et al., 1990
425			27.4			Halite	Das et al., 1990
2100			17.6			barite	Deb et al., 1991
2100			17.9			barite	Deb et al., 1991
2100			19.7			barite	Deb et al., 1991
2100			28.9			barite	Deb et al., 1991
2100			18.8			barite	Deb et al., 1991
2100			21.2			barite	Deb et al., 1991
2100			17.1			barite	Deb et al., 1991
2100			20.0			barite	Deb et al., 1991
2100			19.3			barite	Deb et al., 1991
2100			18.6			barite	Deb et al., 1991
2100			18.4			barite	Deb et al., 1991
2100			18.3			barite	Deb et al., 1991
2100			19.4			barite	Deb et al., 1991
2100			18.0			barite	Deb et al., 1991
2100			18.8			barite	Deb et al., 1991
2100			18.2			barite	Deb et al., 1991
544			38.4			CAS	Fike and Grotzinger, 1998
544			39.0			CAS	Fike and Grotzinger, 1998
544			17.8			CAS	Fike and Grotzinger, 1998
544			39.7			CAS	Fike and Grotzinger, 1998
544			36.1			CAS	Fike and Grotzinger, 1998
544			36.2			CAS	Fike and Grotzinger, 1998
544			36.7			CAS	Fike and Grotzinger, 1998
544			35.0			CAS	Fike and Grotzinger, 1998
544			32.9			CAS	Fike and Grotzinger, 1998
544			33.1			CAS	Fike and Grotzinger, 1998
544			35.9			CAS	Fike and Grotzinger, 1998
544			39.3			CAS	Fike and Grotzinger, 1998
544			38.8			CAS	Fike and Grotzinger, 1998
544			16.6			CAS	Fike and Grotzinger, 1998
544			38.8			CAS	Fike and Grotzinger, 1998
544			38.5			CAS	Fike and Grotzinger, 1998
544			38.7			CAS	Fike and Grotzinger, 1998
544			38.9			CAS	Fike and Grotzinger, 1998
544			39.3			CAS	Fike and Grotzinger, 1998
544			38.9			CAS	Fike and Grotzinger, 1998
544			38.7			CAS	Fike and Grotzinger, 1998
544			39.3			CAS	Fike and Grotzinger, 1998
544			39.3			CAS	Fike and Grotzinger, 1998
544			39.7			CAS	Fike and Grotzinger, 1998
544			39.0			CAS	Fike and Grotzinger, 1998
544			39.6			CAS	Fike and Grotzinger, 1998
544			39.7			CAS	Fike and Grotzinger, 1998
544			39.2			CAS	Fike and Grotzinger, 1998
544			38.9			CAS	Fike and Grotzinger, 1998
544			39.4			CAS	Fike and Grotzinger, 1998
544			39.3			CAS	Fike and Grotzinger, 1998
544			39.8			CAS	Fike and Grotzinger, 1998
544			34.7			CAS	Fike and Grotzinger, 1998
544			40.4			CAS	Fike and Grotzinger, 1998
544			41.2			CAS	Fike and Grotzinger, 1998
544			40.9			CAS	Fike and Grotzinger, 1998
544			40.5			CAS	Fike and Grotzinger, 1998
544			41.1			CAS	Fike and Grotzinger, 1998
544			40.5			CAS	Fike and Grotzinger, 1998

544	40.3	CAS	Fike and Grotzinger, 1998
544	38.7	CAS	Fike and Grotzinger, 1998
544	36.9	CAS	Fike and Grotzinger, 1998
544	39.6	CAS	Fike and Grotzinger, 1998
544	37.9	CAS	Fike and Grotzinger, 1998
544	38.7	CAS	Fike and Grotzinger, 1998
544	40.8	CAS	Fike and Grotzinger, 1998
544	34.2	CAS	Fike and Grotzinger, 1998
544	40.6	CAS	Fike and Grotzinger, 1998
544	33.9	CAS	Fike and Grotzinger, 1998
544	37.8	CAS	Fike and Grotzinger, 1998
544	39.9	CAS	Fike and Grotzinger, 1998
544	10.9	CAS	Fike and Grotzinger, 1998
544	40.6	CAS	Fike and Grotzinger, 1998
544	37.1	CAS	Fike and Grotzinger, 1998
544	41.2	CAS	Fike and Grotzinger, 1998
544	41.4	CAS	Fike and Grotzinger, 1998
544	39.5	CAS	Fike and Grotzinger, 1998
544	42.5	CAS	Fike and Grotzinger, 1998
544	40.4	CAS	Fike and Grotzinger, 1998
544	41.2	CAS	Fike and Grotzinger, 1998
544	41.2	CAS	Fike and Grotzinger, 1998
544	40.1	CAS	Fike and Grotzinger, 1998
544	40.5	CAS	Fike and Grotzinger, 1998
544	29.3	CAS	Fike and Grotzinger, 1998
544	41.3	CAS	Fike and Grotzinger, 1998
544	40.6	CAS	Fike and Grotzinger, 1998
544	33.5	CAS	Fike and Grotzinger, 1998
544	39.1	CAS	Fike and Grotzinger, 1998
544	37.0	CAS	Fike and Grotzinger, 1998
544	36.7	CAS	Fike and Grotzinger, 1998
544	36.7	CAS	Fike and Grotzinger, 1998
544	36.7	CAS	Fike and Grotzinger, 1998
544	38.0	CAS	Fike and Grotzinger, 1998
544	37.0	CAS	Fike and Grotzinger, 1998
544	27.3	CAS	Fike and Grotzinger, 1998
544	31.8	CAS	Fike and Grotzinger, 1998
544	26.7	CAS	Fike and Grotzinger, 1998
544	30.2	CAS	Fike and Grotzinger, 1998
544	23.0	CAS	Fike and Grotzinger, 1998
544	24.1	CAS	Fike and Grotzinger, 1998
544	24.5	CAS	Fike and Grotzinger, 1998
544	25.3	CAS	Fike and Grotzinger, 1998
544	25.7	CAS	Fike and Grotzinger, 1998
544	23.8	CAS	Fike and Grotzinger, 1998
544	25.2	CAS	Fike and Grotzinger, 1998
544	23.7	CAS	Fike and Grotzinger, 1998
544	41.2	CAS	Fike and Grotzinger, 1998
544	39.6	CAS	Fike and Grotzinger, 1998
544	39.3	CAS	Fike and Grotzinger, 1998
544	39.2	CAS	Fike and Grotzinger, 1998
544	41.3	CAS	Fike and Grotzinger, 1998
544	29.7	CAS	Fike and Grotzinger, 1998
544	38.9	CAS	Fike and Grotzinger, 1998
544	38.2	CAS	Fike and Grotzinger, 1998
544	40.7	CAS	Fike and Grotzinger, 1998
544	40.0	CAS	Fike and Grotzinger, 1998
544	40.3	CAS	Fike and Grotzinger, 1998
544	41.1	CAS	Fike and Grotzinger, 1998
544	38.9	CAS	Fike and Grotzinger, 1998
544	39.6	CAS	Fike and Grotzinger, 1998
544	39.7	CAS	Fike and Grotzinger, 1998
544	39.0	CAS	Fike and Grotzinger, 1998
544	39.3	CAS	Fike and Grotzinger, 1998
544	39.7	CAS	Fike and Grotzinger, 1998
544	40.4	CAS	Fike and Grotzinger, 1998
544	38.7	CAS	Fike and Grotzinger, 1998
544	38.9	CAS	Fike and Grotzinger, 1998
544	38.9	CAS	Fike and Grotzinger, 1998
544	39.2	CAS	Fike and Grotzinger, 1998
544	38.9	CAS	Fike and Grotzinger, 1998
544	41.8	CAS	Fike and Grotzinger, 1998

544	39.2	CAS	Fike and Grotzinger, 1998
544	38.3	CAS	Fike and Grotzinger, 1998
544	39.5	CAS	Fike and Grotzinger, 1998
544	39.4	CAS	Fike and Grotzinger, 1998
544	41.8	CAS	Fike and Grotzinger, 1998
544	39.8	CAS	Fike and Grotzinger, 1998
544	42.4	CAS	Fike and Grotzinger, 1998
544	42.3	CAS	Fike and Grotzinger, 1998
544	41.3	CAS	Fike and Grotzinger, 1998
544	39.5	CAS	Fike and Grotzinger, 1998
544	40.2	CAS	Fike and Grotzinger, 1998
544	39.6	CAS	Fike and Grotzinger, 1998
544	40.7	CAS	Fike and Grotzinger, 1998
544	40.8	CAS	Fike and Grotzinger, 1998
544	39.6	CAS	Fike and Grotzinger, 1998
544	40.5	CAS	Fike and Grotzinger, 1998
544	44.3	CAS	Fike and Grotzinger, 1998
544	34.9	CAS	Fike and Grotzinger, 1998
544	37.9	CAS	Fike and Grotzinger, 1998
544	27.1	CAS	Fike and Grotzinger, 1998
544	18.3	CAS	Fike and Grotzinger, 1998
544	39.1	CAS	Fike and Grotzinger, 1998
544	38.4	CAS	Fike and Grotzinger, 1998
544	31.8	CAS	Fike and Grotzinger, 1998
544	33.7	CAS	Fike and Grotzinger, 1998
544	31.9	CAS	Fike and Grotzinger, 1998
544	38.1	CAS	Fike and Grotzinger, 1998
544	37.1	CAS	Fike and Grotzinger, 1998
544	27.8	CAS	Fike and Grotzinger, 1998
544	27.2	CAS	Fike and Grotzinger, 1998
544	31.7	CAS	Fike and Grotzinger, 1998
544	36.5	CAS	Fike and Grotzinger, 1998
544	33.0	CAS	Fike and Grotzinger, 1998
544	29.9	CAS	Fike and Grotzinger, 1998
544	8.0	CAS	Fike and Grotzinger, 1998
544	18.1	CAS	Fike and Grotzinger, 1998
544	27.1	CAS	Fike and Grotzinger, 1998
544	27.0	CAS	Fike and Grotzinger, 1998
544	14.8	CAS	Fike and Grotzinger, 1998
544	18.6	CAS	Fike and Grotzinger, 1998
544	23.3	CAS	Fike and Grotzinger, 1998
544	25.7	CAS	Fike and Grotzinger, 1998
544	13.9	CAS	Fike and Grotzinger, 1998
440	25.0	Gypsum	Fox and Videtich, 1997
440	25.0	Gypsum	Fox and Videtich, 1997
440	25.4	Gypsum	Fox and Videtich, 1997
440	25.9	Gypsum	Fox and Videtich, 1997
440	26.7	Gypsum	Fox and Videtich, 1997
440	25.7	Gypsum	Fox and Videtich, 1997
440	25.5	Gypsum	Fox and Videtich, 1997
440	25.1	Gypsum	Fox and Videtich, 1997
440	25.3	Gypsum	Fox and Videtich, 1997
440	25.4	Gypsum	Fox and Videtich, 1997
440	25.0	Gypsum	Fox and Videtich, 1997
440	25.0	Gypsum	Fox and Videtich, 1997
440	25.6	Gypsum	Gellatly and Lyons, 2005
1200	18.9	CAS	Gellatly and Lyons, 2005
1200	14.0	CAS	Gellatly and Lyons, 2005
1200	15.2	CAS	Gellatly and Lyons, 2005
1200	12.3	CAS	Gellatly and Lyons, 2005
1200	9.9	CAS	Gellatly and Lyons, 2005
1200	9.1	CAS	Gellatly and Lyons, 2005
1200	16.5	CAS	Gellatly and Lyons, 2005
1200	16.4	CAS	Gellatly and Lyons, 2005
1200	18.8	CAS	Gellatly and Lyons, 2005
1200	18.8	CAS	Gellatly and Lyons, 2005
1200	11.8	CAS	Gellatly and Lyons, 2005
1460	15.6	CAS	Gellatly and Lyons, 2005
1460	16.6	CAS	Gellatly and Lyons, 2005
1460	4.7	CAS	Gellatly and Lyons, 2005
1460	14.9	CAS	Gellatly and Lyons, 2005

1460	15.1	CAS	Gellatly and Lyons, 2005
1460	15.1	CAS	Gellatly and Lyons, 2005
1460	1.1	CAS	Gellatly and Lyons, 2005
1460	3.6	CAS	Gellatly and Lyons, 2005
1460	7.6	CAS	Gellatly and Lyons, 2005
1460	12.6	CAS	Gellatly and Lyons, 2005
1460	9.0	CAS	Gellatly and Lyons, 2005
1460	9.8	CAS	Gellatly and Lyons, 2005
1460	12.0	CAS	Gellatly and Lyons, 2005
1460	13.3	CAS	Gellatly and Lyons, 2005
1460	13.1	CAS	Gellatly and Lyons, 2005
1460	13.0	CAS	Gellatly and Lyons, 2005
1460	18.5	CAS	Gellatly and Lyons, 2005
1460	20.3	CAS	Gellatly and Lyons, 2005
1460	17.8	CAS	Gellatly and Lyons, 2005
1460	13.0	CAS	Gellatly and Lyons, 2005
1460	14.0	CAS	Gellatly and Lyons, 2005
1460	14.0	CAS	Gellatly and Lyons, 2005
1460	12.7	CAS	Gellatly and Lyons, 2005
1460	11.9	CAS	Gellatly and Lyons, 2005
1460	10.9	CAS	Gellatly and Lyons, 2005
1460	6.9	CAS	Gellatly and Lyons, 2005
1460	12.0	CAS	Gellatly and Lyons, 2005
1460	11.1	CAS	Gellatly and Lyons, 2005
1460	14.0	CAS	Gellatly and Lyons, 2005
1460	19.7	CAS	Gellatly and Lyons, 2005
1460	18.9	CAS	Gellatly and Lyons, 2005
1460	14.4	CAS	Gellatly and Lyons, 2005
1460	15.2	CAS	Gellatly and Lyons, 2005
1460	11.4	CAS	Gellatly and Lyons, 2005
1460	27.3	CAS	Gellatly and Lyons, 2005
1460	17.9	CAS	Gellatly and Lyons, 2005
1460	13.7	CAS	Gellatly and Lyons, 2005
1460	20.6	CAS	Gellatly and Lyons, 2005
1460	22.9	CAS	Gellatly and Lyons, 2005
1460	21.1	CAS	Gellatly and Lyons, 2005
1460	23.2	CAS	Gellatly and Lyons, 2005
1460	23.8	CAS	Gellatly and Lyons, 2005
1460	19.7	CAS	Gellatly and Lyons, 2005
1460	22.1	CAS	Gellatly and Lyons, 2005
1460	12.0	CAS	Gellatly and Lyons, 2005
1460	24.6	CAS	Gellatly and Lyons, 2005
1460	25.1	CAS	Gellatly and Lyons, 2005
1650	37.0	CAS	Gellatly and Lyons, 2005
1650	14.1	CAS	Gellatly and Lyons, 2005
1650	37.3	CAS	Gellatly and Lyons, 2005
1650	30.1	CAS	Gellatly and Lyons, 2005
1650	30.4	CAS	Gellatly and Lyons, 2005
1650	27.9	CAS	Gellatly and Lyons, 2005
1650	36.4	CAS	Gellatly and Lyons, 2005
1650	30.6	CAS	Gellatly and Lyons, 2005
1650	37.2	CAS	Gellatly and Lyons, 2005
1650	35.2	CAS	Gellatly and Lyons, 2005
1650	37.2	CAS	Gellatly and Lyons, 2005
1650	35.1	CAS	Gellatly and Lyons, 2005
1650	25.0	CAS	Gellatly and Lyons, 2005
1650	27.4	CAS	Gellatly and Lyons, 2005
1650	30.3	CAS	Gellatly and Lyons, 2005
1650	33.0	CAS	Gellatly and Lyons, 2005
1650	27.8	CAS	Gellatly and Lyons, 2005
1650	31.3	CAS	Gellatly and Lyons, 2005
1650	16.5	CAS	Gellatly and Lyons, 2005
1650	31.5	CAS	Gellatly and Lyons, 2005
1650	32.1	CAS	Gellatly and Lyons, 2005
1650	26.4	CAS	Gellatly and Lyons, 2005
1650	29.0	CAS	Gellatly and Lyons, 2005
500	35.6	CAS	Gill et al., 2007
500	34.5	CAS	Gill et al., 2007
500	35.1	CAS	Gill et al., 2007
500	36.9	CAS	Gill et al., 2007
500	36.5	CAS	Gill et al., 2007

500		39.7	CAS	Gill et al., 2007
500		37.3	CAS	Gill et al., 2007
500		45.7	CAS	Gill et al., 2007
500		26.7	CAS	Gill et al., 2007
500		33.3	CAS	Gill et al., 2007
500		32.6	CAS	Gill et al., 2007
500		29.1	CAS	Gill et al., 2007
500		32.0	CAS	Gill et al., 2007
500		26.8	CAS	Gill et al., 2007
500		21.2	CAS	Gill et al., 2007
478		24.0	CAS	Gill et al., 2007
478		22.5	CAS	Gill et al., 2007
478		19.7	CAS	Gill et al., 2007
478		26.3	CAS	Gill et al., 2007
478		24.8	CAS	Gill et al., 2007
478		28.6	CAS	Gill et al., 2007
478		27.0	CAS	Gill et al., 2007
478		27.0	CAS	Gill et al., 2007
478		26.2	CAS	Gill et al., 2007
478		27.1	CAS	Gill et al., 2007
478		26.7	CAS	Gill et al., 2007
478		24.0	CAS	Gill et al., 2007
478		22.5	CAS	Gill et al., 2007
478		26.8	CAS	Gill et al., 2007
478		25.1	CAS	Gill et al., 2007
478		27.1	CAS	Gill et al., 2007
478		26.2	CAS	Gill et al., 2007
478		26.3	CAS	Gill et al., 2007
419		22.3	CAS	Gill et al., 2007
419		22.4	CAS	Gill et al., 2007
419		18.2	CAS	Gill et al., 2007
419		21.9	CAS	Gill et al., 2007
419		24.7	CAS	Gill et al., 2007
419		16.8	CAS	Gill et al., 2007
419		25.2	CAS	Gill et al., 2007
419		11.0	CAS	Gill et al., 2007
419		22.5	CAS	Gill et al., 2007
419		27.0	CAS	Gill et al., 2007
419		23.9	CAS	Gill et al., 2007
419		24.0	CAS	Gill et al., 2007
419		23.3	CAS	Gill et al., 2007
419		20.5	CAS	Gill et al., 2007
419		21.2	CAS	Gill et al., 2007
419		19.0	CAS	Gill et al., 2007
419		20.8	CAS	Gill et al., 2007
419		28.0	CAS	Gill et al., 2007
419		27.2	CAS	Gill et al., 2007
419		29.0	CAS	Gill et al., 2007
419		26.9	CAS	Gill et al., 2007
419		26.1	CAS	Gill et al., 2007
419		29.4	CAS	Gill et al., 2007
419		29.4	CAS	Gill et al., 2007
419		28.7	CAS	Gill et al., 2007
419		28.1	CAS	Gill et al., 2007
419		27.0	CAS	Gill et al., 2007
419		28.0	CAS	Gill et al., 2007
419		27.3	CAS	Gill et al., 2007
419		28.5	CAS	Gill et al., 2007
419		28.5	CAS	Gill et al., 2007
419		29.8	CAS	Gill et al., 2007
419		28.5	CAS	Gill et al., 2007
419		27.4	CAS	Gill et al., 2007
419		25.7	CAS	Gill et al., 2007
340		16.9	CAS	Gill et al., 2007
340		17.5	CAS	Gill et al., 2007
340		19.2	CAS	Gill et al., 2007
340		16.8	CAS	Gill et al., 2007
340		19.6	CAS	Gill et al., 2007
340		19.7	CAS	Gill et al., 2007
600	15.4	32.9	CAS/Phosphorites	Goldberg et al., 2005
600	0.5	20.0	CAS/Phosphorites	Goldberg et al., 2005

600	2.3	16.7			CAS/Phosphorites	Goldberg et al., 2005
600		16.6			CAS/Phosphorites	Goldberg et al., 2005
600	9.4	14.8			CAS/Phosphorites	Goldberg et al., 2005
600	14.7	34.0			CAS/Phosphorites	Goldberg et al., 2005
600	11.7	42.2			CAS/Phosphorites	Goldberg et al., 2005
600	12.2	37.7			CAS/Phosphorites	Goldberg et al., 2005
600	13.9	42.0			CAS/Phosphorites	Goldberg et al., 2005
600	15.4	53.7			CAS/Phosphorites	Goldberg et al., 2005
600	13.8	41.1			CAS/Phosphorites	Goldberg et al., 2005
600	15.5	43.0			CAS/Phosphorites	Goldberg et al., 2005
600	17.1	54.3			CAS/Phosphorites	Goldberg et al., 2005
600	12.8	43.8			CAS/Phosphorites	Goldberg et al., 2005
600	15.0	39.3			CAS/Phosphorites	Goldberg et al., 2005
600	12.8	33.8			CAS/Phosphorites	Goldberg et al., 2005
600	13.1	30.9			CAS/Phosphorites	Goldberg et al., 2005
600	20.1	36.7			CAS/Phosphorites	Goldberg et al., 2005
600	7.1	35.7			CAS/Phosphorites	Goldberg et al., 2005
600	14.8	24.3			CAS/Phosphorites	Goldberg et al., 2005
600	14.7	25.9			CAS/Phosphorites	Goldberg et al., 2005
600	11.8	24.0			CAS/Phosphorites	Goldberg et al., 2005
600	16.3	34.1			CAS/Phosphorites	Goldberg et al., 2005
600	14.0	35.2			CAS/Phosphorites	Goldberg et al., 2005
600	25.1	31.9			CAS/Phosphorites	Goldberg et al., 2005
600	18.3	34.3			CAS/Phosphorites	Goldberg et al., 2005
600	14.7	32.5			CAS/Phosphorites	Goldberg et al., 2005
600	14.4	32.8			CAS/Phosphorites	Goldberg et al., 2005
600	12.6	33.8			CAS/Phosphorites	Goldberg et al., 2005
600	6.3	35.0			CAS/Phosphorites	Goldberg et al., 2005
600	12.9	36.2			CAS/Phosphorites	Goldberg et al., 2005
600	17.8	39.5			CAS/Phosphorites	Goldberg et al., 2005
600	17.0	38.4			CAS/Phosphorites	Goldberg et al., 2005
600	16.4	39.5			CAS/Phosphorites	Goldberg et al., 2005
600	13.8	33.2			CAS/Phosphorites	Goldberg et al., 2005
600	9.8	18.8			CAS/Phosphorites	Goldberg et al., 2005
2200		27.8			Barite	Grinenko et al., 1989
2200		34.2			Barite	Grinenko et al., 1989
2161		13.9	0.00	-0.31	CAS	Guo et al., 2009
2162		13.1	-0.01	-0.27	CAS	Guo et al., 2009
2166		13.0	-0.01	-0.21	CAS	Guo et al., 2009
2170		16.6	-0.16	-0.01	CAS	Guo et al., 2009
2171		16.8	-0.16	-0.11	CAS	Guo et al., 2009
2172		17.0	-0.16	-0.11	CAS	Guo et al., 2009
2173		15.6	-0.07	-0.38	CAS	Guo et al., 2009
2174		11.8	-0.06	-0.18	CAS	Guo et al., 2009
2200		19.7	0.00	0.16	CAS	Guo et al., 2009
2200		30.2	-0.05	0.08	CAS	Guo et al., 2009
2321		25.0	0.03	0.4	CAS	Guo et al., 2009
2322		16.4	0.03	0	CAS	Guo et al., 2009
2323		20.4	0.04	0.1	CAS	Guo et al., 2009
2325		16.1	0.03	0	CAS	Guo et al., 2009
2330		23.3	0.03	0.2	CAS	Guo et al., 2009
2330		24.7	0.00	0.26	CAS	Guo et al., 2009
2330		22.2	0.01	0.11	CAS	Guo et al., 2009
2330		18.5	0.02	0.05	CAS	Guo et al., 2009
2331		24.1	0.08	0.1	CAS	Guo et al., 2009
2338		27.7	0.04	0.3	CAS	Guo et al., 2009
2342		42.3	0.12	0.6	CAS	Guo et al., 2009
2344		28.3	0.09	0.3	CAS	Guo et al., 2009
2349		24.7	0.06	0.15	CAS	Guo et al., 2009
2349		27.6	0.14	0.3	CAS	Guo et al., 2009
2350		27.2	0.18	0.3	CAS	Guo et al., 2009
2382		6.2	0.20	0	CAS	Guo et al., 2009
2388		8.1	0.81	-0.92	CAS	Guo et al., 2009
2388		9.3	0.75	-0.7	CAS	Guo et al., 2009
2415		4.7	0.45	-0.64	CAS	Guo et al., 2009
2439		18.6	0.13	0.4	CAS	Guo et al., 2009
2525		10.5	1.04		CAS	Guo et al., 2009
2550		14.4	1.65	-1.2	CAS	Guo et al., 2009
2560		10.9	2.84	-2	CAS	Guo et al., 2009
6.25		21.8			gypsum	Holser and Kaplan, 1966
6.25		22.4			gypsum	Holser and Kaplan, 1966

6.25	23.9	gypsum	Holser and Kaplan, 1966
6.25	20.9	gypsum	Holser and Kaplan, 1966
6.25	21.1	gypsum	Holser and Kaplan, 1966
6.25	-1.1	gypsum	Holser and Kaplan, 1966
6.25	21.0	gypsum	Holser and Kaplan, 1966
6.25	21.8	gypsum	Holser and Kaplan, 1966
275	11.2	gypsum	Holser and Kaplan, 1966
275	10.8	gypsum	Holser and Kaplan, 1966
275	10.1	gypsum	Holser and Kaplan, 1966
275	10.3	gypsum	Holser and Kaplan, 1966
275	10.6	gypsum	Holser and Kaplan, 1966
275	9.0	gypsum	Holser and Kaplan, 1966
275	9.0	gypsum	Holser and Kaplan, 1966
275	10.7	gypsum	Holser and Kaplan, 1966
275	11.1	gypsum	Holser and Kaplan, 1966
275	9.4	gypsum	Holser and Kaplan, 1966
275	22.5	gypsum	Holser and Kaplan, 1966
275	9.7	gypsum	Holser and Kaplan, 1966
275	9.8	gypsum	Holser and Kaplan, 1966
275	10.3	gypsum	Holser and Kaplan, 1966
275	12.6	gypsum	Holser and Kaplan, 1966
275	11.9	gypsum	Holser and Kaplan, 1966
275	11.7	gypsum	Holser and Kaplan, 1966
275	11.3	gypsum	Holser and Kaplan, 1966
275	10.9	gypsum	Holser and Kaplan, 1966
275	11.5	gypsum	Holser and Kaplan, 1966
275	11.8	gypsum	Holser and Kaplan, 1966
275	12.8	gypsum	Holser and Kaplan, 1966
275	12.7	gypsum	Holser and Kaplan, 1966
275	9.1	gypsum	Holser and Kaplan, 1966
275	9.7	gypsum	Holser and Kaplan, 1966
275	10.5	gypsum	Holser and Kaplan, 1966
275	9.4	gypsum	Holser and Kaplan, 1966
275	10.4	gypsum	Holser and Kaplan, 1966
275	10.0	gypsum	Holser and Kaplan, 1966
275	10.3	gypsum	Holser and Kaplan, 1966
275	11.1	gypsum	Holser and Kaplan, 1966
275	12.4	gypsum	Holser and Kaplan, 1966
275	11.0	gypsum	Holser and Kaplan, 1966
275	11.2	gypsum	Holser and Kaplan, 1966
275	11.3	gypsum	Holser and Kaplan, 1966
275	10.8	gypsum	Holser and Kaplan, 1966
275	10.7	gypsum	Holser and Kaplan, 1966
275	10.5	gypsum	Holser and Kaplan, 1966
275	10.6	gypsum	Holser and Kaplan, 1966
275	10.7	gypsum	Holser and Kaplan, 1966
275	9.6	gypsum	Holser and Kaplan, 1966
275	8.3	gypsum	Holser and Kaplan, 1966
275	10.7	gypsum	Holser and Kaplan, 1966
275	10.5	gypsum	Holser and Kaplan, 1966
275	9.1	gypsum	Holser and Kaplan, 1966
275	9.4	gypsum	Holser and Kaplan, 1966
275	10.8	gypsum	Holser and Kaplan, 1966
275	10.8	gypsum	Holser and Kaplan, 1966
275	10.1	gypsum	Holser and Kaplan, 1966
275	10.0	gypsum	Holser and Kaplan, 1966
275	9.0	gypsum	Holser and Kaplan, 1966
275	9.2	gypsum	Holser and Kaplan, 1966
275	10.1	gypsum	Holser and Kaplan, 1966
275	9.4	gypsum	Holser and Kaplan, 1966
275	9.6	gypsum	Holser and Kaplan, 1966
275	10.6	gypsum	Holser and Kaplan, 1966
275	10.2	gypsum	Holser and Kaplan, 1966
275	10.0	gypsum	Holser and Kaplan, 1966
275	10.2	gypsum	Holser and Kaplan, 1966
28	16.3	gypsum	Holser and Kaplan, 1966
100	21.8	gypsum	Holser and Kaplan, 1966
100	13.4	gypsum	Holser and Kaplan, 1966
100	14.9	gypsum	Holser and Kaplan, 1966
100	16.2	gypsum	Holser and Kaplan, 1966
100	15.1	gypsum	Holser and Kaplan, 1966
100	14.9	gypsum	Holser and Kaplan, 1966

175	16.3	gypsum	Holser and Kaplan, 1966
175	16.5	gypsum	Holser and Kaplan, 1966
432	23.5	gypsum	Holser and Kaplan, 1966
432	26.3	gypsum	Holser and Kaplan, 1966
387	17.2	gypsum	Holser and Kaplan, 1966
387	15.8	gypsum	Holser and Kaplan, 1966
510	48.2	Francolite bound sulfate	Hough et al., 2006
510	47.3	Francolite bound sulfate	Hough et al., 2006
510	46.8	Francolite bound sulfate	Hough et al., 2006
510	45.5	Francolite bound sulfate	Hough et al., 2006
510	47.6	Francolite bound sulfate	Hough et al., 2006
510	46.1	Francolite bound sulfate	Hough et al., 2006
510	48.9	Francolite bound sulfate	Hough et al., 2006
510	49.2	Francolite bound sulfate	Hough et al., 2006
510	49.7	Francolite bound sulfate	Hough et al., 2006
510	48.8	Francolite bound sulfate	Hough et al., 2006
510	46.5	Francolite bound sulfate	Hough et al., 2006
510	50.7	Francolite bound sulfate	Hough et al., 2006
510	51.4	Francolite bound sulfate	Hough et al., 2006
510	51.2	Francolite bound sulfate	Hough et al., 2006
510	50.4	Francolite bound sulfate	Hough et al., 2006
510	51.9	Francolite bound sulfate	Hough et al., 2006
510	51.4	Francolite bound sulfate	Hough et al., 2006
510	52.8	Francolite bound sulfate	Hough et al., 2006
510	52.1	Francolite bound sulfate	Hough et al., 2006
510	53.3	Francolite bound sulfate	Hough et al., 2006
510	55.1	Francolite bound sulfate	Hough et al., 2006
510	56.1	Francolite bound sulfate	Hough et al., 2006
510	62.1	Francolite bound sulfate	Hough et al., 2006
510	44.0	Francolite bound sulfate	Hough et al., 2006
510	47.2	Francolite bound sulfate	Hough et al., 2006
510	45.8	Francolite bound sulfate	Hough et al., 2006
510	50.9	Francolite bound sulfate	Hough et al., 2006
510	50.9	Francolite bound sulfate	Hough et al., 2006
510	50.7	Francolite bound sulfate	Hough et al., 2006
510	44.5	Francolite bound sulfate	Hough et al., 2006
510	49.7	Francolite bound sulfate	Hough et al., 2006
510	46.5	Francolite bound sulfate	Hough et al., 2006
510	38.6	Francolite bound sulfate	Hough et al., 2006
510	40.8	Francolite bound sulfate	Hough et al., 2006
635	27.2	CAS	Hurtgen et al., 2002
635	22.9	CAS	Hurtgen et al., 2002
635	30.3	CAS	Hurtgen et al., 2002
635	28.6	CAS	Hurtgen et al., 2002
635	35.8	CAS	Hurtgen et al., 2002
635	23.1	CAS	Hurtgen et al., 2002
635	24.0	CAS	Hurtgen et al., 2002
635	28.2	CAS	Hurtgen et al., 2002
635	10.5	CAS	Hurtgen et al., 2002
635	25.5	CAS	Hurtgen et al., 2002
640	27.8	CAS	Hurtgen et al., 2002
640	19.4	CAS	Hurtgen et al., 2002
640	13.4	CAS	Hurtgen et al., 2002
640	14.1	CAS	Hurtgen et al., 2002
640	25.1	CAS	Hurtgen et al., 2002
640	15.1	CAS	Hurtgen et al., 2002
640	23.7	CAS	Hurtgen et al., 2002
640	25.1	CAS	Hurtgen et al., 2002
640	22.7	CAS	Hurtgen et al., 2002
640	16.0	CAS	Hurtgen et al., 2002
640	22.2	CAS	Hurtgen et al., 2002
640	22.0	CAS	Hurtgen et al., 2002
640	23.4	CAS	Hurtgen et al., 2002
640	23.1	CAS	Hurtgen et al., 2002
640	17.4	CAS	Hurtgen et al., 2002
640	22.8	CAS	Hurtgen et al., 2002
640	14.0	CAS	Hurtgen et al., 2002
640	13.9	CAS	Hurtgen et al., 2002
640	21.4	CAS	Hurtgen et al., 2002
645	33.9	CAS	Hurtgen et al., 2002
645	30.5	CAS	Hurtgen et al., 2002

658	34.6		CAS	Hurtgen et al., 2002
658	19.1		CAS	Hurtgen et al., 2002
658	15.6		CAS	Hurtgen et al., 2002
658	39.9		CAS	Hurtgen et al., 2002
658	42.3		CAS	Hurtgen et al., 2002
658	51.5		CAS	Hurtgen et al., 2002
658	18.7		CAS	Hurtgen et al., 2002
658	25.0		CAS	Hurtgen et al., 2002
658	12.4		CAS	Hurtgen et al., 2002
658	40.6		CAS	Hurtgen et al., 2002
658	40.9		CAS	Hurtgen et al., 2002
658	30.2		CAS	Hurtgen et al., 2002
658	36.8		CAS	Hurtgen et al., 2002
658	30.5		CAS	Hurtgen et al., 2002
658	31.6		CAS	Hurtgen et al., 2002
1150	11.0		CAS	Hurtgen et al., 2004
1150	11.7		CAS	Hurtgen et al., 2004
1150	12.4		CAS	Hurtgen et al., 2004
1150	13.4		CAS	Hurtgen et al., 2004
1150	13.9		CAS	Hurtgen et al., 2004
632	15.3		CAS	Hurtgen et al., 2004
1150	15.6		CAS	Hurtgen et al., 2004
1150	16.3		CAS	Hurtgen et al., 2004
780	16.3		CAS	Hurtgen et al., 2004
780	16.4		CAS	Hurtgen et al., 2004
900	16.4		CAS	Hurtgen et al., 2004
900	16.7		CAS	Hurtgen et al., 2004
780	18.5		CAS	Hurtgen et al., 2004
780	18.9		CAS	Hurtgen et al., 2004
780	19.0		CAS	Hurtgen et al., 2004
780	19.1		CAS	Hurtgen et al., 2004
900	19.5		CAS	Hurtgen et al., 2004
780	20.3		CAS	Hurtgen et al., 2004
632	20.7		CAS	Hurtgen et al., 2004
780	20.7		CAS	Hurtgen et al., 2004
780	21.4		CAS	Hurtgen et al., 2004
780	21.8		CAS	Hurtgen et al., 2004
780	21.9		CAS	Hurtgen et al., 2004
632	22.1		CAS	Hurtgen et al., 2004
1150	22.7		CAS	Hurtgen et al., 2004
780	22.8		CAS	Hurtgen et al., 2004
632	22.9		CAS	Hurtgen et al., 2004
632	23.1		CAS	Hurtgen et al., 2004
632	23.5		CAS	Hurtgen et al., 2004
632	23.8		CAS	Hurtgen et al., 2004
632	23.9		CAS	Hurtgen et al., 2004
780	25.5		CAS	Hurtgen et al., 2004
632	25.7		CAS	Hurtgen et al., 2004
632	27.3		CAS	Hurtgen et al., 2004
780	27.4		CAS	Hurtgen et al., 2004
632	27.8		CAS	Hurtgen et al., 2004
632	28.2		CAS	Hurtgen et al., 2004
632	28.8		CAS	Hurtgen et al., 2004
632	29.3		CAS	Hurtgen et al., 2004
632	31.5		CAS	Hurtgen et al., 2004
632	32.0		CAS	Hurtgen et al., 2004
510.7	35.6	0.02	CAS	Johnston et al., 2005
517.1	40.4	-0.03	CAS	Johnston et al., 2005
530	33.4	0.00	Gypsum	Johnston et al., 2005
530	31.7	0.00	Gypsum	Johnston et al., 2005
530	32.3	-0.01	Gypsum	Johnston et al., 2005
537	44.7	-0.03	CAS	Johnston et al., 2005
540	33.5	0.02	Gypsum	Johnston et al., 2005
556.5	35.1	-0.01	CAS	Johnston et al., 2005
559.8	39.1	0.01	CAS	Johnston et al., 2005
561.2	34.6	0.00	CAS	Johnston et al., 2005
571	33.2	-0.02	Gypsum	Johnston et al., 2005
571	31.5	0.00	Gypsum	Johnston et al., 2005
571	32.4	0.00	Gypsum	Johnston et al., 2005
571	33.5	-0.16	CAS	Johnston et al., 2005
571	31.1	0.01	CAS	Johnston et al., 2005

750	16.6	-0.01	Gypsum	Johnston et al., 2005
750	17.6	-0.01	Gypsum	Johnston et al., 2005
750	17.2	-0.01	Gypsum	Johnston et al., 2005
850	21.2	-0.01	Gypsum	Johnston et al., 2005
850	19.3	0.02	Gypsum	Johnston et al., 2005
850	21.6	0.02	Gypsum	Johnston et al., 2005
850	20.1	0.02	Gypsum	Johnston et al., 2005
850	23.4	0.00	CAS	Johnston et al., 2005
930	12.2	-0.03	CAS	Johnston et al., 2005
940	31.6	-0.03	CAS	Johnston et al., 2005
1050	32.9	0.03	CAS	Johnston et al., 2005
1050	29.8	0.06	CAS	Johnston et al., 2005
1050	34.7	0.04	CAS	Johnston et al., 2005
1050	34.8	0.06	CAS	Johnston et al., 2005
1050	26.7	0.04	CAS	Johnston et al., 2005
1050	28.6	0.04	CAS	Johnston et al., 2005
1050	32.5	0.02	CAS	Johnston et al., 2005
1200	22.3	-0.02	CAS	Johnston et al., 2005
1300	16.2	-0.05	CAS	Johnston et al., 2005
1300	31.0	0.00	CAS	Johnston et al., 2005
1300	21.6	0.01	CAS	Johnston et al., 2005
1300	28.9	-0.02	CAS	Johnston et al., 2005
1300	24.4	0.00	CAS	Johnston et al., 2005
1450	17.4	-0.07	CAS	Johnston et al., 2005
1450	9.7	-0.02	CAS	Johnston et al., 2005
1450	18.7	-0.05	CAS	Johnston et al., 2005
1450	13.1	-0.03	CAS	Johnston et al., 2005
1600	33.8	-0.09	CAS	Johnston et al., 2005
1658	33.4	0.01	CAS	Johnston et al., 2005
1658	39.1	0.01	CAS	Johnston et al., 2005
1658	33.0	0.01	CAS	Johnston et al., 2005
1658	17.4	0.00	CAS	Johnston et al., 2005
1680	31.6	-0.04	CAS	Johnston et al., 2005
2000	13.7	-0.04	CAS	Johnston et al., 2005
1300	30.6		CAS	Kah et al., 2004
1300	30.9		CAS	Kah et al., 2004
1300	28.4		CAS	Kah et al., 2004
1300	28.8		CAS	Kah et al., 2004
1300	29.2		CAS	Kah et al., 2004
1300	30.7		CAS	Kah et al., 2004
1300	31.1		CAS	Kah et al., 2004
1300	22.5		CAS	Kah et al., 2004
1300	20.1		CAS	Kah et al., 2004
1300	29.0		CAS	Kah et al., 2004
1300	26.4		CAS	Kah et al., 2004
1300	25.7		CAS	Kah et al., 2004
1300	19.3		CAS	Kah et al., 2004
1300	19.4		CAS	Kah et al., 2004
1300	17.3		CAS	Kah et al., 2004
1300	21.6		CAS	Kah et al., 2004
1300	33.2		CAS	Kah et al., 2004
1300	23.0		CAS	Kah et al., 2004
1300	23.1		CAS	Kah et al., 2004
1300	26.5		CAS	Kah et al., 2004
1300	17.5		CAS	Kah et al., 2004
1300	21.2		CAS	Kah et al., 2004
1050	25.2		CAS	Kah et al., 2004
1050	23.6		CAS	Kah et al., 2004
1050	27.0		CAS	Kah et al., 2004
1050	22.6		CAS	Kah et al., 2004
1050	25.2		CAS	Kah et al., 2004
1050	25.3		CAS	Kah et al., 2004
1050	28.6		CAS	Kah et al., 2004
1050	28.4		CAS	Kah et al., 2004
1050	28.4		CAS	Kah et al., 2004
1050	25.1		CAS	Kah et al., 2004
1050	26.1		CAS	Kah et al., 2004
1050	26.1		CAS	Kah et al., 2004
1050	31.2		CAS	Kah et al., 2004
1050	32.6		CAS	Kah et al., 2004
1050	32.7		CAS	Kah et al., 2004

1050	33.7	CAS	Kah et al., 2004
1050	32.8	CAS	Kah et al., 2004
1050	36.7	CAS	Kah et al., 2004
1050	37.8	CAS	Kah et al., 2004
1050	33.2	CAS	Kah et al., 2004
1050	30.6	CAS	Kah et al., 2004
1050	31.2	CAS	Kah et al., 2004
1050	31.3	CAS	Kah et al., 2004
1050	32.5	CAS	Kah et al., 2004
1050	34.3	CAS	Kah et al., 2004
1050	37.5	CAS	Kah et al., 2004
1050	29.1	CAS	Kah et al., 2004
1050	38.5	CAS	Kah et al., 2004
1050	31.7	CAS	Kah et al., 2004
1050	39.8	CAS	Kah et al., 2004
1050	35.7	CAS	Kah et al., 2004
1050	29.2	CAS	Kah et al., 2004
1050	30.5	CAS	Kah et al., 2004
1050	23.6	CAS	Kah et al., 2004
1050	24.0	CAS	Kah et al., 2004
1050	27.9	CAS	Kah et al., 2004
1050	28.5	CAS	Kah et al., 2004
1050	26.6	CAS	Kah et al., 2004
1050	27.2	CAS	Kah et al., 2004
1050	26.9	CAS	Kah et al., 2004
1050	20.1	CAS	Kah et al., 2004
1050	25.7	CAS	Kah et al., 2004
1050	25.6	CAS	Kah et al., 2004
1700	26.4	CAS	Kah et al., 2004
1700	32.1	CAS	Kah et al., 2004
1700	31.5	CAS	Kah et al., 2004
1700	16.5	CAS	Kah et al., 2004
1700	31.3	CAS	Kah et al., 2004
1700	27.8	CAS	Kah et al., 2004
1700	33.0	CAS	Kah et al., 2004
1700	30.3	CAS	Kah et al., 2004
1700	27.4	CAS	Kah et al., 2004
1700	25.0	CAS	Kah et al., 2004
1700	35.1	CAS	Kah et al., 2004
1700	37.2	CAS	Kah et al., 2004
1700	35.2	CAS	Kah et al., 2004
1700	37.2	CAS	Kah et al., 2004
1700	30.6	CAS	Kah et al., 2004
1700	36.4	CAS	Kah et al., 2004
1700	27.9	CAS	Kah et al., 2004
1700	30.4	CAS	Kah et al., 2004
1700	30.1	CAS	Kah et al., 2004
1700	37.3	CAS	Kah et al., 2004
1700	14.1	CAS	Kah et al., 2004
1700	37.0	CAS	Kah et al., 2004
1450	12.0	CAS	Kah et al., 2004
1450	6.9	CAS	Kah et al., 2004
1450	10.9	CAS	Kah et al., 2004
1450	11.9	CAS	Kah et al., 2004
1450	12.7	CAS	Kah et al., 2004
1450	14.0	CAS	Kah et al., 2004
1450	14.0	CAS	Kah et al., 2004
1450	13.0	CAS	Kah et al., 2004
1450	17.8	CAS	Kah et al., 2004
1450	20.3	CAS	Kah et al., 2004
1450	18.5	CAS	Kah et al., 2004
1450	13.0	CAS	Kah et al., 2004
1450	13.1	CAS	Kah et al., 2004
1450	13.3	CAS	Kah et al., 2004
1450	12.0	CAS	Kah et al., 2004
1450	9.8	CAS	Kah et al., 2004
1450	9.0	CAS	Kah et al., 2004
1450	12.6	CAS	Kah et al., 2004
1450	7.6	CAS	Kah et al., 2004
1450	3.6	CAS	Kah et al., 2004
1450	-1.1	CAS	Kah et al., 2004
1450	15.1	CAS	Kah et al., 2004

1450	15.1	CAS	Kah et al., 2004
1450	14.9	CAS	Kah et al., 2004
1450	4.7	CAS	Kah et al., 2004
1450	16.6	CAS	Kah et al., 2004
1450	15.6	CAS	Kah et al., 2004
447	16.3	CAS	Kah et al., 2016
447	17.0	CAS	Kah et al., 2016
447	11.5	CAS	Kah et al., 2016
447	12.8	CAS	Kah et al., 2016
447	16.4	CAS	Kah et al., 2016
447	17.6	CAS	Kah et al., 2016
447	13.5	CAS	Kah et al., 2016
447	15.8	CAS	Kah et al., 2016
447	16.2	CAS	Kah et al., 2016
447	13.0	CAS	Kah et al., 2016
447	14.0	CAS	Kah et al., 2016
447	14.7	CAS	Kah et al., 2016
447	14.2	CAS	Kah et al., 2016
447	16.0	CAS	Kah et al., 2016
447	11.7	CAS	Kah et al., 2016
447	11.5	CAS	Kah et al., 2016
447	21.3	CAS	Kah et al., 2016
447	21.7	CAS	Kah et al., 2016
447	24.0	CAS	Kah et al., 2016
447	17.4	CAS	Kah et al., 2016
447	13.0	CAS	Kah et al., 2016
447	9.9	CAS	Kah et al., 2016
447	8.8	CAS	Kah et al., 2016
447	11.3	CAS	Kah et al., 2016
447	7.2	CAS	Kah et al., 2016
447	7.0	CAS	Kah et al., 2016
447	-1.2	CAS	Kah et al., 2016
447	18.8	CAS	Kah et al., 2016
447	15.5	CAS	Kah et al., 2016
447	18.3	CAS	Kah et al., 2016
447	17.7	CAS	Kah et al., 2016
447	21.4	CAS	Kah et al., 2016
447	12.7	CAS	Kah et al., 2016
447	6.0	CAS	Kah et al., 2016
447	15.8	CAS	Kah et al., 2016
447	28.9	CAS	Kah et al., 2016
447	17.1	CAS	Kah et al., 2016
447	11.8	CAS	Kah et al., 2016
447	17.1	CAS	Kah et al., 2016
447	16.8	CAS	Kah et al., 2016
447	11.6	CAS	Kah et al., 2016
447	13.6	CAS	Kah et al., 2016
447	13.6	CAS	Kah et al., 2016
447	15.3	CAS	Kah et al., 2016
447	14.7	CAS	Kah et al., 2016
447	14.9	CAS	Kah et al., 2016
447	15.5	CAS	Kah et al., 2016
447	14.0	CAS	Kah et al., 2016
447	15.2	CAS	Kah et al., 2016
447	13.3	CAS	Kah et al., 2016
447	15.6	CAS	Kah et al., 2016
447	14.8	CAS	Kah et al., 2016
447	13.5	CAS	Kah et al., 2016
447	13.5	CAS	Kah et al., 2016
447	15.6	CAS	Kah et al., 2016
447	14.9	CAS	Kah et al., 2016
447	9.8	CAS	Kah et al., 2016
447	15.9	CAS	Kah et al., 2016
447	15.8	CAS	Kah et al., 2016
447	7.8	CAS	Kah et al., 2016
447	11.1	CAS	Kah et al., 2016
447	12.0	CAS	Kah et al., 2016
447	14.4	CAS	Kah et al., 2016
447	11.0	CAS	Kah et al., 2016
447	10.2	CAS	Kah et al., 2016
447	18.1	CAS	Kah et al., 2016

447	16.4	CAS	Kah et al., 2016
447	9.2	CAS	Kah et al., 2016
447	14.5	CAS	Kah et al., 2016
447	14.4	CAS	Kah et al., 2016
447	18.1	CAS	Kah et al., 2016
447	14.9	CAS	Kah et al., 2016
447	13.8	CAS	Kah et al., 2016
447	15.3	CAS	Kah et al., 2016
447	12.7	CAS	Kah et al., 2016
447	14.3	CAS	Kah et al., 2016
447	11.3	CAS	Kah et al., 2016
447	14.6	CAS	Kah et al., 2016
447	15.2	CAS	Kah et al., 2016
447	15.0	CAS	Kah et al., 2016
447	14.8	CAS	Kah et al., 2016
447	31.6	CAS	Kah et al., 2016
447	28.7	CAS	Kah et al., 2016
447	30.9	CAS	Kah et al., 2016
447	24.8	CAS	Kah et al., 2016
447	32.9	CAS	Kah et al., 2016
447	31.3	CAS	Kah et al., 2016
447	27.4	CAS	Kah et al., 2016
447	33.7	CAS	Kah et al., 2016
447	30.9	CAS	Kah et al., 2016
447	29.2	CAS	Kah et al., 2016
447	29.9	CAS	Kah et al., 2016
447	33.0	CAS	Kah et al., 2016
447	29.4	CAS	Kah et al., 2016
447	24.6	CAS	Kah et al., 2016
447	29.8	CAS	Kah et al., 2016
447	28.9	CAS	Kah et al., 2016
447	25.0	CAS	Kah et al., 2016
447	28.2	CAS	Kah et al., 2016
447	33.6	CAS	Kah et al., 2016
447	30.0	CAS	Kah et al., 2016
447	38.6	CAS	Kah et al., 2016
447	17.1	CAS	Kah et al., 2016
447	26.8	CAS	Kah et al., 2016
447	36.1	CAS	Kah et al., 2016
447	31.6	CAS	Kah et al., 2016
447	29.0	CAS	Kah et al., 2016
447	29.2	CAS	Kah et al., 2016
447	32.9	CAS	Kah et al., 2016
447	29.9	CAS	Kah et al., 2016
447	19.2	CAS	Kah et al., 2016
447	21.8	CAS	Kah et al., 2016
447	2.6	CAS	Kah et al., 2016
447	18.5	CAS	Kah et al., 2016
447	12.2	CAS	Kah et al., 2016
447	21.8	CAS	Kah et al., 2016
447	13.3	CAS	Kah et al., 2016
447	15.6	CAS	Kah et al., 2016
447	21.1	CAS	Kah et al., 2016
447	18.2	CAS	Kah et al., 2016
447	20.7	CAS	Kah et al., 2016
447	9.7	CAS	Kah et al., 2016
447	24.7	CAS	Kah et al., 2016
447	16.8	CAS	Kah et al., 2016
447	14.7	CAS	Kah et al., 2016
447	24.1	CAS	Kah et al., 2016
447	24.8	CAS	Kah et al., 2016
447	21.5	CAS	Kah et al., 2016
447	22.8	CAS	Kah et al., 2016
447	29.3	CAS	Kah et al., 2016
447	30.4	CAS	Kah et al., 2016
447	28.0	CAS	Kah et al., 2016
447	29.9	CAS	Kah et al., 2016
447	32.9	CAS	Kah et al., 2016
447	31.5	CAS	Kah et al., 2016
447	26.9	CAS	Kah et al., 2016
447	28.7	CAS	Kah et al., 2016
447	25.0	CAS	Kah et al., 2016

447	31.4	CAS	Kah et al., 2016
447	31.1	CAS	Kah et al., 2016
447	28.9	CAS	Kah et al., 2016
447	32.1	CAS	Kah et al., 2016
447	30.9	CAS	Kah et al., 2016
447	32.6	CAS	Kah et al., 2016
447	31.6	CAS	Kah et al., 2016
447	31.3	CAS	Kah et al., 2016
447	29.4	CAS	Kah et al., 2016
447	26.4	CAS	Kah et al., 2016
447	26.1	CAS	Kah et al., 2016
447	14.0	CAS	Kah et al., 2016
447	27.2	CAS	Kah et al., 2016
447	27.1	CAS	Kah et al., 2016
447	23.1	CAS	Kah et al., 2016
447	28.0	CAS	Kah et al., 2016
447	27.5	CAS	Kah et al., 2016
447	26.5	CAS	Kah et al., 2016
447	26.5	CAS	Kah et al., 2016
447	26.9	CAS	Kah et al., 2016
447	27.1	CAS	Kah et al., 2016
447	25.5	CAS	Kah et al., 2016
447	26.3	CAS	Kah et al., 2016
447	24.2	CAS	Kah et al., 2016
447	26.1	CAS	Kah et al., 2016
447	13.2	CAS	Kah et al., 2016
130	15.3	CAS	Kamschulte and Strauss, 2004
132	15.9	CAS	Kamschulte and Strauss, 2004
133	17.0	CAS	Kamschulte and Strauss, 2004
134	18.0	CAS	Kamschulte and Strauss, 2004
134	17.4	CAS	Kamschulte and Strauss, 2004
134	16.2	CAS	Kamschulte and Strauss, 2004
136	18.5	CAS	Kamschulte and Strauss, 2004
136	15.2	CAS	Kamschulte and Strauss, 2004
136	16.7	CAS	Kamschulte and Strauss, 2004
138	16.5	CAS	Kamschulte and Strauss, 2004
139	16.1	CAS	Kamschulte and Strauss, 2004
140	25.0	CAS	Kamschulte and Strauss, 2004
140	21.8	CAS	Kamschulte and Strauss, 2004
140	14.8	CAS	Kamschulte and Strauss, 2004
142	13.3	CAS	Kamschulte and Strauss, 2004
144	12.7	CAS	Kamschulte and Strauss, 2004
154	16.1	CAS	Kamschulte and Strauss, 2004
157	15.3	CAS	Kamschulte and Strauss, 2004
161	16.6	CAS	Kamschulte and Strauss, 2004
161	15.8	CAS	Kamschulte and Strauss, 2004
164	17.5	CAS	Kamschulte and Strauss, 2004
167	20.7	CAS	Kamschulte and Strauss, 2004
170	18.5	CAS	Kamschulte and Strauss, 2004
173	18.1	CAS	Kamschulte and Strauss, 2004
178	18.0	CAS	Kamschulte and Strauss, 2004
184	23.6	CAS	Kamschulte and Strauss, 2004
187	17.4	CAS	Kamschulte and Strauss, 2004
197	14.3	CAS	Kamschulte and Strauss, 2004
208	24.4	CAS	Kamschulte and Strauss, 2004
210	18.5	CAS	Kamschulte and Strauss, 2004
211	18.0	CAS	Kamschulte and Strauss, 2004
214	19.0	CAS	Kamschulte and Strauss, 2004
216	17.4	CAS	Kamschulte and Strauss, 2004
221	19.2	CAS	Kamschulte and Strauss, 2004
225	18.5	CAS	Kamschulte and Strauss, 2004
237	17.5	CAS	Kamschulte and Strauss, 2004
240	20.1	CAS	Kamschulte and Strauss, 2004
242	26.4	CAS	Kamschulte and Strauss, 2004
245	16.7	CAS	Kamschulte and Strauss, 2004
245	15.7	CAS	Kamschulte and Strauss, 2004
246	24.5	CAS	Kamschulte and Strauss, 2004
253	10.9	CAS	Kamschulte and Strauss, 2004
264	12.5	CAS	Kamschulte and Strauss, 2004
289	12.5	CAS	Kamschulte and Strauss, 2004
295	11.8	CAS	Kamschulte and Strauss, 2004

297	12.3	CAS	Kamschulte and Strauss, 2004
298	11.0	CAS	Kamschulte and Strauss, 2004
304	12.9	CAS	Kamschulte and Strauss, 2004
305	13.3	CAS	Kamschulte and Strauss, 2004
306	13.8	CAS	Kamschulte and Strauss, 2004
306	12.6	CAS	Kamschulte and Strauss, 2004
309	12.6	CAS	Kamschulte and Strauss, 2004
310	13.0	CAS	Kamschulte and Strauss, 2004
311	15.4	CAS	Kamschulte and Strauss, 2004
313	15.1	CAS	Kamschulte and Strauss, 2004
316	15.4	CAS	Kamschulte and Strauss, 2004
316	14.5	CAS	Kamschulte and Strauss, 2004
317	15.0	CAS	Kamschulte and Strauss, 2004
318	16.8	CAS	Kamschulte and Strauss, 2004
318	15.0	CAS	Kamschulte and Strauss, 2004
319	15.7	CAS	Kamschulte and Strauss, 2004
321	17.5	CAS	Kamschulte and Strauss, 2004
321	16.7	CAS	Kamschulte and Strauss, 2004
324	15.7	CAS	Kamschulte and Strauss, 2004
324	14.7	CAS	Kamschulte and Strauss, 2004
324	13.5	CAS	Kamschulte and Strauss, 2004
326	16.2	CAS	Kamschulte and Strauss, 2004
326	15.2	CAS	Kamschulte and Strauss, 2004
327	12.1	CAS	Kamschulte and Strauss, 2004
329	14.1	CAS	Kamschulte and Strauss, 2004
330	15.3	CAS	Kamschulte and Strauss, 2004
331	14.0	CAS	Kamschulte and Strauss, 2004
331	13.8	CAS	Kamschulte and Strauss, 2004
331	12.8	CAS	Kamschulte and Strauss, 2004
332	15.0	CAS	Kamschulte and Strauss, 2004
334	14.5	CAS	Kamschulte and Strauss, 2004
334	13.7	CAS	Kamschulte and Strauss, 2004
335	12.9	CAS	Kamschulte and Strauss, 2004
336	15.6	CAS	Kamschulte and Strauss, 2004
337	14.5	CAS	Kamschulte and Strauss, 2004
338	12.8	CAS	Kamschulte and Strauss, 2004
339	13.4	CAS	Kamschulte and Strauss, 2004
343	14.6	CAS	Kamschulte and Strauss, 2004
343	13.7	CAS	Kamschulte and Strauss, 2004
345	15.9	CAS	Kamschulte and Strauss, 2004
346	21.2	CAS	Kamschulte and Strauss, 2004
349	17.7	CAS	Kamschulte and Strauss, 2004
351	18.5	CAS	Kamschulte and Strauss, 2004
353	17.6	CAS	Kamschulte and Strauss, 2004
355	23.3	CAS	Kamschulte and Strauss, 2004
355	21.3	CAS	Kamschulte and Strauss, 2004
360	20.6	CAS	Kamschulte and Strauss, 2004
360	19.7	CAS	Kamschulte and Strauss, 2004
380	22.7	CAS	Kamschulte and Strauss, 2004
380	22.0	CAS	Kamschulte and Strauss, 2004
383	16.4	CAS	Kamschulte and Strauss, 2004
386	17.3	CAS	Kamschulte and Strauss, 2004
391	23.3	CAS	Kamschulte and Strauss, 2004
403	24.5	CAS	Kamschulte and Strauss, 2004
406	28.5	CAS	Kamschulte and Strauss, 2004
408	24.4	CAS	Kamschulte and Strauss, 2004
413	26.6	CAS	Kamschulte and Strauss, 2004
422	25.8	CAS	Kamschulte and Strauss, 2004
426	25.8	CAS	Kamschulte and Strauss, 2004
426	24.8	CAS	Kamschulte and Strauss, 2004
426	24.5	CAS	Kamschulte and Strauss, 2004
427	27.5	CAS	Kamschulte and Strauss, 2004
427	23.4	CAS	Kamschulte and Strauss, 2004
432	24.3	CAS	Kamschulte and Strauss, 2004
434	30.2	CAS	Kamschulte and Strauss, 2004
435	28.9	CAS	Kamschulte and Strauss, 2004
436	35.6	CAS	Kamschulte and Strauss, 2004
436	29.2	CAS	Kamschulte and Strauss, 2004
436	28.2	CAS	Kamschulte and Strauss, 2004
436	27.6	CAS	Kamschulte and Strauss, 2004
437	31.5	CAS	Kamschulte and Strauss, 2004
438	26.2	CAS	Kamschulte and Strauss, 2004

439	14.5	CAS	Kamschulte and Strauss, 2004
441	24.3	CAS	Kamschulte and Strauss, 2004
441	24.0	CAS	Kamschulte and Strauss, 2004
443	27.0	CAS	Kamschulte and Strauss, 2004
443	22.6	CAS	Kamschulte and Strauss, 2004
445	31.6	CAS	Kamschulte and Strauss, 2004
445	21.8	CAS	Kamschulte and Strauss, 2004
445	21.1	CAS	Kamschulte and Strauss, 2004
446	23.0	CAS	Kamschulte and Strauss, 2004
447	32.9	CAS	Kamschulte and Strauss, 2004
454	29.3	CAS	Kamschulte and Strauss, 2004
454	24.5	CAS	Kamschulte and Strauss, 2004
456	27.4	CAS	Kamschulte and Strauss, 2004
461	22.9	CAS	Kamschulte and Strauss, 2004
468	19.1	CAS	Kamschulte and Strauss, 2004
471	26.8	CAS	Kamschulte and Strauss, 2004
472	28.7	CAS	Kamschulte and Strauss, 2004
475	27.8	CAS	Kamschulte and Strauss, 2004
475	25.8	CAS	Kamschulte and Strauss, 2004
477	17.6	CAS	Kamschulte and Strauss, 2004
478	26.8	CAS	Kamschulte and Strauss, 2004
484	29.0	CAS	Kamschulte and Strauss, 2004
484	27.6	CAS	Kamschulte and Strauss, 2004
486	32.3	CAS	Kamschulte and Strauss, 2004
491	30.5	CAS	Kamschulte and Strauss, 2004
510	30.8	CAS	Kamschulte and Strauss, 2004
511	20.9	CAS	Kamschulte and Strauss, 2004
512	36.2	CAS	Kamschulte and Strauss, 2004
512	34.5	CAS	Kamschulte and Strauss, 2004
512	30.6	CAS	Kamschulte and Strauss, 2004
513	29.2	CAS	Kamschulte and Strauss, 2004
514	45.4	CAS	Kamschulte and Strauss, 2004
514	32.5	CAS	Kamschulte and Strauss, 2004
515	27.8	CAS	Kamschulte and Strauss, 2004
516	50.7	CAS	Kamschulte and Strauss, 2004
516	36.4	CAS	Kamschulte and Strauss, 2004
517	46.4	CAS	Kamschulte and Strauss, 2004
517	40.2	CAS	Kamschulte and Strauss, 2004
518	39.1	CAS	Kamschulte and Strauss, 2004
518	34.7	CAS	Kamschulte and Strauss, 2004
519	30.6	CAS	Kamschulte and Strauss, 2004
521	38.5	CAS	Kamschulte and Strauss, 2004
524	36.2	CAS	Kamschulte and Strauss, 2004
526	39.0	CAS	Kamschulte and Strauss, 2004
527	29.7	CAS	Kamschulte and Strauss, 2004
550	34.5	CAS	Kamschulte and Strauss, 2004
553	31.6	CAS	Kamschulte and Strauss, 2004
556	29.4	CAS	Kamschulte and Strauss, 2004
557	37.0	CAS	Kamschulte and Strauss, 2004
558	30.8	CAS	Kamschulte and Strauss, 2004
560	38.2	CAS	Kamschulte and Strauss, 2004
560	34.8	CAS	Kamschulte and Strauss, 2004
562	37.3	CAS	Kamschulte and Strauss, 2004
563	34.2	CAS	Kamschulte and Strauss, 2004
254	11.0	Gypsum	Kamschulte et al., 1998
254	10.7	Gypsum	Kamschulte et al., 1998
254	12.6	Gypsum	Kamschulte et al., 1998
254	11.6	Gypsum	Kamschulte et al., 1998
254	11.0	Gypsum	Kamschulte et al., 1998
254	11.4	Gypsum	Kamschulte et al., 1998
254	11.6	Gypsum	Kamschulte et al., 1998
254	11.7	Gypsum	Kamschulte et al., 1998
254	11.5	Gypsum	Kamschulte et al., 1998
254	11.4	Gypsum	Kamschulte et al., 1998
254	9.7	Gypsum	Kamschulte et al., 1998
254	10.0	Gypsum	Kamschulte et al., 1998
254	11.0	Gypsum	Kamschulte et al., 1998
254	11.7	Gypsum	Kamschulte et al., 1998
254	10.8	Gypsum	Kamschulte et al., 1998
254	10.9	Gypsum	Kamschulte et al., 1998
254	11.1	Gypsum	Kamschulte et al., 1998

254		10.4	Gypsum	Kamschulte et al., 1998
254		10.9	Gypsum	Kamschulte et al., 1998
254		10.3	Gypsum	Kamschulte et al., 1998
254		10.2	Gypsum	Kamschulte et al., 1998
254		11.1	Gypsum	Kamschulte et al., 1998
254		11.5	Gypsum	Kamschulte et al., 1998
254		12.0	Gypsum	Kamschulte et al., 1998
254		11.5	Gypsum	Kamschulte et al., 1998
254		10.4	Gypsum	Kamschulte et al., 1998
254		10.3	Gypsum	Kamschulte et al., 1998
254		10.7	Gypsum	Kamschulte et al., 1998
254		11.2	Gypsum	Kamschulte et al., 1998
254		10.9	Gypsum	Kamschulte et al., 1998
254		11.0	Gypsum	Kamschulte et al., 1998
254		-20.7	Gypsum	Kamschulte et al., 1998
254		-20.6	Gypsum	Kamschulte et al., 1998
254		11.7	Gypsum	Kamschulte et al., 1998
254		10.8	Gypsum	Kamschulte et al., 1998
254		11.4	Gypsum	Kamschulte et al., 1998
254		10.5	Gypsum	Kamschulte et al., 1998
254		10.5	Gypsum	Kamschulte et al., 1998
254		11.2	Gypsum	Kamschulte et al., 1998
254		11.6	Gypsum	Kamschulte et al., 1998
254		10.9	Gypsum	Kamschulte et al., 1998
254		9.8	Gypsum	Kamschulte et al., 1998
254		10.5	Gypsum	Kamschulte et al., 1998
254		11.4	Gypsum	Kamschulte et al., 1998
254		11.2	Gypsum	Kamschulte et al., 1998
254		11.7	Gypsum	Kamschulte et al., 1998
254		10.5	Gypsum	Kamschulte et al., 1998
254		10.5	Gypsum	Kamschulte et al., 1998
254		10.2	Gypsum	Kamschulte et al., 1998
254		10.7	Gypsum	Kamschulte et al., 1998
254		10.3	Gypsum	Kamschulte et al., 1998
254		10.5	Gypsum	Kamschulte et al., 1998
254		-22.5	Gypsum	Kamschulte et al., 1998
254		10.1	Gypsum	Kamschulte et al., 1998
254		10.2	Gypsum	Kamschulte et al., 1998
254		10.3	Gypsum	Kamschulte et al., 1998
254		10.9	Gypsum	Kamschulte et al., 1998
254		11.0	Gypsum	Kamschulte et al., 1998
254		10.9	Gypsum	Kamschulte et al., 1998
254		11.1	Gypsum	Kamschulte et al., 1998
254		11.1	Gypsum	Kamschulte et al., 1998
254		11.4	Gypsum	Kamschulte et al., 1998
127		13.2	Barite, Celestite	Kesler and Jones, 1980
127		14.9	Barite, Celestite	Kesler and Jones, 1980
127		17.9	Barite, Celestite	Kesler and Jones, 1980
127		16.8	Barite, Celestite	Kesler and Jones, 1980
127		17.2	Barite, Celestite	Kesler and Jones, 1980
127		16.4	Barite, Celestite	Kesler and Jones, 1980
127		17.7	Barite, Celestite	Kesler and Jones, 1980
127		18.0	Barite, Celestite	Kesler and Jones, 1980
127		17.2	Barite, Celestite	Kesler and Jones, 1980
127		18.2	Barite, Celestite	Kesler and Jones, 1980
127		16.8	Barite, Celestite	Kesler and Jones, 1980
127		34.2	Barite, Celestite	Kesler and Jones, 1980
127		32.1	Barite, Celestite	Kesler and Jones, 1980
127		38.3	Barite, Celestite	Kesler and Jones, 1980
127		16.3	Barite, Celestite	Kesler and Jones, 1980
127		17.0	Barite, Celestite	Kesler and Jones, 1980
127		13.6	Barite, Celestite	Kesler and Jones, 1980
127		15.4	Barite, Celestite	Kesler and Jones, 1980
127		9.1	Barite, Celestite	Kesler and Jones, 1980
127		6.4	Barite, Celestite	Kesler and Jones, 1980
127		13.2	Barite, Celestite	Kesler and Jones, 1980
635	-0.11		Barite	Killingsworth et al., 2013
635	-0.27		Barite	Killingsworth et al., 2013
635	-0.42		Barite	Killingsworth et al., 2013
635	-0.53		Barite	Killingsworth et al., 2013
635	-0.09		Barite	Killingsworth et al., 2013

635		-0.22		Barite	Killingsworth et al., 2013
635		-0.24		Barite	Killingsworth et al., 2013
635		-0.19		Barite	Killingsworth et al., 2013
635		-0.45		Barite	Killingsworth et al., 2013
635		-0.70		Barite	Killingsworth et al., 2013
635		-0.08		Barite	Killingsworth et al., 2013
635		-0.11		Barite	Killingsworth et al., 2013
635		-0.14		Barite	Killingsworth et al., 2013
635		-0.09		Barite	Killingsworth et al., 2013
635		-0.12		Barite	Killingsworth et al., 2013
635		-0.04		Barite	Killingsworth et al., 2013
635		-0.11		Barite	Killingsworth et al., 2013
635		-0.16		Barite	Killingsworth et al., 2013
2100			5.7	CAS	Krupenik et al., 2011
2100			5.1	CAS	Krupenik et al., 2011
2100			5.1	CAS	Krupenik et al., 2011
2100			5.1	CAS	Krupenik et al., 2011
2100			4.8	CAS	Krupenik et al., 2011
2100			5.2	CAS	Krupenik et al., 2011
2100			5.5	CAS	Krupenik et al., 2011
2100			5.8	CAS	Krupenik et al., 2011
2100			5.9	CAS	Krupenik et al., 2011
2100			6.1	CAS	Krupenik et al., 2011
2100			5.8	CAS	Krupenik et al., 2011
2100			5.8	CAS	Krupenik et al., 2011
2100			5.7	CAS	Krupenik et al., 2011
2100			5.2	CAS	Krupenik et al., 2011
1634			32.4	CAS	Li et al., 2015
1634			32.5	CAS	Li et al., 2015
1634			28.7	CAS	Li et al., 2015
1634			33.7	CAS	Li et al., 2015
1634			33.4	CAS	Li et al., 2015
1634			27.3	CAS	Li et al., 2015
1634			35.5	CAS	Li et al., 2015
1634			37.5	CAS	Li et al., 2015
1634			37.2	CAS	Li et al., 2015
1634			38.2	CAS	Li et al., 2015
1634			37.8	CAS	Li et al., 2015
1634			37.5	CAS	Li et al., 2015
1634			37.8	CAS	Li et al., 2015
1634			40.2	CAS	Li et al., 2015
1634			37.8	CAS	Li et al., 2015
1634			37.8	CAS	Li et al., 2015
1634			39.9	CAS	Li et al., 2015
1634			34.8	CAS	Li et al., 2015
275	16.3			Gypsum	Longinelli and Flora, 2007
275	17.9			Gypsum	Longinelli and Flora, 2007
275	17.0			Gypsum	Longinelli and Flora, 2007
275	16.8			Gypsum	Longinelli and Flora, 2007
275	16.5			Gypsum	Longinelli and Flora, 2007
275	16.7			Gypsum	Longinelli and Flora, 2007
275	15.8		11.9	Gypsum	Longinelli and Flora, 2007
275	16.3			Gypsum	Longinelli and Flora, 2007
275	16.7			Gypsum	Longinelli and Flora, 2007
275	16.2			Gypsum	Longinelli and Flora, 2007
275	17.7			Gypsum	Longinelli and Flora, 2007
275	16.6		12.0	Gypsum	Longinelli and Flora, 2007
275	16.9		12.1	Gypsum	Longinelli and Flora, 2007
275	17.7			Gypsum	Longinelli and Flora, 2007
275	17.2			Gypsum	Longinelli and Flora, 2007
275	16.8			Gypsum	Longinelli and Flora, 2007
275	17.2			Gypsum	Longinelli and Flora, 2007
275	16.7			Gypsum	Longinelli and Flora, 2007
275	15.4		11.4	Gypsum	Longinelli and Flora, 2007
275	15.8			Gypsum	Longinelli and Flora, 2007
229	14.9			Gypsum	Longinelli and Flora, 2007
229	15.9			Gypsum	Longinelli and Flora, 2007
229	14.9			Gypsum	Longinelli and Flora, 2007
229	16.3			Gypsum	Longinelli and Flora, 2007
229	11.7			Gypsum	Longinelli and Flora, 2007
229	14.9		14.7	Gypsum	Longinelli and Flora, 2007

229	15.0				Gypsum	Longinelli and Flora, 2007
229	12.4				Gypsum	Longinelli and Flora, 2007
229	12.6				Gypsum	Longinelli and Flora, 2007
229	15.7	15.0			Gypsum	Longinelli and Flora, 2007
229	13.9				Gypsum	Longinelli and Flora, 2007
229	15.1				Gypsum	Longinelli and Flora, 2007
229	15.3	15.5			Gypsum	Longinelli and Flora, 2007
229	15.6				Gypsum	Longinelli and Flora, 2007
229	14.0				Gypsum	Longinelli and Flora, 2007
229	15.0	14.8			Gypsum	Longinelli and Flora, 2007
229	15.4				Gypsum	Longinelli and Flora, 2007
229	15.1				Gypsum	Longinelli and Flora, 2007
229	16.2				Gypsum	Longinelli and Flora, 2007
229	14.4				Gypsum	Longinelli and Flora, 2007
1560		13.5	-0.01	0.423	CAS	Luo et al., 2015
1560		13.2	0.01	0.254	CAS	Luo et al., 2015
1560		11.9	-0.02	0.445	CAS	Luo et al., 2015
1560		11.7	0.00	0.236	CAS	Luo et al., 2015
1560		14.2	-0.03	0.374	CAS	Luo et al., 2015
1560		13.5	-0.01	0.355	CAS	Luo et al., 2015
1560		12.7	0.01	0.397	CAS	Luo et al., 2015
1560		14.1	-0.01	0.307	CAS	Luo et al., 2015
1560		14.2	-0.02	0.353	CAS	Luo et al., 2015
1560		15.9	0.01	0.391	CAS	Luo et al., 2015
1560		12.4	0.00	0.545	CAS	Luo et al., 2015
1560		13.7	-0.01	0.398	CAS	Luo et al., 2015
1560		11.1	0.01	0.444	CAS	Luo et al., 2015
1560		12.7	0.16	0.402	CAS	Luo et al., 2015
1560		14.6	-0.01	0.436	CAS	Luo et al., 2015
1560		14.9	-0.05	0.441	CAS	Luo et al., 2015
1560		12.5	0.02	0.388	CAS	Luo et al., 2015
1560		15.6	-0.01	0.406	CAS	Luo et al., 2015
1560		14.9	0.01	0.426	CAS	Luo et al., 2015
1560		12.5	-0.03	0.337	CAS	Luo et al., 2015
1560		8.6	0.02	0.238	CAS	Luo et al., 2015
1560		13.0	0.03	0.15	CAS	Luo et al., 2015
1560		12.9	-0.02	0.336	CAS	Luo et al., 2015
1560		12.2	-0.03	0.327	CAS	Luo et al., 2015
1560		12.7	0.02	0.296	CAS	Luo et al., 2015
1560		15.2	-0.04	0.456	CAS	Luo et al., 2015
1560		11.5	-0.03	0.302	CAS	Luo et al., 2015
1560		12.8	-0.02	0.355	CAS	Luo et al., 2015
1560		7.6	-0.03	0.216	CAS	Luo et al., 2015
1560		13.9	0.02	0.303	CAS	Luo et al., 2015
0.078	6.1	20.8			Barite	Markovic et al., 2016
0.078	6.4				Barite	Markovic et al., 2016
0.12	6.5	21.0			Barite	Markovic et al., 2016
0.2	4.4	21.0			Barite	Markovic et al., 2016
0.2	4.7				Barite	Markovic et al., 2016
0.309	5.6	20.8			Barite	Markovic et al., 2016
0.388	5.4	21.0			Barite	Markovic et al., 2016
0.388	5.1				Barite	Markovic et al., 2016
0.475	5.5	21.0			Barite	Markovic et al., 2016
0.475	5.0	21.0			Barite	Markovic et al., 2016
0.475	5.4				Barite	Markovic et al., 2016
0.61	5.6	20.9			Barite	Markovic et al., 2016
0.679	5.6	21.1			Barite	Markovic et al., 2016
0.758	5.8	21.2			Barite	Markovic et al., 2016
0.761	5.5	21.1			Barite	Markovic et al., 2016
0.91	6.3	21.3			Barite	Markovic et al., 2016
1.025	5.9	21.4			Barite	Markovic et al., 2016
1.143	6.2	21.1			Barite	Markovic et al., 2016
1.214	6.6	21.4			Barite	Markovic et al., 2016
1.214	7.2	21.5			Barite	Markovic et al., 2016
1.373	7.4				Barite	Markovic et al., 2016
1.58	6.2				Barite	Markovic et al., 2016
1.58	6.3				Barite	Markovic et al., 2016
1.646	6.6				Barite	Markovic et al., 2016
1.708	6.7	21.8			Barite	Markovic et al., 2016
1.798	6.7				Barite	Markovic et al., 2016
1.922	7.3				Barite	Markovic et al., 2016

1.922	7.1				Barite	Markovic et al., 2016
1.922	7.0				Barite	Markovic et al., 2016
2.012	7.2	21.9			Barite	Markovic et al., 2016
2.143	6.8				Barite	Markovic et al., 2016
2.261	7.0				Barite	Markovic et al., 2016
2.261	7.0				Barite	Markovic et al., 2016
2.261	6.4				Barite	Markovic et al., 2016
2.34	7.3				Barite	Markovic et al., 2016
2.498	8.1				Barite	Markovic et al., 2016
2.498	7.5				Barite	Markovic et al., 2016
2.536	6.7	21.8			Barite	Markovic et al., 2016
2.635	7.2				Barite	Markovic et al., 2016
2.734	7.5				Barite	Markovic et al., 2016
2.734	7.2				Barite	Markovic et al., 2016
2.78	6.7				Barite	Markovic et al., 2016
2.872	7.0				Barite	Markovic et al., 2016
2.976	6.4				Barite	Markovic et al., 2016
3.051	6.7	21.7			Barite	Markovic et al., 2016
3.09	7.7	21.7			Barite	Markovic et al., 2016
3.09		22.0			Barite	Markovic et al., 2016
3.194	7.4				Barite	Markovic et al., 2016
3.194	6.9				Barite	Markovic et al., 2016
3.297	6.9	21.5			Barite	Markovic et al., 2016
3.391	8.0				Barite	Markovic et al., 2016
3.391	7.4				Barite	Markovic et al., 2016
3.556	7.0				Barite	Markovic et al., 2016
3.645	7.5	21.9			Barite	Markovic et al., 2016
3.645	6.8	22.0			Barite	Markovic et al., 2016
3.723	7.2	21.7			Barite	Markovic et al., 2016
3.83	6.8	21.9			Barite	Markovic et al., 2016
3.92	6.7				Barite	Markovic et al., 2016
3.92	6.3				Barite	Markovic et al., 2016
4.016	6.9	21.8			Barite	Markovic et al., 2016
4.131	6.8				Barite	Markovic et al., 2016
0.001		20.9	0.01	-0.438	barite	Masterson et al., 2016
0.001		20.8	0.04	-0.442	barite	Masterson et al., 2016
0.001		20.7	0.06	-0.472	barite	Masterson et al., 2016
0.4		20.9	0.04	-0.443	barite	Masterson et al., 2016
1.937		22.1	0.03	-0.515	barite	Masterson et al., 2016
3.578		21.4	0.06	-0.338	barite	Masterson et al., 2016
4.552		21.8	0.06	-0.089	barite	Masterson et al., 2016
4.85		22.1	0.04	-0.428	barite	Masterson et al., 2016
5.4		21.8	0.03	-0.465	barite	Masterson et al., 2016
6.231		22.2	0.05	-0.448	barite	Masterson et al., 2016
7.854		22.5	0.03	-0.524	barite	Masterson et al., 2016
12.488		22.0	0.03	-0.269	barite	Masterson et al., 2016
12.488		21.9	0.05	-0.033	barite	Masterson et al., 2016
12.774		22.7	0.05	-0.566	barite	Masterson et al., 2016
12.782		22.4	0.04	-0.479	barite	Masterson et al., 2016
13		22.5	0.09	-0.417	barite	Masterson et al., 2016
13.274		22.0	0.06	-0.481	barite	Masterson et al., 2016
13.717		22.1	0.06	-0.411	barite	Masterson et al., 2016
14.054		21.8	0.08	-0.478	barite	Masterson et al., 2016
14.983		21.8	0.04	-0.273	barite	Masterson et al., 2016
18.132		21.8	0.04	-0.304	barite	Masterson et al., 2016
18.132		21.8	0.05	-0.449	barite	Masterson et al., 2016
20.138		21.7	0.02	-0.302	barite	Masterson et al., 2016
23.547		21.9	0.04	-0.410	barite	Masterson et al., 2016
24.144		21.8	0.05	-0.630	barite	Masterson et al., 2016
24.6		21.6	0.04	-0.486	barite	Masterson et al., 2016
24.8		21.4	0.03	-0.228	barite	Masterson et al., 2016
25.679		21.6	0.07	-0.389	barite	Masterson et al., 2016
28.445		21.3	0.02	-0.496	barite	Masterson et al., 2016
31		22.0	0.03	-0.006	barite	Masterson et al., 2016
31		21.7	0.04	-0.413	barite	Masterson et al., 2016
32.5		21.5	0.05	-0.615	barite	Masterson et al., 2016
33.9		21.5	0.04	-0.450	barite	Masterson et al., 2016
34.4		22.8	0.04	-0.194	barite	Masterson et al., 2016
34.5		22.1	0.05	-0.595	barite	Masterson et al., 2016
34.95		22.2	0.03	-0.414	barite	Masterson et al., 2016
35.4		21.8	0.09	-0.067	barite	Masterson et al., 2016

36	21.8	0.05	-0.477	barite	Masterson et al., 2016
36.306	22.5	0.04	-0.531	barite	Masterson et al., 2016
37.5	22.0	0.05	-0.352	barite	Masterson et al., 2016
39.5	22.4	0.04	-0.571	barite	Masterson et al., 2016
41	22.2	0.06	-0.565	barite	Masterson et al., 2016
42.5	22.5	0.05	-0.422	barite	Masterson et al., 2016
49.7	19.3	0.04	-0.024	barite	Masterson et al., 2016
50	18.8	0.08	-0.302	barite	Masterson et al., 2016
50.8	18.1	0.03	-0.439	barite	Masterson et al., 2016
52	17.8	0.03	-0.290	barite	Masterson et al., 2016
52.818	17.4	0.02	-0.374	barite	Masterson et al., 2016
55.4	17.6	0.03	-0.435	barite	Masterson et al., 2016
55.8	18.1	0.02	-0.360	barite	Masterson et al., 2016
55.8	18.0	0.03	-0.291	barite	Masterson et al., 2016
56.53	17.7	0.05	-0.472	barite	Masterson et al., 2016
57.2	17.6	0.02	-0.419	barite	Masterson et al., 2016
59.6	18.1	0.03	-0.491	barite	Masterson et al., 2016
62.2	18.7	0.08	-0.444	barite	Masterson et al., 2016
62.4	19.0	0.04	-0.496	barite	Masterson et al., 2016
64.9745	19.2	0.04	-0.547	barite	Masterson et al., 2016
74.4	19.5	0.05	-0.054	barite	Masterson et al., 2016
76.43	19.2	0.04	-0.362	barite	Masterson et al., 2016
80.32	19.2	0.04	-0.239	barite	Masterson et al., 2016
81.97	19.4	0.04	-0.232	barite	Masterson et al., 2016
83.63	18.5	0.04	-0.576	barite	Masterson et al., 2016
83.9	18.1	0.04	-0.464	barite	Masterson et al., 2016
85.6	18.5	0.03	-0.358	barite	Masterson et al., 2016
91	18.6	0.04	-0.382	barite	Masterson et al., 2016
95	19.4	0.05	-0.444	barite	Masterson et al., 2016
95.78	19.1	0.04	-0.321	barite	Masterson et al., 2016
97	18.2	0.04	-0.448	barite	Masterson et al., 2016
97	19.4	0.05	-0.688	barite	Masterson et al., 2016
98.87	17.9	0.04	-0.498	barite	Masterson et al., 2016
109	16.3	0.07	-0.445	barite	Masterson et al., 2016
110	15.5	0.04	-0.253	barite	Masterson et al., 2016
112.7	16.1	0.03	-0.306	barite	Masterson et al., 2016
116.5	15.4	0.04	-0.438	barite	Masterson et al., 2016
119.6	15.6	0.03	-0.333	barite	Masterson et al., 2016
126.65	20.1	0.03	-0.110	barite	Masterson et al., 2016
730	30.6			CAS	Mazumdar and Strauss, 2006
730	31.8			CAS	Mazumdar and Strauss, 2006
730	31.3			CAS	Mazumdar and Strauss, 2006
730	31.1			CAS	Mazumdar and Strauss, 2006
730	30.0			CAS	Mazumdar and Strauss, 2006
730	34.2			CAS	Mazumdar and Strauss, 2006
730	31.7			CAS	Mazumdar and Strauss, 2006
730	33.5			CAS	Mazumdar and Strauss, 2006
730	27.3			CAS	Mazumdar and Strauss, 2006
730	31.0			CAS	Mazumdar and Strauss, 2006
730	28.7			CAS	Mazumdar and Strauss, 2006
730	31.4			CAS	Mazumdar and Strauss, 2006
730	31.5			CAS	Mazumdar and Strauss, 2006
730	31.0			CAS	Mazumdar and Strauss, 2006
730	31.6			CAS	Mazumdar and Strauss, 2006
730	32.9			CAS	Mazumdar and Strauss, 2006
730	31.1			CAS	Mazumdar and Strauss, 2006
730	36.4			CAS	Mazumdar and Strauss, 2006
730	36.3			CAS	Mazumdar and Strauss, 2006
730	35.0			CAS	Mazumdar and Strauss, 2006
730	36.1			CAS	Mazumdar and Strauss, 2006
730	35.7			CAS	Mazumdar and Strauss, 2006
730	35.7			CAS	Mazumdar and Strauss, 2006
730	34.4			CAS	Mazumdar and Strauss, 2006
730	35.9			CAS	Mazumdar and Strauss, 2006
730	36.5			CAS	Mazumdar and Strauss, 2006
730	36.3			CAS	Mazumdar and Strauss, 2006
730	34.5			CAS	Mazumdar and Strauss, 2006
730	33.4			CAS	Mazumdar and Strauss, 2006
730	34.4			CAS	Mazumdar and Strauss, 2006
730	36.2			CAS	Mazumdar and Strauss, 2006
730	41.8			CAS	Mazumdar and Strauss, 2006

730		42.0	CAS	Mazumdar and Strauss, 2006
730		36.0	CAS	Mazumdar and Strauss, 2006
730		35.7	CAS	Mazumdar and Strauss, 2006
730		33.0	CAS	Mazumdar and Strauss, 2006
730		34.4	CAS	Mazumdar and Strauss, 2006
730		34.3	CAS	Mazumdar and Strauss, 2006
2150		9.2	Gypsum	Master et al., 1993
2150		14.0	Gypsum	Master et al., 1993
630		32.8	Barite	Misi and Veizer, 1998
630		32.8	Barite	Misi and Veizer, 1998
630		29.1	Barite	Misi and Veizer, 1998
630		30.9	Barite	Misi and Veizer, 1998
630		31.9	Barite	Misi and Veizer, 1998
630		29.4	Barite	Misi and Veizer, 1998
630		25.3	Barite	Misi and Veizer, 1998
630		25.9	Barite	Misi and Veizer, 1998
630		29.6	Barite	Misi and Veizer, 1998
630		25.2	Barite	Misi and Veizer, 1998
630		31.4	Barite	Misi and Veizer, 1998
630		26.4	Gypsum	Misi and Veizer, 1998
630		25.8	Gypsum	Misi and Veizer, 1998
14	5.2	6.1	Gypsum	Orti et al., 2010
14	−4.60	6.1	Gypsum	Orti et al., 2010
14	−0.55	−3.2	Gypsum	Orti et al., 2010
14	−4.26	8.6	Gypsum	Orti et al., 2010
14	6.5	9.5	Gypsum	Orti et al., 2010
14	10.1	16.3	Gypsum	Orti et al., 2010
14	6.0	5.0	Gypsum	Orti et al., 2010
14	7.6	6.0	Gypsum	Orti et al., 2010
14	19.0	24.0	Gypsum	Orti et al., 2010
14	3.6	7.7	Gypsum	Orti et al., 2010
14	8.5	9.1	Gypsum	Orti et al., 2010
14	−0.54	2.1	Gypsum	Orti et al., 2010
14	7.7	1.6	Gypsum	Orti et al., 2010
14	6.3	5.5	Gypsum	Orti et al., 2010
14	−3.51	7.9	Gypsum	Orti et al., 2010
14	−6.05	3.9	Gypsum	Orti et al., 2010
14	−1.79	4.9	Gypsum	Orti et al., 2010
14	12.6	26.4	Gypsum	Orti et al., 2010
14	8.5	7.2	Gypsum	Orti et al., 2010
14	19.9	14.9	Gypsum	Orti et al., 2010
14	−0.91	9.1	Gypsum	Orti et al., 2010
14	8.3	11.8	Gypsum	Orti et al., 2010
14	19.3	16.1	Gypsum	Orti et al., 2010
14	5.8	11.0	Gypsum	Orti et al., 2010
14	21.7	14.7	Gypsum	Orti et al., 2010
14	7.0	6.0	Gypsum	Orti et al., 2010
14	5.8	6.2	Gypsum	Orti et al., 2010
0.2		20.9	Barite	Paytan et al., 1998
0.2		21.1	Barite	Paytan et al., 1998
2.2		22.0	Barite	Paytan et al., 1998
2.6		22.0	Barite	Paytan et al., 1998
3.8		21.9	Barite	Paytan et al., 1998
4.8		22.3	Barite	Paytan et al., 1998
5.2		21.8	Barite	Paytan et al., 1998
5.7		22.1	Barite	Paytan et al., 1998
6		22.0	Barite	Paytan et al., 1998
6.4		22.3	Barite	Paytan et al., 1998
6.8		22.3	Barite	Paytan et al., 1998
7.8		21.8	Barite	Paytan et al., 1998
7.8		22.0	Barite	Paytan et al., 1998
8.1		22.3	Barite	Paytan et al., 1998
9.3		21.8	Barite	Paytan et al., 1998
9.7		22.1	Barite	Paytan et al., 1998
10.2		21.9	Barite	Paytan et al., 1998
11.4		22.2	Barite	Paytan et al., 1998
12.1		22.1	Barite	Paytan et al., 1998
12.6		21.9	Barite	Paytan et al., 1998
12.6		22.0	Barite	Paytan et al., 1998
12.7		22.0	Barite	Paytan et al., 1998
12.7		22.7	Barite	Paytan et al., 1998

12.8	22.2	Barite	Paytan et al., 1998
12.9	22.7	Barite	Paytan et al., 1998
13.4	22.1	Barite	Paytan et al., 1998
13.7	22.0	Barite	Paytan et al., 1998
14.2	21.7	Barite	Paytan et al., 1998
15.1	22.0	Barite	Paytan et al., 1998
15.1	22.1	Barite	Paytan et al., 1998
15.7	22.4	Barite	Paytan et al., 1998
16.3	21.8	Barite	Paytan et al., 1998
16.3	22.0	Barite	Paytan et al., 1998
17.2	22.1	Barite	Paytan et al., 1998
18.1	21.9	Barite	Paytan et al., 1998
19	21.8	Barite	Paytan et al., 1998
20	21.6	Barite	Paytan et al., 1998
21	22.0	Barite	Paytan et al., 1998
22.2	22.0	Barite	Paytan et al., 1998
23.5	21.9	Barite	Paytan et al., 1998
24.1	21.9	Barite	Paytan et al., 1998
25.6	21.7	Barite	Paytan et al., 1998
26.4	21.4	Barite	Paytan et al., 1998
26.4	21.8	Barite	Paytan et al., 1998
26.4	21.9	Barite	Paytan et al., 1998
27.4	21.4	Barite	Paytan et al., 1998
28.5	21.2	Barite	Paytan et al., 1998
29	21.3	Barite	Paytan et al., 1998
29	21.5	Barite	Paytan et al., 1998
29.5	21.7	Barite	Paytan et al., 1998
30	21.6	Barite	Paytan et al., 1998
30.8	21.4	Barite	Paytan et al., 1998
31	21.7	Barite	Paytan et al., 1998
32.6	21.6	Barite	Paytan et al., 1998
33.7	22.0	Barite	Paytan et al., 1998
33.8	21.8	Barite	Paytan et al., 1998
34.2	21.6	Barite	Paytan et al., 1998
34.6	21.8	Barite	Paytan et al., 1998
35.1	22.4	Barite	Paytan et al., 1998
35.1	22.5	Barite	Paytan et al., 1998
35.6	22.2	Barite	Paytan et al., 1998
36.5	22.5	Barite	Paytan et al., 1998
37.5	22.1	Barite	Paytan et al., 1998
37.5	22.3	Barite	Paytan et al., 1998
39.4	22.2	Barite	Paytan et al., 1998
40.5	22.3	Barite	Paytan et al., 1998
41.7	22.1	Barite	Paytan et al., 1998
43.8	22.4	Barite	Paytan et al., 1998
44.5	21.9	Barite	Paytan et al., 1998
44.5	22.0	Barite	Paytan et al., 1998
46	21.6	Barite	Paytan et al., 1998
46	21.5	Barite	Paytan et al., 1998
48.2	20.3	Barite	Paytan et al., 1998
49.7	19.1	Barite	Paytan et al., 1998
49.9	19.3	Barite	Paytan et al., 1998
50.2	19.1	Barite	Paytan et al., 1998
51.2	18.7	Barite	Paytan et al., 1998
51.6	18.0	Barite	Paytan et al., 1998
51.9	18.1	Barite	Paytan et al., 1998
53.6	17.8	Barite	Paytan et al., 1998
55.5	17.4	Barite	Paytan et al., 1998
56.4	17.7	Barite	Paytan et al., 1998
57	17.5	Barite	Paytan et al., 1998
57.6	18.2	Barite	Paytan et al., 1998
57.6	18.3	Barite	Paytan et al., 1998
57.9	17.9	Barite	Paytan et al., 1998
57.9	18.0	Barite	Paytan et al., 1998
59.2	18.1	Barite	Paytan et al., 1998
60.7	18.6	Barite	Paytan et al., 1998
60.9	19.0	Barite	Paytan et al., 1998
61.8	19.1	Barite	Paytan et al., 1998
63.9	18.8	Barite	Paytan et al., 1998
65.2	19.0	Barite	Paytan et al., 1998
65.2	18.9	Barite	Paytan et al., 1998
65.5	19.1	Barite	Paytan et al., 1998

66			18.8	Barite	Paytan et al., 1998
66.8			18.8	Barite	Paytan et al., 1998
68.7			18.9	Barite	Paytan et al., 1998
68.7			18.9	Barite	Paytan et al., 1998
70			18.8	Barite	Paytan et al., 1998
71.3			19.1	Barite	Paytan et al., 1998
73			19.2	Barite	Paytan et al., 1998
74.2			19.1	Barite	Paytan et al., 1998
74.4			19.3	Barite	Paytan et al., 1998
75.3			19.4	Barite	Paytan et al., 1998
75.6			19.3	Barite	Paytan et al., 1998
76.4			19.1	Barite	Paytan et al., 1998
78.4			19.0	Barite	Paytan et al., 1998
78.8			19.1	Barite	Paytan et al., 1998
80.3			19.0	Barite	Paytan et al., 1998
82			18.9	Barite	Paytan et al., 1998
83			18.2	Barite	Paytan et al., 1998
83.6			18.4	Barite	Paytan et al., 1998
83.7			18.4	Barite	Paytan et al., 1998
83.9			18.1	Barite	Paytan et al., 1998
85.6			18.3	Barite	Paytan et al., 1998
88.4			18.3	Barite	Paytan et al., 1998
88.4			18.1	Barite	Paytan et al., 1998
91			18.6	Barite	Paytan et al., 1998
93			18.9	Barite	Paytan et al., 1998
93.4			19.1	Barite	Paytan et al., 1998
93.5			19.0	Barite	Paytan et al., 1998
93.6			18.8	Barite	Paytan et al., 1998
93.8			19.0	Barite	Paytan et al., 1998
95			19.2	Barite	Paytan et al., 1998
95.8			19.0	Barite	Paytan et al., 1998
97			19.1	Barite	Paytan et al., 1998
97			18.5	Barite	Paytan et al., 1998
98.9			17.9	Barite	Paytan et al., 1998
98.9			17.8	Barite	Paytan et al., 1998
100			16.3	Barite	Paytan et al., 1998
104			15.6	Barite	Paytan et al., 1998
104			15.6	Barite	Paytan et al., 1998
107			15.7	Barite	Paytan et al., 1998
108			15.9	Barite	Paytan et al., 1998
109			16.1	Barite	Paytan et al., 1998
110			15.9	Barite	Paytan et al., 1998
111.1			16.1	Barite	Paytan et al., 1998
111.5			16.3	Barite	Paytan et al., 1998
111.9			16.1	Barite	Paytan et al., 1998
112			16.6	Barite	Paytan et al., 1998
112			16.0	Barite	Paytan et al., 1998
112			16.3	Barite	Paytan et al., 1998
112.7			16.3	Barite	Paytan et al., 1998
113.1			15.4	Barite	Paytan et al., 1998
116			15.5	Barite	Paytan et al., 1998
116			15.8	Barite	Paytan et al., 1998
116			15.9	Barite	Paytan et al., 1998
116.3			15.3	Barite	Paytan et al., 1998
116.5			15.5	Barite	Paytan et al., 1998
116.5			15.5	Barite	Paytan et al., 1998
119.6			15.5	Barite	Paytan et al., 1998
119.8			16.4	Barite	Paytan et al., 1998
120			17.2	Barite	Paytan et al., 1998
120.5			18.7	Barite	Paytan et al., 1998
120.7			17.8	Barite	Paytan et al., 1998
122.8			19.5	Barite	Paytan et al., 1998
122.8			19.2	Barite	Paytan et al., 1998
125			19.7	Barite	Paytan et al., 1998
126.7			20.0	Barite	Paytan et al., 1998
129.2			20.1	Barite	Paytan et al., 1998
635	13.6	-0.63	23.3	Barite	Peng et al., 2011
635	14.3	-0.63	22.3	Barite	Peng et al., 2011
635	13.4	-0.60	23.7	Barite	Peng et al., 2011
635	14.1	-0.44	26.2	Barite	Peng et al., 2011
635	16.6	-0.43	27.1	Barite	Peng et al., 2011

635	16.0	-0.32	26.3	Barite	Peng et al., 2011
635	15.0	-0.64	25.1	Barite	Peng et al., 2011
635	14.1	-0.69	23.3	Barite	Peng et al., 2011
635	15.2	-0.77	24.0	Barite	Peng et al., 2011
635	14.2	-0.68	23.4	Barite	Peng et al., 2011
635	14.7	-0.69	22.6	Barite	Peng et al., 2011
635	14.9	-0.60	21.7	Barite	Peng et al., 2011
635	13.3	-0.60	23.4	Barite	Peng et al., 2011
635	16.2	-0.45	30.9	Barite	Peng et al., 2011
635	15.6	-0.32	31.0	Barite	Peng et al., 2011
635	14.8	-0.21	29.8	Barite	Peng et al., 2011
635	17.5	-0.42	25.3	Barite	Peng et al., 2011
635	13.9	-0.56	26.4	Barite	Peng et al., 2011
635	19.3		31.2	Barite	Peng et al., 2011
635	15.4	-0.39	29.9	Barite	Peng et al., 2011
635	15.4	-0.32	28.5	Barite	Peng et al., 2011
635	15.8	-0.28	36.2	Barite	Peng et al., 2011
635	16.9	-0.28	35.1	Barite	Peng et al., 2011
635	16.4	-0.39	34.1	Barite	Peng et al., 2011
635	15.2	-0.24	34.6	Barite	Peng et al., 2011
635	15.0	-0.31	29.9	Barite	Peng et al., 2011
635	17.9	-0.22	30.2	Barite	Peng et al., 2011
635	18.0	-0.49	23.1	Barite	Peng et al., 2011
635	17.7	-0.40	26.2	Barite	Peng et al., 2011
635	16.7	-0.34	33.6	Barite	Peng et al., 2011
635	13.6	-0.43	22.8	Barite	Peng et al., 2011
635	14.0	-0.57	22.2	Barite	Peng et al., 2011
635	13.9	-0.50	24.8	Barite	Peng et al., 2011
635	15.3	-0.29	35.2	Barite	Peng et al., 2011
635	16.3	-0.76	23.6	Barite	Peng et al., 2011
635	15.8	-0.31	35.2	Barite	Peng et al., 2011
635	15.3	-0.26	33.3	Barite	Peng et al., 2011
635	15.8	-0.20	35.6	Barite	Peng et al., 2011
635	15.3	-0.33	27.3	Barite	Peng et al., 2011
635	15.6	-0.36	28.3	Barite	Peng et al., 2011
635	16.1	-0.32	28.9	Barite	Peng et al., 2011
635	14.9	-0.22	28.8	Barite	Peng et al., 2011
635	16.3	-0.28	30.4	Barite	Peng et al., 2011
635	17.6	-0.24	24.2	Barite	Peng et al., 2011
635	17.6	-0.35	30.4	Barite	Peng et al., 2011
635	21.3	-0.44	28.2	Barite	Peng et al., 2011
635	19.7	-0.49	27.4	Barite	Peng et al., 2011
635	18.9	-0.28	28.5	Barite	Peng et al., 2011
635	19.1	-0.14	41.7	Barite	Peng et al., 2011
635	20.1	-0.31	31.4	Barite	Peng et al., 2011
635	17.3	-0.56	26.6	Barite	Peng et al., 2011
635	16.0	-0.39	23.6	Barite	Peng et al., 2011
635	14.6	-0.47	27.0	Barite	Peng et al., 2011
635	14.8	-0.86	23.5	Barite	Peng et al., 2011
635	14.1	-0.79	23.7	Barite	Peng et al., 2011
635	14.0	-0.72	21.5	Barite	Peng et al., 2011
635	13.9	-0.68	21.2	Barite	Peng et al., 2011
635	14.7	-0.70	21.1	Barite	Peng et al., 2011
635	18.2	-0.24	35.2	Barite	Peng et al., 2011
635	16.8	-0.24	27.0	Barite	Peng et al., 2011
635	18.2	-0.26	29.9	Barite	Peng et al., 2011
635	16.8	-0.33	33.8	Barite	Peng et al., 2011
635	18.2	-0.37	32.4	Barite	Peng et al., 2011
635	17.6	-0.33	27.6	Barite	Peng et al., 2011
635	20.6	-0.21	29.2	Barite	Peng et al., 2011
635	19.7	-0.30	28.3	Barite	Peng et al., 2011
635	19.1	-0.25		Barite	Peng et al., 2011
635	16.4	-0.26		Barite	Peng et al., 2011
635	16.7	-0.27		Barite	Peng et al., 2011
635	17.3	-0.48		Barite	Peng et al., 2011
635	17.2	-0.47		Barite	Peng et al., 2011
635	16.6			Barite	Peng et al., 2011
635	16.7	-0.74		Barite	Peng et al., 2011
635	15.9	-0.71		Barite	Peng et al., 2011
635	16.5	-0.79		Barite	Peng et al., 2011
635	16.1	-0.74		Barite	Peng et al., 2011
635	16.3	-0.52		Barite	Peng et al., 2011

635	16.4	-0.82	22.0	Barite	Peng et al., 2011
635	17.2	-0.87	21.7	Barite	Peng et al., 2011
635	17.2	-0.84	21.8	Barite	Peng et al., 2011
635	16.8	-0.79	22.1	Barite	Peng et al., 2011
635	15.4	-0.85	22.1	Barite	Peng et al., 2011
635	20.0	-0.43	27.8	Barite	Peng et al., 2011
635	20.6	-0.44	28.1	Barite	Peng et al., 2011
635	21.6	-0.47	28.0	Barite	Peng et al., 2011
635	22.0	-0.50	27.6	Barite	Peng et al., 2011
635	21.5	-0.50	27.5	Barite	Peng et al., 2011
635	19.0	-0.44	31.2	Barite	Peng et al., 2011
635	17.5	-0.39	31.5	Barite	Peng et al., 2011
635	18.4	-0.35	31.7	Barite	Peng et al., 2011
635	17.8	-0.30	31.6	Barite	Peng et al., 2011
635	18.1	-0.31	30.8	Barite	Peng et al., 2011
635	19.5	-0.39	31.8	Barite	Peng et al., 2011
635	17.3	-0.27		Barite	Peng et al., 2011
635	19.6	-0.13		Barite	Peng et al., 2011
635	19.2	-0.24		Barite	Peng et al., 2011
635	17.9	-0.15		Barite	Peng et al., 2011
635	18.9	-0.15		Barite	Peng et al., 2011
635	18.5	-0.15		Barite	Peng et al., 2011
635	18.1	-0.12		Barite	Peng et al., 2011
635	17.0	-0.45	22.4	Barite	Peng et al., 2011
635	19.9	-0.24	28.8	Barite	Peng et al., 2011
635	19.3	-0.26	34.5	Barite	Peng et al., 2011
635	19.5	-0.09	36.5	Barite	Peng et al., 2011
635	19.0	-0.09	36.0	Barite	Peng et al., 2011
635	19.4	-0.16	34.6	Barite	Peng et al., 2011
635	18.9	-0.11	32.7	Barite	Peng et al., 2011
635	19.5	-0.13	31.7	Barite	Peng et al., 2011
635	19.1	-0.41	31.4	Barite	Peng et al., 2011
635	21.9	-0.45	27.2	Barite	Peng et al., 2011
635	21.9	-0.52	27.6	Barite	Peng et al., 2011
635	22.0	-0.47	28.4	Barite	Peng et al., 2011
635	21.7	-0.43	29.0	Barite	Peng et al., 2011
635	22.6	-0.37	28.9	Barite	Peng et al., 2011
635	21.2	-0.47	28.5	Barite	Peng et al., 2011
635	23.3	-0.40	27.9	Barite	Peng et al., 2011
635	22.1	-0.42	27.6	Barite	Peng et al., 2011
635	23.5	-0.45	27.1	Barite	Peng et al., 2011
635	23.2	-0.45	27.1	Barite	Peng et al., 2011
635	18.5	-0.44	26.3	Barite	Peng et al., 2011
635	20.6	-0.57	25.0	Barite	Peng et al., 2011
635	21.4	-0.46	25.4	Barite	Peng et al., 2011
635	20.6	-0.33	25.7	Barite	Peng et al., 2011
635	20.9	-0.48	25.2	Barite	Peng et al., 2011
635	20.9	-0.36	25.3	Barite	Peng et al., 2011
635	21.2	-0.40	26.5	Barite	Peng et al., 2011
635	21.0	-0.38	26.3	Barite	Peng et al., 2011
635	21.4	-0.42	26.8	Barite	Peng et al., 2011
635	21.4	-0.45	26.8	Barite	Peng et al., 2011
635	20.7	-0.41	30.3	Barite	Peng et al., 2011
635	21.1	-0.39	30.5	Barite	Peng et al., 2011
635	19.7	-0.49	27.3	Barite	Peng et al., 2011
635	21.9	-0.46	25.8	Barite	Peng et al., 2011
635	20.9	-0.41	26.0	Barite	Peng et al., 2011
635	20.4	-0.44	25.6	Barite	Peng et al., 2011
635	19.8	-0.35		Barite	Peng et al., 2011
635	20.7	-0.34		Barite	Peng et al., 2011
635	21.9	-0.30		Barite	Peng et al., 2011
635	19.6	-0.56		Barite	Peng et al., 2011
635	19.4	-0.58		Barite	Peng et al., 2011
635	18.9	-0.54		Barite	Peng et al., 2011
635	18.6	-0.13	45.3	Barite	Peng et al., 2011
635	18.0	-0.21	44.3	Barite	Peng et al., 2011
635	18.6	-0.12	42.7	Barite	Peng et al., 2011
635	19.2	-0.11	45.5	Barite	Peng et al., 2011
635	18.4	-0.16	43.2	Barite	Peng et al., 2011
635	19.4	-0.17	42.2	Barite	Peng et al., 2011
635	14.2	-0.32	23.3	Barite	Peng et al., 2011
635	15.8	-0.79	24.3	Barite	Peng et al., 2011

635	16.0	-0.85	23.8	Barite	Peng et al., 2011
635	16.4	-0.82	23.6	Barite	Peng et al., 2011
635	16.4	-0.55	25.2	Barite	Peng et al., 2011
635	14.2	-0.58	26.8	Barite	Peng et al., 2011
635	14.3	-0.59	26.9	Barite	Peng et al., 2011
635	14.0	-0.53	27.8	Barite	Peng et al., 2011
635	13.9	-0.39	29.0	Barite	Peng et al., 2011
635	15.2	-0.85		Barite	Peng et al., 2011
635	16.6	-0.81		Barite	Peng et al., 2011
635	16.0	-0.82		Barite	Peng et al., 2011
635	15.4	-0.86		Barite	Peng et al., 2011
535	15.6		28.9	Anhydrite	Peryt et al., 2010
535	16.9		34.0	Anhydrite	Peryt et al., 2010
535	17.3		22.8	Anhydrite	Peryt et al., 2010
535	13.4		21.6	Anhydrite	Peryt et al., 2010
535	15.5		24.8	Anhydrite	Peryt et al., 2010
535	13.5		28.8	Anhydrite	Peryt et al., 2010
535	16.9		28.6	Anhydrite	Peryt et al., 2010
535	16.4		25.7	Anhydrite	Peryt et al., 2010
535	17.4		28.0	Anhydrite	Peryt et al., 2010
535	17.7		31.2	Anhydrite	Peryt et al., 2010
535	17.3		26.0	Anhydrite	Peryt et al., 2010
535	15.0		32.8	Anhydrite	Peryt et al., 2010
535	12.8		30.3	Anhydrite	Peryt et al., 2010
535			34.5	Anhydrite	Peryt et al., 2010
535	12.9		29.4	Anhydrite	Peryt et al., 2010
535	15.1		31.5	Anhydrite	Peryt et al., 2010
535	16.8		32.3	Anhydrite	Peryt et al., 2010
535	15.9		31.3	Anhydrite	Peryt et al., 2010
535	16.9		31.8	Anhydrite	Peryt et al., 2010
535	13.1		32.2	Anhydrite	Peryt et al., 2010
535	15.2		31.5	Anhydrite	Peryt et al., 2010
535	15.6		29.7	Anhydrite	Peryt et al., 2010
535	17.2		32.2	Anhydrite	Peryt et al., 2010
535	17.8		23.3	Anhydrite	Peryt et al., 2010
535	13.4		24.3	Anhydrite	Peryt et al., 2010
535	12.4		30.5	Anhydrite	Peryt et al., 2010
535	11.9		7.3	Anhydrite	Peryt et al., 2010
535	14.5		22.6	Anhydrite	Peryt et al., 2010
391	17.1		20.2	Anhydrite	Pierre and Rouchy, 1986
391	16.8		20.1	Anhydrite	Pierre and Rouchy, 1986
391	18.7		23.4	Anhydrite	Pierre and Rouchy, 1986
391	19.4		23.5	Anhydrite	Pierre and Rouchy, 1986
391	19.8		20.8	Anhydrite	Pierre and Rouchy, 1986
391	17.9		20.0	Anhydrite	Pierre and Rouchy, 1986
391	19.4		20.5	Anhydrite	Pierre and Rouchy, 1986
391	20.0		20.8	Anhydrite	Pierre and Rouchy, 1986
391	19.8		20.6	Anhydrite	Pierre and Rouchy, 1986
337	15.7		16.4	Anhydrite	Pierre and Rouchy, 1986
337	19.2		19.0	Anhydrite	Pierre and Rouchy, 1986
337	17.3		16.4	Anhydrite	Pierre and Rouchy, 1986
337	16.9		16.2	Anhydrite	Pierre and Rouchy, 1986
337	17.4		15.7	Anhydrite	Pierre and Rouchy, 1986
337	15.7		15.6	Anhydrite	Pierre and Rouchy, 1986
337	15.1		16.0	Anhydrite	Pierre and Rouchy, 1986
337	15.2		15.2	Anhydrite	Pierre and Rouchy, 1986
337	14.6		14.9	Anhydrite	Pierre and Rouchy, 1986
337	14.7		15.2	Anhydrite	Pierre and Rouchy, 1986
337	19.6		17.2	Anhydrite	Pierre and Rouchy, 1986
337	14.4		14.9	Anhydrite	Pierre and Rouchy, 1986
337	15.0		14.0	Anhydrite	Pierre and Rouchy, 1986
337	14.1		14.5	Anhydrite	Pierre and Rouchy, 1986
337	17.5		15.2	Anhydrite	Pierre and Rouchy, 1986
337	17.2		15.2	Anhydrite	Pierre and Rouchy, 1986
337	14.8		15.0	Anhydrite	Pierre and Rouchy, 1986
337	16.2		15.5	Anhydrite	Pierre and Rouchy, 1986
337	15.9		14.6	Anhydrite	Pierre and Rouchy, 1986
337	14.1		15.2	Anhydrite	Pierre and Rouchy, 1986
337	13.7		14.4	Anhydrite	Pierre and Rouchy, 1986
337	14.9		15.1	Anhydrite	Pierre and Rouchy, 1986
337	14.1		14.2	Anhydrite	Pierre and Rouchy, 1986

337	17.4	18.7	Anhydrite	Pierre and Rouchy, 1986
345	18.3	16.6	Anhydrite	Pierre and Rouchy, 1986
345	13.4	13.6	Anhydrite	Pierre and Rouchy, 1986
345	16.1	15.0	Anhydrite	Pierre and Rouchy, 1986
345	16.4	15.2	Anhydrite	Pierre and Rouchy, 1986
345	17.2	15.4	Anhydrite	Pierre and Rouchy, 1986
2100		10.8	Anhydrite	Reuschel et al., 2012
2100		9.5	Anhydrite	Reuschel et al., 2012
2100		9.0	Anhydrite	Reuschel et al., 2012
2100		10.3	Anhydrite	Reuschel et al., 2012
2100		9.1	Anhydrite	Reuschel et al., 2012
2100		8.7	Anhydrite	Reuschel et al., 2012
2100		12.9	Barite	Reuschel et al., 2012
2100		8.4	Barite	Reuschel et al., 2012
2100		10.4	CAS	Reuschel et al., 2012
2100		9.8	CAS	Reuschel et al., 2012
2100		7.8	CAS	Reuschel et al., 2012
2100		9.4	CAS	Reuschel et al., 2012
2100		15.8	CAS	Reuschel et al., 2012
2100		8.3	CAS	Reuschel et al., 2012
2100		8.8	CAS	Reuschel et al., 2012
2100		10.7	CAS	Reuschel et al., 2012
2100		11.3	CAS	Reuschel et al., 2012
220	8.0	15.4	Gypsum	Rick, 1990
220	11.7	16.9	Gypsum	Rick, 1990
220	11.2	16.6	Gypsum	Rick, 1990
220	12.1	15.8	Gypsum	Rick, 1990
220	12.8	17.4	Gypsum	Rick, 1990
220	11.9	16.8	Gypsum	Rick, 1990
220	11.3	17.0	Gypsum	Rick, 1990
220	10.6	14.1	Gypsum	Rick, 1990
220	11.1	14.7	Gypsum	Rick, 1990
220	11.8	14.3	Gypsum	Rick, 1990
220	7.7	14.3	Gypsum	Rick, 1990
220		14.9	Gypsum	Rick, 1990
220		14.9	Gypsum	Rick, 1990
220		15.5	Gypsum	Rick, 1990
220	12.8	14.9	Gypsum	Rick, 1990
220		18.0	Gypsum	Rick, 1990
552		20.9	CAS	Ries et al., 2009
552		15.5	CAS	Ries et al., 2009
551.9		26.0	CAS	Ries et al., 2009
551.8		23.1	CAS	Ries et al., 2009
551.7		15.9	CAS	Ries et al., 2009
551.6		21.3	CAS	Ries et al., 2009
551.6		13.5	CAS	Ries et al., 2009
551.5		19.1	CAS	Ries et al., 2009
551.4		14.2	CAS	Ries et al., 2009
551.4		13.7	CAS	Ries et al., 2009
551.3		16.7	CAS	Ries et al., 2009
551.2		16.6	CAS	Ries et al., 2009
551.1		15.9	CAS	Ries et al., 2009
551.1		20.2	CAS	Ries et al., 2009
551		14.0	CAS	Ries et al., 2009
550.9		14.4	CAS	Ries et al., 2009
550.8		13.7	CAS	Ries et al., 2009
550.8		22.9	CAS	Ries et al., 2009
550.7		16.8	CAS	Ries et al., 2009
550.6		20.4	CAS	Ries et al., 2009
550.5		17.4	CAS	Ries et al., 2009
550.5		16.7	CAS	Ries et al., 2009
550.4		29.5	CAS	Ries et al., 2009
550.3		24.7	CAS	Ries et al., 2009
550.7		29.9	CAS	Ries et al., 2009
550.6		27.5	CAS	Ries et al., 2009
550.5		25.4	CAS	Ries et al., 2009
550.5		29.7	CAS	Ries et al., 2009
550.4		37.4	CAS	Ries et al., 2009
550.3		35.3	CAS	Ries et al., 2009
550.2		35.2	CAS	Ries et al., 2009
550.2		33.5	CAS	Ries et al., 2009

550.1	32.2	CAS	Ries et al., 2009
550	33.2	CAS	Ries et al., 2009
549.9	35.1	CAS	Ries et al., 2009
549.9	38.5	CAS	Ries et al., 2009
549.8	39.0	CAS	Ries et al., 2009
549.7	40.0	CAS	Ries et al., 2009
549.6	18.5	CAS	Ries et al., 2009
549.5	22.5	CAS	Ries et al., 2009
549.5	32.3	CAS	Ries et al., 2009
549.4	31.2	CAS	Ries et al., 2009
549.3	28.3	CAS	Ries et al., 2009
549.2	37.0	CAS	Ries et al., 2009
549.1	38.8	CAS	Ries et al., 2009
549	41.4	CAS	Ries et al., 2009
549	28.2	CAS	Ries et al., 2009
549	39.0	CAS	Ries et al., 2009
548.9	33.4	CAS	Ries et al., 2009
548.9	36.7	CAS	Ries et al., 2009
548.8	37.9	CAS	Ries et al., 2009
548.8	47.0	CAS	Ries et al., 2009
548.7	38.8	CAS	Ries et al., 2009
548.7	35.2	CAS	Ries et al., 2009
548.7	40.8	CAS	Ries et al., 2009
548.6	50.3	CAS	Ries et al., 2009
548.6	47.9	CAS	Ries et al., 2009
548.5	32.9	CAS	Ries et al., 2009
548.5	30.5	CAS	Ries et al., 2009
548.4	44.7	CAS	Ries et al., 2009
548.4	47.3	CAS	Ries et al., 2009
548.3	64.2	CAS	Ries et al., 2009
548.3	54.0	CAS	Ries et al., 2009
548.2	39.2	CAS	Ries et al., 2009
548.2	34.6	CAS	Ries et al., 2009
548.1	30.3	CAS	Ries et al., 2009
548	32.5	CAS	Ries et al., 2009
547.9	45.4	CAS	Ries et al., 2009
547.9	41.0	CAS	Ries et al., 2009
547.8	17.0	CAS	Ries et al., 2009
547.7	19.0	CAS	Ries et al., 2009
547.7	20.5	CAS	Ries et al., 2009
547.6	17.3	CAS	Ries et al., 2009
547.5	17.9	CAS	Ries et al., 2009
547.5	24.2	CAS	Ries et al., 2009
547.4	25.0	CAS	Ries et al., 2009
547.3	16.6	CAS	Ries et al., 2009
547.2	22.5	CAS	Ries et al., 2009
547.1	35.2	CAS	Ries et al., 2009
547	30.5	CAS	Ries et al., 2009
546.9	22.7	CAS	Ries et al., 2009
546.9	37.0	CAS	Ries et al., 2009
546.7	20.9	CAS	Ries et al., 2009
546.7	20.5	CAS	Ries et al., 2009
546.6	28.4	CAS	Ries et al., 2009
546.5	20.8	CAS	Ries et al., 2009
546.4	22.6	CAS	Ries et al., 2009
546.3	32.8	CAS	Ries et al., 2009
546.2	28.1	CAS	Ries et al., 2009
546.2	16.0	CAS	Ries et al., 2009
546.1	16.1	CAS	Ries et al., 2009
545.9	17.4	CAS	Ries et al., 2009
545.9	18.3	CAS	Ries et al., 2009
545.8	19.0	CAS	Ries et al., 2009
545.7	18.7	CAS	Ries et al., 2009
545.6	20.1	CAS	Ries et al., 2009
545.5	20.5	CAS	Ries et al., 2009
545.5	21.2	CAS	Ries et al., 2009
545.4	20.4	CAS	Ries et al., 2009
545.4	18.9	CAS	Ries et al., 2009
545.3	18.8	CAS	Ries et al., 2009
545.2	20.1	CAS	Ries et al., 2009
545.1	17.9	CAS	Ries et al., 2009
545.1	22.9	CAS	Ries et al., 2009

545.1		24.0			CAS	Ries et al., 2009
545		21.3			CAS	Ries et al., 2009
544.9		20.2			CAS	Ries et al., 2009
0	10.9	20.8			Gypsum	Sakai et al., 1972
0	15.8	24.3			Gypsum	Sakai et al., 1972
45	12.2	18.4			Gypsum	Sakai et al., 1972
45	11.7	18.9			Gypsum	Sakai et al., 1972
260	9.8	10.2			Gypsum	Sakai et al., 1972
260	8.3	10.9			Gypsum	Sakai et al., 1972
260	8.1	10.3			Gypsum	Sakai et al., 1972
275	9.3	11.5			Gypsum	Sakai et al., 1972
275	9.9	12.1			Gypsum	Sakai et al., 1972
375	15.1	29.5			Gypsum	Sakai et al., 1972
385	15.0	17.3			Gypsum	Sakai et al., 1972
433	10.6	24.9			Gypsum	Sakai et al., 1972
465	15.9	25.0			Gypsum	Sakai et al., 1972
510	13.1	30.0			Gypsum	Sakai et al., 1972
525	10.5	38.2			Gypsum	Sakai et al., 1972
800	13.3	14.7			Gypsum	Sakai et al., 1972
800	25.0	14.5			Gypsum	Sakai et al., 1972
800	21.9	28.6			Gypsum	Sakai et al., 1972
14	7.7	3.7			Gypsum	Sakai et al., 1972
80	9.5	-28.2			Gypsum	Sakai et al., 1972
120	3.1	-23.3			Gypsum	Sakai et al., 1972
0	9.5	20.3			Gypsum	Sakai et al., 1972
2210		11.3			Gypsum	Schröder, et al., 2008
2210		11.9			Gypsum	Schröder, et al., 2008
570		36.3			Francolite	Shields et al., 2004
570		37.4			Francolite	Shields et al., 2004
570		37.8			Francolite	Shields et al., 2004
570		35.7			Francolite	Shields et al., 2004
570		35.5			Francolite	Shields et al., 2004
570		37.8			Francolite	Shields et al., 2004
570		32.3			Francolite	Shields et al., 2004
570		33.6			Francolite	Shields et al., 2004
570		34.5			Francolite	Shields et al., 2004
570		34.2			Francolite	Shields et al., 2004
570		32.6			Francolite	Shields et al., 2004
570		33.5			Francolite	Shields et al., 2004
570		31.6			Francolite	Shields et al., 2004
381.50		31.5	0.05	-0.192	CAS	Sim et al., 2015
381.64		29.9			CAS	Sim et al., 2015
381.80		33.2			CAS	Sim et al., 2015
381.83		29.7	-0.03	0.080	CAS	Sim et al., 2015
381.85		31.5			CAS	Sim et al., 2015
381.87		28.1			CAS	Sim et al., 2015
381.89		20.6			CAS	Sim et al., 2015
381.92		14.3	-0.03	0.141	CAS	Sim et al., 2015
381.97		21.6			CAS	Sim et al., 2015
382.02		30.5			CAS	Sim et al., 2015
382.09		31.7	0.03	-0.066	CAS	Sim et al., 2015
382.12		34.4			CAS	Sim et al., 2015
382.17		35.4	0.03	-0.110	CAS	Sim et al., 2015
382.19		32.4			CAS	Sim et al., 2015
382.23		16.6			CAS	Sim et al., 2015
382.25		32.2			CAS	Sim et al., 2015
382.28		28.5			CAS	Sim et al., 2015
382.32		32.9	0.06	-0.156	CAS	Sim et al., 2015
382.37		30.2			CAS	Sim et al., 2015
382.63		27.0			CAS	Sim et al., 2015
382.87		30.3			CAS	Sim et al., 2015
383.69		27.0	0.07	-0.124	CAS	Sim et al., 2015
384.73		30.1			CAS	Sim et al., 2015
381.82		27.2			CAS	Sim et al., 2015
381.83		27.9			CAS	Sim et al., 2015
381.85		34.7			CAS	Sim et al., 2015
381.86		36.7			CAS	Sim et al., 2015
381.88		39.8			CAS	Sim et al., 2015
381.89		35.7			CAS	Sim et al., 2015
381.90		23.8			CAS	Sim et al., 2015
381.91		31.6			CAS	Sim et al., 2015

381.92	32.0	CAS	Sim et al., 2015
381.92	36.2	CAS	Sim et al., 2015
381.93	34.8	CAS	Sim et al., 2015
381.93	31.7	CAS	Sim et al., 2015
381.94	33.5	CAS	Sim et al., 2015
381.95	27.9	CAS	Sim et al., 2015
381.95	24.1	CAS	Sim et al., 2015
381.96	26.3	CAS	Sim et al., 2015
381.96	12.6	CAS	Sim et al., 2015
381.97	18.1	CAS	Sim et al., 2015
381.97	22.8	CAS	Sim et al., 2015
381.98	26.2	CAS	Sim et al., 2015
382.06	31.7	CAS	Sim et al., 2015
382.11	31.8	CAS	Sim et al., 2015
382.16	32.4	CAS	Sim et al., 2015
382.24	29.8	CAS	Sim et al., 2015
382.25	28.5	CAS	Sim et al., 2015
382.29	29.8	CAS	Sim et al., 2015
382.32	26.1	CAS	Sim et al., 2015
382.34	28.7	CAS	Sim et al., 2015
382.36	23.5	CAS	Sim et al., 2015
382.38	23.9	CAS	Sim et al., 2015
382.40	29.7	CAS	Sim et al., 2015
375.30	24.5	CAS	Sim et al., 2015
375.44	24.9	CAS	Sim et al., 2015
375.55	24.6	CAS	Sim et al., 2015
375.75	24.9	CAS	Sim et al., 2015
375.86	24.8	CAS	Sim et al., 2015
376.09	22.9	CAS	Sim et al., 2015
376.16	26.2	CAS	Sim et al., 2015
376.21	26.0	CAS	Sim et al., 2015
376.26	25.5	CAS	Sim et al., 2015
376.49	29.6	CAS	Sim et al., 2015
376.73	28.1	CAS	Sim et al., 2015
376.81	28.1	CAS	Sim et al., 2015
377.05	28.4	CAS	Sim et al., 2015
377.22	27.9	CAS	Sim et al., 2015
590	27.6	Gypsum	Strauss, 1993
680	29.6	Gypsum	Strauss, 1993
750	15.1	Gypsum	Strauss, 1993
750	15.6	Gypsum	Strauss, 1993
750	16.0	Gypsum	Strauss, 1993
750	16.4	Gypsum	Strauss, 1993
750	16.5	Gypsum	Strauss, 1993
750	18.6	Gypsum	Strauss, 1993
750	18.8	Gypsum	Strauss, 1993
750	19.1	Gypsum	Strauss, 1993
750	22.9	Gypsum	Strauss, 1993
750	25.5	Gypsum	Strauss, 1993
850	18.6	Gypsum	Strauss, 1993
850	19.1	Gypsum	Strauss, 1993
850	19.2	Gypsum	Strauss, 1993
850	19.4	Gypsum	Strauss, 1993
850	19.4	Gypsum	Strauss, 1993
1350	12.0	Gypsum	Strauss, 1993
1350	13.6	Gypsum	Strauss, 1993
1350	14.4	Gypsum	Strauss, 1993
1350	18.3	Gypsum	Strauss, 1993
3500	2.2	Gypsum	Strauss, 1993
3500	14.9	Gypsum	Strauss, 1993
3500	7.4	Gypsum	Strauss, 1993
3450	2.7	Gypsum	Strauss, 1993
3450	3.9	Gypsum	Strauss, 1993
3450	3.3	Gypsum	Strauss, 1993
3400	3.0	Gypsum	Strauss, 1993
3400	6.0	Gypsum	Strauss, 1993
3400	3.9	Gypsum	Strauss, 1993
3350	3.1	Gypsum	Strauss, 1993
3350	3.8	Gypsum	Strauss, 1993
3350	3.4	Gypsum	Strauss, 1993
3300	4.0	Gypsum	Strauss, 1993

3300	7.5	Gypsum	Strauss, 1993
3300	5.4	Gypsum	Strauss, 1993
2300	12.4	Gypsum	Strauss, 1993
2300	15.6	Gypsum	Strauss, 1993
2300	13.7	Gypsum	Strauss, 1993
1800	17.1	Gypsum	Strauss, 1993
1800	21.2	Gypsum	Strauss, 1993
1800	18.8	Gypsum	Strauss, 1993
1800	1.5	Gypsum	Strauss, 1993
1800	15.0	Gypsum	Strauss, 1993
1800	10.9	Gypsum	Strauss, 1993
1650	18.4	Gypsum	Strauss, 1993
1650	24.7	Gypsum	Strauss, 1993
1650	19.9	Gypsum	Strauss, 1993
1650	19.0	Gypsum	Strauss, 1993
1650	32.0	Gypsum	Strauss, 1993
1650	26.3	Gypsum	Strauss, 1993
1350	13.6	Gypsum	Strauss, 1993
1350	18.3	Gypsum	Strauss, 1993
1350	15.4	Gypsum	Strauss, 1993
1250	15.5	Gypsum	Strauss, 1993
1250	19.8	Gypsum	Strauss, 1993
1250	17.7	Gypsum	Strauss, 1993
1100	15.8	Gypsum	Strauss, 1993
1100	21.0	Gypsum	Strauss, 1993
1100	18.6	Gypsum	Strauss, 1993
1100	13.0	Gypsum	Strauss, 1993
1100	21.0	Gypsum	Strauss, 1993
1100	16.6	Gypsum	Strauss, 1993
1100	20.3	Gypsum	Strauss, 1993
1100	21.0	Gypsum	Strauss, 1993
1100	20.7	Gypsum	Strauss, 1993
1100	14.5	Gypsum	Strauss, 1993
1100	28.6	Gypsum	Strauss, 1993
1100	21.2	Gypsum	Strauss, 1993
1100	4.2	Gypsum	Strauss, 1993
1100	30.2	Gypsum	Strauss, 1993
1100	18.3	Gypsum	Strauss, 1993
1100	21.0	Gypsum	Strauss, 1993
1100	19.6	Gypsum	Strauss, 1993
650	29.6	Gypsum	Strauss, 1993
590	27.6	Gypsum	Strauss, 1993
550	30.8	Gypsum	Strauss et al., 2001
550	33.4	Gypsum	Strauss et al., 2001
550	33.4	Gypsum	Strauss et al., 2001
550	32.5	Gypsum	Strauss et al., 2001
550	31.2	Gypsum	Strauss et al., 2001
550	29.5	Gypsum	Strauss et al., 2001
550	34.2	Gypsum	Strauss et al., 2001
550	35.6	Gypsum	Strauss et al., 2001
550	30.6	Gypsum	Strauss et al., 2001
550	27.5	Gypsum	Strauss et al., 2001
550	34.9	Gypsum	Strauss et al., 2001
550	34.6	Gypsum	Strauss et al., 2001
550	34.1	Gypsum	Strauss et al., 2001
550	29.8	Gypsum	Strauss et al., 2001
550	28.0	Gypsum	Strauss et al., 2001
550	39.7	Gypsum	Strauss et al., 2001
550	34.2	Gypsum	Strauss et al., 2001
550	34.8	Gypsum	Strauss et al., 2001
550	34.4	Gypsum	Strauss et al., 2001
550	35.4	Gypsum	Strauss et al., 2001
550	33.9	Gypsum	Strauss et al., 2001
550	35.2	Gypsum	Strauss et al., 2001
550	29.0	Gypsum	Strauss et al., 2001
550	28.7	Gypsum	Strauss et al., 2001
550	29.7	Gypsum	Strauss et al., 2001
5	20.2	CAS	Strauss, 1999
15	22.1	CAS	Strauss, 1999
25	16.5	CAS	Strauss, 1999
35	21.5	CAS	Strauss, 1999

45	19.8	CAS	Strauss, 1999
55	17.2	CAS	Strauss, 1999
65	18.2	CAS	Strauss, 1999
75	16.2	CAS	Strauss, 1999
85	18.2	CAS	Strauss, 1999
95	15.0	CAS	Strauss, 1999
105	15.6	CAS	Strauss, 1999
115	14.5	CAS	Strauss, 1999
125	15.6	CAS	Strauss, 1999
135	15.5	CAS	Strauss, 1999
155	17.1	CAS	Strauss, 1999
175	16.8	CAS	Strauss, 1999
195	11.7	CAS	Strauss, 1999
205	11.8	CAS	Strauss, 1999
225	16.4	CAS	Strauss, 1999
235	17.1	CAS	Strauss, 1999
245	25.9	CAS	Strauss, 1999
255	10.9	CAS	Strauss, 1999
265	12.4	CAS	Strauss, 1999
305	14.6	CAS	Strauss, 1999
315	15.8	CAS	Strauss, 1999
345	15.9	CAS	Strauss, 1999
365	27.6	CAS	Strauss, 1999
375	20.5	CAS	Strauss, 1999
385	20.2	CAS	Strauss, 1999
395	19.7	CAS	Strauss, 1999
415	28.2	CAS	Strauss, 1999
425	24.8	CAS	Strauss, 1999
455	25.4	CAS	Strauss, 1999
475	24.1	CAS	Strauss, 1999
535	30.3	CAS	Strauss, 1999
2260	11.4	Gypsum	Taylor 1970
2260	16.0	Gypsum	Taylor 1970
491	19.1	CAS	Thompson and Kah, 2012
490.7	16.3	CAS	Thompson and Kah, 2012
490.4	17.0	CAS	Thompson and Kah, 2012
490	11.6	CAS	Thompson and Kah, 2012
489.8	13.4	CAS	Thompson and Kah, 2012
489.5	11.0	CAS	Thompson and Kah, 2012
489.1	16.1	CAS	Thompson and Kah, 2012
488.9	11.2	CAS	Thompson and Kah, 2012
488.5	13.9	CAS	Thompson and Kah, 2012
488.2	17.3	CAS	Thompson and Kah, 2012
487.9	10.1	CAS	Thompson and Kah, 2012
487.6	18.8	CAS	Thompson and Kah, 2012
487.1	17.9	CAS	Thompson and Kah, 2012
486.8	18.7	CAS	Thompson and Kah, 2012
486.2	15.6	CAS	Thompson and Kah, 2012
485.9	17.4	CAS	Thompson and Kah, 2012
485.6	11.7	CAS	Thompson and Kah, 2012
485.3	19.9	CAS	Thompson and Kah, 2012
485	18.5	CAS	Thompson and Kah, 2012
484.6	13.1	CAS	Thompson and Kah, 2012
484	19.5	CAS	Thompson and Kah, 2012
483.7	12.2	CAS	Thompson and Kah, 2012
483.4	15.3	CAS	Thompson and Kah, 2012
483.1	14.9	CAS	Thompson and Kah, 2012
482.8	17.3	CAS	Thompson and Kah, 2012
482.5	17.0	CAS	Thompson and Kah, 2012
482.2	20.1	CAS	Thompson and Kah, 2012
481.9	19.0	CAS	Thompson and Kah, 2012
481.6	13.4	CAS	Thompson and Kah, 2012
481.3	19.8	CAS	Thompson and Kah, 2012
481	18.3	CAS	Thompson and Kah, 2012
480.8	16.6	CAS	Thompson and Kah, 2012
480.5	16.6	CAS	Thompson and Kah, 2012
480.2	15.0	CAS	Thompson and Kah, 2012
479.9	15.7	CAS	Thompson and Kah, 2012
479.6	15.6	CAS	Thompson and Kah, 2012
479.3	12.3	CAS	Thompson and Kah, 2012
479	15.3	CAS	Thompson and Kah, 2012

479	15.3	CAS	Thompson and Kah, 2012
478.8	17.1	CAS	Thompson and Kah, 2012
478.6	18.3	CAS	Thompson and Kah, 2012
478.4	23.5	CAS	Thompson and Kah, 2012
478.1	19.6	CAS	Thompson and Kah, 2012
477.9	19.0	CAS	Thompson and Kah, 2012
477.7	21.7	CAS	Thompson and Kah, 2012
477.5	23.3	CAS	Thompson and Kah, 2012
477.2	14.9	CAS	Thompson and Kah, 2012
477	21.2	CAS	Thompson and Kah, 2012
476.8	25.3	CAS	Thompson and Kah, 2012
476.6	23.8	CAS	Thompson and Kah, 2012
476.4	24.5	CAS	Thompson and Kah, 2012
476.2	20.2	CAS	Thompson and Kah, 2012
476	23.9	CAS	Thompson and Kah, 2012
475.8	6.6	CAS	Thompson and Kah, 2012
475.7	26.5	CAS	Thompson and Kah, 2012
475.5	26.6	CAS	Thompson and Kah, 2012
475.3	25.5	CAS	Thompson and Kah, 2012
475.1	20.7	CAS	Thompson and Kah, 2012
474.9	22.0	CAS	Thompson and Kah, 2012
474.7	27.6	CAS	Thompson and Kah, 2012
474.4	23.8	CAS	Thompson and Kah, 2012
474.2	6.1	CAS	Thompson and Kah, 2012
474	21.5	CAS	Thompson and Kah, 2012
473.8	26.7	CAS	Thompson and Kah, 2012
473.6	25.0	CAS	Thompson and Kah, 2012
473.4	6.1	CAS	Thompson and Kah, 2012
473.2	22.5	CAS	Thompson and Kah, 2012
473	23.7	CAS	Thompson and Kah, 2012
472.7	26.3	CAS	Thompson and Kah, 2012
472.5	22.2	CAS	Thompson and Kah, 2012
472.3	15.5	CAS	Thompson and Kah, 2012
472	20.2	CAS	Thompson and Kah, 2012
471.8	17.1	CAS	Thompson and Kah, 2012
471.6	24.2	CAS	Thompson and Kah, 2012
471.4	16.8	CAS	Thompson and Kah, 2012
471.2	19.7	CAS	Thompson and Kah, 2012
471	23.7	CAS	Thompson and Kah, 2012
470.7	5.6	CAS	Thompson and Kah, 2012
470.5	19.7	CAS	Thompson and Kah, 2012
470.3	19.6	CAS	Thompson and Kah, 2012
470.1	15.6	CAS	Thompson and Kah, 2012
469.8	19.4	CAS	Thompson and Kah, 2012
469.6	16.4	CAS	Thompson and Kah, 2012
469.4	19.4	CAS	Thompson and Kah, 2012
469.2	16.8	CAS	Thompson and Kah, 2012
469	13.5	CAS	Thompson and Kah, 2012
471.2	25.1	CAS	Thompson and Kah, 2012
471	25.0	CAS	Thompson and Kah, 2012
470.7	27.1	CAS	Thompson and Kah, 2012
470.7	23.6	CAS	Thompson and Kah, 2012
470.7	20.9	CAS	Thompson and Kah, 2012
470.7	21.5	CAS	Thompson and Kah, 2012
470.6	20.6	CAS	Thompson and Kah, 2012
470.3	24.4	CAS	Thompson and Kah, 2012
470.1	26.2	CAS	Thompson and Kah, 2012
469.9	25.8	CAS	Thompson and Kah, 2012
469.7	23.2	CAS	Thompson and Kah, 2012
469.4	23.7	CAS	Thompson and Kah, 2012
469.2	21.1	CAS	Thompson and Kah, 2012
468.9	13.9	CAS	Thompson and Kah, 2012
468.7	27.1	CAS	Thompson and Kah, 2012
468.4	23.5	CAS	Thompson and Kah, 2012
468.2	21.9	CAS	Thompson and Kah, 2012
467.9	19.0	CAS	Thompson and Kah, 2012
467.8	19.6	CAS	Thompson and Kah, 2012
472.7	6.1	CAS	Thompson and Kah, 2012
471.7	6.2	CAS	Thompson and Kah, 2012
471.5	5.8	CAS	Thompson and Kah, 2012
471.3	6.0	CAS	Thompson and Kah, 2012
471	6.0	CAS	Thompson and Kah, 2012

470.8	6.0	CAS	Thompson and Kah, 2012
470.6	5.9	CAS	Thompson and Kah, 2012
470.4	5.7	CAS	Thompson and Kah, 2012
470.1	5.8	CAS	Thompson and Kah, 2012
469.9	6.0	CAS	Thompson and Kah, 2012
469.7	6.2	CAS	Thompson and Kah, 2012
469.5	5.9	CAS	Thompson and Kah, 2012
469.3	5.8	CAS	Thompson and Kah, 2012
469.1	22.1	CAS	Thompson and Kah, 2012
468.9	20.1	CAS	Thompson and Kah, 2012
468.6	19.1	CAS	Thompson and Kah, 2012
468.4	18.3	CAS	Thompson and Kah, 2012
468.2	15.3	CAS	Thompson and Kah, 2012
468	13.0	CAS	Thompson and Kah, 2012
467.8	23.0	CAS	Thompson and Kah, 2012
467.6	23.7	CAS	Thompson and Kah, 2012
467.3	25.7	CAS	Thompson and Kah, 2012
467.1	22.8	CAS	Thompson and Kah, 2012
466.9	22.2	CAS	Thompson and Kah, 2012
477.1	7.0	CAS	Thompson and Kah, 2012
477	7.0	CAS	Thompson and Kah, 2012
477	6.8	CAS	Thompson and Kah, 2012
476.9	7.0	CAS	Thompson and Kah, 2012
476.8	6.9	CAS	Thompson and Kah, 2012
476.7	7.2	CAS	Thompson and Kah, 2012
476.6	7.3	CAS	Thompson and Kah, 2012
476.5	6.9	CAS	Thompson and Kah, 2012
476.4	6.9	CAS	Thompson and Kah, 2012
476.3	6.9	CAS	Thompson and Kah, 2012
476.3	7.2	CAS	Thompson and Kah, 2012
476.2	7.0	CAS	Thompson and Kah, 2012
476.2	7.1	CAS	Thompson and Kah, 2012
476.1	7.1	CAS	Thompson and Kah, 2012
476	6.7	CAS	Thompson and Kah, 2012
475.9	7.2	CAS	Thompson and Kah, 2012
475.8	7.0	CAS	Thompson and Kah, 2012
475.7	6.8	CAS	Thompson and Kah, 2012
475.6	6.9	CAS	Thompson and Kah, 2012
475.5	7.0	CAS	Thompson and Kah, 2012
475.5	6.6	CAS	Thompson and Kah, 2012
475.4	6.7	CAS	Thompson and Kah, 2012
475.3	6.6	CAS	Thompson and Kah, 2012
475.2	6.4	CAS	Thompson and Kah, 2012
475.1	6.2	CAS	Thompson and Kah, 2012
475	6.5	CAS	Thompson and Kah, 2012
474.9	7.0	CAS	Thompson and Kah, 2012
474.8	6.7	CAS	Thompson and Kah, 2012
474.8	7.0	CAS	Thompson and Kah, 2012
474.7	7.1	CAS	Thompson and Kah, 2012
474.6	7.0	CAS	Thompson and Kah, 2012
474.5	7.0	CAS	Thompson and Kah, 2012
474.4	7.3	CAS	Thompson and Kah, 2012
474.3	7.7	CAS	Thompson and Kah, 2012
474.2	9.6	CAS	Thompson and Kah, 2012
474.1	10.8	CAS	Thompson and Kah, 2012
474.1	14.3	CAS	Thompson and Kah, 2012
473.6	28.7	CAS	Thompson and Kah, 2012
473.3		CAS	Thompson and Kah, 2012
473.1	30.9	CAS	Thompson and Kah, 2012
473	24.8	CAS	Thompson and Kah, 2012
472.7	32.9	CAS	Thompson and Kah, 2012
472.5	31.3	CAS	Thompson and Kah, 2012
472.2	27.4	CAS	Thompson and Kah, 2012
472	33.7	CAS	Thompson and Kah, 2012
471.8	25.0	CAS	Thompson and Kah, 2012
471.8	30.9	CAS	Thompson and Kah, 2012
471.6	29.2	CAS	Thompson and Kah, 2012
471.3	29.9	CAS	Thompson and Kah, 2012
471.1	33.0	CAS	Thompson and Kah, 2012
470.9	29.4	CAS	Thompson and Kah, 2012
470.6	24.6	CAS	Thompson and Kah, 2012
470.4	29.8	CAS	Thompson and Kah, 2012

470.2	28.9	CAS	Thompson and Kah, 2012
469.9	25.0	CAS	Thompson and Kah, 2012
469.7	28.2	CAS	Thompson and Kah, 2012
469.4	33.6	CAS	Thompson and Kah, 2012
469.2	30.0	CAS	Thompson and Kah, 2012
468.9	38.6	CAS	Thompson and Kah, 2012
468.7	17.1	CAS	Thompson and Kah, 2012
468.5	26.8	CAS	Thompson and Kah, 2012
468.3	31.8	CAS	Thompson and Kah, 2012
468	31.6	CAS	Thompson and Kah, 2012
467.8	29.0	CAS	Thompson and Kah, 2012
467.5	29.2	CAS	Thompson and Kah, 2012
467.3	32.9	CAS	Thompson and Kah, 2012
467.1	29.9	CAS	Thompson and Kah, 2012
466.8		CAS	Thompson and Kah, 2012
466.5	19.2	CAS	Thompson and Kah, 2012
466.1	21.8	CAS	Thompson and Kah, 2012
465.8	2.6	CAS	Thompson and Kah, 2012
465.6	18.5	CAS	Thompson and Kah, 2012
465.4	12.2	CAS	Thompson and Kah, 2012
465.1	21.8	CAS	Thompson and Kah, 2012
464.9	13.3	CAS	Thompson and Kah, 2012
464.7	15.6	CAS	Thompson and Kah, 2012
464.5	21.1	CAS	Thompson and Kah, 2012
464.2	18.2	CAS	Thompson and Kah, 2012
464	20.7	CAS	Thompson and Kah, 2012
463.8	9.7	CAS	Thompson and Kah, 2012
547	33.1	CAS	Tostevin et al., 2017
547	29.0	CAS	Tostevin et al., 2017
547	24.2	CAS	Tostevin et al., 2017
547	29.5	CAS	Tostevin et al., 2017
547	39.3	CAS	Tostevin et al., 2017
547	27.8	CAS	Tostevin et al., 2017
547	27.5	CAS	Tostevin et al., 2017
547	29.2	CAS	Tostevin et al., 2017
547	21.9	CAS	Tostevin et al., 2017
547	32.8	CAS	Tostevin et al., 2017
547	36.7	CAS	Tostevin et al., 2017
547	35.0	CAS	Tostevin et al., 2017
547	40.1	CAS	Tostevin et al., 2017
547	38.3	CAS	Tostevin et al., 2017
547	29.5	CAS	Tostevin et al., 2017
547	31.6	CAS	Tostevin et al., 2017
547	32.1	CAS	Tostevin et al., 2017
547	28.4	CAS	Tostevin et al., 2017
547	30.0	CAS	Tostevin et al., 2017
547	32.2	CAS	Tostevin et al., 2017
547	34.6	CAS	Tostevin et al., 2017
547	29.8	CAS	Tostevin et al., 2017
547	39.9	CAS	Tostevin et al., 2017
547	33.2	CAS	Tostevin et al., 2017
547	26.3	CAS	Tostevin et al., 2017
547	32.3	CAS	Tostevin et al., 2017
547	33.9	CAS	Tostevin et al., 2017
547	31.4	CAS	Tostevin et al., 2017
547	30.7	CAS	Tostevin et al., 2017
547	33.7	CAS	Tostevin et al., 2017
547	26.8	CAS	Tostevin et al., 2017
547	38.9	CAS	Tostevin et al., 2017
547	38.7	CAS	Tostevin et al., 2017
547	41.4	CAS	Tostevin et al., 2017
547	35.6	CAS	Tostevin et al., 2017
547	27.2	CAS	Tostevin et al., 2017
547	35.9	CAS	Tostevin et al., 2017
547	37.1	CAS	Tostevin et al., 2017
547	39.3	CAS	Tostevin et al., 2017
547	41.5	CAS	Tostevin et al., 2017
547	39.1	CAS	Tostevin et al., 2017
547	43.1	CAS	Tostevin et al., 2017
547	42.7	CAS	Tostevin et al., 2017
547	37.4	CAS	Tostevin et al., 2017

547		37.5		CAS	Tostevin et al., 2017
547		45.4		CAS	Tostevin et al., 2017
547		33.4		CAS	Tostevin et al., 2017
547		37.2		CAS	Tostevin et al., 2017
547		39.9		CAS	Tostevin et al., 2017
547		38.9		CAS	Tostevin et al., 2017
547		29.7		CAS	Tostevin et al., 2017
0		21.8	0.05	Seawater	Tostevin et al., 2014
0		20.2	0.05	Seawater	Tostevin et al., 2014
0		21.3	0.05	Seawater	Tostevin et al., 2014
0		21.4	0.05	Seawater	Tostevin et al., 2014
0		21.3	0.05	Seawater	Tostevin et al., 2014
0		21.2	0.05	Seawater	Tostevin et al., 2014
0		21.5	0.06	Seawater	Tostevin et al., 2014
0		21.0	0.06	Seawater	Tostevin et al., 2014
0		21.2	0.06	Seawater	Tostevin et al., 2014
0		21.1	0.05	Seawater	Tostevin et al., 2014
0		21.6	0.05	Seawater	Tostevin et al., 2014
0		21.0	0.05	Seawater	Tostevin et al., 2014
0		21.6	0.06	Seawater	Tostevin et al., 2014
0		22.1	0.05	Seawater	Tostevin et al., 2014
0		21.1	0.03	Seawater	Tostevin et al., 2014
0		21.5	0.04	Seawater	Tostevin et al., 2014
0		21.7	0.06	Seawater	Tostevin et al., 2014
0		22.1	0.04	Seawater	Tostevin et al., 2014
0		20.5	0.05	Seawater	Tostevin et al., 2014
0		21.1	0.06	Seawater	Tostevin et al., 2014
0		20.4	0.06	Seawater	Tostevin et al., 2014
0		21.4	0.05	Seawater	Tostevin et al., 2014
0		21.2	0.05	Seawater	Tostevin et al., 2014
0		21.1	0.05	Seawater	Tostevin et al., 2014
0		21.0	0.05	Seawater	Tostevin et al., 2014
0		21.1	0.04	Seawater	Tostevin et al., 2014
0		21.4	0.05	Seawater	Tostevin et al., 2014
0		21.1	0.04	Seawater	Tostevin et al., 2014
0.1	7.7			Barite	Turchyn and Schrag, 2004
0.1	7.9			Barite	Turchyn and Schrag, 2004
0.1	7.3			Barite	Turchyn and Schrag, 2004
0.1	8.8			Barite	Turchyn and Schrag, 2004
0.5	7.8			Barite	Turchyn and Schrag, 2004
0.03	7.7			Barite	Turchyn and Schrag, 2004
0.03	8.4			Barite	Turchyn and Schrag, 2004
0.9	8.6			Barite	Turchyn and Schrag, 2004
0.9	10.2			Barite	Turchyn and Schrag, 2004
0.9	10.5			Barite	Turchyn and Schrag, 2004
2.3	13.0			Barite	Turchyn and Schrag, 2004
2.3	13.2			Barite	Turchyn and Schrag, 2004
2.3	13.5			Barite	Turchyn and Schrag, 2004
2.3	13.7			Barite	Turchyn and Schrag, 2004
2.7	12.1			Barite	Turchyn and Schrag, 2004
2.7	12.4			Barite	Turchyn and Schrag, 2004
2.7	14.2			Barite	Turchyn and Schrag, 2004
2.7	14.7			Barite	Turchyn and Schrag, 2004
2.7	13.3			Barite	Turchyn and Schrag, 2004
2.3	11.2			Barite	Turchyn and Schrag, 2004
2.3	12.8			Barite	Turchyn and Schrag, 2004
2.3	13.5			Barite	Turchyn and Schrag, 2004
2.3	14.0			Barite	Turchyn and Schrag, 2004
2.3	14.1			Barite	Turchyn and Schrag, 2004
3.88	10.9			Barite	Turchyn and Schrag, 2004
3.88	11.1			Barite	Turchyn and Schrag, 2004
3.88	11.5			Barite	Turchyn and Schrag, 2004
5.69	10.0			Barite	Turchyn and Schrag, 2004
5.69	10.6			Barite	Turchyn and Schrag, 2004
8.2	9.9			Barite	Turchyn and Schrag, 2004
8.2	10.0			Barite	Turchyn and Schrag, 2004
8.2	10.1			Barite	Turchyn and Schrag, 2004
3.12	12.5			Barite	Turchyn and Schrag, 2004
3.12	13.0			Barite	Turchyn and Schrag, 2004
4	11.6			Barite	Turchyn and Schrag, 2004
4	11.8			Barite	Turchyn and Schrag, 2004

4	11.9	Barite	Turchyn and Schrag, 2004
4	12.1	Barite	Turchyn and Schrag, 2004
4.2	10.5	Barite	Turchyn and Schrag, 2004
4.2	10.5	Barite	Turchyn and Schrag, 2004
4.2	10.6	Barite	Turchyn and Schrag, 2004
4.2	11.0	Barite	Turchyn and Schrag, 2004
4.6	10.9	Barite	Turchyn and Schrag, 2004
4.6	11.4	Barite	Turchyn and Schrag, 2004
4.6	11.4	Barite	Turchyn and Schrag, 2004
4.6	11.8	Barite	Turchyn and Schrag, 2004
5.2	9.2	Barite	Turchyn and Schrag, 2004
5.2	9.7	Barite	Turchyn and Schrag, 2004
5.2	9.7	Barite	Turchyn and Schrag, 2004
5.4	9.3	Barite	Turchyn and Schrag, 2004
5.4	9.4	Barite	Turchyn and Schrag, 2004
5.4	9.6	Barite	Turchyn and Schrag, 2004
5.6	8.4	Barite	Turchyn and Schrag, 2004
5.6	8.7	Barite	Turchyn and Schrag, 2004
5.6	9.3	Barite	Turchyn and Schrag, 2004
0.03	8.1	Barite	Turchyn and Schrag, 2004
1	10.2	Barite	Turchyn and Schrag, 2004
1	10.3	Barite	Turchyn and Schrag, 2004
1	10.3	Barite	Turchyn and Schrag, 2004
1	10.4	Barite	Turchyn and Schrag, 2004
1.2	8.9	Barite	Turchyn and Schrag, 2004
1.2	9.0	Barite	Turchyn and Schrag, 2004
1.2	9.4	Barite	Turchyn and Schrag, 2004
1.4	9.3	Barite	Turchyn and Schrag, 2004
1.4	9.5	Barite	Turchyn and Schrag, 2004
1.4	9.6	Barite	Turchyn and Schrag, 2004
1.6	10.1	Barite	Turchyn and Schrag, 2004
1.6	10.3	Barite	Turchyn and Schrag, 2004
2.4	13.9	Barite	Turchyn and Schrag, 2004
2.4	14.0	Barite	Turchyn and Schrag, 2004
2.4	14.1	Barite	Turchyn and Schrag, 2004
0.9	10.1	Barite	Turchyn and Schrag, 2004
0.9	10.7	Barite	Turchyn and Schrag, 2004
0.9	9.7	Barite	Turchyn and Schrag, 2004
0.9	9.8	Barite	Turchyn and Schrag, 2004
0.9	9.9	Barite	Turchyn and Schrag, 2004
0.9	10.1	Barite	Turchyn and Schrag, 2004
0.9	10.1	Barite	Turchyn and Schrag, 2004
0.9	10.2	Barite	Turchyn and Schrag, 2004
0.9	10.5	Barite	Turchyn and Schrag, 2004
0.9	10.7	Barite	Turchyn and Schrag, 2004
1.3	8.8	Barite	Turchyn and Schrag, 2004
1.3	9.2	Barite	Turchyn and Schrag, 2004
1.5	10.1	Barite	Turchyn and Schrag, 2004
1.5	10.3	Barite	Turchyn and Schrag, 2004
1.5	11.4	Barite	Turchyn and Schrag, 2004
1.7	10.6	Barite	Turchyn and Schrag, 2004
1.7	11.8	Barite	Turchyn and Schrag, 2004
3.5	11.1	Barite	Turchyn and Schrag, 2004
3.5	11.3	Barite	Turchyn and Schrag, 2004
3.5	11.4	Barite	Turchyn and Schrag, 2004
3.8	10.1	Barite	Turchyn and Schrag, 2004
3.8	10.1	Barite	Turchyn and Schrag, 2004
3.8	10.2	Barite	Turchyn and Schrag, 2004
3.9	11.3	Barite	Turchyn and Schrag, 2004
4.1	9.0	Barite	Turchyn and Schrag, 2004
4.1	9.6	Barite	Turchyn and Schrag, 2004
4.1	9.8	Barite	Turchyn and Schrag, 2004
4.3	10.8	Barite	Turchyn and Schrag, 2004
4.3	11.0	Barite	Turchyn and Schrag, 2004
4.3	11.3	Barite	Turchyn and Schrag, 2004
4.4	9.0	Barite	Turchyn and Schrag, 2004
4.4	9.2	Barite	Turchyn and Schrag, 2004
4.4	9.3	Barite	Turchyn and Schrag, 2004
4.7	9.8	Barite	Turchyn and Schrag, 2004
4.9	11.2	Barite	Turchyn and Schrag, 2004
4.9	11.3	Barite	Turchyn and Schrag, 2004
4.9	11.9	Barite	Turchyn and Schrag, 2004

5.1	10.0		Barite	Turchyn and Schrag, 2004
5.1	10.4		Barite	Turchyn and Schrag, 2004
5.1	10.4		Barite	Turchyn and Schrag, 2004
5.3	9.8		Barite	Turchyn and Schrag, 2004
5.3	9.8		Barite	Turchyn and Schrag, 2004
5.3	10.1		Barite	Turchyn and Schrag, 2004
5.5	9.7		Barite	Turchyn and Schrag, 2004
5.5	10.4		Barite	Turchyn and Schrag, 2004
5.5	10.5		Barite	Turchyn and Schrag, 2004
5.5	11.4		Barite	Turchyn and Schrag, 2004
5.7	8.9		Barite	Turchyn and Schrag, 2004
5.7	9.4		Barite	Turchyn and Schrag, 2004
5.7	9.4		Barite	Turchyn and Schrag, 2004
5.9	9.2		Barite	Turchyn and Schrag, 2004
5.9	9.6		Barite	Turchyn and Schrag, 2004
5.9	10.1		Barite	Turchyn and Schrag, 2004
6.2	8.8		Barite	Turchyn and Schrag, 2004
6.2	8.9		Barite	Turchyn and Schrag, 2004
6.2	9.3		Barite	Turchyn and Schrag, 2004
6.5	8.1		Barite	Turchyn and Schrag, 2004
6.5	8.5		Barite	Turchyn and Schrag, 2004
6.5	8.7		Barite	Turchyn and Schrag, 2004
6.8	8.7		Barite	Turchyn and Schrag, 2004
6.8	9.1		Barite	Turchyn and Schrag, 2004
6.8	9.7		Barite	Turchyn and Schrag, 2004
7.1	9.0		Barite	Turchyn and Schrag, 2004
7.1	9.2		Barite	Turchyn and Schrag, 2004
7.1	9.4		Barite	Turchyn and Schrag, 2004
7.4	9.3		Barite	Turchyn and Schrag, 2004
7.4	10.2		Barite	Turchyn and Schrag, 2004
7.4	11.0		Barite	Turchyn and Schrag, 2004
8.8	8.9		Barite	Turchyn and Schrag, 2004
8.8	9.6		Barite	Turchyn and Schrag, 2004
8.8	9.9		Barite	Turchyn and Schrag, 2004
0.55	7.9		Barite	Turchyn and Schrag, 2004
0.55	7.9		Barite	Turchyn and Schrag, 2004
0.55	8.0		Barite	Turchyn and Schrag, 2004
3.5	13.8		Barite	Turchyn and Schrag, 2004
5.45	8.9		Barite	Turchyn and Schrag, 2004
5.45	8.9		Barite	Turchyn and Schrag, 2004
1.2	10.0		Barite	Turchyn and Schrag, 2004
1.2	10.1		Barite	Turchyn and Schrag, 2004
1.2	10.3		Barite	Turchyn and Schrag, 2004
1.2	10.5		Barite	Turchyn and Schrag, 2004
1.9	10.7		Barite	Turchyn and Schrag, 2004
1.9	11.6		Barite	Turchyn and Schrag, 2004
1.9	11.7		Barite	Turchyn and Schrag, 2004
1.9	11.8		Barite	Turchyn and Schrag, 2004
1.9	11.9		Barite	Turchyn and Schrag, 2004
1.9	12.0		Barite	Turchyn and Schrag, 2004
1.9	12.5		Barite	Turchyn and Schrag, 2004
46.01		20.7	CAS	Turchyn et al., 2009
54.13		18.9	CAS	Turchyn et al., 2009
55.18		18.7	CAS	Turchyn et al., 2009
55.83		19.5	CAS	Turchyn et al., 2009
55.97		18.6	CAS	Turchyn et al., 2009
56.22		19.1	CAS	Turchyn et al., 2009
56.43		19.3	CAS	Turchyn et al., 2009
56.91		19.9	CAS	Turchyn et al., 2009
59.05		20.0	CAS	Turchyn et al., 2009
46.34		21.1	CAS	Turchyn et al., 2009
41.04		20.8	CAS	Turchyn et al., 2009
43.14		20.9	CAS	Turchyn et al., 2009
33.5		21.5	CAS	Turchyn et al., 2009
34		21.2	CAS	Turchyn et al., 2009
34.5		21.4	CAS	Turchyn et al., 2009
103		19.7	CAS	Turchyn et al., 2009
102		17.0	CAS	Turchyn et al., 2009
101		18.0	CAS	Turchyn et al., 2009
100		18.1	CAS	Turchyn et al., 2009
93.4		19.0	CAS	Turchyn et al., 2009

93.1		18.3	CAS	Turchyn et al., 2009
100		11.9	CAS	Turchyn et al., 2009
83.9		22.4	CAS	Turchyn et al., 2009
116		13.2	CAS	Turchyn et al., 2009
122.81		16.6	CAS	Turchyn et al., 2009
126.65		24.5	CAS	Turchyn et al., 2009
129.17		16.5	CAS	Turchyn et al., 2009
68.65		21.1	CAS	Turchyn et al., 2009
74.4		21.4	CAS	Turchyn et al., 2009
83.7		21.2	CAS	Turchyn et al., 2009
83.9		19.9	CAS	Turchyn et al., 2009
85.6		20.7	CAS	Turchyn et al., 2009
95		19.6	CAS	Turchyn et al., 2009
110		20.8	CAS	Turchyn et al., 2009
112		11.1	CAS	Turchyn et al., 2009
119.6		18.2	CAS	Turchyn et al., 2009
116.5		18.6	CAS	Turchyn et al., 2009
120		13.4	CAS	Turchyn et al., 2009
125		-16.1	CAS	Turchyn et al., 2009
				Turchyn et al., 2009
46.01		20.1	Barite	Turchyn et al., 2009
54.13		16.9	Barite	Turchyn et al., 2009
55.18		16.8	Barite	Turchyn et al., 2009
55.83		17.0	Barite	Turchyn et al., 2009
55.97		17.2	Barite	Turchyn et al., 2009
56.22		17.5	Barite	Turchyn et al., 2009
56.43		17.6	Barite	Turchyn et al., 2009
56.91		17.4	Barite	Turchyn et al., 2009
59.05		17.8	Barite	Turchyn et al., 2009
46.34		20.1	Barite	Turchyn et al., 2009
41.04		20.9	Barite	Turchyn et al., 2009
43.14		20.3	Barite	Turchyn et al., 2009
33.5		20.4	Barite	Turchyn et al., 2009
34		20.3	Barite	Turchyn et al., 2009
34.5		20.6	Barite	Turchyn et al., 2009
103		15.5	Barite	Turchyn et al., 2009
102		15.4	Barite	Turchyn et al., 2009
101		15.7	Barite	Turchyn et al., 2009
100		17.0	Barite	Turchyn et al., 2009
93.4		17.7	Barite	Turchyn et al., 2009
93.1		17.3	Barite	Turchyn et al., 2009
100		15.5	Barite	Turchyn et al., 2009
83.9		18.5	Barite	Turchyn et al., 2009
116		15.7	Barite	Turchyn et al., 2009
122.81		18.9	Barite	Turchyn et al., 2009
126.65		19.7	Barite	Turchyn et al., 2009
129.17		20.0	Barite	Turchyn et al., 2009
68.65		18.9	Barite	Turchyn et al., 2009
74.4		19.2	Barite	Turchyn et al., 2009
83.7		18.2	Barite	Turchyn et al., 2009
83.9		17.9	Barite	Turchyn et al., 2009
85.6		18.2	Barite	Turchyn et al., 2009
95		18.2	Barite	Turchyn et al., 2009
110		14.6	Barite	Turchyn et al., 2009
112		14.2	Barite	Turchyn et al., 2009
119.6		14.9	Barite	Turchyn et al., 2009
116.5		14.8	Barite	Turchyn et al., 2009
120		15.9	Barite	Turchyn et al., 2009
125		19.4	Barite	Turchyn et al., 2009
				Turchyn et al., 2009
118.77	16.3		CAS	Turchyn et al., 2009
117.68	15.3		CAS	Turchyn et al., 2009
116.55	14.4		CAS	Turchyn et al., 2009
115.48	14.6		CAS	Turchyn et al., 2009
114.55	0.5		CAS	Turchyn et al., 2009
110.89	13.2		CAS	Turchyn et al., 2009
110.55	4.9		CAS	Turchyn et al., 2009
110.12	9.9		CAS	Turchyn et al., 2009
109.56	10.5		CAS	Turchyn et al., 2009
109.03	16.8		CAS	Turchyn et al., 2009
108.57	13.9		CAS	Turchyn et al., 2009
107.4	12.1		CAS	Turchyn et al., 2009

106.84	15.3	CAS	Turchyn et al., 2009
106.21	15.4	CAS	Turchyn et al., 2009
105.39	14.5	CAS	Turchyn et al., 2009
105.19	16.4	CAS	Turchyn et al., 2009
104.49	13.7	CAS	Turchyn et al., 2009
104	16.9	CAS	Turchyn et al., 2009
103.42	17.8	CAS	Turchyn et al., 2009
102.85	17.0	CAS	Turchyn et al., 2009
102.63	13.8	CAS	Turchyn et al., 2009
102.4	17.4	CAS	Turchyn et al., 2009
102.27	14.6	CAS	Turchyn et al., 2009
102.05	13.7	CAS	Turchyn et al., 2009
101.83	18.0	CAS	Turchyn et al., 2009
101.75	17.2	CAS	Turchyn et al., 2009
101.66	16.7	CAS	Turchyn et al., 2009
101.57	15.3	CAS	Turchyn et al., 2009
101.44	16.5	CAS	Turchyn et al., 2009
101.36	14.8	CAS	Turchyn et al., 2009
101.27	15.4	CAS	Turchyn et al., 2009
101.19	16.2	CAS	Turchyn et al., 2009
101.03	14.8	CAS	Turchyn et al., 2009
100.91	15.9	CAS	Turchyn et al., 2009
100.63	16.2	CAS	Turchyn et al., 2009
100.42	16.8	CAS	Turchyn et al., 2009
100.11	15.7	CAS	Turchyn et al., 2009
99.97	15.4	CAS	Turchyn et al., 2009
99.83	16.3	CAS	Turchyn et al., 2009
99.58	16.2	CAS	Turchyn et al., 2009
99.44	15.4	CAS	Turchyn et al., 2009
99.38	16.3	CAS	Turchyn et al., 2009
99.3	15.5	CAS	Turchyn et al., 2009
99.04	16.3	CAS	Turchyn et al., 2009
98.98	16.3	CAS	Turchyn et al., 2009
98.85	18.3	CAS	Turchyn et al., 2009
98.7	19.7	CAS	Turchyn et al., 2009
98.41	19.4	CAS	Turchyn et al., 2009
98.34	17.3	CAS	Turchyn et al., 2009
98.29	17.9	CAS	Turchyn et al., 2009
98.12	18.6	CAS	Turchyn et al., 2009
98	18.8	CAS	Turchyn et al., 2009
97.82	16.4	CAS	Turchyn et al., 2009
97.73	16.2	CAS	Turchyn et al., 2009
97.68	16.9	CAS	Turchyn et al., 2009
97.59	17.4	CAS	Turchyn et al., 2009
97.54	17.3	CAS	Turchyn et al., 2009
97.45	15.3	CAS	Turchyn et al., 2009
97.36	15.6	CAS	Turchyn et al., 2009
97.28	16.4	CAS	Turchyn et al., 2009
97.2	19.9	CAS	Turchyn et al., 2009
97.13	18.9	CAS	Turchyn et al., 2009
97.05	18.2	CAS	Turchyn et al., 2009
96.98	17.6	CAS	Turchyn et al., 2009
96.92	17.5	CAS	Turchyn et al., 2009
96.85	17.9	CAS	Turchyn et al., 2009
96.79	18.0	CAS	Turchyn et al., 2009
96.7	17.6	CAS	Turchyn et al., 2009
96.62	17.3	CAS	Turchyn et al., 2009
96.55	18.0	CAS	Turchyn et al., 2009
96.46	19.0	CAS	Turchyn et al., 2009
96.36	17.9	CAS	Turchyn et al., 2009
96.29	18.8	CAS	Turchyn et al., 2009
96.22	19.9	CAS	Turchyn et al., 2009
96.17	19.8	CAS	Turchyn et al., 2009
96.01	19.8	CAS	Turchyn et al., 2009
95.92	18.7	CAS	Turchyn et al., 2009
95.69	19.7	CAS	Turchyn et al., 2009
95.62	20.0	CAS	Turchyn et al., 2009
95.32	20.2	CAS	Turchyn et al., 2009
94.74	17.1	CAS	Turchyn et al., 2009
94.4	16.2	CAS	Turchyn et al., 2009
94.29	17.8	CAS	Turchyn et al., 2009
93.98	20.5	CAS	Turchyn et al., 2009

93.96	21.0	CAS	Turchyn et al., 2009
93.91	21.2	CAS	Turchyn et al., 2009
93.79	20.5	CAS	Turchyn et al., 2009
93.76	19.6	CAS	Turchyn et al., 2009
93.65	20.1	CAS	Turchyn et al., 2009
93.56	20.0	CAS	Turchyn et al., 2009
93.4	19.2	CAS	Turchyn et al., 2009
93.27	20.1	CAS	Turchyn et al., 2009
92.91	19.3	CAS	Turchyn et al., 2009
135.03	8.2	Barite	Turchyn et al., 2009
118.77	8.1	Barite	Turchyn et al., 2009
117.68	8.7	Barite	Turchyn et al., 2009
115.48	9.0	Barite	Turchyn et al., 2009
111.88	9.3	Barite	Turchyn et al., 2009
110.89	9.5	Barite	Turchyn et al., 2009
110.12	9.5	Barite	Turchyn et al., 2009
108.57	9.3	Barite	Turchyn et al., 2009
108.06	9.5	Barite	Turchyn et al., 2009
107.4	9.0	Barite	Turchyn et al., 2009
105.39	9.4	Barite	Turchyn et al., 2009
104.49	8.5	Barite	Turchyn et al., 2009
103.42	13.8	Barite	Turchyn et al., 2009
102.85	14.3	Barite	Turchyn et al., 2009
102.63	14.9	Barite	Turchyn et al., 2009
102.27	15.3	Barite	Turchyn et al., 2009
102.05	15.2	Barite	Turchyn et al., 2009
101.83	16.4	Barite	Turchyn et al., 2009
101.75	15.5	Barite	Turchyn et al., 2009
100.91	15.4	Barite	Turchyn et al., 2009
100.63	14.0	Barite	Turchyn et al., 2009
100.42	11.7	Barite	Turchyn et al., 2009
100.11	9.3	Barite	Turchyn et al., 2009
99.97	10.2	Barite	Turchyn et al., 2009
99.83	11.6	Barite	Turchyn et al., 2009
99.44	10.0	Barite	Turchyn et al., 2009
99.16	14.3	Barite	Turchyn et al., 2009
98.98	11.7	Barite	Turchyn et al., 2009
98.93	14.3	Barite	Turchyn et al., 2009
98.85	14.6	Barite	Turchyn et al., 2009
98.41	13.3	Barite	Turchyn et al., 2009
98.41	13.1	Barite	Turchyn et al., 2009
98.08	12.8	Barite	Turchyn et al., 2009
98	13.0	Barite	Turchyn et al., 2009
97.9	12.5	Barite	Turchyn et al., 2009
96.92	10.3	Barite	Turchyn et al., 2009
96.7	8.9	Barite	Turchyn et al., 2009
94.95	9.9	Barite	Turchyn et al., 2009
94.89	9.3	Barite	Turchyn et al., 2009
94.63	9.7	Barite	Turchyn et al., 2009
94.4	10.6	Barite	Turchyn et al., 2009
94.29	10.5	Barite	Turchyn et al., 2009
93.98	13.7	Barite	Turchyn et al., 2009
93.76	18.7	Barite	Turchyn et al., 2009
93.56	16.6	Barite	Turchyn et al., 2009
91.15	10.0	Barite	Turchyn et al., 2009
90.79	12.5	Barite	Turchyn et al., 2009
90.44	12.1	Barite	Turchyn et al., 2009
89.38	15.3	Barite	Turchyn et al., 2009
85.4	16.4	Barite	Turchyn et al., 2009
83.99	14.8	Barite	Turchyn et al., 2009
83.88	12.2	Barite	Turchyn et al., 2009
83.77	11.5	Barite	Turchyn et al., 2009
83.22	9.5	Barite	Turchyn et al., 2009
82.85	4.2	Barite	Turchyn et al., 2009
11.75	13.4	Barite	Turchyn and Schrag, 2006
17.85	12.4	Barite	Turchyn and Schrag, 2006
25.1	11.7	Barite	Turchyn and Schrag, 2006
25.37	11.0	Barite	Turchyn and Schrag, 2006
26.95	11.8	Barite	Turchyn and Schrag, 2006
29.04	12.1	Barite	Turchyn and Schrag, 2006
29.9	12.0	Barite	Turchyn and Schrag, 2006

30.03	11.6	Barite	Turchyn and Schrag, 2006
30.65	11.1	Barite	Turchyn and Schrag, 2006
31.07	11.6	Barite	Turchyn and Schrag, 2006
31.39	11.4	Barite	Turchyn and Schrag, 2006
31.62	11.5	Barite	Turchyn and Schrag, 2006
31.99	11.9	Barite	Turchyn and Schrag, 2006
9.79	10.7	Barite	Turchyn and Schrag, 2006
10.78	10.2	Barite	Turchyn and Schrag, 2006
14.34	14.3	Barite	Turchyn and Schrag, 2006
14.97	12.0	Barite	Turchyn and Schrag, 2006
9.46	11.2	Barite	Turchyn and Schrag, 2006
9.97	12.1	Barite	Turchyn and Schrag, 2006
10.71	12.1	Barite	Turchyn and Schrag, 2006
11.72	10.8	Barite	Turchyn and Schrag, 2006
12.54	14.9	Barite	Turchyn and Schrag, 2006
13.61	12.6	Barite	Turchyn and Schrag, 2006
14.51	12.9	Barite	Turchyn and Schrag, 2006
15.94	11.9	Barite	Turchyn and Schrag, 2006
19.97	10.9	Barite	Turchyn and Schrag, 2006
22.2	11.0	Barite	Turchyn and Schrag, 2006
22.8	11.8	Barite	Turchyn and Schrag, 2006
26.2	10.8	Barite	Turchyn and Schrag, 2006
26.81	10.9	Barite	Turchyn and Schrag, 2006
30.97	11.8	Barite	Turchyn and Schrag, 2006
17.44	11.7	Barite	Turchyn and Schrag, 2006
18.89	10.8	Barite	Turchyn and Schrag, 2006
10.56	11.7	Barite	Turchyn and Schrag, 2006
13.21	13.5	Barite	Turchyn and Schrag, 2006
17.25	12.8	Barite	Turchyn and Schrag, 2006
19.48	12.3	Barite	Turchyn and Schrag, 2006
20.38	11.3	Barite	Turchyn and Schrag, 2006
15.97	12.9	Barite	Turchyn and Schrag, 2006
37.71	10.8	Barite	Turchyn and Schrag, 2006
47.02	10.1	Barite	Turchyn and Schrag, 2006
48.99	10.8	Barite	Turchyn and Schrag, 2006
52.1	11.4	Barite	Turchyn and Schrag, 2006
60.37	11.5	Barite	Turchyn and Schrag, 2006
62.75	10.8	Barite	Turchyn and Schrag, 2006
63.26	10.8	Barite	Turchyn and Schrag, 2006
65.69	9.6	Barite	Turchyn and Schrag, 2006
33.9	10.9	Barite	Turchyn and Schrag, 2006
34.1	10.4	Barite	Turchyn and Schrag, 2006
34.3	10.7	Barite	Turchyn and Schrag, 2006
34.3	10.7	Barite	Turchyn and Schrag, 2006
52.17	12.2	Barite	Turchyn and Schrag, 2006
52.84	13.5	Barite	Turchyn and Schrag, 2006
54.13	12.2	Barite	Turchyn and Schrag, 2006
55.18	13.7	Barite	Turchyn and Schrag, 2006
55.83	13.3	Barite	Turchyn and Schrag, 2006
55.97	13.6	Barite	Turchyn and Schrag, 2006
56.22	12.7	Barite	Turchyn and Schrag, 2006
56.43	11.8	Barite	Turchyn and Schrag, 2006
56.91	11.6	Barite	Turchyn and Schrag, 2006
59.05	11.5	Barite	Turchyn and Schrag, 2006
46.01	11.0	Barite	Turchyn and Schrag, 2006
47.34	11.7	Barite	Turchyn and Schrag, 2006
49.42	11.6	Barite	Turchyn and Schrag, 2006
51.35	12.8	Barite	Turchyn and Schrag, 2006
25.5	12.4	Barite	Turchyn and Schrag, 2006
27.5	11.6	Barite	Turchyn and Schrag, 2006
28.5	14.7	Barite	Turchyn and Schrag, 2006
29.5	12.9	Barite	Turchyn and Schrag, 2006
37.5	11.2	Barite	Turchyn and Schrag, 2006
38.5	9.8	Barite	Turchyn and Schrag, 2006
39.5	10.0	Barite	Turchyn and Schrag, 2006
40.5	10.1	Barite	Turchyn and Schrag, 2006
41.5	10.7	Barite	Turchyn and Schrag, 2006
34.5	10.6	Barite	Turchyn and Schrag, 2006
36.07	10.5	Barite	Turchyn and Schrag, 2006
37	11.0	Barite	Turchyn and Schrag, 2006
38.25	13.1	Barite	Turchyn and Schrag, 2006
39.05	11.3	Barite	Turchyn and Schrag, 2006

40.16	10.5		Barite	Turchyn and Schrag, 2006
41.04	10.8		Barite	Turchyn and Schrag, 2006
43.14	11.7		Barite	Turchyn and Schrag, 2006
44.34	11.8		Barite	Turchyn and Schrag, 2006
45.31	12.2		Barite	Turchyn and Schrag, 2006
46.34	11.4		Barite	Turchyn and Schrag, 2006
388		20.4	CAS	Ueda et al., 1987
388		21.3	CAS	Ueda et al., 1987
388		23.6	CAS	Ueda et al., 1987
388		19.5	CAS	Ueda et al., 1987
388		24.6	CAS	Ueda et al., 1987
388		23.5	CAS	Ueda et al., 1987
388		19.6	CAS	Ueda et al., 1987
388		22.6	CAS	Ueda et al., 1987
388		23.5	CAS	Ueda et al., 1987
388		16.8	CAS	Ueda et al., 1987
388		19.4	CAS	Ueda et al., 1987
388		20.7	CAS	Ueda et al., 1987
388		24.5	CAS	Ueda et al., 1987
388		18.3	CAS	Ueda et al., 1987
388		5.0	CAS	Ueda et al., 1987
388		23.0	CAS	Ueda et al., 1987
388		21.0	CAS	Ueda et al., 1987
388		23.9	CAS	Ueda et al., 1987
82	15.1	18.4	Gypsum	Utrilla et al., 1992
82	12.1	19.2	Gypsum	Utrilla et al., 1992
82	16.3	19.0	Gypsum	Utrilla et al., 1992
82	12.7	17.9	Gypsum	Utrilla et al., 1992
82	15.6	18.6	Gypsum	Utrilla et al., 1992
82	12.3	19.2	Gypsum	Utrilla et al., 1992
82	11.1	18.9	Gypsum	Utrilla et al., 1992
82	12.6	16.3	Gypsum	Utrilla et al., 1992
215	13.9	14.8	Gypsum	Utrilla et al., 1992
215	9.7	14.8	Gypsum	Utrilla et al., 1992
215	10.2	13.3	Gypsum	Utrilla et al., 1992
215	8.9	13.9	Gypsum	Utrilla et al., 1992
215	9.0	13.5	Gypsum	Utrilla et al., 1992
215	9.4	13.8	Gypsum	Utrilla et al., 1992
215	12.2	14.5	Gypsum	Utrilla et al., 1992
215	12.6	12.9	Gypsum	Utrilla et al., 1992
215	10.9	12.9	Gypsum	Utrilla et al., 1992
215	10.4	12.5	Gypsum	Utrilla et al., 1992
215	12.5	11.5	Gypsum	Utrilla et al., 1992
215	12.4	12.2	Gypsum	Utrilla et al., 1992
215	11.5	12.5	Gypsum	Utrilla et al., 1992
215	10.9	15.8	Gypsum	Utrilla et al., 1992
215	13.5	11.9	Gypsum	Utrilla et al., 1992
215	13.1	10.2	Gypsum	Utrilla et al., 1992
215	12.6	12.1	Gypsum	Utrilla et al., 1992
215	14.9	14.5	Gypsum	Utrilla et al., 1992
215	14.1	14.6	Gypsum	Utrilla et al., 1992
215	11.7	13.7	Gypsum	Utrilla et al., 1992
215	11.5	16.6	Gypsum	Utrilla et al., 1992
215	13.8	14.1	Gypsum	Utrilla et al., 1992
215	18.0	12.8	Gypsum	Utrilla et al., 1992
14	18.3	12.1	Gypsum	Utrilla et al., 1992
14	13.0	12.0	Gypsum	Utrilla et al., 1992
14	14.5	14.8	Gypsum	Utrilla et al., 1992
14	17.5	10.2	Gypsum	Utrilla et al., 1992
14	17.0	10.7	Gypsum	Utrilla et al., 1992
14	18.0	9.9	Gypsum	Utrilla et al., 1992
14	17.5	10.5	Gypsum	Utrilla et al., 1992
14	14.9	12.1	Gypsum	Utrilla et al., 1992
14	17.7	14.5	Gypsum	Utrilla et al., 1992
28	14.1	11.5	Gypsum	Utrilla et al., 1992
28	17.3	12.4	Gypsum	Utrilla et al., 1992
28	14.2	11.1	Gypsum	Utrilla et al., 1992
28	16.7	10.2	Gypsum	Utrilla et al., 1992
28	15.5	12.4	Gypsum	Utrilla et al., 1992
28	16.8	12.2	Gypsum	Utrilla et al., 1992
28	17.0	11.4	Gypsum	Utrilla et al., 1992

28	15.2	16.4	Gypsum	Utrilla et al., 1992
28	13.9	15.6	Gypsum	Utrilla et al., 1992
28	14.4	14.8	Gypsum	Utrilla et al., 1992
28	12.7	12.4	Gypsum	Utrilla et al., 1992
45	16.9	12.8	Gypsum	Utrilla et al., 1992
45	16.6	12.3	Gypsum	Utrilla et al., 1992
45	17.2	11.6	Gypsum	Utrilla et al., 1992
45	15.8	11.9	Gypsum	Utrilla et al., 1992
45	14.5	11.3	Gypsum	Utrilla et al., 1992
45	16.5	14.1	Gypsum	Utrilla et al., 1992
45	17.1	8.8	Gypsum	Utrilla et al., 1992
45	16.4	11.2	Gypsum	Utrilla et al., 1992
45	16.0	12.8	Gypsum	Utrilla et al., 1992
45	15.4	16.2	Gypsum	Utrilla et al., 1992
45	14.6	16.6	Gypsum	Utrilla et al., 1992
45	16.1	15.5	Gypsum	Utrilla et al., 1992
45	14.3	14.6	Gypsum	Utrilla et al., 1992
45	17.4	14.9	Gypsum	Utrilla et al., 1992
45	15.7	15.4	Gypsum	Utrilla et al., 1992
60	13.3	16.1	Gypsum	Utrilla et al., 1992
60	16.9	14.9	Gypsum	Utrilla et al., 1992
60	15.0	15.7	Gypsum	Utrilla et al., 1992
60	14.1	23.8	Gypsum	Utrilla et al., 1992
40	12.4	20.2	Gypsum	Utrilla et al., 1992
40	12.2	20.9	Gypsum	Utrilla et al., 1992
40	11.1	20.1	Gypsum	Utrilla et al., 1992
40	10.9	20.2	Gypsum	Utrilla et al., 1992
40	12.0	21.4	Gypsum	Utrilla et al., 1992
40	11.5	22.0	Gypsum	Utrilla et al., 1992
40	12.1	21.9	Gypsum	Utrilla et al., 1992
40	12.0	21.0	Gypsum	Utrilla et al., 1992
40	10.5	23.7	Gypsum	Utrilla et al., 1992
40	12.3	21.0	Gypsum	Utrilla et al., 1992
40	11.3	20.3	Gypsum	Utrilla et al., 1992
40	10.6	20.5	Gypsum	Utrilla et al., 1992
40	10.4	20.2	Gypsum	Utrilla et al., 1992
40	11.2	21.7	Gypsum	Utrilla et al., 1992
40	11.3	21.5	Gypsum	Utrilla et al., 1992
40	11.6	22.3	Gypsum	Utrilla et al., 1992
40	11.5	22.4	Gypsum	Utrilla et al., 1992
40	14.0	23.8	Gypsum	Utrilla et al., 1992
40	11.9	21.8	Gypsum	Utrilla et al., 1992
45	13.4	21.3	Gypsum	Utrilla et al., 1992
45	12.4	21.3	Gypsum	Utrilla et al., 1992
45	12.8	21.0	Gypsum	Utrilla et al., 1992
45	13.5	21.7	Gypsum	Utrilla et al., 1992
45	13.0	21.5	Gypsum	Utrilla et al., 1992
45	12.0	21.5	Gypsum	Utrilla et al., 1992
45	12.9	20.2	Gypsum	Utrilla et al., 1992
45	12.5	21.4	Gypsum	Utrilla et al., 1992
45	11.1	21.5	Gypsum	Utrilla et al., 1992
45	14.7	21.5	Gypsum	Utrilla et al., 1992
45	11.9	21.5	Gypsum	Utrilla et al., 1992
45	11.9	21.8	Gypsum	Utrilla et al., 1992
45	18.1	15.4	Gypsum	Utrilla et al., 1992
14	15.5	17.9	Gypsum	Utrilla et al., 1992
14	16.4	18.5	Gypsum	Utrilla et al., 1992
14	15.7	16.3	Gypsum	Utrilla et al., 1992
14	13.6	14.8	Gypsum	Utrilla et al., 1992
14	13.6	16.4	Gypsum	Utrilla et al., 1992
14	18.3	18.7	Gypsum	Utrilla et al., 1992
14	16.2		Gypsum	Utrilla et al., 1992
14	15.1	16.3	Gypsum	Utrilla et al., 1992
14	16.9	16.3	Gypsum	Utrilla et al., 1992
20	17.2	17.2	Gypsum	Utrilla et al., 1992
20	16.3	19.1	Gypsum	Utrilla et al., 1992
20	17.7	17.1	Gypsum	Utrilla et al., 1992
20	16.5	17.7	Gypsum	Utrilla et al., 1992
20	16.0	15.2	Gypsum	Utrilla et al., 1992
20	16.8	16.5	Gypsum	Utrilla et al., 1992
20	17.3	17.2	Gypsum	Utrilla et al., 1992
20	17.6	18.2	Gypsum	Utrilla et al., 1992

20	18.1	19.4	Gypsum	Utrilla et al., 1992
20	17.1	17.8	Gypsum	Utrilla et al., 1992
20	16.5	17.3	Gypsum	Utrilla et al., 1992
20	15.5	17.6	Gypsum	Utrilla et al., 1992
20	18.9	17.7	Gypsum	Utrilla et al., 1992
20	15.0	18.6	Gypsum	Utrilla et al., 1992
56	15.0	19.1	Gypsum	Utrilla et al., 1992
56	17.9	18.9	Gypsum	Utrilla et al., 1992
56	18.8	18.4	Gypsum	Utrilla et al., 1992
56	14.7	17.2	Gypsum	Utrilla et al., 1992
56	17.5	16.1	Gypsum	Utrilla et al., 1992
60	17.1	15.0	Gypsum	Utrilla et al., 1992
60	15.9	13.7	Gypsum	Utrilla et al., 1992
60	12.9	18.0	Gypsum	Utrilla et al., 1992
17	14.2	18.4	Gypsum	Utrilla et al., 1992
17	11.3	18.4	Gypsum	Utrilla et al., 1992
17	15.9	18.5	Gypsum	Utrilla et al., 1992
17	14.6	17.7	Gypsum	Utrilla et al., 1992
17	15.3	19.7	Gypsum	Utrilla et al., 1992
17	13.6	19.0	Gypsum	Utrilla et al., 1992
17	14.4	19.1	Gypsum	Utrilla et al., 1992
17	15.4	19.7	Gypsum	Utrilla et al., 1992
17	15.8	19.1	Gypsum	Utrilla et al., 1992
17	15.4	18.5	Gypsum	Utrilla et al., 1992
17	14.3	19.2	Gypsum	Utrilla et al., 1992
17	13.9	12.5	Gypsum	Utrilla et al., 1992
20	13.7	15.8	Gypsum	Utrilla et al., 1992
20	13.5	14.7	Gypsum	Utrilla et al., 1992
20	13.6	13.8	Gypsum	Utrilla et al., 1992
20	18.4	15.6	Gypsum	Utrilla et al., 1992
20	18.3	16.6	Gypsum	Utrilla et al., 1992
20	19.3	15.2	Gypsum	Utrilla et al., 1992
20	19.7	15.7	Gypsum	Utrilla et al., 1992
20	11.8	12.2	Gypsum	Utrilla et al., 1992
14	13.0	14.7	Gypsum	Utrilla et al., 1992
14	19.0	14.1	Gypsum	Utrilla et al., 1992
14	17.1	15.8	Gypsum	Utrilla et al., 1992
14	18.5	15.8	Gypsum	Utrilla et al., 1992
14	-0.5	9.1	Gypsum	Utrilla et al., 1992
14	8.8	5.0	Gypsum	Utrilla et al., 1992
2100		32.1	Gypsum	Velikoslavinsky
515		32.2	CAS	Wotte et al., 2012
515		28.9	CAS	Wotte et al., 2012
515		30.5	CAS	Wotte et al., 2012
515			CAS	Wotte et al., 2012
515		27.1	CAS	Wotte et al., 2012
515		29.4	CAS	Wotte et al., 2012
515		29.8	CAS	Wotte et al., 2012
515		29.2	CAS	Wotte et al., 2012
515		30.7	CAS	Wotte et al., 2012
515		29.7	CAS	Wotte et al., 2012
515		30.5	CAS	Wotte et al., 2012
515		29.6	CAS	Wotte et al., 2012
515		29.0	CAS	Wotte et al., 2012
515		30.3	CAS	Wotte et al., 2012
515		30.5	CAS	Wotte et al., 2012
515		28.9	CAS	Wotte et al., 2012
515		29.3	CAS	Wotte et al., 2012
515		27.3	CAS	Wotte et al., 2012
515		27.1	CAS	Wotte et al., 2012
515		28.7	CAS	Wotte et al., 2012
515		27.8	CAS	Wotte et al., 2012
515		25.0	CAS	Wotte et al., 2012
515		25.8	CAS	Wotte et al., 2012
515		27.1	CAS	Wotte et al., 2012
515		29.6	CAS	Wotte et al., 2012
515		30.1	CAS	Wotte et al., 2012
515		27.7	CAS	Wotte et al., 2012
515		27.6	CAS	Wotte et al., 2012
515		28.7	CAS	Wotte et al., 2012
515		28.5	CAS	Wotte et al., 2012

515	29.1		CAS	Wotte et al., 2012
515	27.8		CAS	Wotte et al., 2012
515	21.3		CAS	Wotte et al., 2012
515	23.0		CAS	Wotte et al., 2012
515	24.7		CAS	Wotte et al., 2012
515	30.3		CAS	Wotte et al., 2012
515	26.8		CAS	Wotte et al., 2012
515	26.4		CAS	Wotte et al., 2012
515	27.3		CAS	Wotte et al., 2012
515	27.9		CAS	Wotte et al., 2012
515	28.2		CAS	Wotte et al., 2012
515	27.6		CAS	Wotte et al., 2012
515	27.7		CAS	Wotte et al., 2012
515	27.8		CAS	Wotte et al., 2012
515	28.2		CAS	Wotte et al., 2012
515	28.2		CAS	Wotte et al., 2012
515	26.7		CAS	Wotte et al., 2012
515	28.1		CAS	Wotte et al., 2012
515	27.6		CAS	Wotte et al., 2012
515	26.4		CAS	Wotte et al., 2012
515	26.7		CAS	Wotte et al., 2012
515	22.0		CAS	Wotte et al., 2012
515	25.8		CAS	Wotte et al., 2012
515	17.6		CAS	Wotte et al., 2012
515	17.9		CAS	Wotte et al., 2012
515	25.7		CAS	Wotte et al., 2012
515	25.1		CAS	Wotte et al., 2012
515	22.5		CAS	Wotte et al., 2012
515	25.9		CAS	Wotte et al., 2012
515	26.8		CAS	Wotte et al., 2012
515	26.9		CAS	Wotte et al., 2012
515	27.4		CAS	Wotte et al., 2012
515	27.0		CAS	Wotte et al., 2012
515	26.9		CAS	Wotte et al., 2012
515	22.8		CAS	Wotte et al., 2012
515	25.3		CAS	Wotte et al., 2012
515	26.9		CAS	Wotte et al., 2012
515	26.9		CAS	Wotte et al., 2012
515	27.6		CAS	Wotte et al., 2012
515	27.4		CAS	Wotte et al., 2012
515	17.1		CAS	Wotte et al., 2012
515	24.5		CAS	Wotte et al., 2012
515	19.1		CAS	Wotte et al., 2012
515	25.4		CAS	Wotte et al., 2012
515	27.5		CAS	Wotte et al., 2012
515	26.9		CAS	Wotte et al., 2012
515	27.5		CAS	Wotte et al., 2012
515	26.9		CAS	Wotte et al., 2012
515	25.2		CAS	Wotte et al., 2012
515	13.1		CAS	Wotte et al., 2012
515	33.2		CAS	Wotte et al., 2012
515	19.9		CAS	Wotte et al., 2012
515	26.6		CAS	Wotte et al., 2012
515	25.8		CAS	Wotte et al., 2012
515	30.0		CAS	Wotte et al., 2012
515	33.0		CAS	Wotte et al., 2012
248.2	21.2		Gypsum	Worden et al., 1997
248.2	18.4		Gypsum	Worden et al., 1997
248.2	15.2		Gypsum	Worden et al., 1997
248.2	15.8		Gypsum	Worden et al., 1997
248.2	14.8		Gypsum	Worden et al., 1997
248.2	16.2		Gypsum	Worden et al., 1997
248.2	15.0		Gypsum	Worden et al., 1997
248.2	14.0		Gypsum	Worden et al., 1997
248.2	12.1		Gypsum	Worden et al., 1997
248.2	9.6		Gypsum	Worden et al., 1997
248.2	11.5		Gypsum	Worden et al., 1997
208.6	15.7	-0.05	CAS	Wu et al., 2014
209.2	34.3	-0.02	CAS	Wu et al., 2014
211.9	18.3	0.04	CAS	Wu et al., 2014
214.7	17.9	-0.01	CAS	Wu et al., 2014

220.3	18.2	0.00	CAS	Wu et al., 2014
225	19.6	-0.01	CAS	Wu et al., 2014
226	18.8	0.01	CAS	Wu et al., 2014
226.9	19.5	0.02	CAS	Wu et al., 2014
228.4	19.9	-0.01	CAS	Wu et al., 2014
229.8	16.5	0.00	CAS	Wu et al., 2014
231	24.0	-0.03	CAS	Wu et al., 2014
233.7	17.5	-0.03	CAS	Wu et al., 2014
234.1	16.9	-0.05	CAS	Wu et al., 2014
235.2	17.3	0.00	CAS	Wu et al., 2014
236.2	29.6	0.01	CAS	Wu et al., 2014
236.9	36.3	0.00	CAS	Wu et al., 2014
237.1	23.0	0.00	CAS	Wu et al., 2014
237.8	17.8	0.00	CAS	Wu et al., 2014
238	19.5	0.01	CAS	Wu et al., 2014
238.2	32.7	0.01	CAS	Wu et al., 2014
238.4	30.2	0.03	CAS	Wu et al., 2014
238.7	31.4	0.01	CAS	Wu et al., 2014
238.8	29.6	0.00	CAS	Wu et al., 2014
239	27.0	-0.01	CAS	Wu et al., 2014
239.3	22.2	-0.03	CAS	Wu et al., 2014
239.5	28.0	0.01	CAS	Wu et al., 2014
239.6	25.2	0.00	CAS	Wu et al., 2014
240.1	21.7	0.04	CAS	Wu et al., 2014
241.4	20.0	-0.07	CAS	Wu et al., 2014
245	16.3	0.02	CAS	Wu et al., 2014
245.7	26.5	0.01	CAS	Wu et al., 2014
246.9	16.7	0.01	CAS	Wu et al., 2014
248.4	21.5	-0.07	CAS	Wu et al., 2014
251.3	14.9	0.01	CAS	Wu et al., 2014
255	15.9	-0.01	CAS	Wu et al., 2014
256.1	23.4	-0.01	CAS	Wu et al., 2014
256.7	11.9	-0.06	CAS	Wu et al., 2014
258	16.9	0.03	CAS	Wu et al., 2014
259	15.9	0.00	CAS	Wu et al., 2014
268.8	22.2	0.00	CAS	Wu et al., 2014
275.5	16.4	0.02	CAS	Wu et al., 2014
280	16.9	0.01	CAS	Wu et al., 2014
284.7	13.7	-0.02	CAS	Wu et al., 2014
290	13.3	0.02	CAS	Wu et al., 2014
291	11.7	-0.03	CAS	Wu et al., 2014
291.6	13.2	-0.02	CAS	Wu et al., 2014
292.1	12.8	0.04	CAS	Wu et al., 2014
293.3	15.2	0.02	CAS	Wu et al., 2014
295.1	11.0	-0.02	CAS	Wu et al., 2014
297.3	15.8	0.07	CAS	Wu et al., 2014
297.7	12.3	0.01	CAS	Wu et al., 2014
298.6	11.8	-0.02	CAS	Wu et al., 2014
299.6	8.4	-0.02	CAS	Wu et al., 2014
301.5	14.0	-0.02	CAS	Wu et al., 2014
302.4	9.8	-0.08	CAS	Wu et al., 2014
303.1	12.1	0.00	CAS	Wu et al., 2014
303.4	12.7	0.00	CAS	Wu et al., 2014
303.6	11.0	-0.02	CAS	Wu et al., 2014
303.8	12.3	-0.02	CAS	Wu et al., 2014
304.9	10.9	0.00	CAS	Wu et al., 2014
305.4	12.3	0.01	CAS	Wu et al., 2014
308.2	14.5	0.03	CAS	Wu et al., 2014
308.7	14.0	-0.01	CAS	Wu et al., 2014
308.8	14.2	-0.01	CAS	Wu et al., 2014
308.9	15.0	0.03	CAS	Wu et al., 2014
309.1	14.4	-0.01	CAS	Wu et al., 2014
309.2	13.7	0.02	CAS	Wu et al., 2014
310.2	10.6	-0.01	CAS	Wu et al., 2014
310.8	15.1	-0.01	CAS	Wu et al., 2014
313.8	12.5	-0.06	CAS	Wu et al., 2014
314.5	11.9	-0.02	CAS	Wu et al., 2014
315.2	12.0	-0.02	CAS	Wu et al., 2014
316.8	10.1	-0.02	CAS	Wu et al., 2014
317.7	21.1	0.01	CAS	Wu et al., 2014
331.8	16.6	0.01	CAS	Wu et al., 2014
332.7	16.2	0.06	CAS	Wu et al., 2014

333.4	15.7	-0.02	CAS	Wu et al., 2014
334.1	12.5	-0.03	CAS	Wu et al., 2014
334.2	17.5	-0.02	CAS	Wu et al., 2014
334.4	14.0	-0.04	CAS	Wu et al., 2014
334.5	18.5	-0.05	CAS	Wu et al., 2014
335.3	14.6	0.00	CAS	Wu et al., 2014
335.4	15.4	0.02	CAS	Wu et al., 2014
336.5	18.1	-0.02	CAS	Wu et al., 2014
336.7	21.0	-0.04	CAS	Wu et al., 2014
337.5	14.2	0.03	CAS	Wu et al., 2014
337.7	13.1	-0.01	CAS	Wu et al., 2014
338.2	18.8	-0.03	CAS	Wu et al., 2014
338.4	18.3	0.00	CAS	Wu et al., 2014
339.4	14.1	0.01	CAS	Wu et al., 2014
339.7	16.7	0.02	CAS	Wu et al., 2014
340	14.5	0.01	CAS	Wu et al., 2014
340.2	27.3	0.00	CAS	Wu et al., 2014
340.3	19.9	0.01	CAS	Wu et al., 2014
340.5	18.3	-0.01	CAS	Wu et al., 2014
340.6	12.8	-0.02	CAS	Wu et al., 2014
341.6	19.5	-0.04	CAS	Wu et al., 2014
341.8	21.7	0.01	CAS	Wu et al., 2014
342.7	19.6	-0.02	CAS	Wu et al., 2014
343.1	16.8	-0.03	CAS	Wu et al., 2014
343.4	16.3	-0.03	CAS	Wu et al., 2014
343.6	20.3	-0.03	CAS	Wu et al., 2014
343.8	10.0	-0.06	CAS	Wu et al., 2014
343.8	17.4	-0.03	CAS	Wu et al., 2014
345.2	19.5	0.01	CAS	Wu et al., 2014
345.3	19.1	0.01	CAS	Wu et al., 2014
346.2	22.2	-0.01	CAS	Wu et al., 2014
346.3	16.6	-0.01	CAS	Wu et al., 2014
346.4	21.9	-0.02	CAS	Wu et al., 2014
346.7	17.3	0.00	CAS	Wu et al., 2014
347.2	21.2	0.00	CAS	Wu et al., 2014
348.7	21.7	0.00	CAS	Wu et al., 2014
349	22.4	0.00	CAS	Wu et al., 2014
350.8	23.9	0.04	CAS	Wu et al., 2014
350.9	22.2	0.05	CAS	Wu et al., 2014
351.5	20.2	0.02	CAS	Wu et al., 2014
351.9	18.5	0.03	CAS	Wu et al., 2014
351.9	20.3	0.03	CAS	Wu et al., 2014
352.1	20.2	0.04	CAS	Wu et al., 2014
353.1	18.0	0.02	CAS	Wu et al., 2014
354.2	11.8	-0.03	CAS	Wu et al., 2014
354.4	19.3	-0.01	CAS	Wu et al., 2014
354.7	21.2	0.00	CAS	Wu et al., 2014
355.9	21.0	0.01	CAS	Wu et al., 2014
357.2	14.8	-0.05	CAS	Wu et al., 2014
359	22.7	0.00	CAS	Wu et al., 2014
360.9	23.8	0.03	CAS	Wu et al., 2014
366.2	19.7	-0.01	CAS	Wu et al., 2014
367.7	26.0	0.00	CAS	Wu et al., 2014
369	17.8	0.00	CAS	Wu et al., 2014
370.1	33.0	0.00	CAS	Wu et al., 2014
372	37.5	0.04	CAS	Wu et al., 2014
373.7	21.6	0.01	CAS	Wu et al., 2014
377.6	19.3	0.01	CAS	Wu et al., 2014
378.6	22.4	0.02	CAS	Wu et al., 2014
379.7	21.9	0.04	CAS	Wu et al., 2014
380.9	17.2	0.00	CAS	Wu et al., 2014
381.9	24.5	0.03	CAS	Wu et al., 2014
383.5	19.3	-0.04	CAS	Wu et al., 2014
384.5	31.1	0.03	CAS	Wu et al., 2014
385.7	17.7	0.01	CAS	Wu et al., 2014
385.8	16.4	0.01	CAS	Wu et al., 2014
385.9	14.0	-0.02	CAS	Wu et al., 2014
386.6	11.0	-0.04	CAS	Wu et al., 2014
388.6	20.4	0.03	CAS	Wu et al., 2014
439.8	26.2	0.02	CAS	Wu et al., 2014
440.5	21.2	0.01	CAS	Wu et al., 2014
443.2	25.1	0.01	CAS	Wu et al., 2014

447.3	28.0	0.02	CAS	Wu et al., 2014
453.6	23.3	0.00	CAS	Wu et al., 2014
457.2	21.4	-0.01	CAS	Wu et al., 2014
459.9	32.4	0.04	CAS	Wu et al., 2014
470.7	26.5	-0.01	CAS	Wu et al., 2014
474.4	35.9	0.00	CAS	Wu et al., 2014
1100	14.3		CAS	Ueda et al., 1987
1100	4.2		CAS	Ueda et al., 1987
1100	0.8		CAS	Ueda et al., 1987
1100	7.0		CAS	Ueda et al., 1987
1100	8.8		CAS	Ueda et al., 1987
1100	12.8		CAS	Ueda et al., 1987
1900	25.9		CAS	Ueda 1990
1900	23.6		CAS	Ueda 1990
1900	27.3		CAS	Ueda 1990
211.8	19.6	0.04	CAS	Wu et al., 2010
213.3	19.8	0.01	CAS	Wu et al., 2010
214.7	18.2	0.02	CAS	Wu et al., 2010
218.8	18.8	0.01	CAS	Wu et al., 2010
224.2	20.0	0.03	CAS	Wu et al., 2010
224.7	19.1	-0.01	CAS	Wu et al., 2010
236.2	18.0	0.03	CAS	Wu et al., 2010
241.2	27.8	0.02	CAS	Wu et al., 2010
241.4	27.6	0.04	CAS	Wu et al., 2010
244.4	17.0	0.04	CAS	Wu et al., 2010
244.8	17.3	0.04	CAS	Wu et al., 2010
244.9	24.5	0.07	CAS	Wu et al., 2010
510.3	37.9	0.00	CAS	Wu et al., 2010
511.7	29.6	-0.01	CAS	Wu et al., 2010
512.9	29.5	-0.02	CAS	Wu et al., 2010
518.1	35.2	-0.05	CAS	Wu et al., 2010
557.4	31.9	0.00	CAS	Wu et al., 2010
561.3	38.6	0.02	CAS	Wu et al., 2010
541	42.4	0.06	CAS	Wu et al., 2015
541	38.8	0.07	CAS	Wu et al., 2015
541	39.6	0.01	CAS	Wu et al., 2015
541	42.2	0.02	CAS	Wu et al., 2015
541	39.7	0.06	CAS	Wu et al., 2015
541	39.8	0.03	CAS	Wu et al., 2015
541	40.9	0.04	CAS	Wu et al., 2015
541	41.6	0.07	CAS	Wu et al., 2015
541	40.3	0.03	CAS	Wu et al., 2015
541	41.3	0.06	CAS	Wu et al., 2015
541	40.0	0.05	CAS	Wu et al., 2015
541	39.7	0.03	CAS	Wu et al., 2015
541	40.4	0.03	CAS	Wu et al., 2015
541	41.6	0.01	CAS	Wu et al., 2015
541	40.0	0.05	CAS	Wu et al., 2015
541	40.3	0.06	CAS	Wu et al., 2015
541	33.4	0.02	CAS	Wu et al., 2015
541	26.8	0.01	CAS	Wu et al., 2015
541	27.4	0.02	CAS	Wu et al., 2015
560	27.2	0.01	CAS	Wu et al., 2015
560	26.7	0.01	CAS	Wu et al., 2015
560	25.9	0.04	CAS	Wu et al., 2015
560	25.7	0.02	CAS	Wu et al., 2015
560	22.0	0.01	CAS	Wu et al., 2015
560	22.1	0.01	CAS	Wu et al., 2015
560	23.3	0.03	CAS	Wu et al., 2015
560	23.6	0.01	CAS	Wu et al., 2015
560	26.2	-0.01	CAS	Wu et al., 2015
560	24.0	0.03	CAS	Wu et al., 2015
560	18.2	0.04	CAS	Wu et al., 2015
560	24.7	0.02	CAS	Wu et al., 2015
560	23.9	0.03	CAS	Wu et al., 2015
560	22.3	0.02	CAS	Wu et al., 2015
560	24.2	0.02	CAS	Wu et al., 2015
560	23.2	0.02	CAS	Wu et al., 2015
560	21.3	0.03	CAS	Wu et al., 2015
560	25.2	0.04	CAS	Wu et al., 2015
560	24.4	0.02	CAS	Wu et al., 2015

560	25.7	0.01	CAS	Wu et al., 2015
560	24.2	0.03	CAS	Wu et al., 2015
600	27.9	0.01	CAS	Wu et al., 2015
600	27.8	-0.01	CAS	Wu et al., 2015
600	21.5	0.07	CAS	Wu et al., 2015
600	23.6	0.02	CAS	Wu et al., 2015
600	26.5	-0.01	CAS	Wu et al., 2015
600	25.2	-0.01	CAS	Wu et al., 2015
600	21.5	0.02	CAS	Wu et al., 2015
600	19.1	0.01	CAS	Wu et al., 2015
600	23.8	0.00	CAS	Wu et al., 2015
600	23.0	-0.01	CAS	Wu et al., 2015
600	20.6	0.05	CAS	Wu et al., 2015
600	22.2	0.02	CAS	Wu et al., 2015
630	18.4	0.00	CAS	Wu et al., 2015
630	22.3	0.00	CAS	Wu et al., 2015
630	21.0	0.04	CAS	Wu et al., 2015
630	22.7	-0.05	CAS	Wu et al., 2015